CANADIAN THESES

THÈSES CANADIENNES

NOTICE

The quality of this microfiche is heavily dependent upon the quality of the original thesis submitted for microfilming. Every effort has been made to ensure the highest quality of reproduction possible.

If pages are missing, contact the university which granted the degree.

Some pages may have indistinct print especially if the original pages were typed with a poor typewriter ribbon or if the university sent us an inferior photocopy.

Previously copyrighted materials (journal articles, published tests, etc.) are not filmed.

AVIS

La qualité de cette microfiche dépend grandement de la qualité de la thèse soumise au microfilmage. Nous avons tout fait pour assurer une qualité supérieure de reproduction.

S'il manque des pages, veuillez communiquer avec l'université qui a conféré le grade.

La qualité d'impression de certaines pages peut laisser à désirer, surtout si les pages originales ont été dactylographiées à l'aide d'un ruban usé ou si l'université nous a fait parvenir une photocopie de qualité inférieure.

Les documents qui font déjà l'objet d'un droit d'auteur (articles de revue, examens publiés, etc.) ne sont pas microfilmés.

THIS DISSERTATION HAS BEEN MICROFILMED EXACTLY AS RECEIVED

LA THÈSE A ÉTÉ MICROFILMÉE TELLE QUE NOUS L'AVONS REÇUE

Analysis and Design of Forced Commutated Cycloconverters for Three and Single Phase Applications

Shahidul Islam Khan

A Thesis

in

The Department

of

Electrical Engineering

Presented in Partial Fulfillment of the Requirements
for the Degree of Doctor of Philosophy at
Concordia University
Montréal, Québec, Canada

November 1986

ISBN 0-315-35513-1

ABSTRACT

Analysis and Design of Forced Commutated Cycloconverters for Three and Single Phase Applications

Shahidul Islam Khan, Ph.D.
Concordia University, 1986

Full automation in manufacturing processes has generated a considerable research interest towards the "next generation" of solid state power converters. These converters are expected to be rugged, cheap and compact enough to be mounted on the frames of their respective motors. These requirements can not be satisfied by existing converter structures because of the bulky L-C components which comprise the various converter filters. To meet these requirements some Forced Commutated Cycloconverter (FCC) structures with improved performance characteristics interms of voltage utilization and generated harmonic distortion are proposed, analysed and experimentally verified in this thesis.

To analyse the aforementioned FCC structures a generalized FCC switching matrix model has been developed. Using this converter model and two distinct modes of operation, a systematic and comprehensive FCC analysis and design approach is established. This approach is subsequently used to analyse and design a number of practical FCC structures suitable for low, medium and high frequency industrial

applications. For example, the proposed three to three phase FCC is targeted towards variable speed ac drive applications while the proposed single to three phase FCC could find extensive use in rural or lightly industrialized areas.

Finally, in order to establish the feasibility of the proposed new FCC topologies and associated frequency, voltage and phase conversion methods, analytical computer based results are verified experimentally.

ACKNOWLEDGEMENTS

The author would like to thank Dr. Phoivos D. Ziogas and Dr. Muhammad H. Rashid for suggesting the topic, and providing encouragement, guidance, support, and friendship during the course of this investigation, and throughout the author's graduate career.

The financial assistance received from the National Science and Engineering Research Council of Canada, the FCAR of Quebec Government and the teaching assistantship from the department of Electrical Engineering are gratefully acknowledged.

My indebtness to my friend and research colleague, Mr. Prasad Enjeti for the interesting discussions we shared.

Help given by Mr. Danny Juras in the laboratory is very much appreciated.

The author is grateful to Mrs. Krishna Shewtahal for her sincere effort in typing the manuscript.

Dedicated to my wife Anisa
and son Asif

TABLE OF CONTENTS

Page

Page

Page

LIST OF FIGURES

Page

LIST OF TABLES

LIST OF ACRONYMS

NCC	Naturally Commutated Cycloconverter
FCC	Forced Commutated Cycloconverter
SF	Switching Function
DMO	Direct Mode of Operation
IMO	Indirect Mode of Operation
PWM	Pulse Width Modulation
pf	Power Factor
SPWM	Sinusoidal Pulse Width Modulation
MSPWM	Modified Sinusoidal Pulse Width Modulation
UPS	Uninterruptible Power Supply
HFL	High Frequency Link

LIST OF SYMBOLS

A_c	Amplitude of carrier signal
A_r	Amplitude of reference signal
A_n	Amplitude of the nth harmonic component
B_n	Amplitude of the nth harmonic component
C	Capacitor
d_l	Order of lower dominant harmonic component
d_h	Order of higher dominant harmonic component
f_c	Carrier frequency
f_{ch}	Chopping frequency per converter switch
f_i	Input frequency of the FCC
f_o	Output frequency of the FCC
f_r	Reference frequency
f_{rt}	Relative frequency of subharmonics
f_s	Switching frequency
I_a, I_b, I_c	Input line currents of the FCC
I_{an}, I_{bn}, I_{cn}	Input phase currents
I_A, I_B, I_C	Output line currents of the FCC
I_A', I_B', I_C'	Output phase currents of the FCC
I_{AN}, I_{BN}, I_{CN}	Output phase currents
N_p	Number of pulses per cycle
N_p	Number of pulses in first 60^0 internal
M_f	Modulation factor
$S_d(\omega_s t)$	DMO cycloconverter switching function
$S_i(\omega_o t)$	IMO cycloconverter inverter switching function
$S_r(\omega_i t)$	IMO cycloconverter rectifier switching function

V_{an}, V_{bn}, V_{cn}	Input phase voltages
V_{AN}, V_{BN}, V_{CN}	Output phase voltages
V_{ab}, V_{bc}, V_{ca}	Input line voltages
V_{AB}, V_{BC}, V_{CA}	Output line voltages
V_{FB}	Peak switch blocking voltage
ω_i	Angular frequency of input voltage
ω_o	Angular frequency of output voltage

CHAPTER 1

INTRODUCTION

1.1 Introduction

Utilities generate and supply the consumers with electric power which is of fixed frequency and voltage. There are many applications, however, where the fixed frequency and voltage is of no use to the consumer and where variable frequency and voltage are required. They include [1]-[5]; variable frequency speed control for ac drives, constant frequency power supplies, controllable VAr generators for voltage support and power factor correction, and ac system interties (see also Table 1.1). This incompatibility between available electric power and required electric power can be solved by using an appropriate power conditioning interface between the source and the load. This interface should have the characteristics of accepting fixed frequency and voltage and delivering variable frequency and voltage. In short it must exhibit the transfer characteristics of a generalized frequency/voltage transformer. These characteristics are analytically depicted in Fig. 1.1.

Furthermore, this hypothetical ideal frequency/voltage transformer is by definition assumed to have complete functional flexibility of independently transforming frequencies and voltages and also generating sinusoidal terminal voltages and currents. Another important property of this frequency/-voltage transformer is that; it must be theoritically loss-

TABLE 1.1: Applications of Frequency/Voltage Transformer

A. Medium Frequency Applications

1. Variable frequency ac drive
   - Textile manufacturing
   - Chemical processing
   - Glass manufacturing
   - Machine tools
   - Polymer forming
   - Food processing
   - Material handling and packaging
   - Printing and paper making
   - Grinders
   - Pumps
   - Mine Hoist
   - Cranes

2. Constant frequency power supplies

   - Aircraft power supplies
   - Mobile ground power generating stations

3. Controllable VAr supply for energy saving

   - Centrifugal pumps
   - Electric fans
   - Power factor correction

4. Transportation

   - Electric locomotive

B. High Frequency Applications

   - Switch-mode rectifiers
   - Battery chargers
   - Linking asynchronous utility lines
   - Induction heating

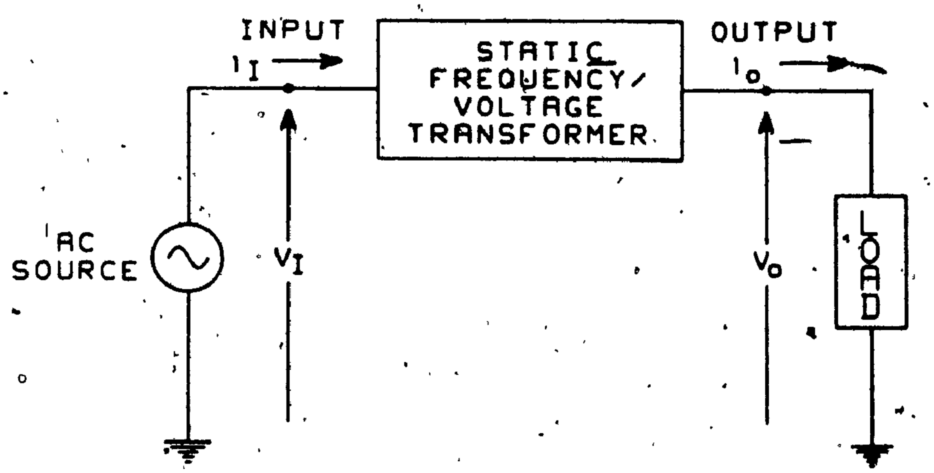

	Input	Output
Excitation:	$v_I = V_I \sin\omega_I t$	$v_o = V_o \sin\omega_o t$
Response:	$i_I = I_I \sin(\omega_I t + \phi_I)$	$i_o = I_o \sin(\omega_o t + \phi_o)$
Given:	$V_I,\ \omega_I$	$Z_o,\ \phi_o$
Controllable:	$Z_I,\ \phi_I$	$V_o,\ \omega_o$

Restriction:

$$P_I = V_I I_I \cos\phi_I = P_o = V_o I_o \cos\phi_o$$

Fig. 1.1: Simplified functional representation of the ideal hypothetical frequency/voltage transformer.

less. Therefore, the real power at the input terminals must be equal to the real power at the output terminals. Also, power must be able to flow in either direction through it.

1.2 Generalized Transformer Implementation

1.2.1 Electromechanical Converter

The first attempt to implement such a practical generalized transformer (i.e. one that generate variable output frequency and voltage) employed a mechanical variable- speed motor-alternator set. This rotary converter had the following limitations [6]-[7]:

i) The motor-alternator speed had to be changed to produce a frequency change with a resulting poor dynamic response for the combined motor-alternator induction motor drive system.

ii) The amplitude of the alternator voltage is proportional to the rate of cutting magnetic flux, which means that at low speeds, in spite of raising the alternator field excitation to a maximum, the amplitude of the output voltage would be very small, and the unit would be incapable of providing the constant voltage/Hz required for constant torque requirement of the ac drive.

iii) Installation as well as life cycle cost is high.

iv) Initial and on going maintenance cost is high.

v) Non-evolutionary.

Due to these disadvantages the rotary converter has been almost completely replaced by the static frequency converter.

1.2.2 DC Link Frequency Changer

The second attempt to implement the subject generalized frequency/voltage transformer employs electronic means and in particular a static dc link frequency changer [8]-[9]. In this case, the fixed frequency fixed voltage ac supply is first rectified and converted into an intermediate stage dc source as shown in Fig. 1.2. The dc source voltage is then inverted at desired output frequency and voltage. The successful application of this type of static frequency changers (dc link frequency changers) was mainly due to the emergence of a new electronic switching device [10] called silicon controlled rectifier (SCR) which was made available in early nineteen sixties. With this switch, frequency and voltage control could be done economically and effectively within the inverter. Although this type of variable frequency static converter is suitable for most variable frequency variable voltage applications discussed earlier, it also has several disadvantages especially when the inverter is of six pulse type. These include [11]-[12]:

i) Input current contains large low order harmonics associated with six pulse rectifier, consequently it requires a large ac filter.

ii) Harmonic content of inverter generated input (dc) current is also high.

iii) Inherent slow response due to the presence of dc link filter inductor and capacitor and the front end phase controlled rectifier.

iv) Non-evolutionary circuit topology.

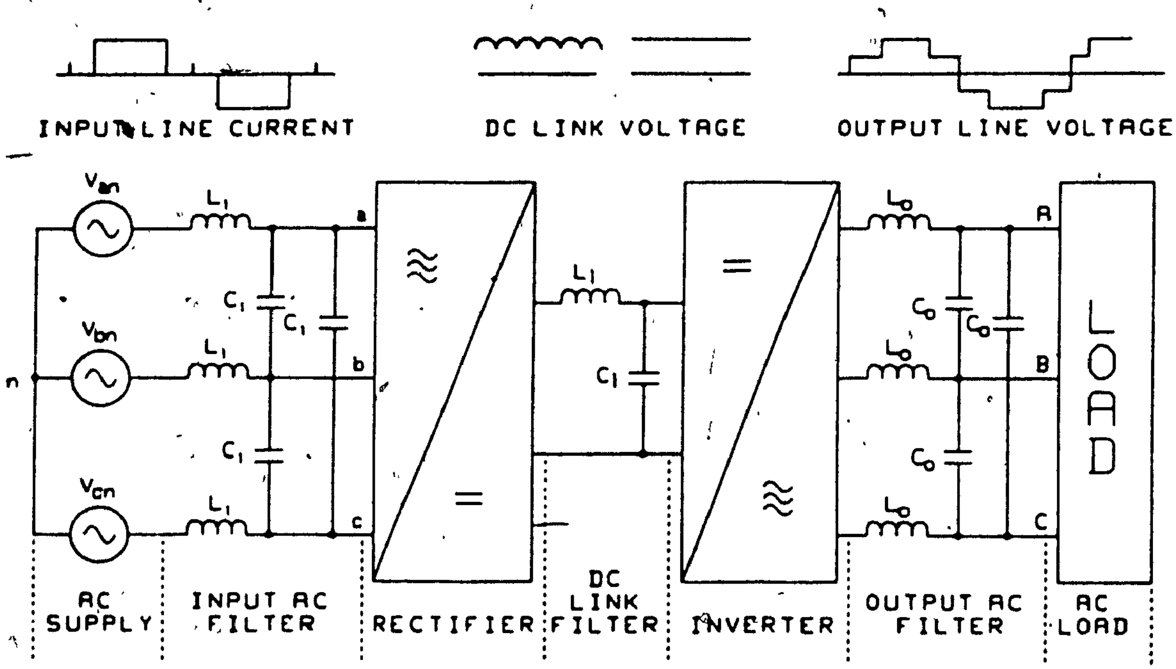

Fig. 1.2: Simplified block diagram representation of a three-phase dc link frequency changer.

Large harmonic contents both in input ac current and dc link stage current make it mandatory to have large dc link and input (ac) filters. Moreover, this topology cannot take advantage of evolutionary new semiconductor devices [13].

1.2.3 Naturally Commutated Cycloconverter (NCC)

The naturally commutated cycloconverter (Fig. 1.3) offers yet another approach in implementing (by electronic means) the subject generalized transformer. The cycloconverter, in its basic form, consists merely of a collection of static switches connected directly between the input ac system and the load circuit and the basic principle of power conversion is to fabricate an output waveform having the desired frequency, simply by opening and closing the switches according to a predetermined temporal sequence. Naturally commutated cycloconverters (NCCs) [14]-[15] are simple, easy to operate and suitable mainly for applications with low load frequency requirements. Main disadvantages of NCC includes [16]:

i) Limited output frequency ($f_o < f_i$) range (Fig. 1.3).

ii) Generation of sub-harmonics both in output voltages and input currents.

iii) Input displacement angle (p.f.) is always lagging irrespective of load power factor.

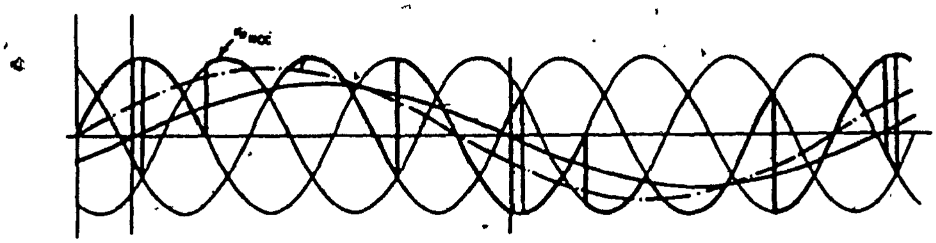

output line voltage

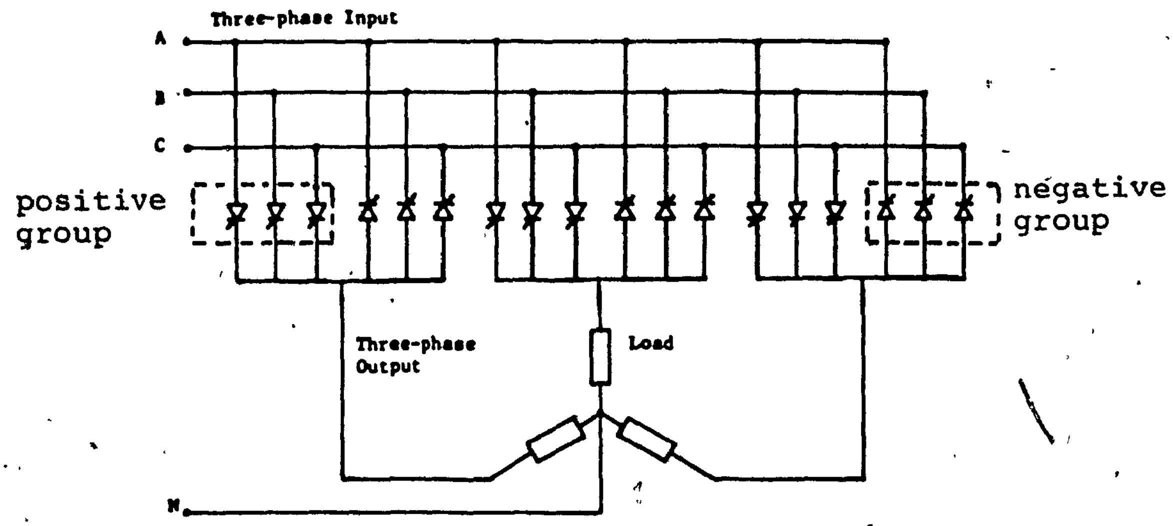

Fig. 1.3: Naturally commutated cycloconverter topology.

1.2.4 Forced Commutated Cycloconverter (FCC)

It has been shown earlier that cycloconverters simplify the process of frequency and voltage transformation by eliminating one stage of power processing, i.e. the dc link stage. For this reason the NCC is obviously a better choice. However, the inherent operating and output frequency limitations of NCC implies further circuit refinements. Such a refinement is the introduction of forced commutation.

Forced commutation unlike natural commutation is the method of 'forcibly' turning on and off of a switch at any required instant irrespective of direction of current or voltage. By using forced commutation the output frequency can be made higher (unrestricted) than the input frequency and also generated harmonics can be better controlled. Thus FCC becomes the best possible means of realizing the subject generalized frequency/voltage static transformer. Because of its frequency related operating characteristics the new converter structure is also known as the "Unrestricted Frequency Changer" or UFC. Most of the investigations on UFC were performed by Gyugyi and Pelly [1],[17]. The performance characteristics of these UFC's are satisfactory. However, they contain sub-harmonics and their spectral characteristics contain low order harmonics. This problem is particularily acute when the output voltage is low. In such cases the amplitude of the unwanted harmonic components becomes higher than the amplitude of the fundamental component. Consequently system performance becomes heavily influenced by harmonic behaviour. In spite of the enormous potential for application of frequency/voltage converters (UFCs), further development and application of UFC was delayed due to two main reasons: limited capability of power devices (in terms of price and switching characteristics) and intrinsic circuit limitations.

Recent advancement in semiconductor technology, however, has shown renewed interest in UFCs and specially Forced Commutated Cycloconverters (FFCs). The power semiconductor industry has lately been making available faster, cheaper, and more efficient switching devices [2], [13] in modular integrated form. The most significant of these devices include; the power MOSFET, asymmetrical thyristors (ASCR), reverse conducting thyristors, gate-turn-off thyristor (GTO), FET - gated bipolar transistor (FGT), gate assisted turn-off thyristors (GATT), etc.

Based on these developments Venturini first proposed and investigated [29] a "generalized transformer" electronic circuit capable of frequency, voltage and power factor transformation. In this circuit model an imaginative PWM voltage control scheme has been also introduced which in principle can eliminate any number of unwanted harmonics and is also free of sub-harmonics. However, the voltage utilization of this scheme is very low [29].

The work presented [18]-[19] here proposes some novel Forced Commutated Cycloconverter structures (e.g. Fig. 1.4) which have improved performance characteristics.

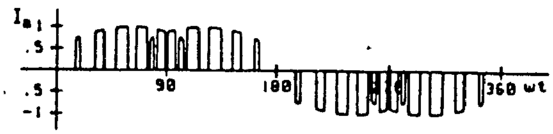

input line current

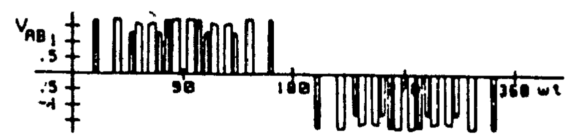

output line voltage

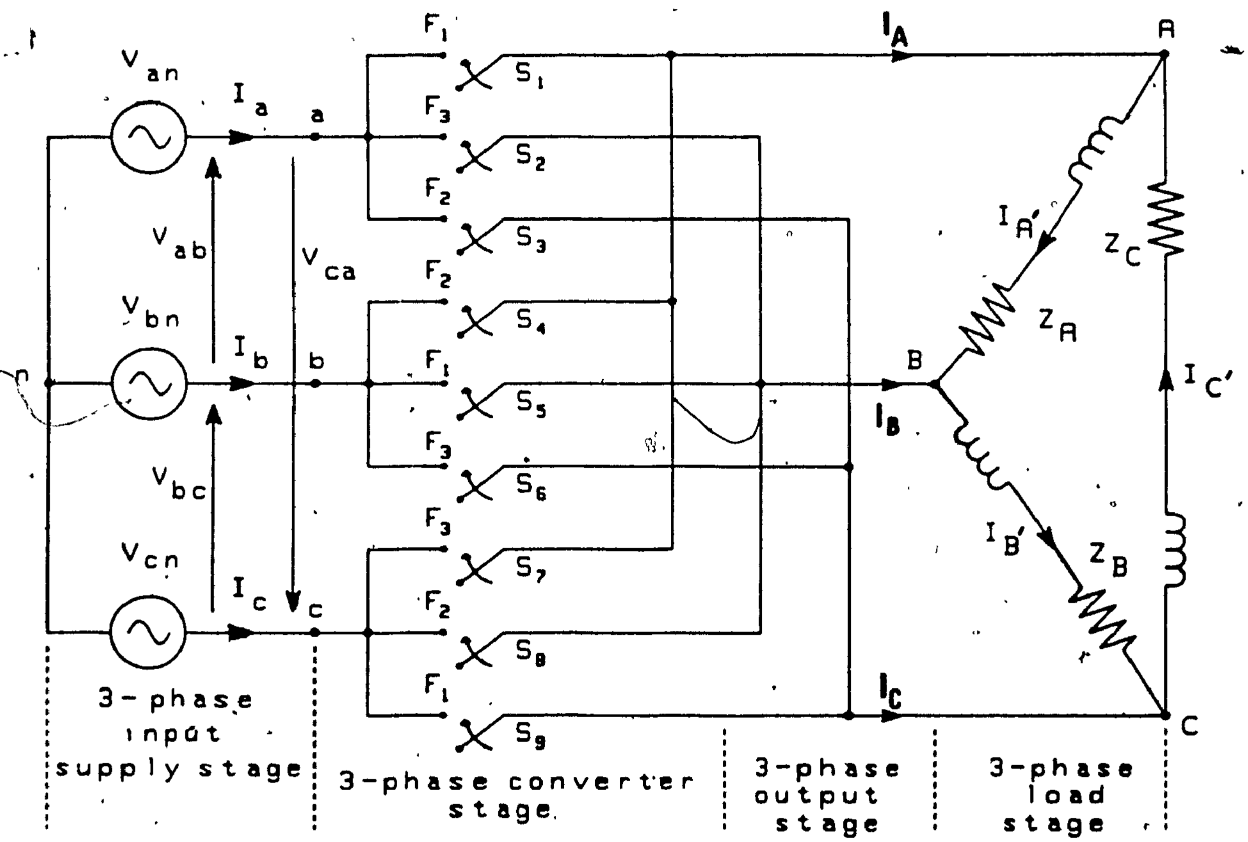

Fig. 1.4: Simplified circuit diagram of the proposed Forced Commutated Cycloconverter structure with improved performance characteristics.

1.3 Review of Previous Work

The first static frequency transformer characterized by variable frequency ratio and bidirectional power flow was proposed [20] by Hazeltine. He established the fundamental principle of constructing output voltage of required frequency from the segments of multiphase input voltages. He then proposed the use of various arrangements of electric valves to switch the load sequentially, thus obtaining the output voltage of required frequency. The frequency changer proposed by Hazeltine was capable of bidirectional power flow and had the flexibility of changing the input-output frequency ratio employing simple control techniques. However, the frequency changer could not be implemented successfully due to lack of suitable electric valves at that time.

A different frequency changer was developed independently by Schenkel [21] and Von Issendorf [22] in early nineteen thirties. These frequency changers used the principle of phase controlled mercury arc converters and were capable of bidirectional power flow. However, the major drawback of the scheme was the attainable output frequency which was less than the input frequency. Nevertheless, the system had two important features that ensured its usefulness in practical application: first, it employed mercury arc valves, which were available with adequate ratings; second, voltage control could be achieved by controlling the ignition angle of the valves. This frequency converter [15], [23] was originally designed to convert the standard three-phase, 50Hz, ac power to single-phase ac power at 15, 16 2/3 or 25Hz, which was used for traction purpose in Europe.

A thorough review on the subject of mercury arc frequency converter was given by Rissik [24]-[25] who introduced the term 'cycloconversion' to designate the process by which an alternating voltage wave of lower frequency is constructed from successive voltage waves of a higher frequency multiphase supply. He also designated the static frequency converters using the above principle as cycloconverter.

In spite of enormous potential of frequency converter, no major contribution has been reported until early nineteen sixties when the new power semiconductor device (SCR) was available in the market.

The first unified treatment of frequency changers as a family of static converters was published by Pelly and Gyugyi in two separate books [1], [17]. Out of different frequency changer structures treated there, the most promising one is Unrestricted Frequency Changer (UFC). In addition to allowing bilateral power flow, this UFC's offer an unlimited output frequency range, good input voltage utilization, do not generate subharmonics and require only nine bidirectional switches (for 3-phase to 3-phase conversion) and relatively low switching frequencies. The main disadvantage of this UFC structure [1] is that they generate large unwanted input current and output voltage harmonics. The order of these harmonics is generally low which makes it difficult to filter them out. This is particularly true with low voltage conditions where the amplitude of the unwanted harmonics can even exceed the amplitude of the wanted fundamental voltage/ current components. Consequently, the advantage gained (over dc link frequency changer) by eliminating the dc link filter is in most cases offset by the presence of large ac filters.

A method of direct frequency conversion using 18(or 12) transistor-diode pairs for three (single) phase controlled current output operation was proposed by Daniels et. al. [26]-[27]. This converter allows bidirectional power flow and is of unrestricted frequency type. The control technique uses continuous monitoring and controlling of load current using slit-width modulation.

Rodriguez proposed and presented a simulation [28] of control technique for direct frequency conversion using bidirectional switches. The converter works with a fixed switching frequency and the modulation is performed by using a high frequency dither (carrier) signal superimposed to a low-frequency control (modulating) voltage. The proposed control strategy is based on the concept of fictitious bipolar source. Neither the quality (spectra) of voltage and current, nor any experimental verification is presented.

The proposed control technique of Daniels and Rodriguez creates no low order harmonics in input current. But their control system has the inherent problems of:

i) High switching frequency.

ii) Low voltage utilization as switching is controlled by monitoring the output current at all time.

iii) As the modulation technique involves some sort of frequency modulation it is difficult to design associated output/input filter.

iv) Loss of control if one or more phases open as current monitoring is used.

Finally a 'generalised transformer' electronic circuit capable of frequency, voltage and power factor change has been proposed and demonstrated by Venturini [29]. This direct frequency converter is characterised by sinusoidal waveforms both at input and output ports, bidirectionality, independent control over input and output frequency, amplitude and phase displacement. This 3-phase frequency transformer constitutes of 9 bidirectional switches. A prototype was successfully implemented as new semiconductor switches became available in the market. Although the output voltage and input current are free of low order harmonics, the voltage utilization of this converter is low. Maximum attainable output voltage is 50% of respective input voltage. However, it has been recently reported [30] that deliberate addition of extra components in the switching function increases the voltage gain from 0.5 to 0.866. However, this is achieved at the expense of even higher switching frequencies and control circuit complexity.

1.4 Scope of the Thesis

The main disadvantages of the previously reviewed FCC structures could be summarised as follows:

i) Unrestricted frequency changers (UFCs) contain low order harmonics of considerable amplitude.

ii) Gain of Venturini's generalised frequency/voltage transformer is very low.

On a parallel development, the power semiconductor industry has been making available faster, cheaper, and more efficient switching devices in modular integrated form. To exploit these features towards producing cheaper and more compact variable speed motor drive units, the static converter industry is showing considerable interest in converter structures that rely mainly on semiconductor components and require only few and small passive components. However, because of the aforementioned disadvantages existing FCC structures cannot be used to achieve these objectives.

The scope and objective of this thesis is to provide solutions to the aforementioned problems of high harmonic contents and low voltage utilization of FCCs for variable speed ac motor drives.

Further thesis contributions include the proposal of novel three phase to three phase, three phase to single phase high frequency FCCs for applications that require compact and light weight power supplies. Finally, this thesis presents also a novel single to three phase FCC with potential applications in rural areas where frequently only single phase ac mains is available.

In particular the contents of this thesis have been organised as follows:

A generalized FCC switching model with N-phase inputs and M-phase outputs is developed in Chapter 2. This model is next used to provide analytical generalized expressions for the dependent input/output FCC variables such as output voltages, input currents. The same model is also used to evaluate FCC transfer characteristics such as voltage and current gains.

In Chapter 3, the performance of three phase to three phase FCC for ac drives applications is investigated extensively by using the analysis method developed in Chapter 2 for two different modes of operation. Relevant component ratings, efficiency figures are derived with various switching functions. Circuit protection is also discussed. Finally predicted results are verified by simulation and as well as experimentally on laboratory prototype units.

In Chapter 4, the analysis presented in Chapter 3 is repeated for three phase to single phase FCC for single phase variable voltage variable frequency ac source applications. Both direct and indirect mode of operation is considered for performance evaluation. Some of the predicted analytical results are verified experimentally.

In Chapter 5, a novel single phase to three phase FCC particularly suitable for rural areas is analysed and evaluated in detail. A laboratory prototype is also built and tested to verify the analytically predicted results.

In Chapter 6, the performance of all FCC structures proposed in Chapters 3 and 4 is analysed under high frequency operating conditions, to determine suitable FCCs in high frequency link applications. Some of the proposed structures are built and tested in the laboratory.

Chapter 7 reviews the entire work presented in this thesis and presents relevant conclusions. It also focuses on future research in the areas of circuit analysis and relevant applications of forced commutated cycloconverters (FCCs).

CHAPTER 2

MODELLING AND ANALYSIS OF FORCED COMMUTATED CYCLOCONVERTERS

2.1 Introduction

The objective of this chapter is to develop a switching model suitable for the analysis and evaluation of performance characteristics of Forced Commutated Cycloconverters (FCC). To achieve this objective the cycloconverter (in its ideal form) is modelled as a circuit matrix consisting of [NxM] switching elements (Fig. 2.1). The proposed matrix representation of this generalized converter allows us to understand easily the process of voltage, current, frequency, phase and amplitude transformation. This model is used throughout the thesis to study the performance characteristics of different FCC structures. Elements of this circuit matrix modelling the converter represent the switching elements of an actual converter.

In addition to the modelling of converter, this chapter also analyses respective generalized input-output waveforms and their spectra. Input-output waveforms of such converters are dependent functions of actual switching patterns, according to which the converter switching operation is carried out. Switching patterns are determined by various pulse width modulation techniques and accordingly the switches operate in ON/OFF mode rather than continuous mode for higher power conversion efficiencies. Consequently the resulting input/output current/voltage waveforms are periodic and contain numerous harmonics and therefore can be for analysis convenience represented by respective Fourier series expressions. The fundamental and dominant harmonics of these waveforms are dependent on respective output frequencies and modulation techniques. This spectral information is essential for the design of converters as well as input-output filters.

The matrix model of the converter is analyzed using two different approaches; namely Direct Mode of Operation (DMO) and Indirect Mode of Operation (IMO). Merits and demerits of these modes of operation interms of voltage utilization and harmonic contents are discussed in details.

2.2 Modelling of Cycloconverter

The model of a converter structure capable of performing the voltage, current, frequency, phase and amplitude transformation is shown in Fig. 2.1. This switching model [31] comprises of an "input matrix" of [Nx1] dimension, "converter switching" matrix of [MxN] dimension and an "output matrix" of [Mx1] dimension. Two methods of power control namely direct and indirect cycloconversion can be realized with this converter model. These two methods are based, one on direct and the other indirect approaches of power conversion and allow effective elimination of all subharmonics from the respective output stages.

2.2.1 Direct Mode of Operation (DMO) Cycloconverter

This mode is based on the principle that "the multiplication of a set of Nx1 sinusoidal quantities (e.g. input voltage matrix) by a compatible set of MxN balanced sinusoidal quantities (e.g. converter transfer matrix) yields a third set of Mx1 sinusoidal quantities (e.g. output voltage matrix) that are also balanced and free of subharmonic components". Therefore, the analytical representation of the DMO converter interms of output voltage $[V_o(\omega_o t)]$ and input current $[I_i(\omega_i t)]$, becomes:

$$[V_o(\omega_o t)] = [F_d(\omega_s t)][V_i(\omega_i t)]$$

$$\begin{bmatrix} V_{o,1} \\ \vdots \\ V_{o,\ell} \\ \vdots \\ V_{o,M} \end{bmatrix} = A \begin{bmatrix} f_{1,1} & \cdots & f_{1,p} & \cdots & f_{1,N} \\ \vdots & & & & \\ f_{q,1} & \cdots & f_{q,p} & \cdots & f_{q,N} \\ \vdots & & & & \\ f_{M,1} & \cdots & f_{M,p} & \cdots & F_{M,N} \end{bmatrix} \cdot B \begin{bmatrix} V_{i,1} \\ \vdots \\ V_{i,p} \\ \vdots \\ V_{i,N} \end{bmatrix}$$

$$= A \begin{bmatrix} \cos(\omega_s t) \cdots\cdots \cos(\omega_s t - \frac{(p-1)}{N}360^\circ) \cdots\cdots \cos(\omega_s t - \frac{(N-1)}{N}360^\circ) \\ \vdots \\ \cos(\omega_s t + \frac{(q-1)}{M}360^\circ) \cdots \cos(\omega_s t - \frac{(p-1)}{N}360^\circ + \frac{(q-1)}{M}360^\circ) \cdots \cos(\omega_s t - \frac{(N-1)}{N}360^\circ + \frac{(q-1)}{M}360^\circ) \\ \vdots \\ \cos(\omega_s t + \frac{(M-1)}{M}360^\circ) \cdots \cos(\omega_s t - \frac{(p-1)}{N}360^\circ + \frac{(M-1)}{M}360^\circ) \cdots \cos(\omega_s t - \frac{(N-1)}{N}360^\circ + \frac{(M-1)}{M}360^\circ) \end{bmatrix}$$

$$\cdot B \begin{bmatrix} \cos(\omega_i t) \\ \vdots \\ \cos(\omega_i t - \frac{(p-1)}{N} 360^\circ) \\ \vdots \\ \cos(\omega_i t - \frac{(N-1)}{N} 360^\circ) \end{bmatrix}$$

$$= \frac{NAB}{2} \begin{bmatrix} \cos(\omega_o t) \\ \vdots \\ \cos(\omega_o t - \frac{(q-1)}{M} 360^\circ) \\ \vdots \\ \cos(\omega_o t - \frac{(M-1)}{M} 360^\circ) \end{bmatrix} \tag{2.1a}$$

and

$$[I_i(\omega_i t)] = [F_d(\omega_s t)]^T [I_o(\omega_o t)]$$

$$\begin{bmatrix} I_{i,1} \\ \vdots \\ I_{i,p} \\ \vdots \\ I_{i,N} \end{bmatrix} = A \begin{bmatrix} f_{1,1} \cdots & f_{q,1} \cdots & f_{M,1} \\ \vdots & & \\ f_{1,p} \cdots & f_{q,p} \cdots & f_{M,p} \\ \vdots & & \\ f_{1,N} \cdots & f_{q,N} \cdots & f_{M,N} \end{bmatrix} \cdot B \begin{bmatrix} I_{o,1} \\ \vdots \\ I_{o,q} \\ \vdots \\ I_{o,M} \end{bmatrix}$$

$$= A \begin{bmatrix} \cos(\omega_s t) \cdots\cdots & \cos(\omega_s t + \frac{(q-1)}{M} 360^\circ) \cdots\cdots & \cos(\omega_s t + \frac{(M-1)}{M} 360^\circ) \\ \vdots & & \\ \cos(\omega_s t - \frac{(p-1)}{N} 360^\circ) \cdots & \cos(\omega_s t - \frac{(p-1)}{N} 360^\circ + \frac{(q-1)}{M} 360^\circ) \cdots & \cos(\omega_s t - \frac{(p-1)}{N} 360^\circ + \frac{(M-1)}{M} 360^\circ) \\ \vdots & & \\ \cos(\omega_s t - \frac{(N-1)}{N} 360^\circ) \cdots & \cos(\omega_s t - \frac{(N-1)}{N} 360^\circ + \frac{(q-1)}{M} 360^\circ) \cdots & \cos(\omega_s t - \frac{(N-1)}{N} 360^\circ + \frac{(M-1)}{M} 360^\circ) \end{bmatrix}$$

$$\cdot B \begin{bmatrix} \cos(\omega_o t) \\ \vdots \\ \cos(\omega_o t - \frac{(q-1)}{M} 360^\circ) \\ \vdots \\ \cos(\omega_o t - \frac{(M-1)}{M} 360^\circ) \end{bmatrix}$$

$$= \frac{MAB}{2} \begin{bmatrix} \cos(\omega_i t) \\ \vdots \\ \cos(\omega_i t - \frac{(p-1)}{N} 360^\circ) \\ \vdots \\ \cos(\omega_i t - \frac{(N-1)}{N} 360^\circ) \end{bmatrix} \qquad (2.1b)$$

and

$$f_{q,p}(t) = A \cos(\omega_s t - \frac{(p-1)}{N} 360^\circ + \frac{(q-1)}{M} 360^\circ) \qquad (2.2)$$

A cycloconverter structure capable of performing voltage, current, frequency, phase and amplitude transformations given in ((2.1a), (2.1b)) is illustrated in Fig. 2.1. This figure intentionaly depicts the converter circuits as an MxN matrix [32] of active elements (i.e. active element matrix) so that there is a one to one correspondance between respective entries of the "converter transfer" and the "active element" matrices. This correspondence is analyticaly stated in (2.2), where the $f_{q,p}(t)$ entry of the transfer matrix $[F_d(\omega_s t)]$, describes the transfer characteristics of the $S_{q,p}$ active element of the converter element matrix.

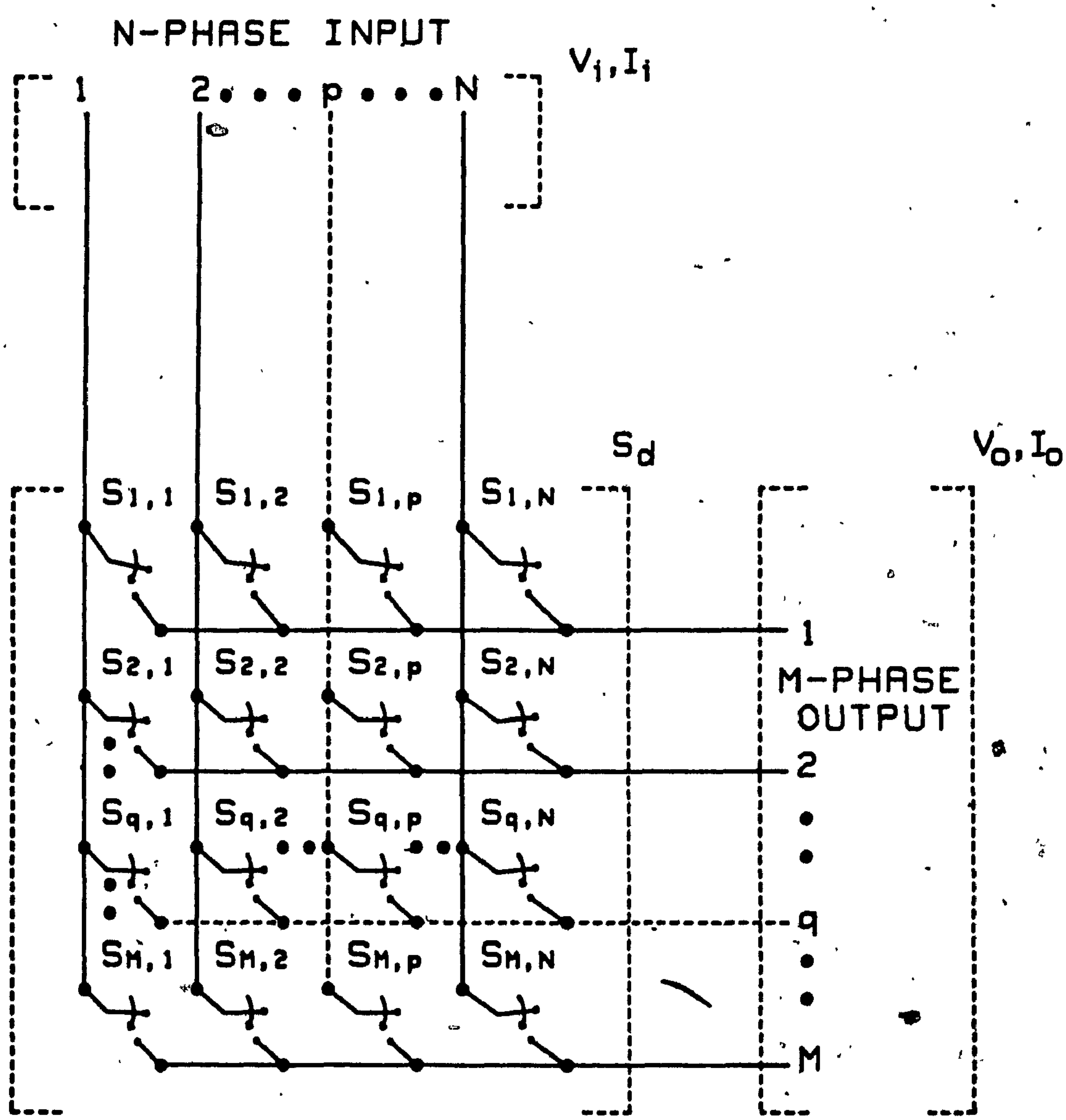

Fig. 2.1: Generalized Forced Commutated Cycloconverter (FCC) topology for N input and M output phases.

Furthermore, the matching of the "converter transfer" and "active element" matrices yields two important results. First, it allows straight-forward derivation of the "transfer matrix" from the "element matrix" and second it allows the straight-forward synthesis of the "active element" matrix (i.e. converter circuit) from the respective "transfer matrix". These features have the advantage of finding a transfer matrix when the circuit topology (i.e. active element matrix) is known. On the other hand a suitable circuit topology can be determined for any specified "transfer matrix".

2.2.2 Indirect Mode of Operation (IMO) Cycloconverter

This mode of operation is based on the following principles,

i) "The multiplication of a set of 1xN balanced sinusoidal quantities (i.e. fictitious rectifier transfer matrix), $[F_r(\omega_i t)]$ by a compatible set of Nx1 sinusoidal quantities (e.g. input voltage matrix), $[V_i(\omega_i t)]$ yields a dc quantity free of any harmonics".

ii) "Further multiplication of the aforementioned dc quantity (e.g. fictitious rectifier output voltage) by a set of Mx1 balanced sinusoidal quantities (i.e. fictitious inverter transfer matrix), $[F_i(\omega_o t)]$ yields a second set of Mx1 balanced and harmonic free sinusoidal quantities (e.g. output voltage matrix), $[V_o(\omega_o t)]$".

Therefore, the analytical expression for the IMO type of converter interms of the converter output voltages $[V_o(\omega_o t)]$ and input currents $[I_i(\omega_i t)]$ can be expressed as follows:

$$[v_o(\omega_o t)] = [F_i(\omega_o t)][F_r(\omega_i t)][V_i(\omega_i t)]$$

$$\begin{bmatrix} V_{o,1} \\ \vdots \\ V_{o,q} \\ \vdots \\ V_{o,M} \end{bmatrix} = A \begin{bmatrix} \cos(\omega_o t) \\ \vdots \\ \cos(\omega_o t - \frac{(q-1)}{M} 360^\circ) \\ \vdots \\ \cos(\omega_o t - \frac{(M-1)}{M} 360^\circ) \end{bmatrix}$$

$$\cdot B[\cos(\omega_i t) \ldots \cos(\omega_i t - \frac{(p-1)}{N} 360^\circ) \ldots \cos(\omega_i t - \frac{(N-1)}{N} 360^\circ)]$$

$$\cdot C \begin{bmatrix} \cos(\omega_i t) \\ \vdots \\ \cos(\omega_i t - \frac{(p-1)}{N} 360^\circ) \\ \vdots \\ \cos(\omega_i t - \frac{(N-1)}{N} 360^\circ) \end{bmatrix}$$

$$= A \begin{bmatrix} \cos(\omega_o t) \\ \vdots \\ \cos(\omega_o t - \frac{(q-1)}{M} 360^\circ) \\ \vdots \\ \cos(\omega_o t - \frac{(M-1)}{M} 360^\circ) \end{bmatrix} \cdot \frac{NBC}{2}$$

$$= \frac{NABC}{2} \begin{bmatrix} \cos(\omega_o t) \\ \vdots \\ \cos(\omega_o t - \frac{(q-1)}{M} 360^\circ) \\ \vdots \\ \cos(\omega_o t - \frac{(M-1)}{M} 360^\circ) \end{bmatrix} \quad (2.3a)$$

and

$$[I_i(\omega_i t)] = [F_r(\omega_i t)]^T [F_i(\omega_o t)]^T [I_o(\omega_o t)]$$

$$\begin{bmatrix} I_{i,1} \\ \vdots \\ I_{i,p} \\ \vdots \\ I_{i,N} \end{bmatrix} = B \begin{bmatrix} \cos(\omega_i t) \\ \vdots \\ \cos(\omega_i t - \frac{(p-1)}{N} 360^\circ) \\ \vdots \\ \cos(\omega_i t - \frac{(N-1)}{N} 360^\circ) \end{bmatrix}$$

$$\cdot A[\cos(\omega_o t) \ldots \cos(\omega_o t - \frac{(q-1)}{M} 360^\circ) \ldots \cos(\omega_o t - \frac{(M-1)}{M} 360^\circ)]$$

$$\cdot C \begin{bmatrix} \cos(\omega_o t) \\ \vdots \\ \cos(\omega_o t - \frac{(q-1)}{M} 360^\circ) \\ \vdots \\ \cos(\omega_o t - \frac{(M-1)}{M} 360^\circ) \end{bmatrix}$$

$$= \frac{MABC}{2} \begin{bmatrix} \cos(\omega_i t) \\ \vdots \\ \cos(\omega_i t - \frac{(p-1)}{N} 360^\circ) \\ \vdots \\ \cos(\omega_i t - \frac{(N-1)}{N} 360^\circ) \end{bmatrix} \qquad (2.3b)$$

Furthermore, the transformations shown in (2.3a) and (2.3b) can also be realized with the converter structure shown in Fig. 2.1.

2.3 Practical Cycloconverter Structure

Generalized N-input, M-output voltage/frequency/phase static transformer topology (Fig. 2.1) discussed in the previous section can be readily used to realise practical FCC circuits for a specified number of input/output phases (N,M). A simplified FCC circuit topology that results from the generalized model shown in Fig. 2.1, N=M=3 is illustrated in Fig. 2.2. This converter structure is capable of voltage/frequency transformation from fixed frequency/voltage 3-phase input to variable frequency 3-phase voltage output.

This FCC topology (Fig. 2.2) comprises of 9(=3x3) "active elements" since the "transfer matrix" is of dimension [3x3] (i.e. N=3, M=3). The active elements are the physical static converter switches. As the converter should be capable of power flow in both direction, the switches are

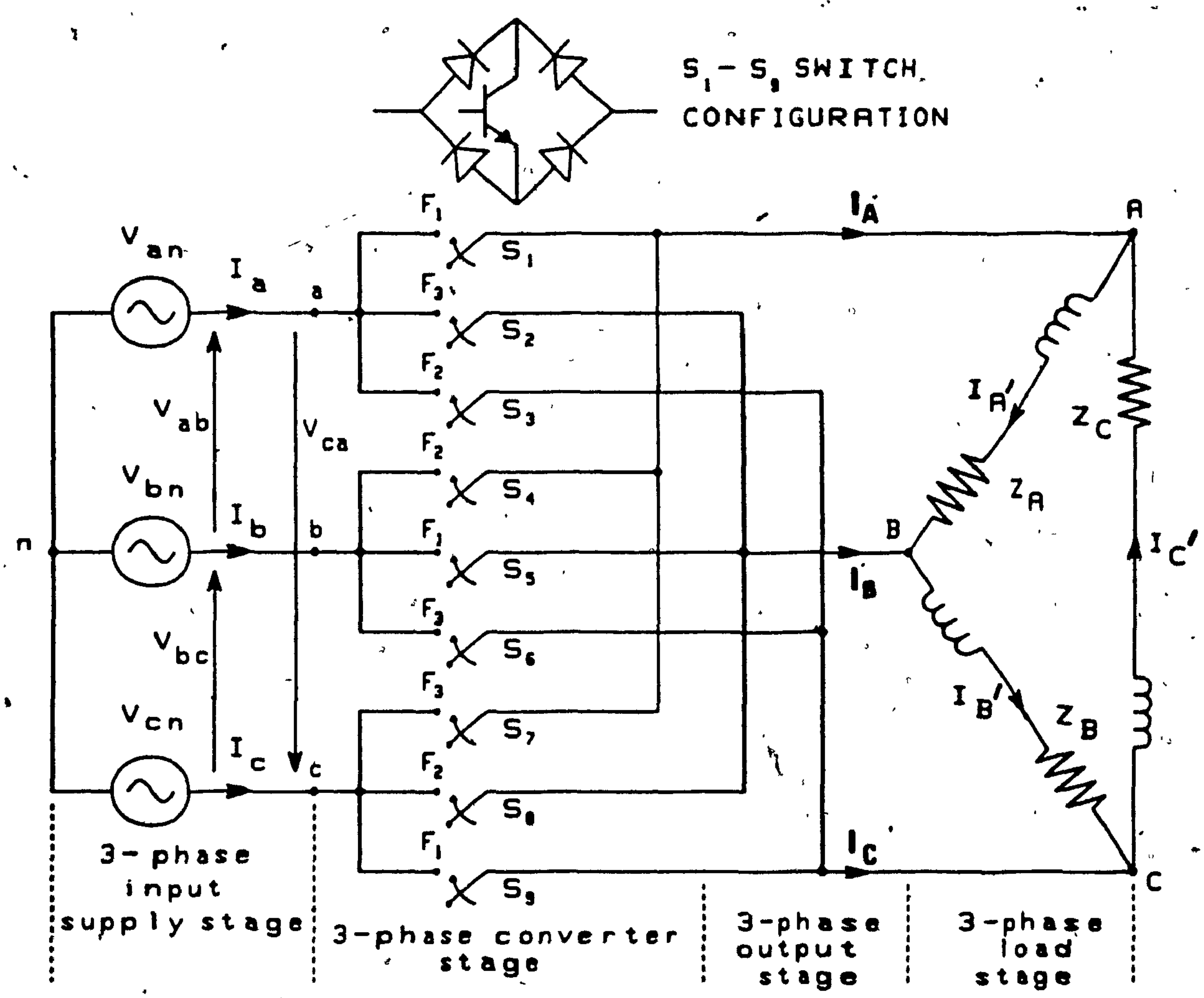

Fig. 2.2: Simplifier circuit diagram of a three-phase to three-phase cycloconverter.

bidirectional. The physical composition of each of the 9 bilateral switches, S_1 to S_9 are shown ~~on~~ top of Fig. 2.2. Other realizations are also possible. Moreover, a bilateral four quadrant switch has been lately produced in integrated form for low power applications. These switches are gated according to some predetermined gating scheme directly related to particular PWM scheme used.

2.4 [3 x 3] Cycloconverter Operation

The operation of the cycloconverter shown in Fig. 2.2 is explained next, after the converter transfer matrix is first chosen. Both modes of operation, i.e. DMO and IMO are explained separately as follows:

2.4.1 Direct Mode of Operation (DMO)

For a 3-phase to 3-phase cycloconverter operating under DMO principle, the converter "transfer matrix" (2.1a), can be rewritten as:

$$[F_d(\omega_s t)] = A \begin{bmatrix} f_{1,1} & f_{1,2} & f_{1,3} \\ f_{2,1} & f_{2,2} & f_{2,3} \\ f_{3,1} & f_{3,2} & f_{3,3} \end{bmatrix} \qquad (2.4a)$$

The converter transfer matrix elements $f_{1,1}$, $f_{1,2}$, etc. can be expressed as F_1, F_2 and F_3, where,

$$F_1 = f_{1,1}$$

$$F_2 = f_{1,2} = F_1 \angle{-120^\circ}$$

and $$F_3 = f_{1,3} = F_1 \angle{-240^\circ} \qquad (2.4b)$$

Equation (2.1a) can be simplified as;

$$[V_o(\omega_o t)] = 1 \begin{bmatrix} F_1 & F_2 & F_3 \\ F_3 & F_1 & F_2 \\ F_2 & F_3 & F_1 \end{bmatrix} .1 \begin{bmatrix} V_{ab} \\ V_{bc} \\ V_{ca} \end{bmatrix}$$

$$\begin{bmatrix} V_{AB} \\ V_{BC} \\ V_{CA} \end{bmatrix} = \begin{bmatrix} F_1 V_{ab} + F_2 V_{bc} + F_3 V_{ca} \\ F_3 V_{ab} + F_1 V_{bc} + F_2 V_{ca} \\ F_2 V_{ab} + F_3 V_{bc} + F_1 V_{ca} \end{bmatrix} \qquad (2.4c)$$

or,

$$V_{AB} = V_{ab}F_1 + V_{bc}F_2 + V_{ca}F_3$$

$$V_{BC} = V_{ab}F_3 + V_{bc}F_1 + V_{ca}F_2 \qquad (2.4d)$$

$$V_{CA} = V_{ab}F_2 + V_{bc}F_3 + V_{ca}F_1$$

The realization of (2.4d) on a cycloconverter structure (Fig. 2.2) for a particular modulation scheme (uniform PWM scheme, Fig. 2.3), can be explained as follows;

Considering switch matrix element F_1, bilateral switches S_1, S_5 and S_9 are turned ON whenever F_1 has the values of one (Fig. 2.3b), thus connecting the three cycloconverter input terminals a, b, c to the three respective output terminals A, B, C (Fig. 2.2). Whenever F_1 has the value of zero, two of the three switches are turned OFF (in this case S5 and S9), while at the same time the remaining two of the three switches connected to the input terminal a, S_2 and S_3, are turned ON. With switches S_1, S_2 and S_3 simultaneously ON, all three output voltages becomes zero, thus disconnecting the output from the input terminals. This mode of ON-OFF operation lasts for 120^0 interval of the period of the output voltage. For the next 120^0 interval cycloconverter operation is determined by switching matrix element F_2 (instead of F_1). Consequently, the function performed by switches S_1, S_5, S_9 is now performed by S_3, S_4, S_8 and the function performed by switches S_1, S_2, S_3 is now performed by S_4, S_5, S_6. A similar switch by switch substitution occurs during the third (and final) 120^0 interval of the period of the output voltage. The resulting gating signals for the nine cycloconverter switches are shown in Fig. 2.3f. However, the switching matrix elements and the gating signals are identical when the modulation factor, $M_f = 1$.

In the same manner, the operation of DMO cycloconverter can be explained for any other type of switch matrix i.e. PWM scheme.

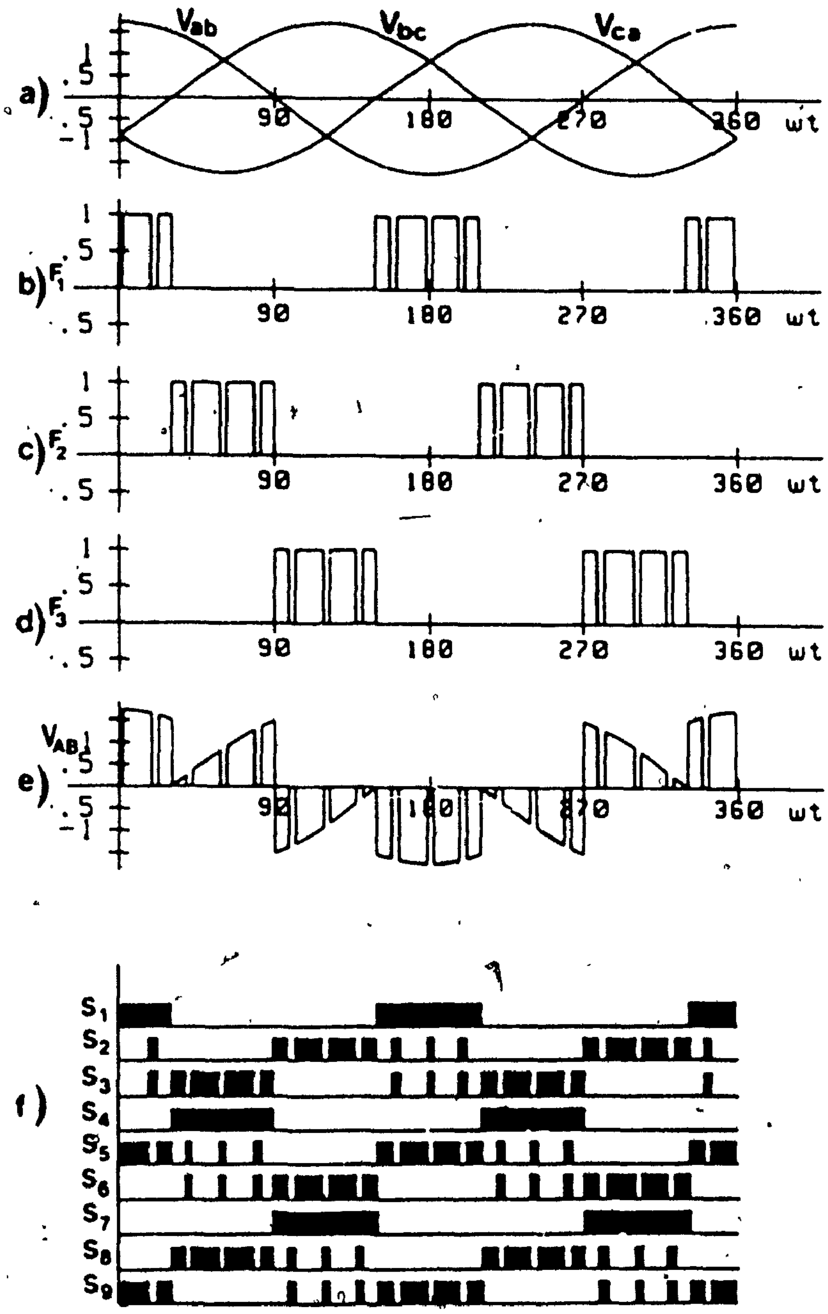

Fig. 2.3: Waveforms obtained with DMO uniform PWM scheme at modulation index, $M_f = 0.8$. (a) Three input line voltages. (b)-(d) F_1, F_2, F_3 switch matrix elements. (e) Output line voltage, V_{AB}. (f) Gating strategy for S_1-S_9 switches.

2.4.2 Indirect Mode of Operation (IMO)

Indirect Mode of Operation, as described in sub-section 2.2.2, is a two step process. No straight forward method (like DMO) of describing the combined rectifier and inverter transfer matrices has yet been reported. The 3-phase to 3-phase converter transfer matrix can be derived from the general equation, (2.3a) as follows;

$$[V_o(\omega_o t)] = [F_i(\omega_o t)][F_r(\omega_i t)][V_i(\omega_i t)]$$

$$\begin{bmatrix} V_{AB} \\ V_{BC} \\ V_{CA} \end{bmatrix} = 1 \begin{bmatrix} \cos(\omega_o t) \\ \cos(\omega_o t - 120^\circ) \\ \cos(\omega_o t - 240^\circ) \end{bmatrix}$$

$$\cdot 1[\cos(\omega_i t) \quad \cos(\omega_i t - 120^\circ) \quad \cos(\omega_i t - 240^\circ)] \cdot 1 \begin{bmatrix} \cos(\omega_i t) \\ \cos(\omega_i t - 120^\circ) \\ \cos(\omega_i t - 240^\circ) \end{bmatrix}$$

$$= \begin{bmatrix} \cos(\omega_o t) \\ \mathrm{Cos}(\omega_o t - 120^\circ) \\ \cos(\omega_o t - 240^\circ) \end{bmatrix} \cdot \frac{3}{2}$$

$$= \frac{3}{2} \begin{bmatrix} \cos(\omega_o t) \\ \cos(\omega_o t - 120^\circ) \\ \cos(\omega_o t - 240^\circ) \end{bmatrix} \quad (2.5)$$

Equation (2.5) shows that IMO converter transfer matrix consists of two terms, rectifier transfer matrix, $F_r(\omega_i t)$, at input frequency, f_i and inverter transfer matrix, $F_i(\omega_o t)$, at output frequency, f_o. Consequently, multiplication of the three input ac voltages with the rectifier transfer matrix can be viewed as a fictitious rectification, while multiplication of the rectified voltage with the inverter transfer matrix can be viewed as inversion. Waveforms representing the rectifier and inverter transfer matrices are illustrated in Fig. 2.4b and d, respectively (for simplicity, only one of the required three waveforms is shown in each case). Fig. 2.4c depicts the fictitious dc voltage and Fig. 2.4e depicts the resulting ac voltage, V_{AB}. Moreover, the gating strategy (for the 9 switches) which yields the required V_{AB} voltage is shown in Fig. 2.4f.

2.5 Harmonic Analysis

Practical power converters operate in ON/OFF mode employing switches rather than in continuous mode. Consequently, the switch matrix elements, i.e. switching functions described in previous section are actually 'trains' of rectangular pulses of uniform or sine modulated widths and as such, they possess frequency spectra comprised of infinite

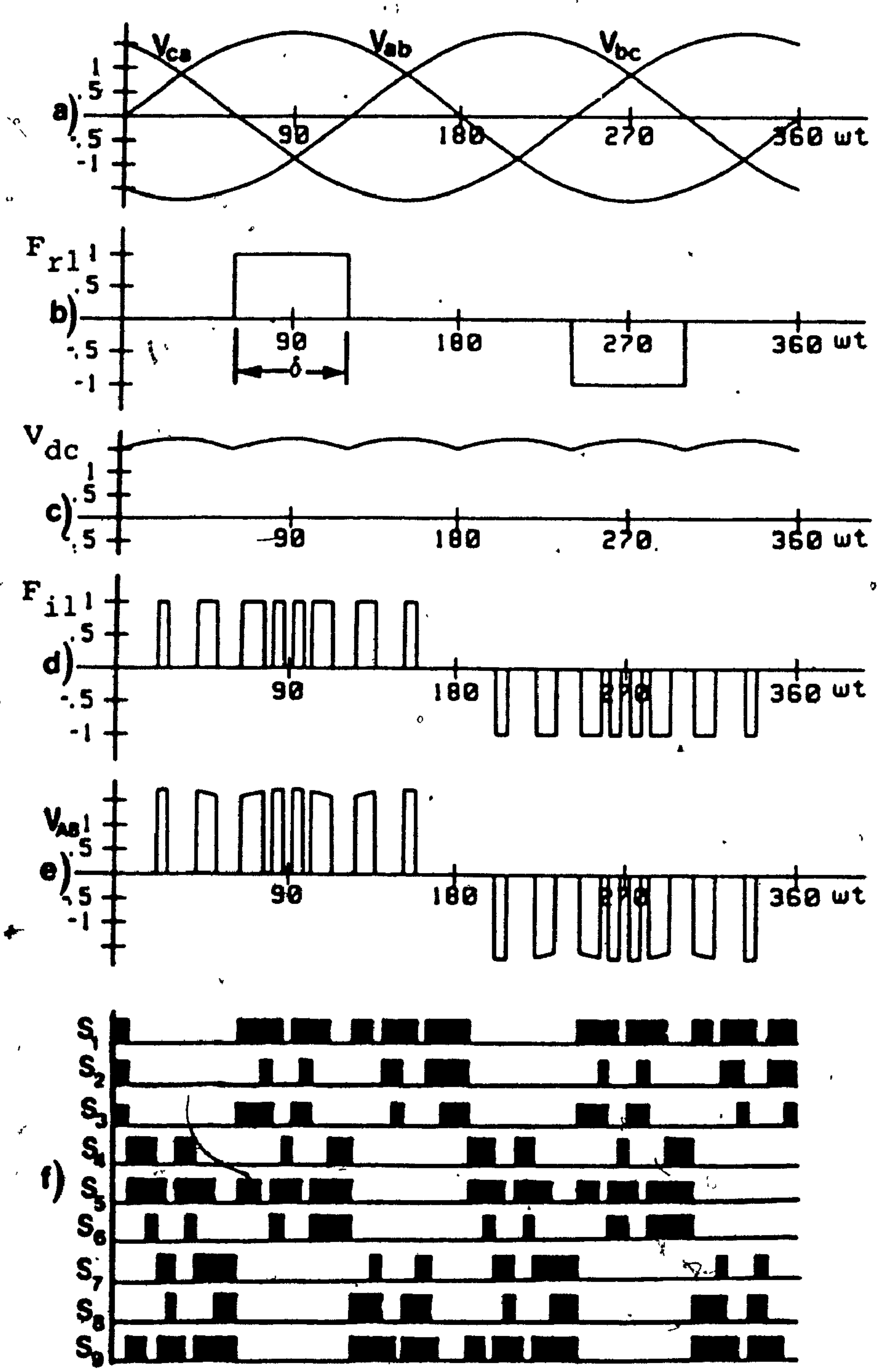

Fig. 2.4: Waveforms obtained with IMO mixed modulation scheme. (a) Three input line voltages. (b) Fictitious rectifier switching matrix element, F_{r1} (one of the three). (c) Fictitious dc voltage, V_{dc}. (d) Fictitious inverter switching matrix element, F_{i1} (one of the three). (e) Output line voltage, V_{AB}. (f) Gating strategy for S_1- S_9 switches.

series of harmonic components. Harmonics associated with switching functions, output voltages and input currents for direct and indirect cycloconversion methods are discussed in details in the following sub-sections.

For simplicity, the analysis is performed for 3-phase to 3-phase cycloconverter. This analytical approach is equally valid for 3-phase to 1-phase and 1-phase to 3-phase cycloconverters, which are described in Chapter 4 and 5 respectively.

2.5.1 Direct Mode of Operation Switching Function, $[S_d(\omega_s t)]$

It is obvious from the introduction presented, that the practical counterpart of switch matrix element, i.e. switching function has infinitely more harmonic components than originally considered transfer matrix elements. Therefore, the equation (2.2) can be rewritten as,

$$S_{q,p}(t) = A_o + A_1 \mathrm{Cos}(\omega_s t - \frac{(p-1)}{N} 360^\circ + \frac{(q-1)}{M} 360^\circ)$$

$$+ \sum_{n=2,3,4}^{\infty} A_n \cos(n(\omega_s t - \frac{(p-1)}{N} 360^\circ + \frac{(q-1)}{M} 360^\circ)) \qquad (2.6)$$

2.5.1.1 DMO Output Voltage Spectrum

The practical switching matrix can be described interms of converter transfer matrix elements as;

$$[S_d(\omega_s t)] = \begin{bmatrix} F_1 & F_2 & F_3 \\ F_3 & F_1 & F_2 \\ F_2 & F_3 & F_1 \end{bmatrix}$$

$$= \begin{bmatrix} A_o + \sum_{n=1,2}^{\infty} A_n \cos(n(\omega_s t)) & A_o + \sum_{n=1,2}^{\infty} A_n \cos(n(\omega_s t-120^o)) & A_o + \sum_{n=1,2}^{\infty} A_n \cos(n(\omega_s t-240^o)) \\ A_o + \sum_{n=1,2}^{\infty} A_n \cos(n(\omega_s t-240^o)) & A_o + \sum_{n=1,2}^{\infty} A_n \cos(n(\omega_s t)) & A_o + \sum_{n=1,2}^{\infty} A_n \cos(n(\omega_s t-120^o)) \\ A_o + \sum_{n=1,2}^{\infty} A_n \cos(n(\omega_s t-120^o)) & A_o + \sum_{n=1,2}^{\infty} A_n \cos(n(\omega_s t-240^o)) & A_o + \sum_{n=1,2}^{\infty} A_n \cos(n(\omega_s t)) \end{bmatrix}$$

(2.7)

and the analytical expression for output voltages (Fig. 2.3), $[V_o(\omega_o t)]$, for a 3-phase to 3-phase DMO cycloconverter becomes

$$[V_o(\omega_o t)] = \begin{bmatrix} F_1 & F_2 & F_3 \\ F_3 & F_1 & F_2 \\ F_2 & F_3 & F_1 \end{bmatrix} \cdot \begin{bmatrix} V_{an} \\ V_{bn} \\ V_{cn} \end{bmatrix}$$

or,

$$\begin{bmatrix} V_{AN} \\ V_{BN} \\ V_{CN} \end{bmatrix} = \frac{3A_1 V_i}{2} \begin{bmatrix} \cos(\omega_o t) \\ \cos(\omega_o t-240^o) \\ \cos(\omega_o t-120^o) \end{bmatrix} + [S_{dH}(\omega_s t] \cdot V_i \begin{bmatrix} \cos(\omega_i t) \\ \cos(\omega_i t-120^o) \\ \cos(\omega_i t-240^o) \end{bmatrix}$$

(2.8)

where

$$[S_{dh}(\omega_s t)] = \begin{bmatrix} \sum_{n=2,3}^{\infty} A_n\cos(n(\omega_s t)) & \sum_{n=2,3}^{\infty} A_n\cos(n(\omega_s t-120^\circ)) & \sum_{n=2,3}^{\infty} A_n\cos(n(\omega_s t-240^\circ)) \\ \sum_{n=2,3}^{\infty} A_n\cos(n(\omega_s t-240^\circ)) & \sum_{n=2,3}^{\infty} A_n\cos(n(\omega_s t)) & \sum_{n=2,3}^{\infty} A_n\cos(n(\omega_s t-120^\circ)) \\ \sum_{n=2,3}^{\infty} A_n\cos(n(\omega_s t-120^\circ)) & \sum_{n=2,3}^{\infty} A_n\cos(n(\omega_s t-240^\circ)) & \sum_{n=2,3}^{\infty} A_n\cos(n(\omega_s t)) \end{bmatrix} \tag{2.9}$$

Comparing equation (2.9) with the general equation (2.1a) of the DMO shows that the difference between practical and ideal DMO cycloconverter output voltages is an infinite series of harmonics represented by the product,

$$[V_{oh}(\omega_o t)] = [V_i(\omega_i t)][S_{dh}(\omega_s t)] \tag{2.10}$$

The Lth component $V_o(L\omega_o t)$ in this series is obtained by setting $n = \ell$ in (2.9) and then evaluating (2.10). After some analytical simplification (given in Appendix A), (2.10) yields,

$$V_o(L\omega_o t) = \frac{3A_\ell V_i}{2} \cos[(\ell\omega_s \pm \omega_i)t]$$

or,

$$V_o(L\omega_o t) = \frac{3A_\ell V_i}{2} \cos[\ell\omega_o + (\ell \pm 1)\omega_i t]$$

for $\ell = n = (3I \mp 1)$, $I = 1,2,3....$ integer (2.11a) and $\quad V_o(L\omega_o t) = 0, \text{ for } \ell \neq (3I \mp 1)$ (2.11b)

Also $L\omega_o = \ell\omega_s \pm \omega_i$, for $\ell = (3I\mp1)$, I = 1,2,3.... integer (2.12a)

and since, $\omega_s = \omega_i + \omega_o$,

$$L\omega_o = \ell\omega_o + (\ell\pm1)\omega_i = [\ell + (\ell \pm 1)\frac{\omega_i}{\omega_o}]\omega_o$$

$$\Rightarrow \quad L = \ell + (\ell\pm1)\frac{\omega_i}{\omega_o} \tag{2.12b}$$

Finally, from (2.11a) and (2.8),

$$\frac{|V_o(Lw_o t)|}{|V_{o1}(\omega_o t)|} = \frac{A_\ell}{A_1} \tag{2.13}$$

where $|V_o(L\omega_o t)|$ and $|V_{o1}(\omega_o t)|$ are the amplitudes of the Lth harmonic and fundamental components of the cycloconverter output voltages $[V_o(\omega_o t)]$, respectively.

Equation (2.11) implies that the lowest possible ℓ is $\ell=2$, (2.11a), consequently the lowest possible frequency component $V_o(L\omega_o t)$ in the cycloconverter output voltage is given by,

$$V_o(L\omega_o t) = \frac{3A_2V_i}{2}\cos(2\omega_s + \omega_i)t \tag{2.14a}$$

$$L\omega_o = 2\omega_s + \omega_i = 2\omega_o + 3\omega_i \tag{2.14b}$$

Consequently, it can be concluded that $[S_d(\omega_s t)]$ type of transfer functions do not generate subharmonic (i.e. $L < 1$) frequency components in the output voltage $[V_o(\omega_o t)]$ spectrum. Also, from (2.12) and (2.13) the following can be concluded:

1) If low-order harmonics, such as $\ell = 2,4,5,\ldots,$ etc., are eliminated from the switching function $[S_d(\omega_s t)]$ spectrum (as with the case shown in Fig. 2.5), respective low-order L harmonics will also be eliminated from the output voltage, $[V_o(\omega_o t)]$ spectrum.

2) The normalized values A_ℓ/A_1 of the $[S_d(\omega_s t)]$ harmonic components are identical to the respective values of the $[V_o(\omega_o t)]$ harmonic components. Consequently, $[V_o(\omega_o t)]$ can be improved by improving the $[S_d(\omega_s t)]$ spectrum. These conclusions became possible due to the novel analytical technique developed for analysis of DMO cycloconverter, in section 2.2.1.

2.5.1.2 DMO Input Current Spectrum

The input current (Fig. 2.5) spectrum for the DMO cycloconverter can be calculated in the same manner as the output voltage spectrum computed in sub-section 2.5.1.1. The equation for input current of a practical 3-phase to 3-phase DMO cycloconverter can be expressed as follows;

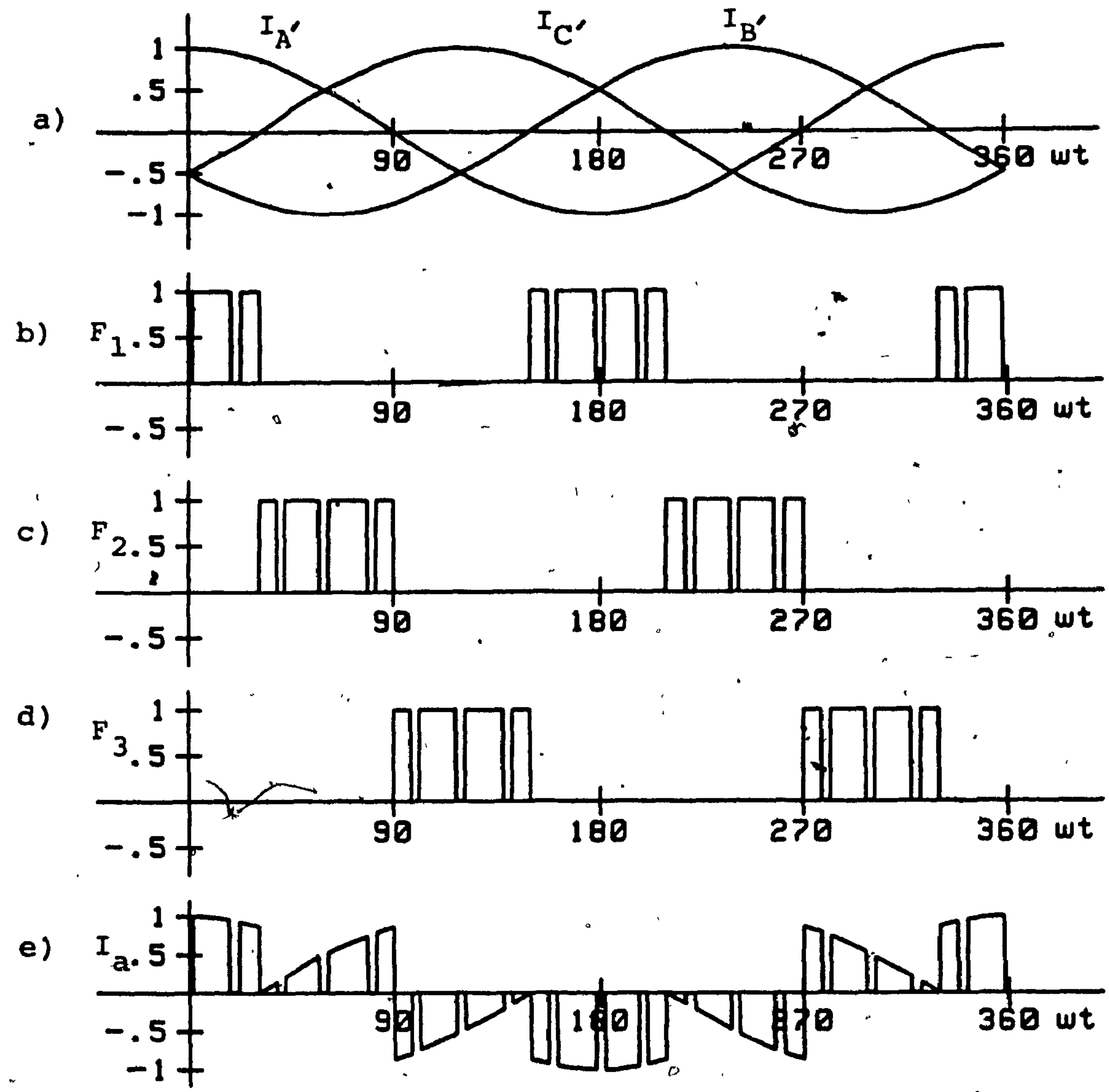

Fig. 2.5: Input current waveform obtained with DMO uniform PWM scheme. (a) Three output phase currents. (b)-(d) F_1, F_2, F_3 switch matrix elements. (e) Resulting input line current, I_a.

$$[I_i(\omega_i t)] = \begin{bmatrix} F_1 & F_3 & F_2 \\ F_2 & F_1 & F_3 \\ F_3 & F_2 & F_1 \end{bmatrix} \cdot \begin{bmatrix} I_A \\ I_B \\ I_C \end{bmatrix}$$

or,

$$\begin{bmatrix} I_a \\ I_b \\ I_c \end{bmatrix} = \frac{3A_1 I_o}{2} \begin{bmatrix} \cos(\omega_i t) \\ \cos(\omega_i t-120^\circ) \\ \cos(\omega_i t-240^\circ) \end{bmatrix} + [S_{dh}(\omega_s t)].I_o \begin{bmatrix} \cos(\omega_o t) \\ \cos(\omega_o t-120^\circ) \\ \cos(\omega_o t-240^\circ) \end{bmatrix}$$

$$= \frac{3A_1 I_o}{2} \begin{bmatrix} \cos(\omega_i t) \\ \cos(\omega_i t-120^\circ) \\ \cos(\omega_i t-240^\circ) \end{bmatrix} + \sum_{n=2,5,8}^{\infty} \frac{3A_n I_o}{2} \begin{bmatrix} \cos(n\omega_s+\omega_o)t \\ \cos((n\omega_s+\omega_o)t-n120^\circ) \\ \cos((n\omega_s+\omega_o)t-n240^\circ) \end{bmatrix}$$

$$+ \sum_{n=4,7,10}^{\infty} \frac{3A_n I_o}{2} \begin{bmatrix} \cos(n\omega_s-\omega_o)t \\ \cos((n\omega_s-\omega_o)t-n120^\circ) \\ \cos((n\omega_s-\omega_o)t-n240^\circ) \end{bmatrix} \qquad (2.15)$$

The harmonic content of the input current is similar to output voltage the main difference being the order of the harmonic components, which are well above the fundamental frequency ω_i. Equation (2.14b) in this case becomes;

$$L\omega_i = 2\omega_s + \omega_o = 2\omega_i + 3\omega_o. \qquad (2.16)$$

2.5.1.3 Gain of DMO Cycloconverter

A comparative evaluation of the fundamental components of the input and output voltages and the respective currents, obtained from (2.8), (2.15) and (2.9), yields that the circuits shown in Figs. 2.1 and 2.2 can also be viewed as a generalized solid state frequency transformer whose turns ratio is given by

$$\frac{N_s}{N_p} = \frac{V_{out}}{V_{in}} = \frac{I_{in}}{I_{out}} = \frac{\frac{3A_1 V_i}{2}}{V_i} = \frac{\frac{3A_1 I_o}{2}}{I_o} = \frac{3A_1}{2}. \tag{2.17a}$$

Furthermore, the values of A_1 can easily be found once the switching patterns for $[F_1 \;\; F_2 \;\; F_3]$ functions have been established. By noting that these three patterns can never overlap (overlapping is equivalent to short circuiting source voltages), and their maximum span being 120° per cycle, the maximum value for A_1 can be expressed as,

$$A_1, \max = \frac{2 \cdot 2}{2\pi} \int_0^{\pi/3} 1.\ \cos \omega t \ d(\omega t) = \frac{\sqrt{3}}{\pi}$$

$$\Rightarrow \frac{N_s}{N_p}, \max = \frac{3\sqrt{3}}{2\pi} = 0.827 \tag{2.17b}$$

Thus the maximum turns ratio between the secondary and the primary of the static frequency changer is 0.827 and the minimum obtainable is 0.5 (for a distributed switching function Fig. 3.4, Chapter 3).

$$A_1, \text{ min} = \frac{1}{3} \Rightarrow \frac{N_s}{N_p}, \text{ min} = \frac{1}{2} = 0.5 \qquad (2.17c)$$

Also for the switching function shown in Fig. 2.4b this value becomes,

$$A_1, \text{ max} = \frac{2}{\pi} \int_0^{\pi} \sin \omega t \; d(\omega t) = \frac{4}{\pi} \cdot \sin \frac{\delta}{2} = \frac{2}{\pi} \text{ when } \delta = \pi/3$$

$$\Rightarrow \frac{N_s}{N_p}, \text{ max} = \frac{3}{2} \cdot \frac{2}{\pi} = 0.955 \qquad (2.17d)$$

2.5.2 Indirect Mode of Operation Switching Function, $[S_i(\omega_o t)][S_r(\omega_i t)]$

The practical cycloconverter switch matrix elements, i.e. switching function for IMO consist of uniform or modulated width pulses (Fig. 2.6). Therefore, the practical 1,p element of, (2.3a) the (fictitious) rectifier switching matrix, $[F_r(w_i t)]$ i.e. $[S_r(\omega_i t)]$ becomes

$$S_{1,p}(t) = B_1 \cos(\omega_i t - \frac{(p-1)}{N} 360^\circ)$$

$$+ \sum_{n=3,5,7}^{\infty} B_n \cos(n(\omega_i t - \frac{(p-1)}{N} 360^\circ)) \qquad (2.18a)$$

and the q,1 element of the respective inverter switching matrix, $[F_i(\omega_o t)]$, (2.3a), i.e. $[S_i(\omega_o t)]$ becomes,

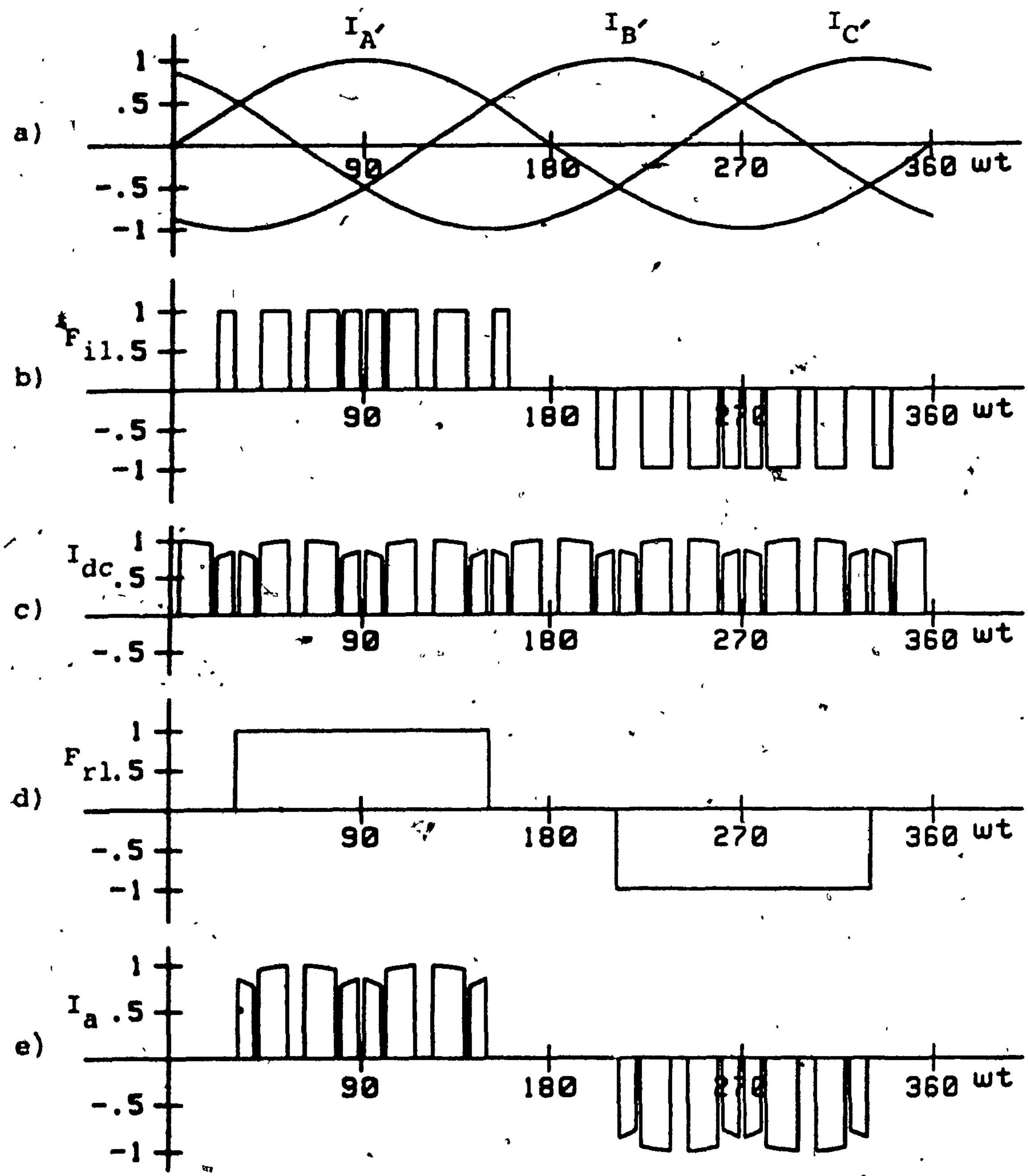

Fig. 2.6: Input current waveform obtained with IMO mixed modulation scheme. (a) Three output phase currents. (b) Fictitious inverter switching matrix element, F_{i1} (one of the three). (c) Fictitious dc current, I_{dc}. (d) Fictitious rectifier switching matrix element, F_{r1} (one of the three). (e) Resulting input line current, I_a.

$$S_{q,1}(t) = A_1 \cos(\omega_o t - \frac{(q-1)}{M} 360^\circ)$$

$$+ \sum_{m=3,5,7}^{\infty} A_m \cos(m(\omega_o t - \frac{(q-1)}{M} 360^\circ)) \qquad (2.18b)$$

2.5.2.1 IMO Output Voltage Spectrum

The analytical equation for output voltage (Fig. 2.4) of practical IMO cycloconverter for a 3-phase to 3-phase conversion can be re-written from (2.3a) as follows;

$$[V_o(\omega_o t)] = [S_i(\omega_o t)][S_r(\omega_i t)][V_i(\omega_i t)]$$

$$= \begin{bmatrix} \sum_{n=1,2}^{\infty} A_n \cos(n\omega_o t) \\ \sum_{n=1,2}^{\infty} A_n \cos(n(\omega_o t-120^\circ)) \\ \sum_{n=1,2}^{\infty} A_n \cos(n(\omega_o t-240^\circ)) \end{bmatrix}$$

$$\cdot \begin{bmatrix} \sum_{m=1,2}^{\infty} B_m \cos(m\omega_i t) & \sum_{m=1,2}^{\infty} B_m \cos(m(\omega_i t-120^\circ)) & \sum_{m=1,2}^{\infty} B_m \cos(m(\omega_i t-240^\circ)) \end{bmatrix}$$

$$\cdot V_i \begin{bmatrix} \cos(\omega_i t) \\ \cos(\omega_i t-120^\circ) \\ \text{cps}(\omega_i t-240^\circ) \end{bmatrix}$$

$$= \frac{3A_1B_1V_i}{2}\begin{bmatrix}\cos(\omega_o t)\\ \cos(\omega_o t-120^\circ)\\ \cos(\omega_o t-240^\circ)\end{bmatrix} + \frac{3B_1V_i}{2}\begin{bmatrix}\sum\limits_{n=5,7}^{\infty} A_n\cos(n\omega_o t)\\ \sum\limits_{n=5,7}^{\infty} A_n\cos(n(\omega_o t-120^\circ))\\ \sum\limits_{n=5,7}^{\infty} A_n\cos(n(\omega_o t-240^\circ))\end{bmatrix}$$

$$+ [S_{ih}(\omega_o t)][S_{rh}(\omega_i t)] \cdot V_i \begin{bmatrix}\cos(\omega_i t)\\ \cos(\omega_i t-120^\circ)\\ \cos(\omega_i t-240^\circ)\end{bmatrix} \tag{2.19}$$

where

$$[S_{ih}(\omega_o t)][S_{rh}(\omega_i t)] = \begin{bmatrix}A_1\cos(\omega_o t) + \sum\limits_{n=5,7}^{\infty} A_n\cos(n\omega_o t)\\ A_1\cos(\omega_o t-120^\circ) + \sum\limits_{n=5,7}^{\infty} A_n\cos(n(\omega_o t-120^\circ))\\ A_1\cos(\omega_o t-120^\circ) + \sum\limits_{n=5,7}^{\infty} A_n\cos(n(\omega_o t-240^\circ))\end{bmatrix}$$

$$\cdot \left[\sum_{m=3,4}^{\infty} B_m\cos(m\omega_i t) \quad \sum_{m=3,4}^{\infty} B_m\cos(m(\omega_i t-120^\circ)) \quad \sum_{m=3,4}^{\infty} B_m\cos(m(\omega_i t-240^\circ))\right] \tag{2.20}$$

Comparing (2.19) and (2.3a) yields that the difference between practical and ideal IMO cycloconverter output voltage is again an infinite series of harmonics represented by the product,

$$[V_{oh}(\omega_o t)] = \frac{3B_1V_i}{2}\begin{bmatrix}\sum_{n=5,7}^{\infty} A_n\cos(n\omega_o t)\\ \sum_{n=5,7}^{\infty} A_n\cos(n(\omega_o t-120^\circ))\\ \sum_{n=5,7}^{\infty} A_n\cos(n(\omega_o t-240^\circ))\end{bmatrix} + [S_{ih}(\omega_o t)][S_{rh}(\omega_i t)]$$

$$\cdot V_i\begin{bmatrix}\cos(\omega_i t)\\ \cos(\omega_i t-120^\circ)\\ \cos(\omega_i t-240^\circ)\end{bmatrix} \tag{2.21}$$

Substitution of $[S_{ih}(\omega_o t)][S_{rh}(\omega_i t)]$ from (2.20) into (2.21) and evaluating only for the phase A voltage, i.e. $[V_{oh,A}(\omega_o t)]$ yields,

$$[V_{oh,A}(\omega_o t)] = \frac{3B_1V_i}{2}\sum_{n=5,7}^{\infty} A_n\cos(n\omega_o t)$$

$$+\frac{3A_1V_i}{2}\sum_{m=6,12,18}^{\infty}(B_{m-1}+B_{m+1})\cos((m\omega_i \pm \omega_o)t)$$

$$+\frac{3V_i}{2}\sum_{m=6,12}^{\infty}\ \sum_{n=5,7}^{\infty}(B_{m-1}+B_{m+1})A_n\cos((m\omega_i+n\omega_o)t)$$

$$+\frac{3V_i}{2}\sum_{m=6,12}^{\infty}\ \sum_{n=5,7}^{\infty}(B_{m-1}+B_{m+1})A_n\cos((m\omega_i-n\omega_o)t) \tag{2.22}$$

Equation (2.22) implies that the IMO cycloconverter output voltage $[V_o(\omega_o t)]$ contains spectral components at frequencies

$$\begin{aligned} \omega_{h1} &= m\omega_i + \omega_o \\ \omega_{h2} &= m\omega_i - \omega_o \\ \omega_{h3} &= m\omega_i + n\omega_o \\ \omega_{h4} &= m\omega_i - n\omega_o \end{aligned} \qquad (2.23)$$

where m=6,12,18,... and n=5,7,.... Moreover, spectral components with frequencies $\omega_h < \omega_o$ are known as subharmonic components or subharmonics. These low-frequency large-amplitude subharmonics contribute to a number of problems including magnetic saturation, torque pulsations, energy losses, light flickering, etc. For these reasons they should be avoided whenever possible.

Of the four sets of frequency components in (2.23), the ω_{h2} and ω_{h4} sets may contain subharmonics (i.e., $\omega_h < \omega_o$) components. In particular, as ω_o increases, ω_{h2} decreases, and when $\omega_{h2} = 6\omega_i - \omega_o < \omega_o$, the first subharmonics appears. Therefore, to avoid subharmonics the following conditions have to be satisfied.

$$\omega_o < 3\omega_i \text{ or } f_o < 3f_i \qquad (2.24)$$

$$\Rightarrow \text{ for } f_i = 60 \text{ Hz},\ f_o < 180 \text{ Hz} \qquad (2.25a)$$

where f_i and f_o are the cycloconverter input and output frequencies respectively.

Further study has proved that subharmonics which appear at a relative frequency, f_{rt}, given by;

$$f_{rt} = \frac{6f_i - f_o}{f_o} = \frac{6f_i}{f_o} - 1 \qquad (2.25b)$$

has its magnitude of about 2.9% of the fundamental. For output frequencies higher than $3f_i$ there will be subharmonics, however, their magnitude will be insignificant (2.9% of input voltage).

Equation (2.25) implies that, for $f_i = 60$ Hz (and assuming that respective $[S_{ih}(\omega_o t)]$ spectrum contains 5th and 7th harmonic components) the upper limit on the frequency f_o before subharmonics begin to appear in the output voltage $[V_o(\omega_o t)]$ spectrum is at $f_o = 180$ Hz. However, another method to raise f_o above 180 Hz is by eliminating respective B_{m-1} and B_{m+1} harmonic coefficient (2.22) from the spectrum of $[S_{rh}(\omega_i t)]$ switching function (2.20). This can be achieved by selecting a suitable PWM scheme.

Regarding the ω_{h4} set of spectral components (2.23), subharmonics can be avoided if the following conditions are satisfied

$$\omega_{h4} = |m\omega_i - n\omega_o| > \omega_o \qquad (2.26)$$

$$\Rightarrow \frac{m}{n+1} > \frac{\omega_o}{\omega_i} \text{ or } \frac{m}{n-1} < \frac{\omega_o}{\omega_i}$$

$$\Rightarrow \frac{m}{n+1} > \frac{f_o}{f_i} \tag{2.27}$$

or,
$$\frac{m}{n-1} < \frac{f_o}{f_i}. \tag{2.28}$$

It can be noted that in theory inequalities (2.27) and (2.28) cannot be satisfied for all m and n values since, as implied by (2.22), $m=6,12,18,\ldots\ldots, \infty$ and $n=5,7,11,\ldots\ldots, \infty$. In practice, however, these inequalities can be satisfied and yield subharmonics of negligible amplitudes, if the mf_i and $(n\pm1)\,f_o$ are assumed to represent only the frequencies of the dominant $B_m\cos(m\omega_i)$ and $A_n\cos(n\omega_o)$ harmonic components in (2.22). Under this assumption, (2.27) can be satisfied with the type of $[S_i(\omega_o t)][S_r(\omega_i t)]$ function shown in Fig. 2.6.

2.5.2.2 IMO Input Current Spectrum

The equation for input current of a practical 3-phase to 3-phase cycloconverter can be written from (2.3b) as follows,

$$[I_i(\omega_i t)]=[S_r(\omega_i t)]^T[S_i(\omega_o t)]^T[I_o(\omega_o t)]$$

$$\begin{bmatrix} I_a \\ I_b \\ I_c \end{bmatrix} = \begin{bmatrix} \sum_{m=1,2}^{\infty} B_m\cos(m\omega_i t) \\ \sum_{m=1,2}^{\infty} B_m\cos(m(\omega_i t-120^\circ)) \\ \sum_{m=1,2}^{\infty} B_m\cos(m(\omega_i t-240^\circ)) \end{bmatrix}.$$

$$[\sum_{n=1,2}^{\infty} A_n \cos(n\omega_o t) \quad \sum_{n=1,2}^{\infty} A_n \cos(n(\omega_o t-120^\circ)) \quad \sum_{n=1,2}^{\infty} A_n \cos(n(\omega_o t-240^\circ))]$$

$$\cdot I_o \begin{bmatrix} \cos(\omega_o t) \\ \cos(\omega_o t-120^\circ) \\ \cos(\omega_o t-240^\circ) \end{bmatrix}$$

$$\begin{bmatrix} I_a \\ I_b \\ I_c \end{bmatrix} = \frac{3A_1 B_1 I_o}{2} \begin{bmatrix} \cos(\omega_i t) \\ \cos(\omega_i t-120^\circ) \\ \cos(\omega_i t-240^\circ) \end{bmatrix} + \frac{3A_1 I_o}{2} \sum_{m=3,5,7}^{\infty} B_m \begin{bmatrix} \cos(m\omega_i t) \\ \cos(m(\omega_i t-120^\circ)) \\ \cos(m(\omega_i t-240^\circ)) \end{bmatrix}$$

$$+ \frac{3I_o}{2} \sum_{m=1,3,5}^{\infty} \sum_{n=6,12,18}^{\infty} B_n (A_{m-1} + A_{m+1})$$

$$\cdot \begin{bmatrix} \cos(m\omega_i \pm n\omega_o)t \\ \cos((m\omega_i \pm n\omega_o)t - (m120^\circ \pm n120^\circ)) \\ \cos((m\omega_i \pm n\omega_o)t - (m240^\circ \pm n240^\circ)) \end{bmatrix} \qquad (2.29)$$

The spectral nature of the input current is similar to the output voltage. However, the order of the harmonic components is high enough permitting easy filtering.

2.5.2.3 Gain of IMO Cycloconverter

Like DMO approach, (2.17), (2.19) and (2.29) also show that the IMO cycloconverter (Fig. 2.2) output voltages [V_{AN} V_{BN} V_{CN}] and input currents [I_a I_b I_c] consist of their fundamental (i.e. wanted) components and an infinite series of harmonic (i.e. unwanted) components. Also, (2.17a) shows that the equivalent solid state transformer turns ratio for IMO cycloconverter shown in Fig. 2.2 is given by;

$$\frac{N_S}{N_P} = \frac{V_{out}}{V_{in}} = \frac{I_{in}}{I_{out}} = \frac{\frac{3A_1 B_1 V_i}{2}}{V_i} = \frac{\frac{3A_1 B_1 I_o}{2}}{I_o} = \frac{3A_1 B_1}{2} \qquad (2.30a)$$

Fig. 2.6b and 2.6d show that maximum A_1 and B_1 values are

$$A_1, \max = \frac{2}{\pi} \int_0^{\pi} \sin \omega t \; d(\omega t) = \frac{4}{\pi} \cdot \frac{\sqrt{3}}{2}$$

$$(2.30b)$$

and B_1, $\max = \frac{2}{\pi} \int_0^{\pi} \sin \omega t \; d(\omega t) = \frac{2}{\pi}$

Therefore,

$$\frac{N_S}{N_P}, \max = \frac{3(\frac{4}{2} \cdot \frac{\sqrt{3}}{\pi}) \cdot (\frac{2}{\pi})}{2} = \frac{6\sqrt{3}}{\pi^2} = 1.053 \qquad (2.30c)$$

which is a significant improvement over the values obtained from (2.17).

2.6 Conclusions

A generalized circuit model of frequency/voltage converter is presented in this chapter. This model has been utilized to predict the behavior of cycloconverters with any number of input-output phases. Furthermore, two modes of converter operation have been identified. By appropriate combination of mode of operation and switching function, FCCs can be made to yield high quality output voltage and input current waveforms with low harmonic content and insignificant output voltage derating.

CHAPTER 3

THREE PHASE TO THREE PHASE CYCLOCONVERTER

3.1 Introduction

The generalized cycloconverter with N input and M output phases discussed in Chapter 2 has been analyzed throughly and implemented for three input and three output phases in this chapter. Motivation behind this analysis and design is due to the potential for extensive application of this type of FCC in high power applications. The advantages of FCC over the dc link frequency changer has been discussed in Chapter 1, Sections 1.2.2 and 1.2.4.

The concepts of switching function and switching patterns are also discussed here. These concepts can be applied to various FCC schemes. The content of this chapter can be summarised as follows;

i) System description and operating principle.

ii) Different DMO and IMO schemes and their evaluation.

iii) Simulation of the various schemes proposed in this chapter.

iv) Design criteria for the proposed structures.

v) Design example and experimental verifications of two of the proposed schemes.

3.2 System Description and Mode of Operation

Fig. 3.1 shows the simplified circuit diagram of a 3-phase to 3-phase cycloconverter derived from the generalized converter diagram shown in Fig. 2.1, Chapter 2 by

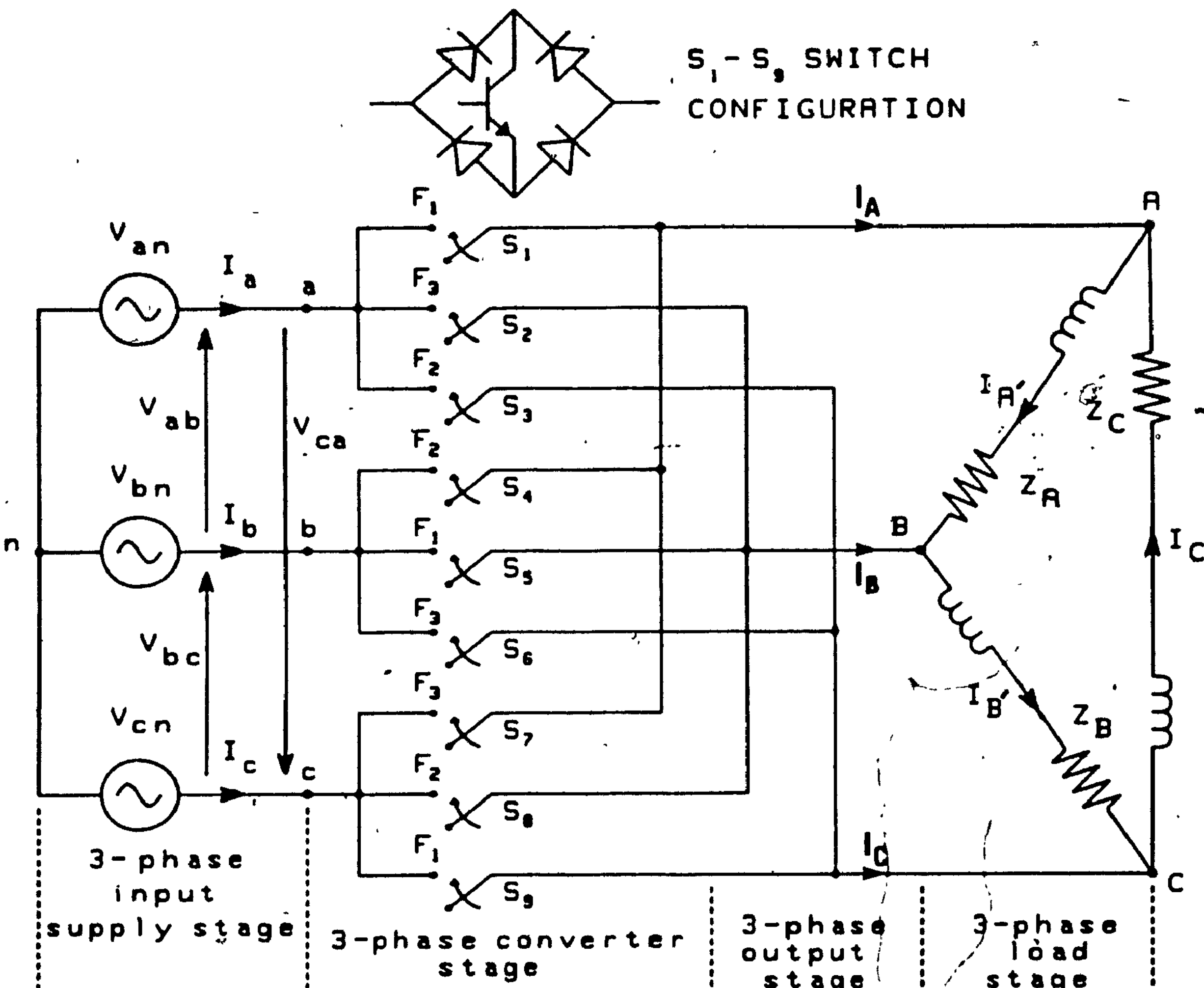

Fig. 3.1: Simplified circuit diagram of the proposed three-phase to three-phase forced commutated cycloconverter structure.

setting N=M=3. It consists of a 3-phase mains supply, the 3-phase converter and a 3-phase balanced load. The 3-phase mains is assumed to be balanced and distortion free. Switches S_1 to S_9 are assumed to be ideal and composed of four diodes and a gate turn-off device, such as bipolar transistor, MOSFET's, GTO's, etc. The load could be an ac load or a step up/down frequency converter. However, for the shake of simplicity, resistive-inductive type of load has been assumed.

The proposed three-phase to three-phase FCC converter structure can operate under either the DMO or the IMO mode. These two operating modes have been explained in subsections 2.4.1 and 2.4.2 of Chapter 2. For both modes, switches S_1 to S_9 are commanded by the gating signals which are determined by the control scheme used. Consequently the rate of repetition of ON and OFF (closing and opening) of these nine switches with respect to the input cycle is determined by the required output frequency.

3.3 Switching Functions

The realization of the 'converter transfer matrix' can be achieved only by means of a set of switches which operate according to a predetermined switching pattern. The switching function for a single switch assumes unit value whenever the switch is closed and a zero value whenever the switch is opened. In a converter, each switch is closed and opened according to a predetermined repetitive pattern; hence, its switching function will take the form of a train of pulses of unit amplitude. Neither the pulses nor the intervening zero-value periods have necessarily the same time duration; however, the requirement that a repetitive switching pattern must exist means that the function must at least consist of repetitive groups of pulses. The simplest, or unmodulated, switching functions have pulses of the same time duration and zero intervals with the same property. A more complex type with differing pulse durations and various interspersed zero times, is termed as a pulse width modulated (PWM) switching function. By modulating the pulse widths, harmonic content of the resultant waveform improves and voltage control at the output is achieved. In the case of a variable frequency converter, the selection of a suitable modulation strategy is of utmost importance. This is particularly true when the output voltage shape and the frequency spectrum change with a corresponding change in output frequency.

There are various types of modulation techniques [33]-[37] reported in the literature, e.g. single-pulse modulation, multi-pulse modulation, sinusoidal-pulse modulation, sinusoidal pulse-width modulation, etc.

The techniques available differ in the harmonic content that they produce and in the output voltage gain. Thus the acceptable harmonic content and resulting voltage gain are the factors that determine the choice of a particular PWM technique. Some of the modulation techniques used in this thesis are described in the following sections.

3.3.1 Single-Pulse Modulation

The switching function waveforms of the single-pulse modulation scheme is illustrated in Fig. 3.2. For the purpose of analysis it is assumed that the pulse width can be varied by equal angular intervals on both sides from the centre of the pulse, thus resulting in variation of the pulse width δ over the range $0 < \delta < \pi$ radian.

The waveform can be described by the Fourier series,

$$SF = A_o + \sum_{n=1,2,3}^{\infty} (A_n \cos n\omega t + B_n \text{Sin } n\omega t) \quad (3.1)$$

where

$$B_n = \frac{2}{\pi} \int_0^{\pi} \sin n\omega t \; d(\omega t)$$

$$= \frac{4}{n\pi} \sin \frac{n\delta}{2}, \text{ n is odd}$$

and

$$A_o = 0, \; A_n = 0$$

and the corresponding harmonics i.e. A_n values are shown in Fig. 3.2b for the value of $\delta = 120^o$. This PWM technique is used in IMO cycloconverter. Variation of pulse width δ is possible in 3-phase to single-phase IMO cycloconverter. For three to three-phase IMO cycloconverter δ is fixed at 120^o.

3.3.2 Uniform Pulse Width Modulation (UPWM)

Uniform pulse width modulated switching function pattern is obtained by comparing a single pulse with triangular carrier wave as shown in Fig. 3.3. The frequency spectrum can be changed by varying the number of triangles in the carrier wave. This also changes the number of pulses. The UPWM waveform can be represented by its Fourier series as,

$$SF = A_o + \sum_{n=1,2,3}^{\infty} (A_n \cos n\omega t + B_n \sin n\omega t) \qquad (3.2)$$

where $A_o = \frac{1}{3}$

$$A_n = \sum_{p=1}^{N_p} \frac{2}{\pi} \int_{\alpha_p}^{\alpha_{p+1}} \cos n\alpha \, d\alpha$$

$$B_n = 0$$

and N_p = no. of pulses per cycle

= no. of triangles + 1

Associated frequency spectra of this type of switching function is plotted in Fig. 3.3b for modulation index, $M_f = 1$ and four pulses per cycle. This PWM technique is used in DMO cycloconverter.

3.3.3 Sinusoidal Pulse Width Modulation (SPWM)

A particular type of sinusoidal pulse width modulation technique proposed by Venturini [29] which in principle can eliminate any number of low-order harmonics is shown in Fig.

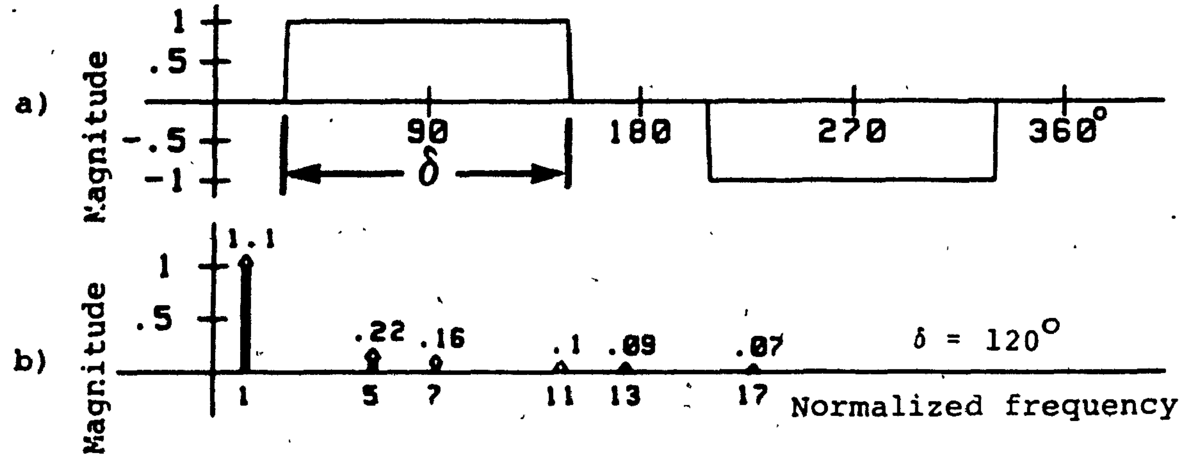

Fig. 3.2: Single pulse modulation switching function
a) The switching function.
b) Respective frequency spectrum.

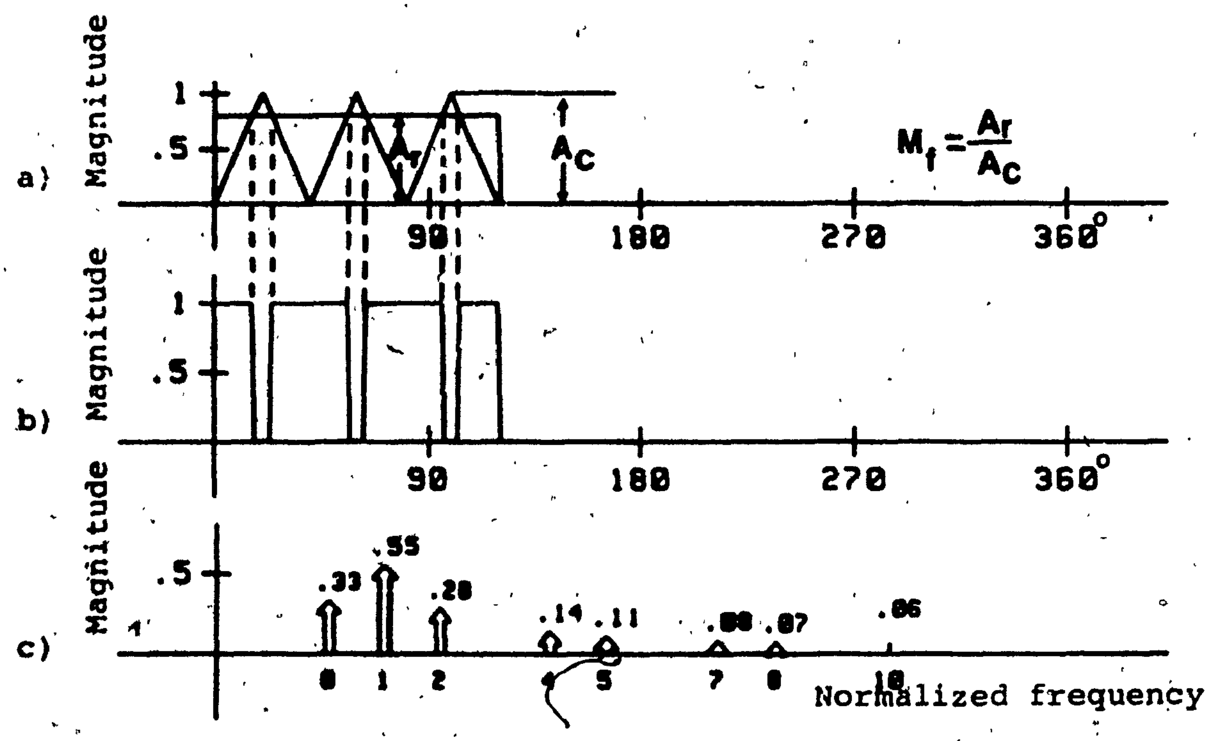

Fig. 3.3: Uniform pulse width modulated switching function.
a) Derivation of UPWM switching function.
b) Resulting switching function.
c) Respective frequency spectrum.

3.4. Switching function pattern for 3-phase frequency converter is calculated as

$$t_1^k = \frac{T_{seq}}{3} (1 + 2q.\ \sin (k.\ T_{seq}.\ \omega_m))$$

$$t_2^k = \frac{T_{seq}}{3} (1 + 2q.\ \sin (k.\ T_{seq}.\ \omega_m - 2\pi/3)) \quad (3.3)$$

$$t_3^k = \frac{T_{seq}}{3} (1 + 2q.\ \sin (k.\ T_{seq}.\ \omega_m - 4\pi/3))$$

where $t_1^k + t_2^k + t_3^k = T_{seq} = \frac{1}{f_{seq}}$

ω_m = input voltage angular frequency,

q = no. of segments of input voltage frequency.

The Fourier series of this function contains A_o, A_n and B_n coefficients. The frequency spectrum of this function is shown in Fig. 3.4b. This PWM technique is used in DMO cycloconverters.

3.3.4 Modified Sinusoidal Pulse Width Modulation (MSPWM)

The modified sinusoidal pulse width modulation [37] switching function pattern is obtained by comparing the triangular carrier wave with the reference sine wave. This technique is used in IMO cycloconverters. The carrier wave is applied only during the first and last 60^o intervals per half-cycle i.e. 0^o-60^o and 120^o-180^o. The intersection points between the carrier and reference waves are the pulses (Fig. 3.5a and b). Middle pulses between 60^o and 120^o of the switching function pattern are determined by considering the mirror image of the pulses in the first and last 60° intervals, while the next half-cycle of the patterns can be readily determined by considering the half wave symmetry of the waveform. The width of the pulses and consequently the amplitude of the Fourier coefficients can be varied by varying the modulation index, M_f. The normal operation of a balanced three-phase system requires that the following correspondence between the carrier frequency and the reference frequency be satisfied,

$$f_c/f_r = 6N_p + 3, \quad N_p = 1,2,3,... \tag{3.4}$$

where

N_p = number of pulses in the first 60° interval. Therefore, the number of pulses per cycle, N_T, is given by:

$$N_T = 8N_p \tag{3.5}$$

An excellent property of this variable pattern MSPWM is that the dominant harmonic can be pushed further away from the fundamental component by varying the number of pulses which can be expressed as;

$$\begin{aligned} d_l &= 6N_p + 1 \\ d_h &= 6N_p + 5 \end{aligned} \tag{3.6}$$

3.4 Direct Mode of Operation (DMO) Cycloconverter

Direct mode of operation (DMO) is a one step process in which output voltage is constructed by direct multiplication

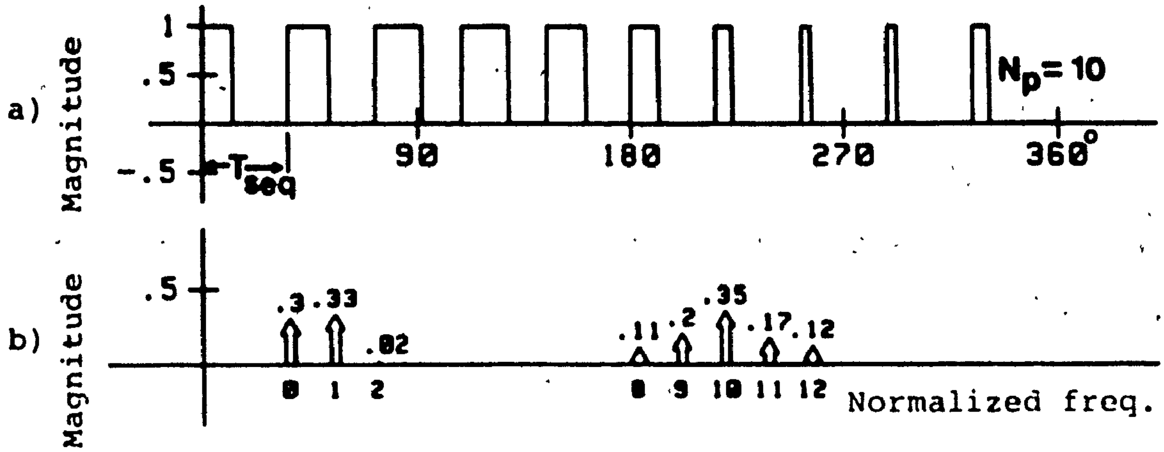

Fig. 3.4: Sinusoidal pulse width modulation switching function.
a) The switching pattern.
b) Respective frequency spectrum.

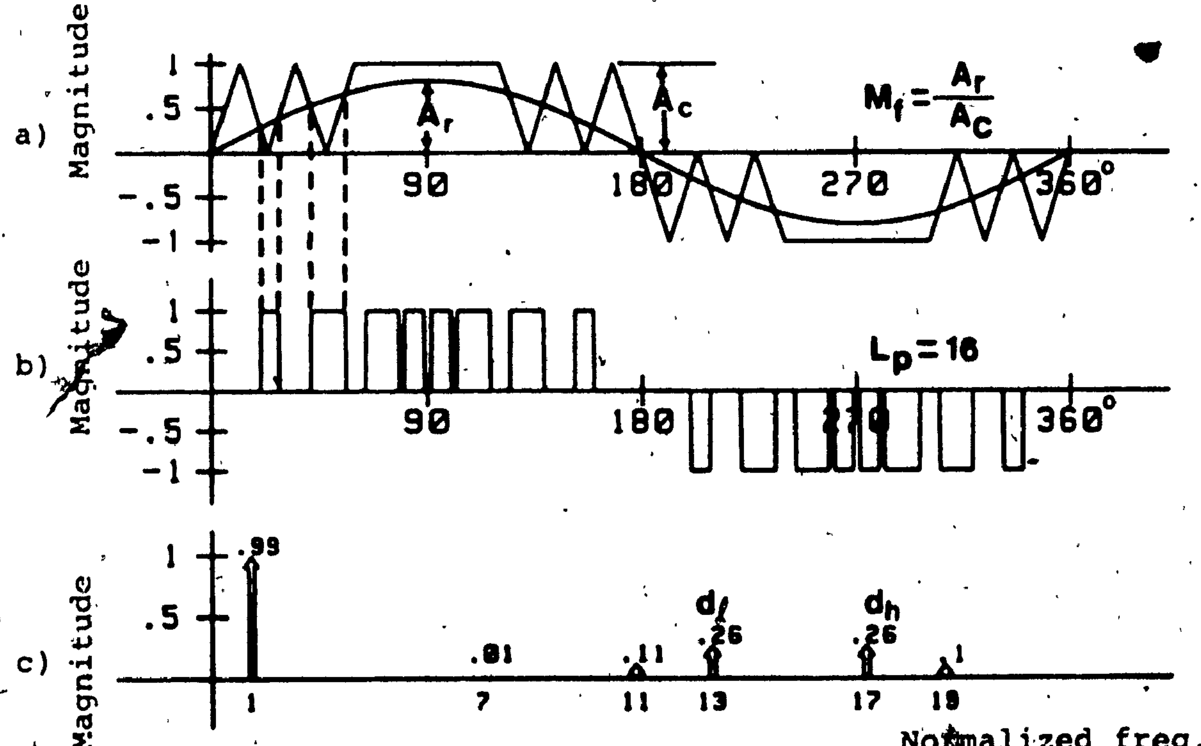

Fig. 3.5: Modified sinusoidal pulse width modulation switching function.
a) Derivation of MSPWM.
b) Resulting switching function.
c) Respective frequency spectrum.

of input voltages by the respective converter transfer matrix. This process can be illustrated by a diagram shown in Fig. 3.6, where F_1 is one of the three (F_1, F_2, F_3) converter transfer matrix elements. Two of the several switching function patterns described in the previous section can be applied to DMO cycloconverter. First the respective output voltage and input current expression for three phase DMO converter are described and subsequently the two schemes are analysed.

The practical equation for the voltage of a 3-phase to 3-phase DMO FCCs which is derived in (2.8), Chapter 2 is once again described here to maintain continuity.

$$\begin{bmatrix} V_{AN} \\ V_{BN} \\ V_{CN} \end{bmatrix} = \frac{3A_1V_i}{2} \begin{bmatrix} \cos(\omega_o t) \\ \cos(\omega_o t-240^\circ) \\ \cos(\omega_o t-120^\circ) \end{bmatrix} +$$

$$\begin{bmatrix} \sum_{n=2,3}^{\infty} A_n\cos(n(\omega_s t)) & \sum_{n=2,3}^{\infty} A_n\cos(n(\omega_s t-120^\circ)) & \sum_{n=2,3}^{\infty} A_n\cos(n(\omega_s t-240^\circ)) \\ \sum_{n=2,3}^{\infty} A_n\cos(n(\omega_s t-240^\circ)) & \sum_{n=2,3}^{\infty} A_n\cos(n(\omega_s t)) & \sum_{n=2,3}^{\infty} A_n\cos(n(\omega_s t-120^\circ)) \\ \sum_{n=2,3}^{\infty} A_n\cos(n(\omega_s t-120^\circ)) & \sum_{n=2,3}^{\infty} A_n\cos(n(\omega_s t-240^\circ)) & \sum_{n=2,3}^{\infty} A_n\cos(n(\omega_s t)) \end{bmatrix}$$

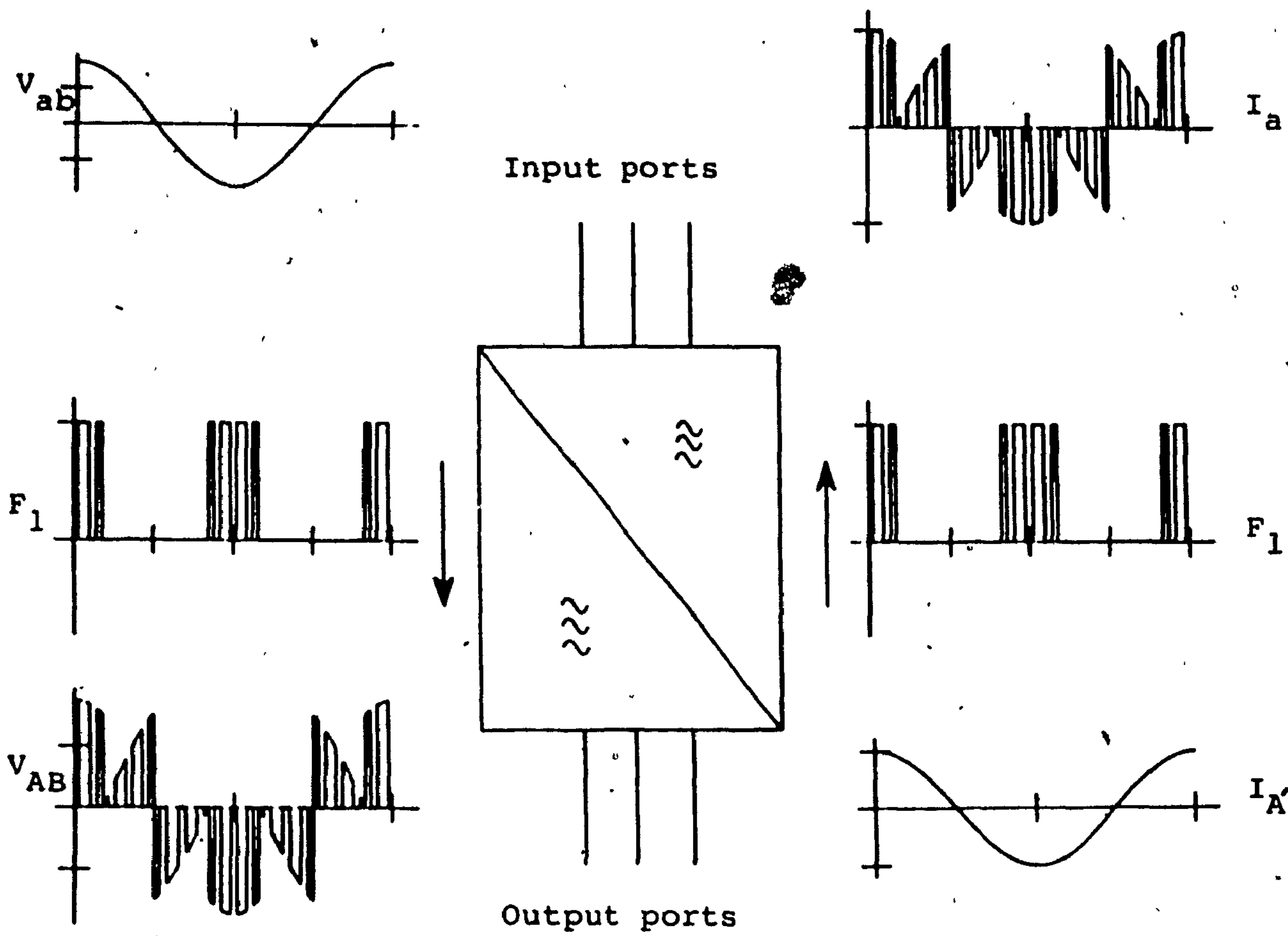

Fig. 3.6: Diagram showing power conversion process for DMO FCC output voltage and input current.

$$\cdot V_i \begin{bmatrix} \cos(\omega_i t) \\ \cos(\omega_i t-120^\circ) \\ \cos(\omega_i t-240^\circ) \end{bmatrix}$$

$$= \frac{3A_1 V_i}{2} \begin{bmatrix} \cos(\omega_o t) \\ \cos(\omega_o t-240^\circ) \\ \cos(\omega_o t-120^\circ) \end{bmatrix} + \sum_{n=2,5,8}^{\infty} \frac{3A_n V_i}{2} \begin{bmatrix} \cos((n\omega_s+\omega_i)t) \\ \cos((n\omega_s+\omega_i)t-n240^\circ) \\ \cos((n\omega_s+\omega_i)t-n120^\circ) \end{bmatrix}$$

$$+ \sum_{n=4,7,10}^{\infty} \frac{3A_n V_i}{2} \begin{bmatrix} \cos((n\omega_s-\omega_i)t) \\ \cos((n\omega_s-\omega_i)t-n240^\circ) \\ \cos((n\omega_s-\omega_i)t-n120^\circ) \end{bmatrix} \qquad (3.7)$$

Equation (3.7) shows that output voltage spectrum contains a fundamental component of amplitude $\frac{3}{2}$ A_1 and harmonic component of $\frac{3A_n}{2}$ whose frequency is determined by $(n\omega_s \pm \omega_i)$ term.

The input current equation for this practical 3-phase cycloconverter is expressed as follows;

$$\begin{bmatrix} I_a \\ I_b \\ I_c \end{bmatrix} = \frac{3A_1 I_o}{2} \begin{bmatrix} \cos(\omega_i t) \\ \cos(\omega_i t-120^\circ) \\ \cos(\omega_i t-240^\circ) \end{bmatrix} + \sum_{n=2,5,8}^{\infty} \frac{3A_n I_o}{2} \begin{bmatrix} \cos((n\omega_s+\omega_o)t) \\ \cos((n\omega_s+\omega_o)t-n120^\circ) \\ \cos((n\omega_s+\omega_o)t-n240^\circ) \end{bmatrix}$$

$$+ \sum_{n=4,7,10,..}^{\infty} \frac{3A_n I_o}{2} \begin{bmatrix} \cos((n\omega_s-\omega_o)t) \\ \cos((n\omega_s-\omega_o)t-n120^{o}) \\ \cos((n\omega_s-\omega_o)t-n240^{o}) \end{bmatrix} \quad (3.8)$$

Input current spectrum contains harmonics at frequencies of $(n\omega_s \pm \omega_o)$, which can be expressed in terms of input frequency of ω_i. Then the order of the harmonics is given by $(n \pm 1)\omega_o + \omega_i$.

3.4.1 DMO FCC with Uniform PWM (Scheme #1)

Scheme #1 is a DMO FCC using uniform PWM switching function. Output voltage and input current waveforms are shown in Figs. 3.7 and 3.8 respectively. With this type of switching function, the general equation for the chopping frequency per converter switch f_{ch}, is given by,

$$f_{ch} = \frac{2}{3}\,(2N_p+1).f_s = \frac{2}{3}(2N_p+1).(f_i+f_o) \qquad (3.9)$$

where N_p is the number of pulses in one period of F_1 switching function component waveform.

Furthermore, Table 3.1 illustrates the order and amplitude of the frequency components for switching function component waveforms, expressed in per unit (where the amplitude of the line input voltages has been taken as 1p.u. V). In particular, the first and second columns of this table show that there are two dominant switching function (SF) harmonics at n=2 and n=4. As predicted by (2.11), Chapter 2, these SF harmonics are reflected onto the spectrum of the FCC output line voltages as also dominant harmonics with frequencies

$$f_{o,d1} = 2f_o + 3f_1, \quad f_{o,d2} = 4f_o + 3f_i \tag{3.10}$$

and amplitudes

$$|V_{o,d1}| = \frac{3A_2}{2}, \quad |V_{o,d2}| = \frac{3A_4}{2} \tag{3.11}$$

The third and fourth columns in this table verify the earlier prediction.

Finally, the mechanism for obtaining output voltage control can be demonstrated with reference to Fig. 3.3 and (3.7) as follow;

The amplitude A_1 of the fundamental component $A_1 \cos(\omega_s t)$, (3.7), of F_1, F_2, F_3 SF components is directly proportional to the A_r/A_c amplitude ratio (Fig. 3.3a). Moreover, the amplitude of the fundamental component of the output line voltage V_o is given, (3.7), by

$$V_{o1} = \frac{3A_1 V_i}{2}.$$

Consequently, V_{o1} is proportional to M_f and can be controlled by electronically controlling A_r/A_c ratio.

Input current waveform and the corresponding frequency spectrum are shown in Fig. 3.8 and Table 3.2 respectively. Magnitude of harmonics is same as the output voltage although their order is changed. This is because now the spectrum is in terms of the input frequency. As predicted in (3.8) and (2.16), Chapter 2, the dominant harmonics are at $2f_o + 3f_i = 5.75$ and $4f_o + 3f_i = 7.75\ f_o$. In Fig. 3.8a, output line current I_C is leading I_B as the output line voltage V_{CA} is

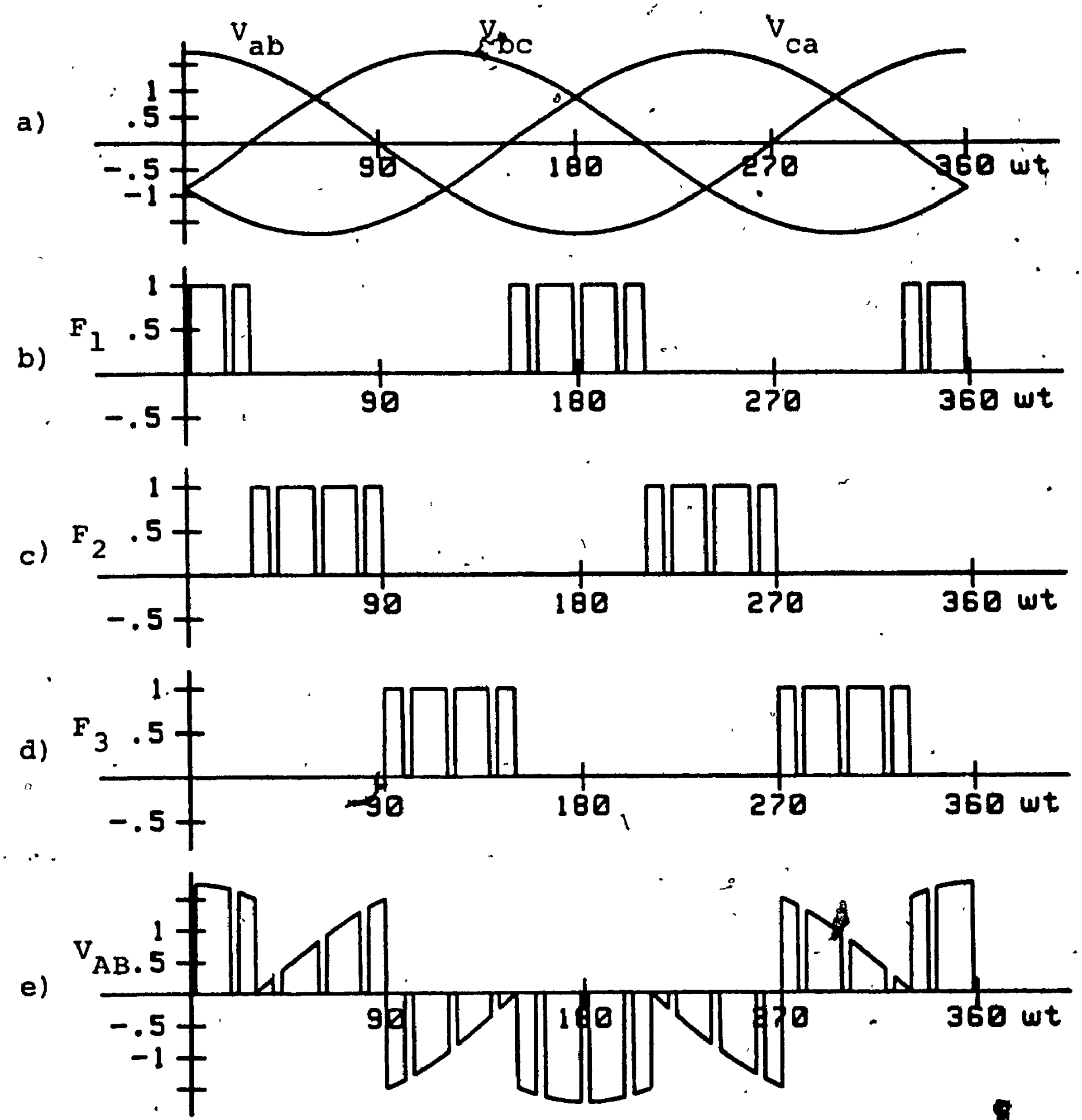

Fig. 3.7: Output voltage waveform obtained with DMO uniform PWM (scheme #1).
a) Three input line voltages.
b)-d) F_1, F_2, F_3 switching function components.
e) Resulting output line voltage, V_{AB}.

TABLE 3.1

FREQUENCY SPECTRA OF WAVEFORMS ASSOCIATED WITH FCC INPUT CURRENT SHOWN IN FIG. 3.7

Harmonic coefficients of switching function (Fig. 3.7b)		Harmonic coefficients of resulting line voltage, V_{AB} (Fig. 3.7e) for $f_o = 75$ Hz $= 1.25\, f_i$		
		Amplitude V_{AB}		
Order (n)	Amplitude (A_n)	Order (kf_o)	p.u. (1)	% (1)
dc	0.33			
1	0.55	f_o	0.83	83
2	0.28	$f_{o,d1}=2f_o+3f_i=4.4f_o$	0.41	41
4	0.14	$f_{o,d2}=4f_o+3f_i=6.4f_o$	0.21	21
5	0.11	$9.8f_o$	0.17	17
7	0.08	$11.8f_o$	0.12	12
8	0.07	$15.2f_o$	0.10	10
10	0.06	$17.2f_o$	0.08	8
16	0.04	$20.6f_o$	0.08	8
17	0.03	$25.2f_o$	0.06	6
19	0.03	$28.0f_o$	0.05	5

(1) Input line voltages have been taken as 1 p.u. volt and 100% volt.

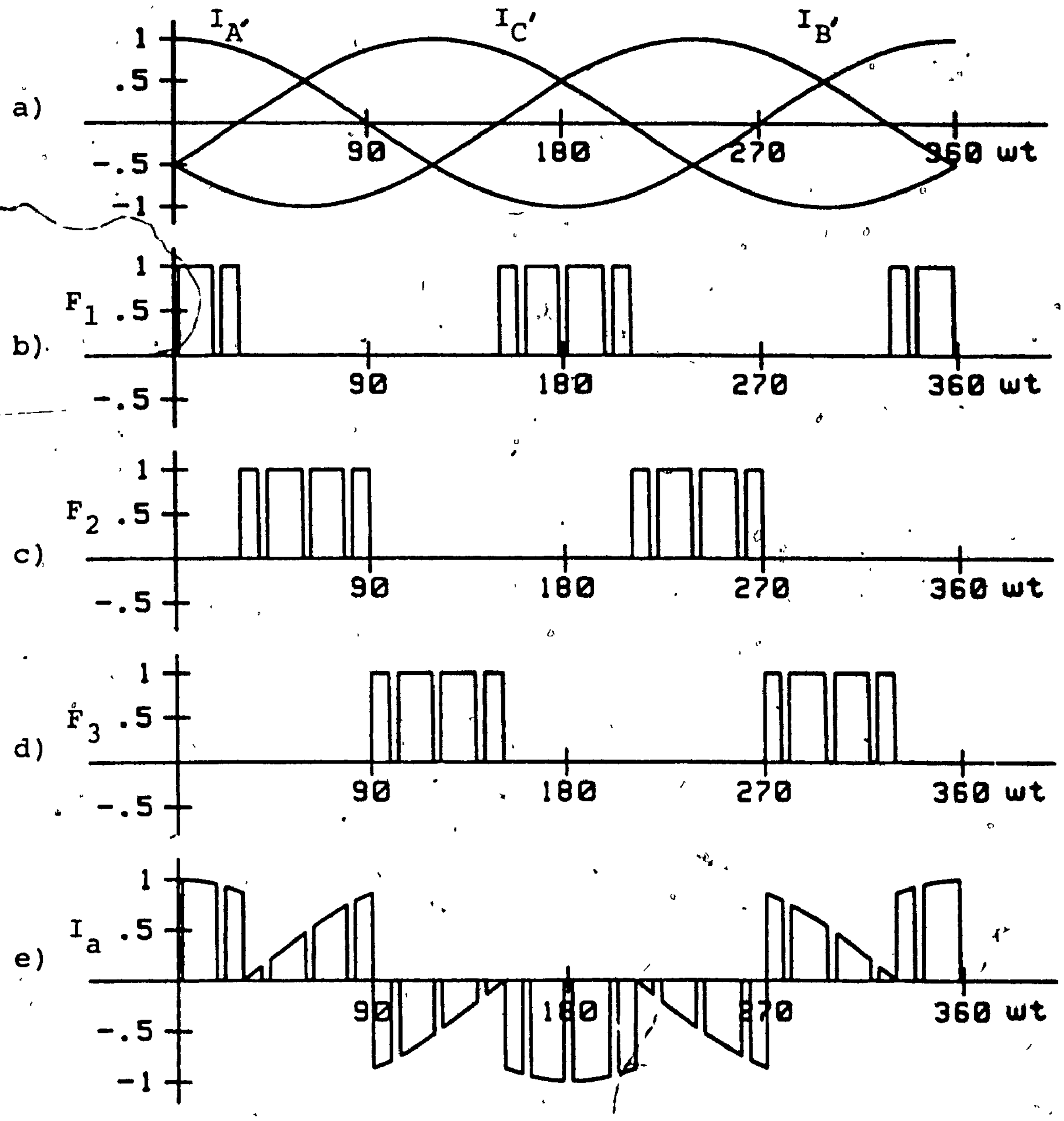

Fig. 3.8: Input current waveform obtained with DMO uniform PWM (scheme #1)
a) Three output phase currents.
b) - d) F_1, F_2, F_3 switching function components.
e) Resulting input current, I_a.

TABLE 3.2

FREQUENCY SPECTRA OF WAVEFORMS ASSOCIATED WITH FCC INPUT CURRENT SHOWN IN FIG. 3.8

Harmonic coefficients of switching function (Fig. 3.8b)		Harmonic coefficients of resulting input phase current I_{an}, (Fig. 3.8e) for $f_o = 75$ Hz $= 1.25\ f_i$		
			Amplitude, I_{an}	
Order (n)	Amplitude (A_n)	Order (kf_i)	p.u.(1)	%(1)
dc	0.33			
1	0.55	f_i	0.83	83
2	0.28	$f_{o,d1}=2f_i+3f_o=5.75f_i$	0.41	41
4	0.14	$f_{o,d2}=4f_i+3f_o=7.75f_i$	0.21	21
5	0.11	$12.5f_i$	0.17	17
7	0.08	$14.5f_i$	0.12	12
8	0.07	$19.25f_i$	0.10	10
10	0.06	$21.25f_i$	0.08	8
16	0.04	$26.0f_i$	0.08	8
17	0.03	$28.0f_i$	0.06	6
19	0.03	$32.75f_i$	0.06	6

1) Output phase currents have been taken as 1 p.u. current and 100% current

leading V_{BC} by 120^o in (3.7).

3.4.2 DMO FCC with Sine PWM (Scheme #2)

The switching function components and output voltage waveforms associated with this technique are shown in Fig. 3.9. From Fig. 3.9 and 3.1 it is apparent that (3.7) and (3.8) are also applicable here. However, in this case F_1, F_2 and F_3 SF components do not contain any low-order harmonics (Table 3.3, column 1 and 2) and consequently the output voltage is free from low-order harmonics. This is achieved by pulsewidth modulating the switching function in sinusoidal fashion illustrated in Fig. 3.4a. With this technique the dominant harmonic frequencies in the output voltage waveforms are closely related to the number of pulses N_p per SF period and clustered around the frequency point,

$$f_d = N_p \cdot f_o + (N_p - 1)\, f_i . \qquad (3.12)$$

Consequently, by increasing the N_p value the f_d value can be increased accordingly. A similar relation, however, exists between N_p and chopping frequency per converter switch f_{ch}, specifically,

$$f_{ch} = N_p \cdot f_s = N_p(f_i + f_o). \qquad (3.13)$$

Consequently, practical f_{ch} values are a compromise between converter switching losses and motor (load) harmonic losses.

The only serious drawback with this technique is that the amplitude of the resulting fundamental component of the output voltage has also been reduced to half (50%) the value of the respective input voltage (Table 3.3). This is less than the previous technique (Scheme #1).

Because this SPWM switching function offers the advantages of yielding sinusoidal output voltages and input currents, a serious effort had been undertaken to improve its respective voltage gain. As a result it has been reported [30] that the deliberate addition of the components $C_1 = 1/6 \cos 4\omega_i t$, and $C_2 = \frac{0.29}{3} \cos (3\omega_o + \omega_i)t$ in the switching function $[F_1\ F_2\ F_3]$ ((2.4), section 2.4.1, Chapter 2) increases voltage gain from 0.5 to 0.866 ((2.17), section 2.5.1.3 Chapter 2). It has also been reported [30], however, this gain is achieved at the cost of a significant increase in switching frequencies and complexity of control circuit hardware.

Input current waveform and spectra are shown in Fig. 3.10 and Table 3.4. The spectrum is similar to output voltage when $f_i = f_o$. The spectrum is different when the output frequency is different than input frequency, which can be verified from Tables 3.3 and 3.4.

3.5 Indirect Mode of Operation (IMO) Cycloconverter

Characteristics of FCC operating under IMO have been thoroughly analyzed in this section. Reconstruction of the output voltage from the input voltages is carried out in two stages. These two steps have been discussed in subsection

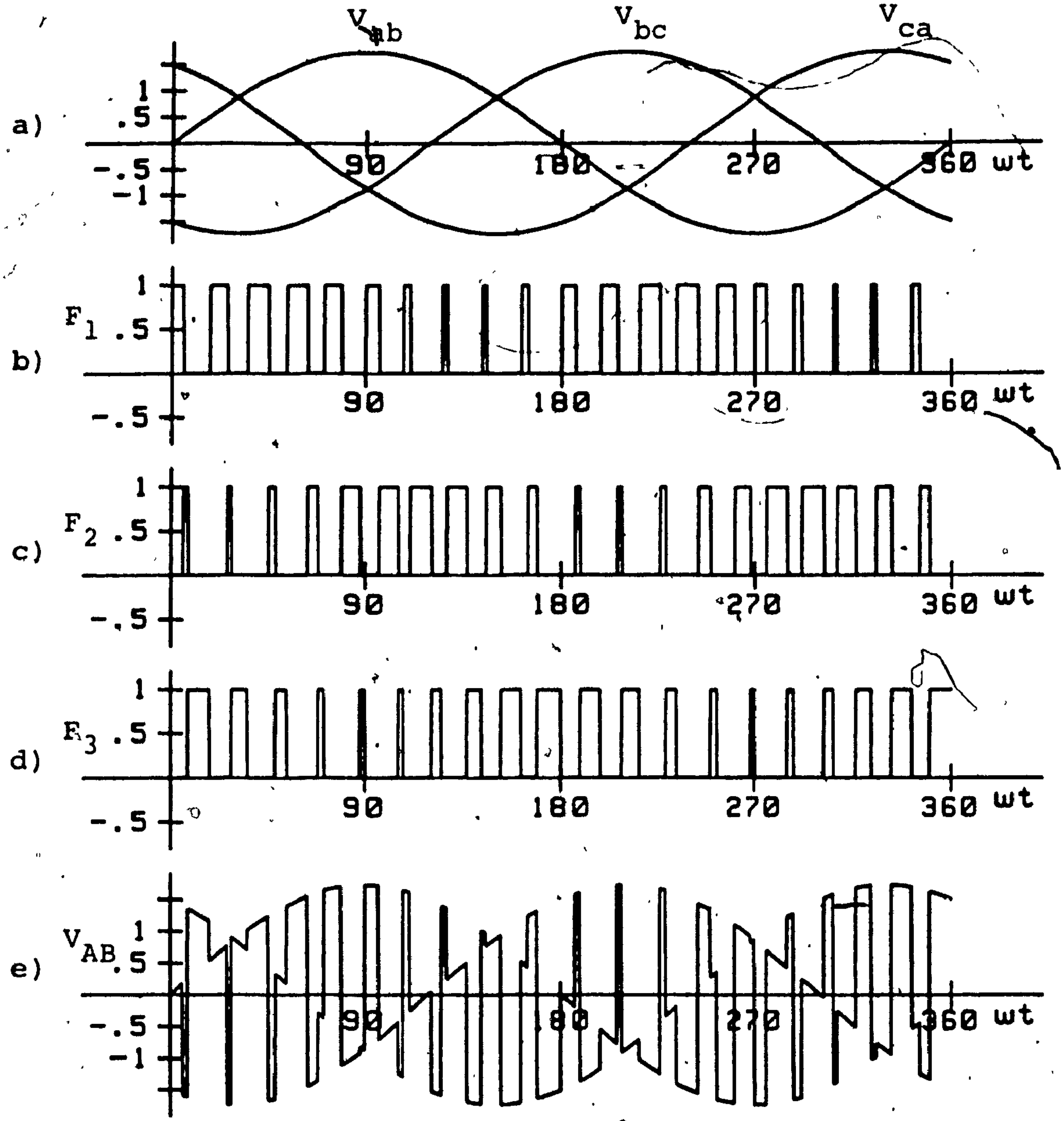

Fig. 3.9: Output voltage waveform obtained with DMO sine PWM (scheme #2).
a) Three input line voltages.
b) - d) F_1, F_2, F_3 switching function components.
e) Resulting output line voltages, V_{AB}.

TABLE 3.3

FREQUENCY SPECTRA OF WAVEFORMS ASSOCIATED WITH FCC OUTPUT VOLTAGE SHOWN IN FIG. 3.9

Harmonic coefficients of switching functions (Fig. 3.9b)		Harmonic coefficients of resulting line voltage, V_{AB}, (Fig. 3.9e), for $f_o = 75$ Hz $= 1.25\ f_i$		
		Amplitude, V_{AB}		
Order (n)	Amplitude (C_n)	Order (kf_o)	p.u.(1)	%(1)
1	0.33	f_o	0.50	50
		. . .		
2	0.02	$f_{d-2} = 26f_o$	0.12	12
3	-	$f_{d-1} = 26.2f_o$	0.28	28
. . .				
N_p-2	0.11	$f_d = 28f_o$	0.37	37
N_p-1	0.20	$f_{d+1} = 29.6f_o$	0.23	23
$N_p=16$	0.35	$f_{d+2} = 29.8f_o$	0.24	24
N_p+1	0.17	$f_{d+3} = 31.4f_o$	0.26	26
N_p+2	0.12			

(1) Output phase currents have been taken as 1 p.u. current and 100% current.

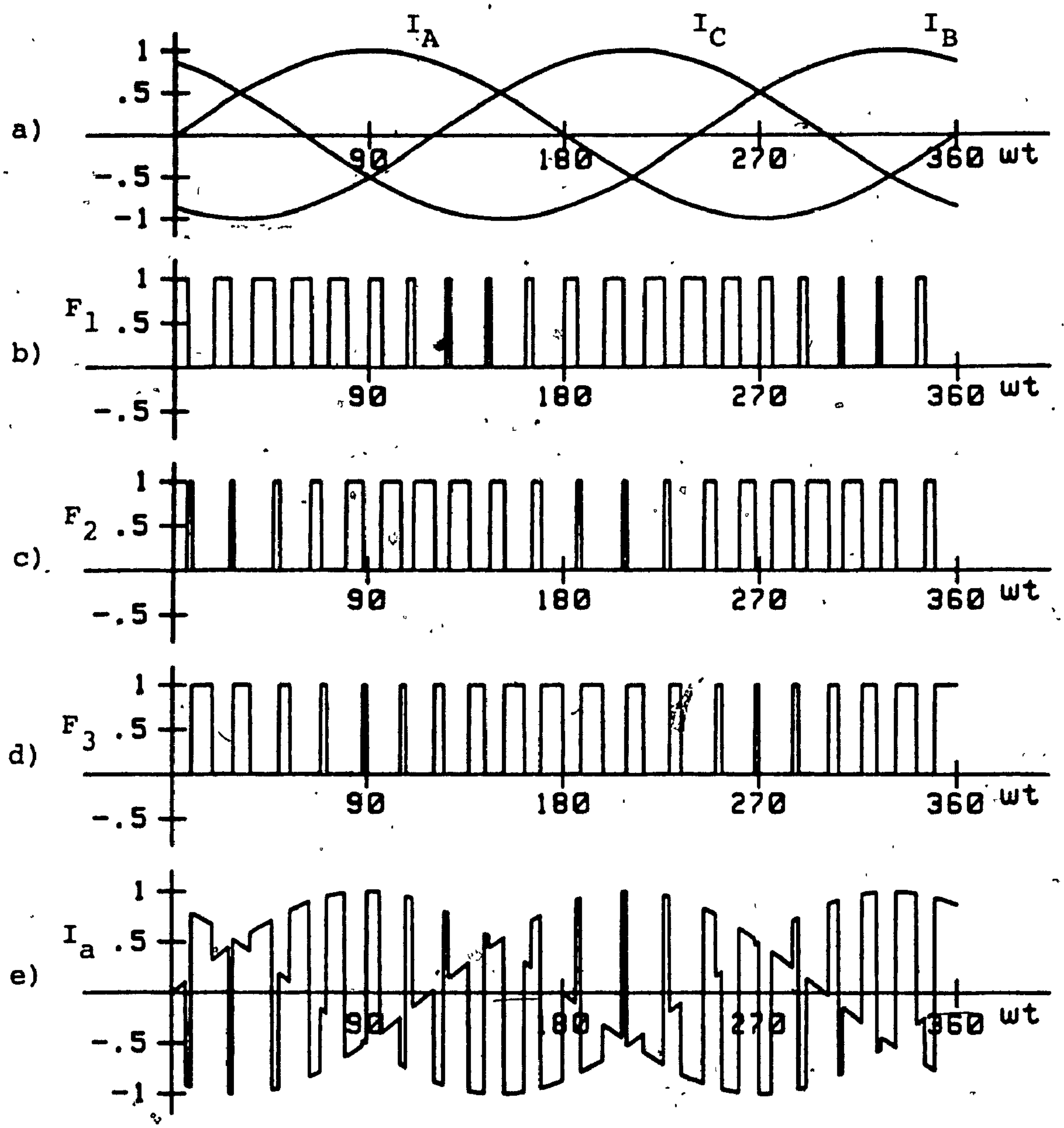

Fig. 3.10: Input current waveform obtained with DMO sine PWM (scheme #2).
a) Three output line currents.
b) - d) F_1, F_2, F_3 switching function components.
e) Resulting input current, I_a.

TABLE 3.4				
FREQUENCY SPECTRA OF WAVEFORMS ASSOCIATED WITH FCC INPUT CURRENT SHOWN IN FIG. 3.10				
Harmonic coefficients of switching function (Fig. 3.10b)		Harmonic coefficients of resulting input phase current I_{an}, (Fig. 3.10e) for $f_o = 75$ Hz $= 1.25f_i$		
		Amplitude, I_{an}		
Order (n)	Amplitude (C_n)	Order (kf_i)	(1) p.u.	(1) %
1	0.33	f_i	0.50	50
2	0.02			
3	--	$f_{d-2}=32.5\ f_i$	0.12	12
		$f_{d-1}=32.75f_i$	0.28	28
N_{p-2}	0.11			
N_{p-1}	0.20	$f_d=35f_i$	0.37	37
$N_{p=16}$	0.35	$f_{d+1}=37f_i$	0.23	23
N_{p+1}	0.17	$f_{d+2}=37.25f_i$	0.24	24
N_{p+2}	0.12	$f_{d+3}=39.25f_i$	0.26	26

1) Output phase currents have been taken as 1 p.u. current and 100% current

2.2.2, Chapter 2 and are shown graphically in Fig. 3.11. Reconstructing the input current is basically the reverse process of output voltage construction, i.e. output current multiplied by inverter SF produces the fictitious dc current. Next, this dc current multiplied by rectifier function yields the input ac current.

The practical equations for output voltages and inputs for IMO FCCs are restated here as;

$$\begin{bmatrix} V_{AN} \\ V_{BN} \\ V_{CN} \end{bmatrix} = \frac{3A_1B_1V_i}{2}\begin{bmatrix} \cos(\omega_o t) \\ \cos(\omega_o t-120^\circ) \\ \cos(\omega_o t-240^\circ) \end{bmatrix} + \frac{3A_1V_i}{2}\sum_{k=3,5,7}^{\infty} B_k \begin{bmatrix} \cos(k\omega_o t) \\ \cos(k(\omega_o t-120^\circ)) \\ \cos(k(\omega_o t-240^\circ)) \end{bmatrix}$$

$$+ \frac{3V_i}{2}\sum_{k=1,3,5}^{\infty}\ \sum_{n=6,12,18}^{\infty} B_k(A_{n-1} + A_{n+1})$$

$$\begin{bmatrix} \cos((k\omega_o \pm n\omega_i)t) \\ \cos((k\omega_o \pm n\omega_i)t - (k120^\circ \pm n120^\circ)) \\ \cos((k\omega_o \pm n\omega_i)t - (k240^\circ \pm n240^\circ)) \end{bmatrix} \qquad (3.14)$$

and

$$\begin{bmatrix} I_a \\ I_a \\ I_c \end{bmatrix} = \frac{3A_1B_1I_o}{2}\begin{bmatrix} \cos(\omega_i t) \\ \cos(\omega_i t-120^\circ) \\ \cos(\omega_i t-240^\circ) \end{bmatrix} + \frac{3B_1I_o}{2}\sum_{n=3,5,7}^{\infty} A_n \begin{bmatrix} \cos(n\omega_i t) \\ \cos(n(\omega_i t-120^\circ)) \\ \cos(n(\omega_i t-240^\circ)) \end{bmatrix}$$

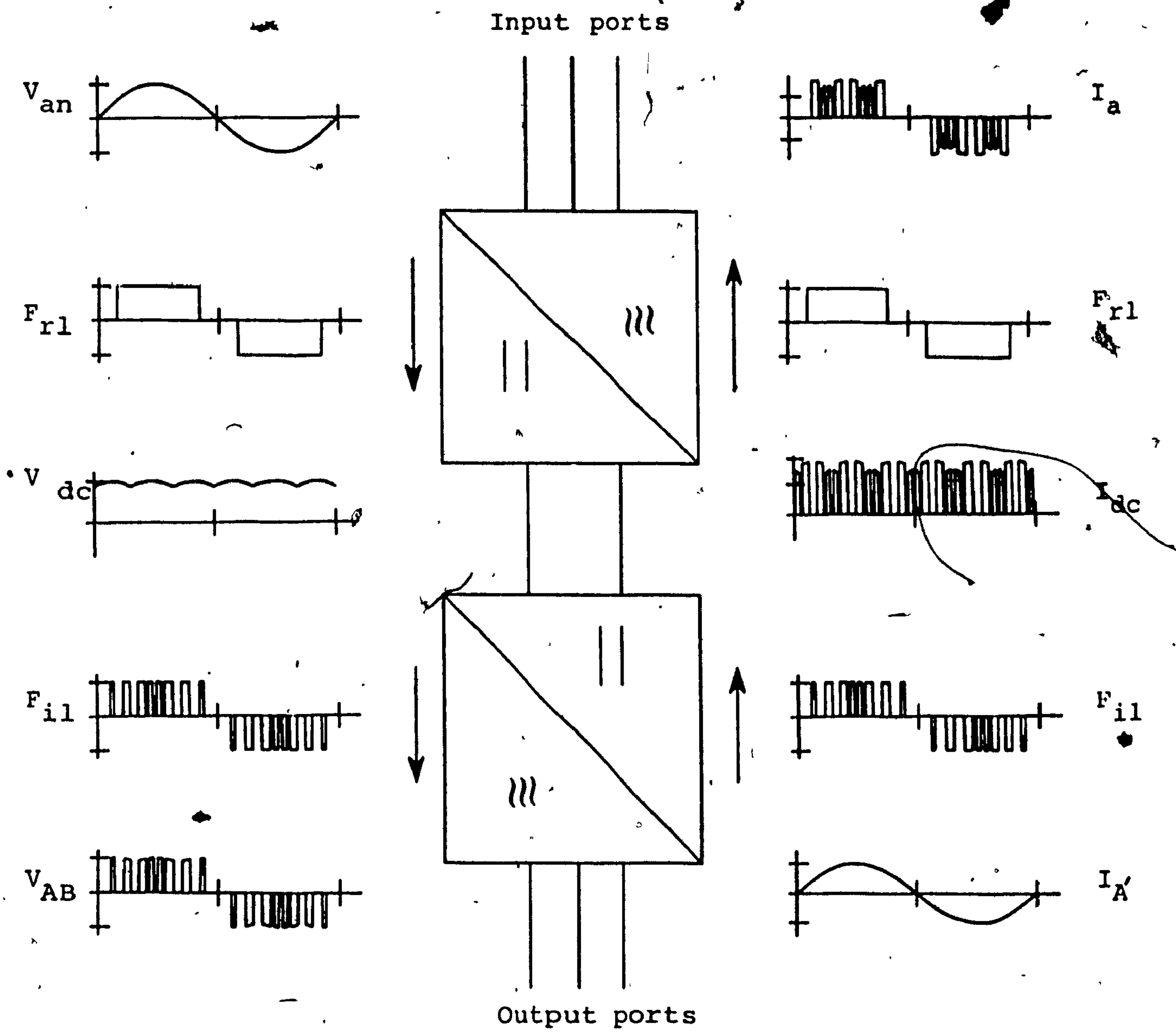

Fig. 3.11: Diagram showing power conversion process for IMO FCC output voltage and input current.

$$+ \frac{3I_o}{2} \sum_{n=1,3,5}^{\infty} \sum_{k=6,12,18}^{\infty} A_n(B_{k-1}+B_{k+1}) \begin{bmatrix} \cos((n\omega_i \pm k\omega_o)t \\ \cos((n\omega_i \pm k\omega_o)t-120^\circ(n\pm k)) \\ \cos((n\omega_i \pm k\omega_o)t-240^\circ(n\pm k)) \end{bmatrix} \tag{3.15}$$

Analytically IMO is a two step process. Therefore, various combination of switching function patterns for fictitious rectification and inversion stages are possible. These mixed modulation schemes can be grouped as,

i) Rectifying function single pulse and inverting function MSPWM, Scheme #1.

ii) Rectifying function MSPWM and inverting function single pulse, Scheme #2.

iii) Rectifying and inverting functions are both MSPWM, Scheme #3.

iv) Rectifying and inverting functions are both single pulse, Scheme #4.

These four IMO schemes are described and analysed as follows;

3.5.1 IMO FCC Scheme #1

In this scheme rectifying SF is a single pulse of 60° duration (line function) or of 120° duration (phase function) and the inverting SF is MSPWM. Fig. 3.12 depicts the waveform associated with this mixed modulation scheme. Rectifying SF (Fig. 3.12b) is at input frequency, f_i and the inverting SF is at output frequency, f_o. For simplicity and easy visual understanding all the waveforms of this chapter are drawn at equal input and output frequencies, although all the schemes (both DMO and IMO) are valid for any other output frequency. A few waveforms at different output frequency are shown in subsequent chapters. Resulting output line voltage, V_{AB} is shown in Fig. 3.12e. Also, the gating strategy for the nine cycloconverter switches which yields the required output voltage, V_{AB} is shown in Fig. 3.12f. From this figure, it can be shown that the per switch maximum chopping frequency f_{ch} is given by

$$f_{ch} = (\frac{N_p}{2} + 2)\ f_o \qquad (3.16)$$

Furthermore, careful examination of (3.14) and (3.15) reveals that spectral shaping is also possible for all the mixed modulation IMO schemes. Tables 3.5 and 3.6 show the output voltage and input current spectra for this scheme. Since f_o has been selected less than $3f_i$ (to satisfy (2.24), Chapter 2) and $nf_i = 5f_i \ll (k-1)f_o = 11f_o$ (to satisfy (2.28), Chapter 2), the resulting V_{AB} spectrum does not contain any perceptible harmonics. Low-order V_{AB} harmonics (up to $10f_o$) have also been eliminated. Moreover, the fundamental V_{AB} component has remained significantly higher than the respective component obtained with DMO approach (Table 3.1). Finally, it can be noted that the amplitude of this component can be varied by varying the modulation index, M_f as shown in Fig. 3.5.

Equations (3.14) and (3.15), also reveal a potential problem with this IMO technique. Specifically, the term $\cos(\pm(k\omega_o - n\omega_i))$ can yield harmonic components of very low frequencies (i.e. sub-harmonics) for the cases where

$$k\omega_o \approx n\omega_i. \qquad (3.17)$$

Since these sub-harmonics can cause flux imbalance in input/output transformers, excite resonant frequencies in input L-C "tanks", and deteriorate the performance of magnetic loads, they should be carefully avoided. This can be accomplished by separating components of the "rectifying" and "inverting" switching functions included in (3.14) and (3.15). For example, the significant spectral components generated by the "rectifying" function in fictitious dc Fig. 3.12c, are the 360 Hz and 720 Hz harmonics. Now, if as shown in Fig. 3.12d, the "inverting" function is chosen such that its first significant harmonics component occurs at a frequency well above the 720 Hz point, then the FCC output voltage and input currents will be practically free of sub-harmonics. This statement can be verified by examining relevant output voltage and input current data contained in Tables 3.5 and 3.6. Input current waveform and respective frequency spectrum are shown in Fig. 3.13 and Table 3.6. This spectrum is very similar to 3-phase 6-diode rectifier input current. It contains 5th and 7th harmonics of 19% and 17% of fundamental component respectively. Subharmonics is less than 1%.

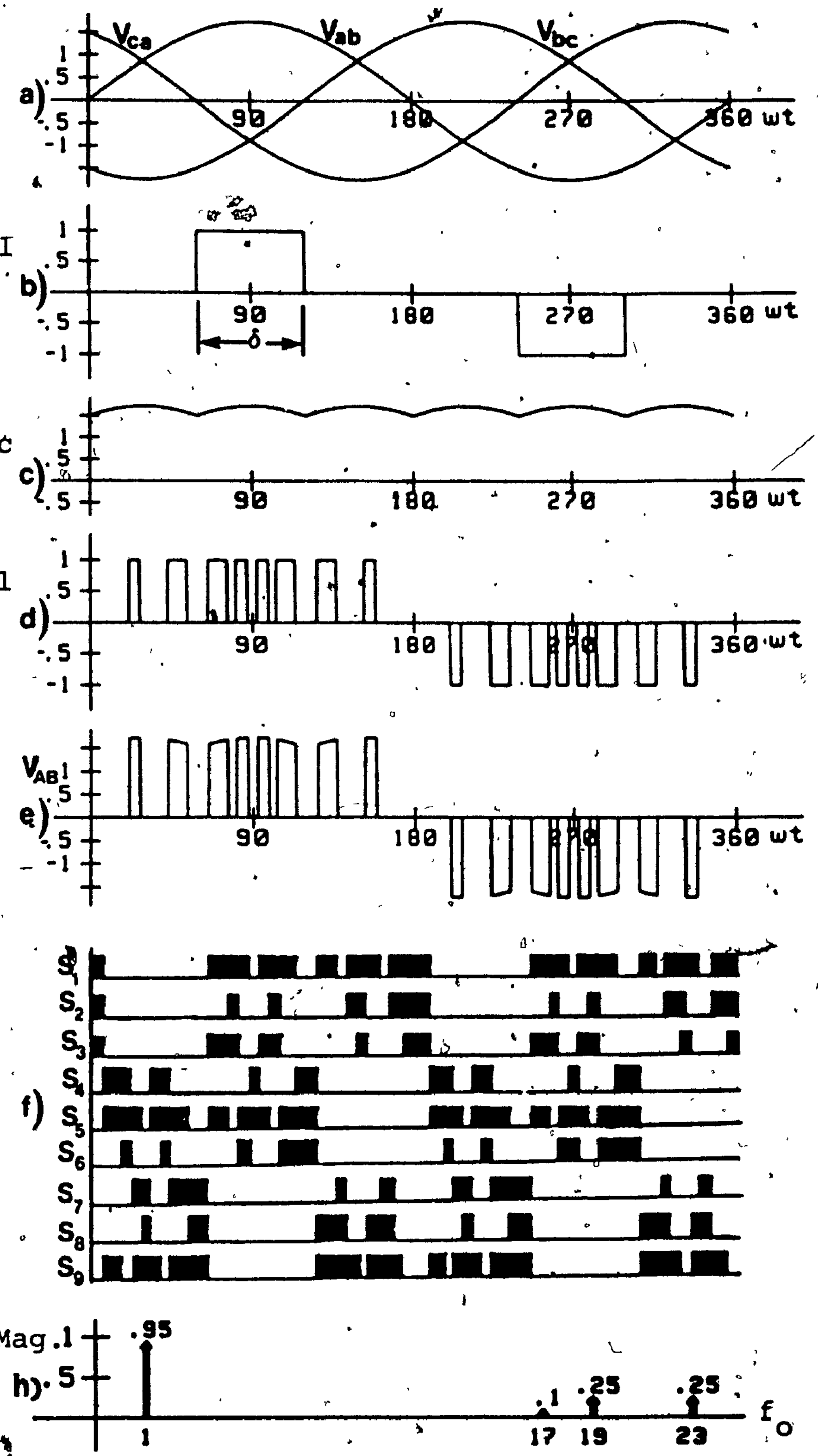

Fig. 3.12: Output voltage waveform obtained with IMO FCC Scheme #1.
a) - e) Process of output voltage, V_{AB} construction. f) Gating strategy for S_1 - S_9 switches. g) Analytically predicted frequency spectrum of V_{AB}.

TABLE 3.5

FREQUENCY SPECTRA OF WAVEFORMS ASSOCIATED WITH FCC OUTPUT VOLTAGE SHOWN IN FIG. 3.12

Harmonic coefficients of rectifier and inverter switching function (Fig. 3.12b and 3.12d)				Harmonic coefficients of resulting output phase voltage, V_{AN} (Fig. 3.12e) for $f_o = 75$ Hz $= 1.25f_i$		
Rectifier SF		Inverter SF		Amplitude, V_{AN}		
Order (n)	Amplitude (A_n)	Order (k)	Amplitude (B_k)	Order (kf_o)	(1) p.u.	(1) %
1	0.64	1	0.99	f_o	0.95	95
3	0.42	3	--	$3.8f_o$	0.03	3
5	0.13	5	--	$5f_o$	0.01	1
7	0.09	7	0.01	$7f_o$	0.01	1
				⋮		
9	0.14	9	--	$f_{d-2}=11f_o$	0.10	10
11	0.06	11	0.11	$f_{d-1}=13f_o$	0.25	25
13	0.05	13	0.26	$f_d=15f_o$	--	-
15	0.09	15	-			
17	0.04	17	0.26	$f_{d+1}=17f_o$	0.25	25
19	0.03	19	0.10	$f_{d+2}=19f_o$	0.10	10

(1) Input phase voltages have been taken as 1 p.u. volt and 100% volt.

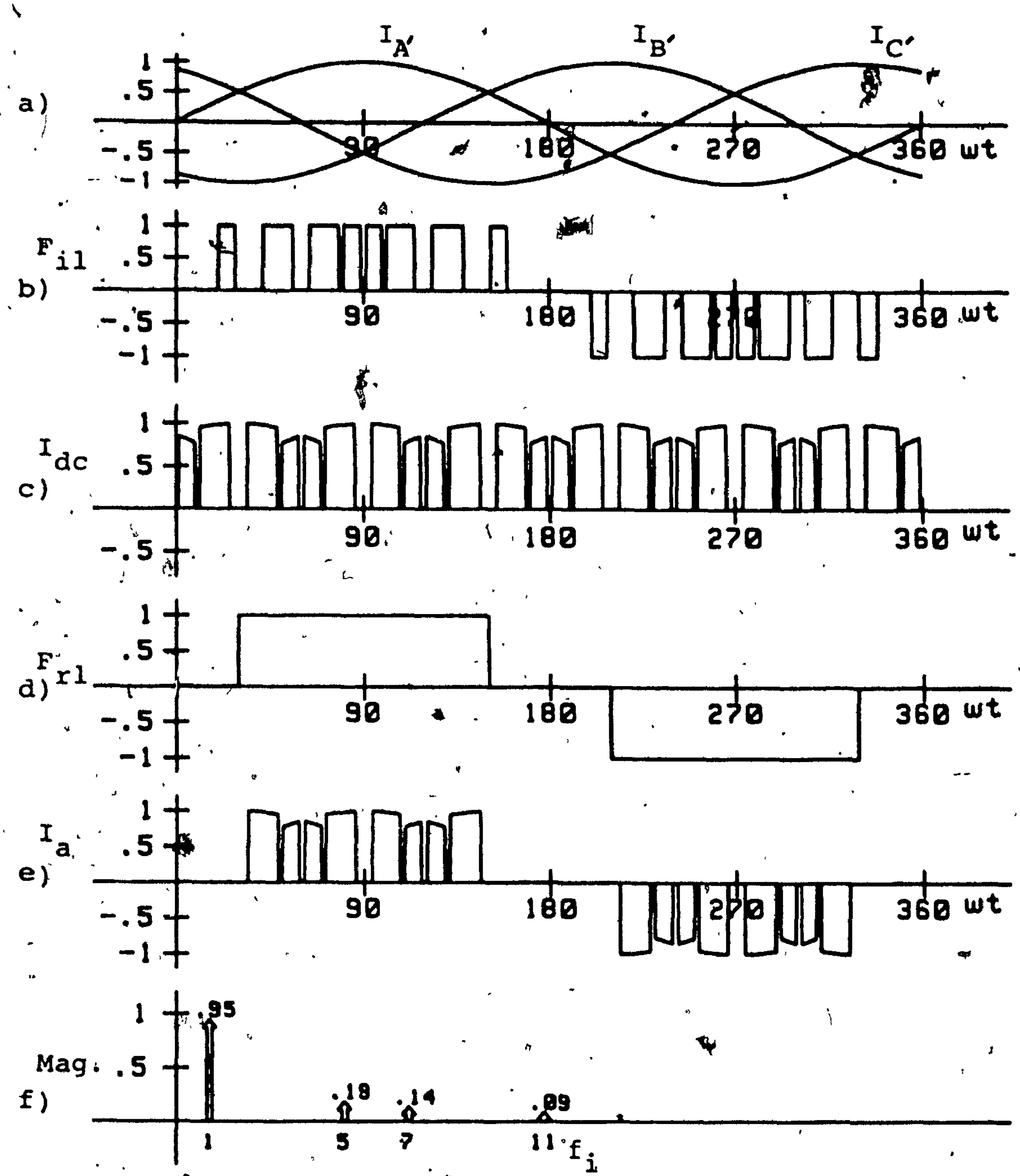

Fig. 3.13: Input current waveform obtained with IMO FCC scheme #1.
a) Three output phase current. b) Fictitious inverter SF (one of the three). c) Fictitious rectifier current. d) Fictitious rectifier SF (one of the three). e) Resulting input current. f) Analytically predicted frequency spectrum of I_a.

TABLE 3.6						
FREQUENCY SPECTRA OF WAVEFORMS ASSOCIATED WITH FCC INPUT CURRENT SHOWN IN FIG. 3.13						
Harmonic coefficients of inverter and rectifier switching function (Fig. 3.13b and 3.13d)				Harmonic coefficients of resulting input phase current, I_{an}, (Fig. 3.13e) for f_o = 75 Hz = 1.25 f_i		
Inverter SF		Rectifier SF		Amplitude, I_{an}		
Order (k)	Amplitude (B_k)	Order (n)	Amplitude (A_n)	Order (kf_i)	(1) p.u.	(1) %
				$0.5f_i$	0.00105	0.11
1	0.99	1	1.10	f_i	0.95	95
5	--	5	0.22	$5f_i$	0.19	19
7	0.01	7	0.16	$7f_i$	0.14	14
11	0.11	11	0.10	$11f_i$	0.09	9
13	0.26	13	0.09	$13f_i$	0.07	7
17	0.26	17	0.07	$17f_i$	0.06	6
19	0.10	19	0.06	$19f_i$	0.05	5

(1) Output phase currents have been taken as 1 p.u. current and 100% current.

3.5.2 IMO FCC Scheme #2

A different class of IMO FCC scheme with mixed modulation is shown in Fig. 3.14. In this scheme rectifying SF is MSPWM and inverting SF is single pulse. The advantage of this over the previous scheme #1 is that it yields subharmonics free output voltage waveform at substantially higher f_o value. However, low order harmonics in V_{AB} cannot be eliminated with this technique, as shown in Table 3.7.

Input current and respective frequency spectrum are shown in Fig. 3.15 and Table 3.8. The input current spectrum is, however, better than the previous scheme, i.e. low order harmonics are eliminated.

3.5.3 IMO FCC Scheme #3

Another class of IMO FCC scheme with mixed modulation is shown in Fig. 3.16 and 3.17. In this case MSPWM switching function is applied to both the rectifying and inverting stages. Complete spectral separation, like scheme #2, is not possible in this scheme. The solution in this case is to select the number of pulses of the "rectifying" function (Fig. 3.16b) and of the "inverting" function (Fig. 3.16d) such that the condition $n\omega_i = k\omega_o$, (3.17) is never satisfied. The simplest approach in this case is to maintain "rectifying" switching patter fixed (since input frequency, f_i is fixed) and vary the number of pulses of the "inverting" function (as the output frequency, f_o varies). IMO FCC output voltage and input current spectra obtained with this

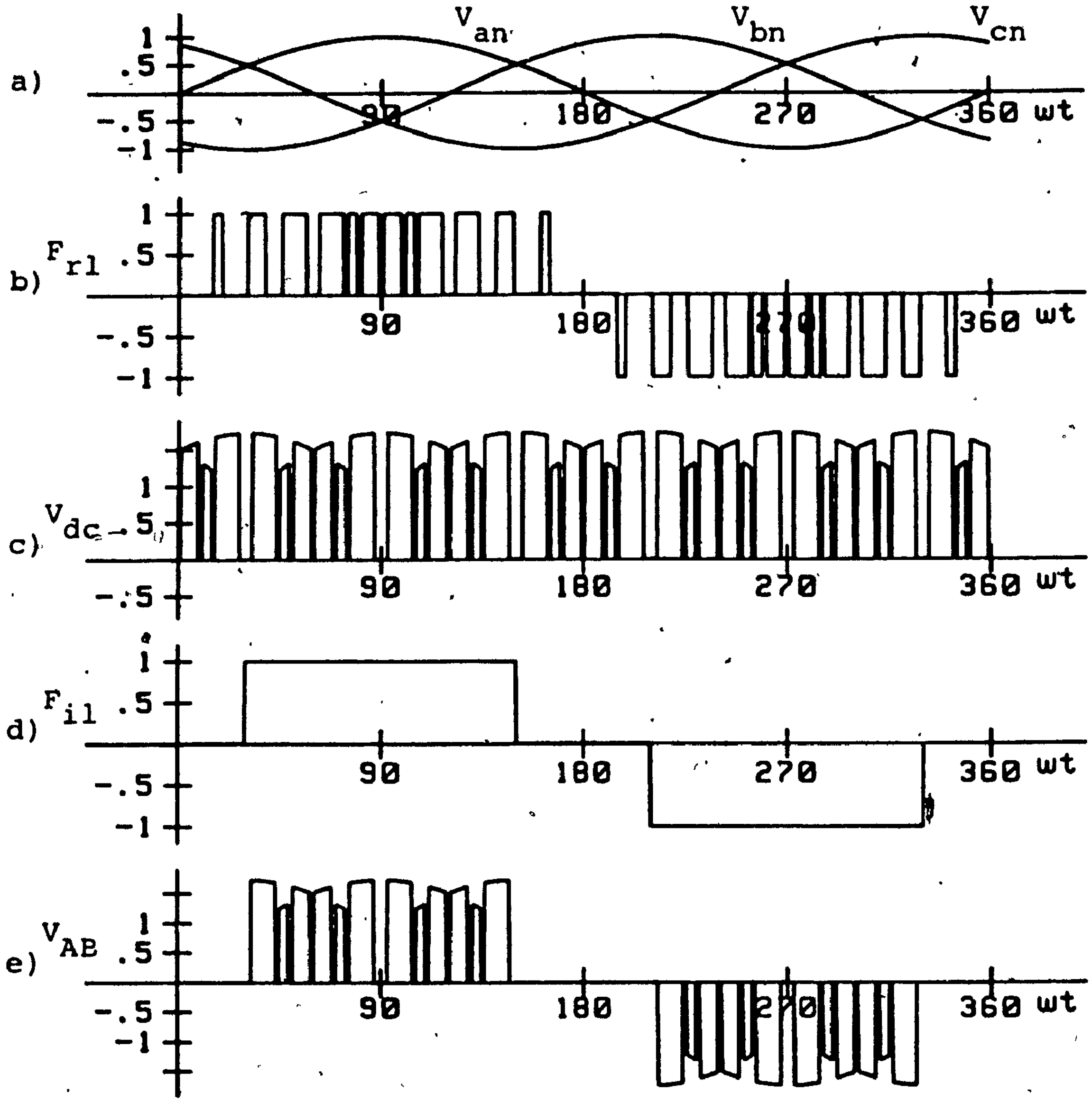

Fig. 3.14: Output voltage waveform obtained with IMO FCC scheme #2. a) Three input voltages. b) Fictitious rectifier SF (one of the three) c) Fictitious rectifier voltage. d) Fictitious inverter SF (one of the three). e) Resulting output line voltage, V_{AB}.

TABLE 3.7

FREQUENCY SPECTRA OF WAVEFORMS ASSOCIATED WITH FCC OUTPUT VOLTAGE SHOWN IN FIG. 3.14

Harmonic coefficients of rectifier and inverter switching function (Fig. 3.14b and 3.14d)				Harmonic coefficients of resulting output phase voltage, V_{AN} (Fig. 3.14e) for $f_o = 75$ Hz $= 1.25f_i$		
Rectifier SF		Inverter SF		Amplitude, V_{AN}		
Order (n)	Amplitude (A_n)	Order (k)	Amplitude (B_k)	Order (kf_o)	(1) p.u.	(1) %
1	0.99	1	1.10	f_o	0.95	95
3	--	3	--	$5f_o$	0.20	20
5	--	5	0.22	$7f_o$	0.14	14
7	--	7	0.16	$11f_o$	0.09	9
9	--	9	--	$13f_o$	0.07	7
11	0.11	11	0.10	$13.4f_o$	0.08	8
13	0.26	13	0.09	$15.4f_o$	0.08	8
15	--	15	--	--		
17	0.26	17	0.07	--		

(1) Input phase voltages have been taken as 1 p.u. volt and 100% volt.

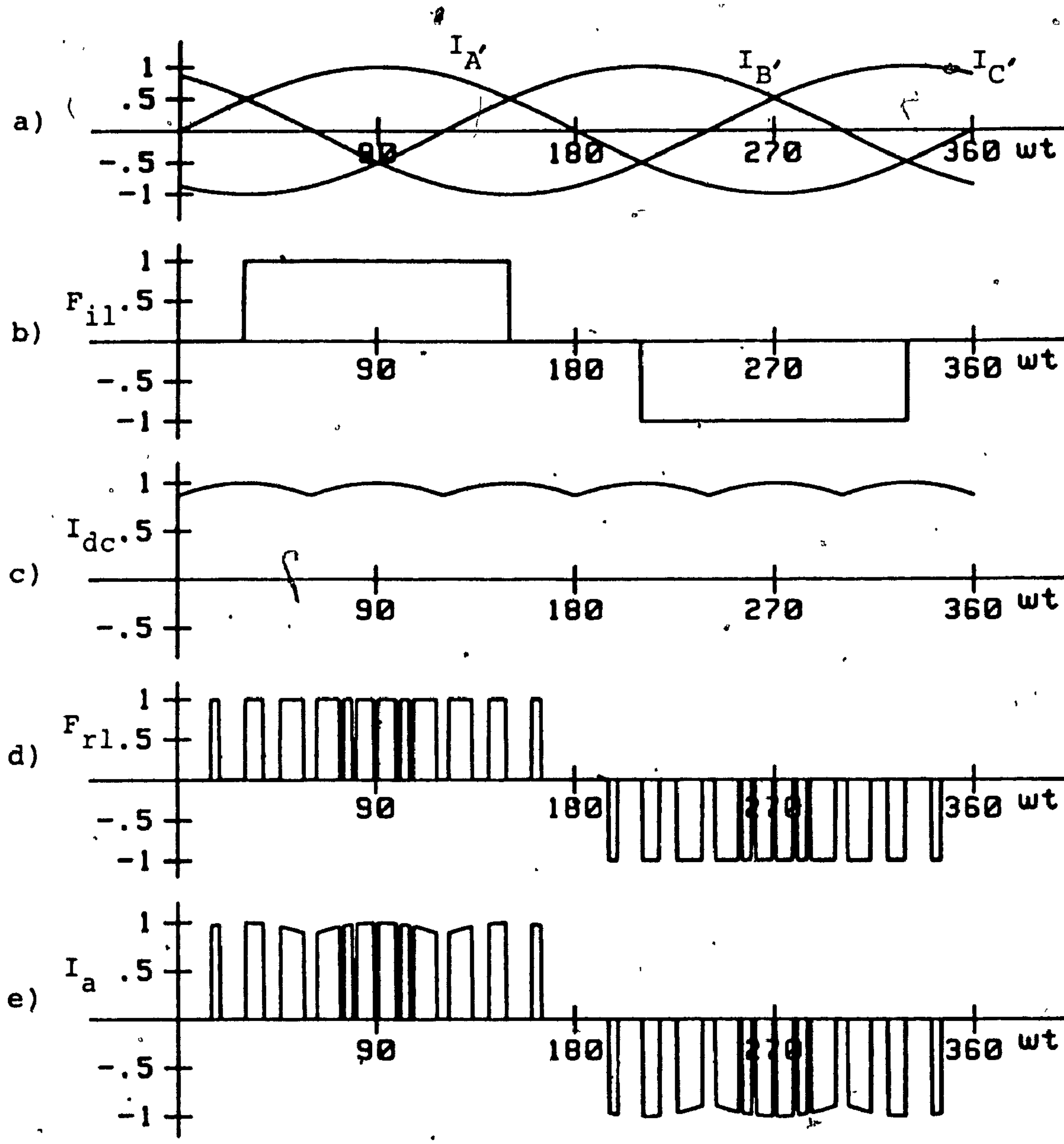

Fig. 3.15: Input current waveform obtained with IMO FCC scheme #2. a) Three output phase current. b) Fictitious inverter SF. c) Fictitious rectifier current, I_{dc}. d) Fictitious rectifier SF. e) Resulting input current, I_a.

TABLE 3.8

FREQUENCY SPECTRA OF WAVEFORMS ASSOCIATED WITH FCC INPUT CURRENT SHOWN IN FIG. 3.15

Harmonic coefficients of inverter and rectifier switching function (Fig. 3.15b and 3.15d)				Harmonic coefficients of resulting input phase current, I_{an}, (Fig. 3.15e) for f_o = 75 Hz = 1.25 f_i		
Inverter SF		Rectifier SF		Amplitude, I_{an}		
Order (k)	Amplitude (B_k)	Order (n)	Amplitude (A_n)	Order (kf_i)	(1) p.u.	(1) %
1	1.10	1	0.99	f_i	0.96	96
3	--	3	--	$7f_i$	0.01	1
5	0.22	5	--	$11f_i$	0.08	8
7	0.16	7	--	$13f_i$	0.28	28
9	--	9	--	$17f_i$	0.25	25
11	0.10	11	0.11	$19f_i$	0.10	10
13	0.09	13	0.26	$23f_i$	0.04	4
17	0.07	17	0.26			
19	0.06	19	0.10			

(1) Output phase currents have been taken as 1 p.u. current and 100% current.

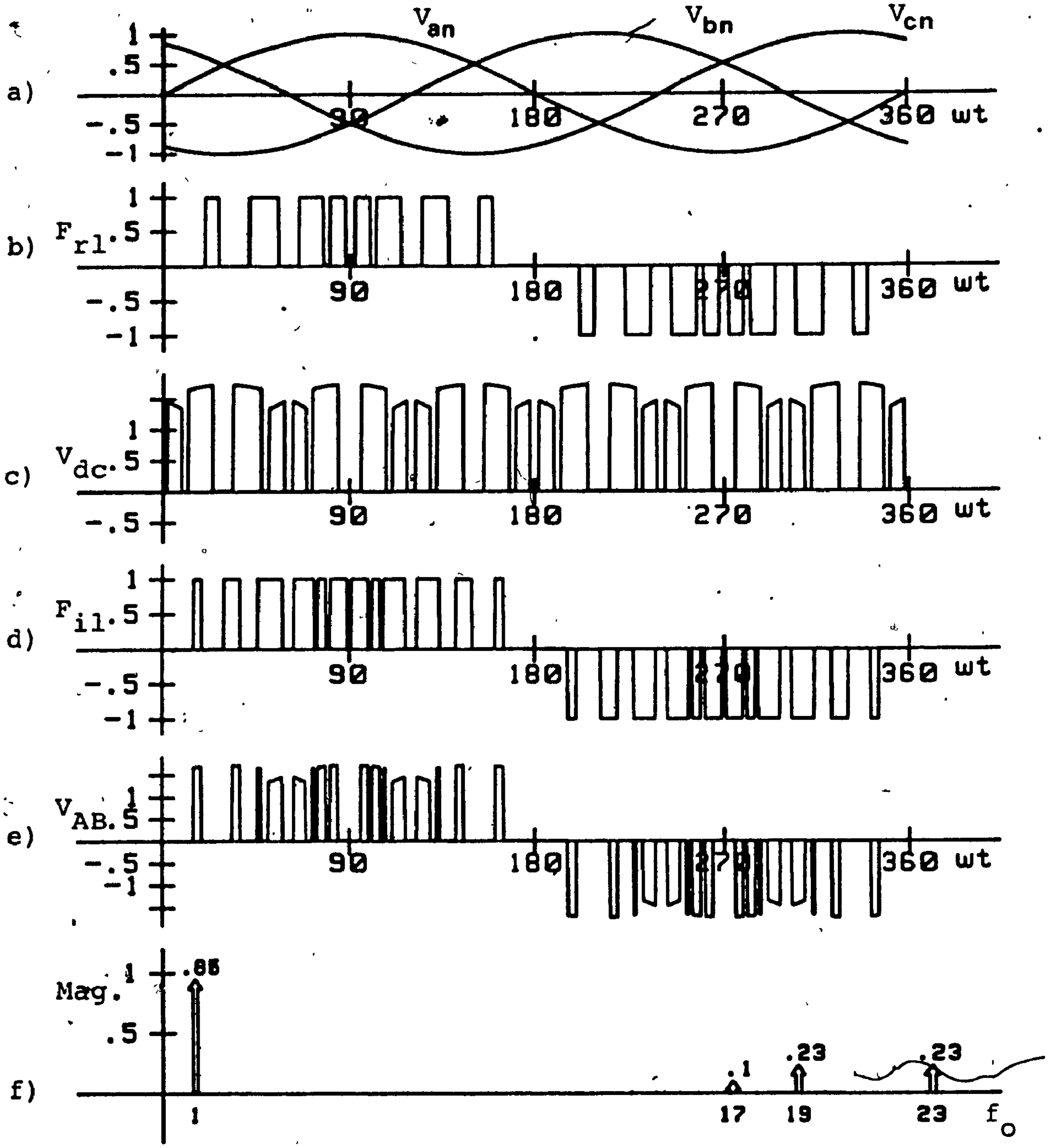

Fig. 3.16: Output voltage waveform obtained with IMO FCC scheme #3.
a) - e) Process of output voltage, V_{AB} construction.
f) Analytically predicted frequency spectrum of V_{AB}.

TABLE 3.9						
FREQUENCY SPECTRA OF WAVEFORMS ASSOCIATED WITH FCC OUTPUT VOLTAGE SHOWN IN FIG. 3.16						
Harmonic coefficients of rectifier and inverter switching function (Fig. 3.16b and 3.16d)				Harmonic coefficients of resulting output phase voltage, V_{AN} (Fig. 3.16e) for f_o= 75 Hz = 1.25f_i		
Rectifier SF		Inverter SF		Amplitude, V_{AN}		
Order (n)	Amplitude (A_n)	Order (k)	Amplitude (B_k)	Order (kf_o)	(1) p.u.	(1) %
1	0.99	1	0.99	0.2f_o	0.02	2
3	--	3	--	f_o	0.86	86
5	--	5	--	3.8f_o	0.02	2
7	--	7	--	4.6f_o	0.02	2
9	--	9	--	13.4f_o	0.06	6
11	--	11	--	15.4f_o	0.06	6
13	--	13	--	17f_o	0.10	10
15	--	15	--	18.2f_o	0.06	6
17	0.11	17	0.11			
19	0.26	19	0.15	19f_o	0.22	22

(1) Input phase voltages have been taken as 1 p.u. volt and 100% volt.

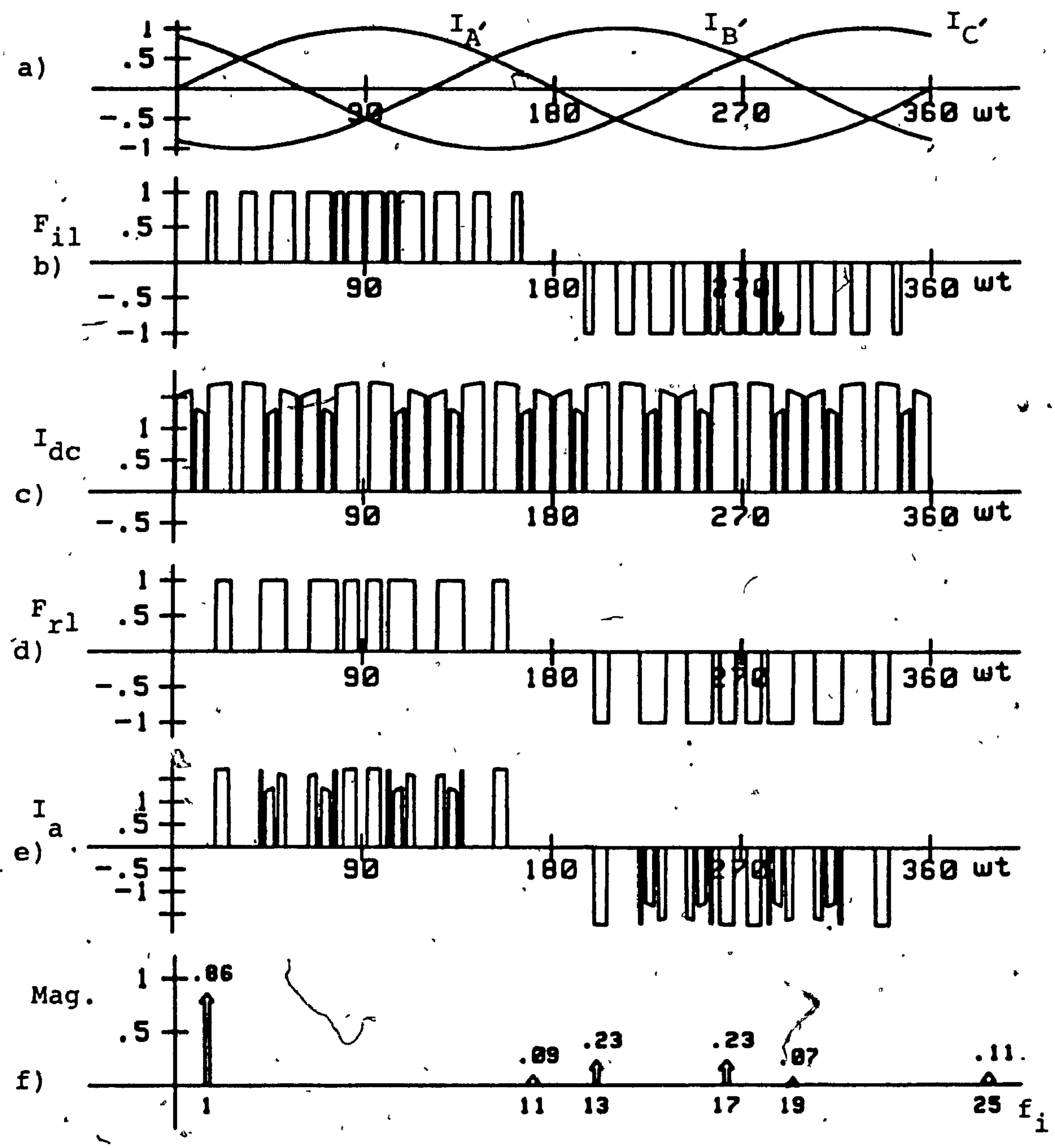

Fig. 3.17: Input current waveform obtained with IMO FCC Scheme #3.
a) - e) Process of input current, I_a construction.
f) Analytically predicted frequency spectrum of I_a.

TABLE 3.10						
FREQUENCY SPECTRA OF WAVEFORMS ASSOCIATED WITH FCC INPUT CURRENT SHOWN IN FIG. 3.17						
Harmonic coefficients of inverter and rectifier switching function (Fig. 3.17b and 3.17d)				Harmonic coefficients of resulting input phase current, I_{an}, (Fig. 3.17e) for $f_o = 75$ Hz $= 1.25\ f_i$		
Inverter SF		Rectifier SF		Amplitude, I_{an}		
Order (k)	Amplitude (B_k)	Order (n)	Amplitude (A_n)	Order (kf_i)	(1) p.u.	(1) %
				$0.5f_i$	0.02	2
1	0.99	1	0.99	f_i	0.86	86
3	--	3	--	$3.5f_i$	0.02	2
5	--	5	--	$7f_i$	0.02	2
7	--	7	--	$11f_i$	0.02	2
11	--	11	--	$17f_i$	0.10	10
13	--	13	--	$19f_i$	0.22	22
17	0.11	17	0.11			
19	0.26	19	0.26			

(1) Output phase currents have been taken as 1 p.u. current and 100% current.

sub-harmonics control strategy are shown in Tables 3.9 and 3.10 respectively for a particular ratio of output to input frequencies. Contents of these table verify the effectiveness of the proposed strategy. Low order harmonics from output voltage and input current as well as significant sub- harmonics is eliminated.

3.5.4 IMO FCC Scheme #4

The final class of IMO FCC scheme with mixed modulation is shown in Figs. 3.18 and 3.19. In this case both switching functions are single pulse. This scheme produces the maximum output of 105% (of input voltage), (Table 3.11). However, its output voltage spectrum contains 5th and 7th harmonics of 21% and 15% respectively of the fundamental component. This is typical of a 6 diode bridge rectifiers. And the input current fundamental component is also 105% (of output current), (Table 3.12). But, as usual it contains 5th and 7th harmonics of significant amplitudes. This scheme may not be suitable for high performance system, but is quite effective for systems which are insensitive to harmonics.

3.6 Evaluation of the Schemes

To facilitate the evaluation of the FCC, DMO and IMO schemes discussed in this chapter, the main features of each scheme are summarized and presented in Table 3.13. These features imply that regarding voltage utilization, harmonic distortion, switching frequencies, and complexity of imple-

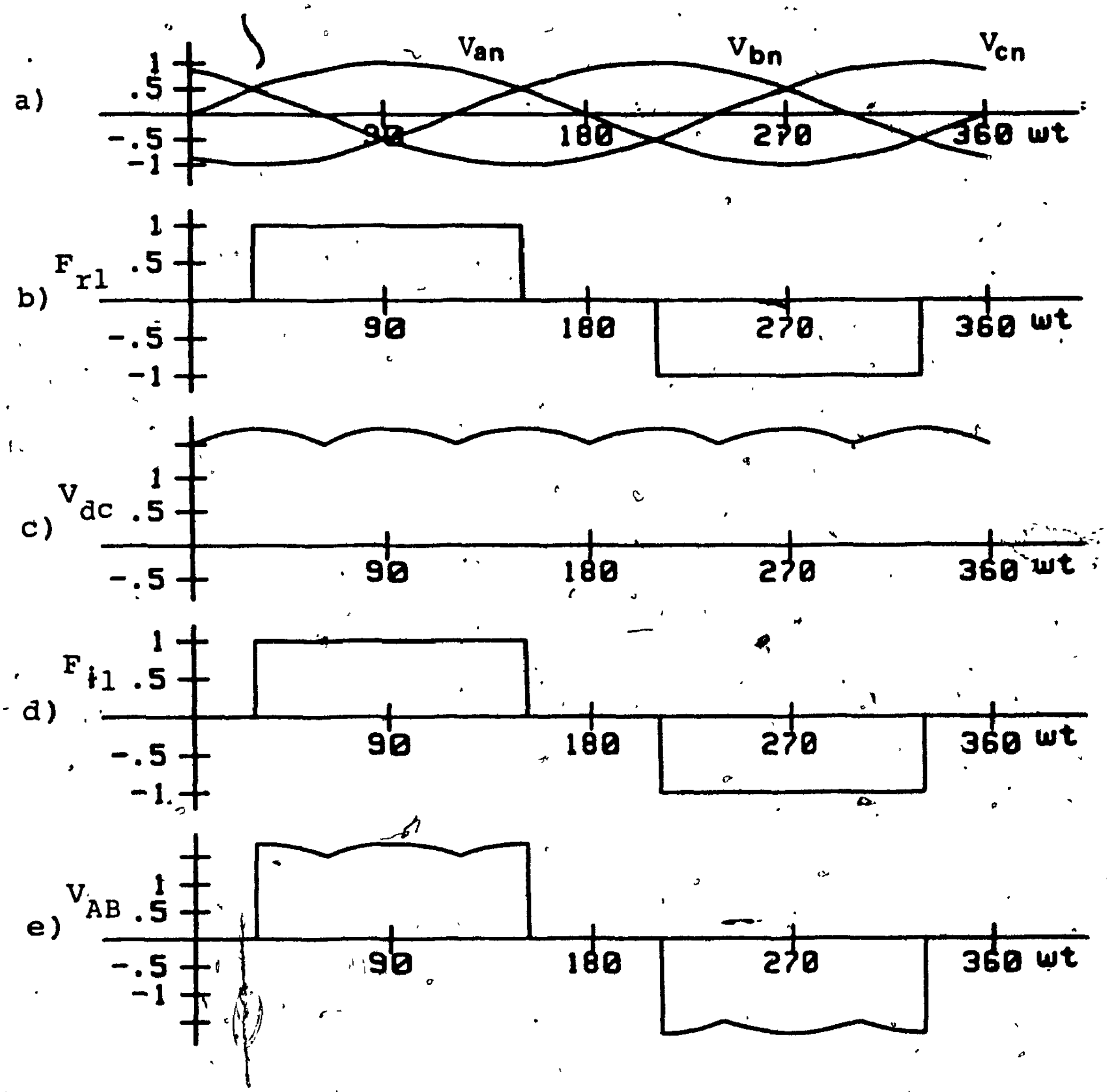

Fig. 3.18: Output voltage waveform obtained with IMO FCC Scheme #4.

TABLE 3.11						
FREQUENCY SPECTRA OF WAVEFORMS ASSOCIATED WITH FCC OUTPUT VOLTAGE SHOWN IN FIG. 3.18						
Harmonic coefficients of rectifier and inverter switching function (Fig. 3.18b and 3.18d)				Harmonic coefficients of resulting output phase voltage, V_{AN} (Fig. 3.18e) for $f_o = 75$ Hz $= 1.25f_i$		
Rectifier SF		Inverter SF		Amplitude, V_{AN}		
Order (n)	Amplitude (A_n)	Order (k)	Amplitude (B_k)	Order (kf_o)	(1) p.u.	(1) %
				$0.2f_o$	0.006	.6
1	1.10	1	1.10	f_o	1.05	105
				$3.8f_o$	0.03	3
3	--	3	--	$5f_o$	0.21	21
5	0.22	5	0.22	$5.8f_o$	0.03	3
7	0.16	7	0.16	$7f_o$	0.15	15
9	--	9	--			
11	0.10	11	0.10	$11f_o$	0.09	9
13	0.09	13	0.09	$13f_o$	0.08	8
15	--	15	--	$17f_o$	0.06	6
17	0.07	17	0.07	$19f_o$	0.06	6
19	0.06	19	0.06			

(1) Input phase voltages have been taken as 1 p.u. volt and 100% volt.

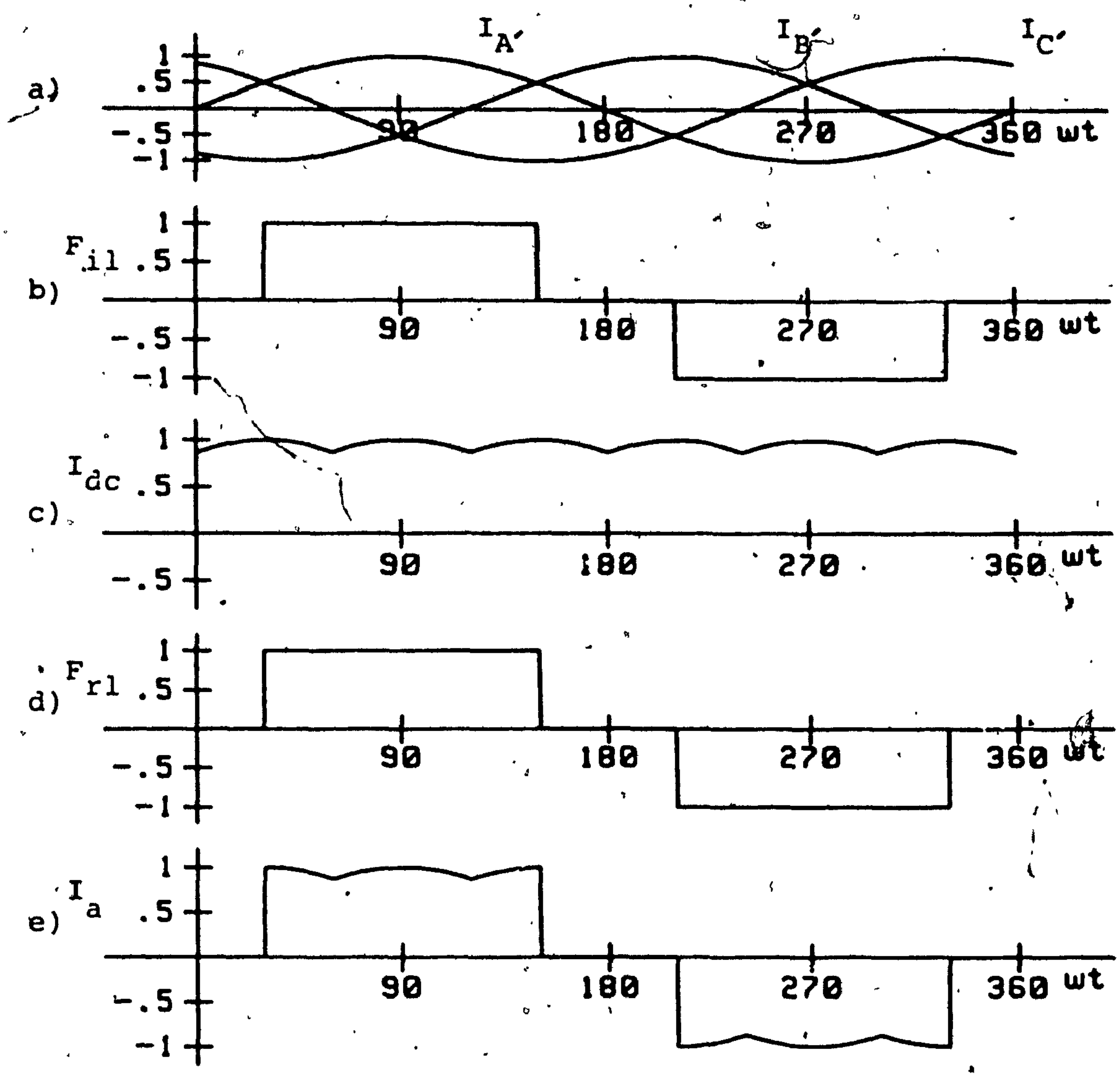

Fig. 3.19: Input current waveform obtained with IMO FCC Scheme #4.

TABLE 3.12						
FREQUENCY SPECTRA OF WAVEFORMS ASSOCIATED WITH FCC INPUT CURRENT SHOWN IN FIG. 3.19						
Harmonic coefficients of inverter and rectifier switching function (Fig. 3.19b and 3.19d)				Harmonic coefficients of resulting input phase current, I_{an}, (Fig. 3.19e) for f_o = 75 Hz = 1.25 f_i		
Inverter SF		Rectifier SF		Amplitude, I_{an}		
Order (k)	Amplitude (B_k)	Order (n)	Amplitude (A_n)	Order (kf_i)	(1) p.u.	(1) %
				$0.5f_i$	0.004	.4
1	1.10	1	1.10	f_i	1.05	105
3	--	3	--	$5f_i$	0.21	21
5	0.22	5	0.22	$6.5f_i$	0.03	3
7	0.16	7	0.16	$7f_i$	0.15	15
11	0.10	11	0.10	$8.5f_i$	0.03	3
13	0.09	13	0.09	$11f_i$	0.10	10
15	--	15	--	$13f_i$	0.08	8
17	0.07	17	0.07	$17f_i$	0.06	6
19	0.06	19	0.06	$19f_i$	0.06	6

(1) Output phase currents have been taken as 1 p.u. current and 100% current.

mentation, each scheme has its own advantages and disadvantages. Consequently, respective PWM schemes should be chosen by carefully matching load requirements with the scheme characteristics. For example, if a truly unrestricted output frequency range is required and the load is rather insensitive to voltage harmonics then the DMO scheme #1 shown in Fig. 3.7 should be chosen. If, however, the output frequency range is limited within 0-180 Hz, then the IMO scheme #1 shown in Fig. 3.12 should be chosen because it combines high voltage utilization with low harmonic distortion.

3.7 Simulated Results

To verify key analytical results, the discussed FCC schemes are tested by simulating on a HP 9836 - DATA 6000 system. A dedicated computer program simulating the precise opening and closing of the nine bilateral switches (S_1 to S_9) is employed to generate the output voltage waveforms shown in Figs. 3.7, 3.9, 3.12, 3.14 and 3.16 (DMO Schemes #1 and #2, and IMO Schemes #1, #2, and #3). Further processing of these waveforms on the DATA 6000 waveform analyzer yields the respective frequency spectra shown in Fig. 3.20. Comparison between analytically predicted frequency spectra (Tables 3.1, 3.3, 3.5, 3.7, 3.9) and spectra obtained by simulation shows that they are in close agreement.

TABLE 3.13

PERFORMANCE CHARACTERISTICS OF DMO AND IMO SCHEMES SHOWN IN FIGS. 3.7-3.10 AND 3.12-3.17

Criteria	DMO		IMO			
	Scheme #1 (Fig.3.7)	Scheme #2 (Fig.3. 9)	Scheme #1 (Fig.3.12)	Scheme #2 (Fig.3.14)	Scheme #3 (Fig.3.16)	Scheme #4 (Fig.3.18)
Output/ input voltage ratio	Average (0.83)	Low (0.50)	High (0.95)	High (0.95)	Average (0.85)	High (1.05)
Output frequency range	Unres-tricted	Unres-tricted	<180 Hz	<300 Hz	<300 Hz	<300 Hz
Attenua-tion of low order harmonics in output voltage/ input current	Low/low	High/high	High/low	Low/high	High/high	Low/low
Subhar-monics in output voltage/ input current	None	None	Negligible	Negligible	Can be controlled to an acceptable level	Negligible
Switching frequen-cies	Average	High	High	High	High	Average
Control logic complexity	Average	High	High	High	High	Average

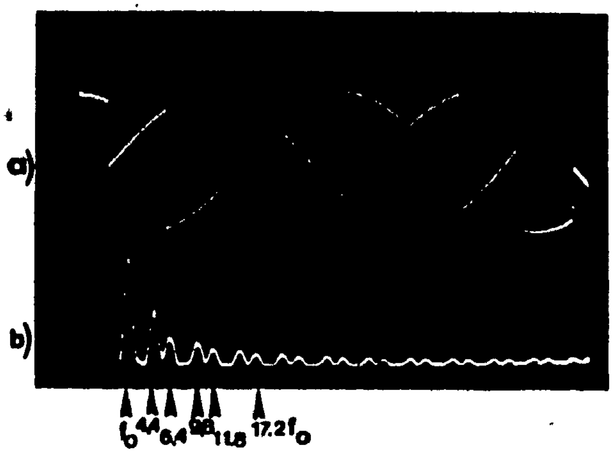

DMO Scheme #1 (Table 3.1)

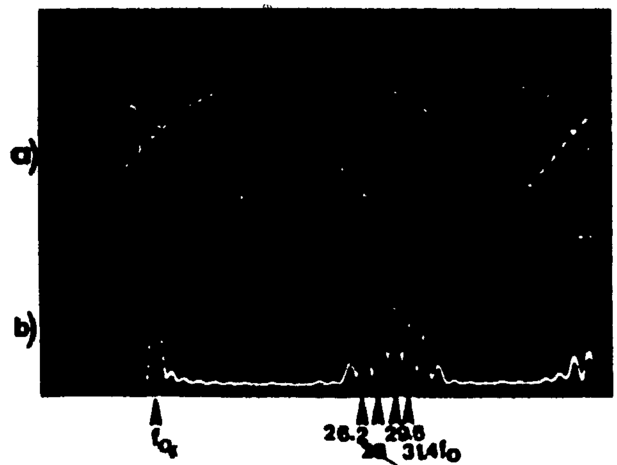

DMO Scheme #2 (Table 3.3)

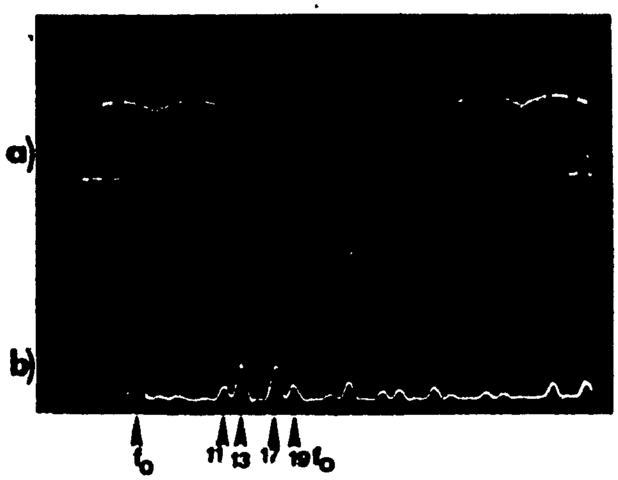

IMO Scheme #1 (Table 3.5)

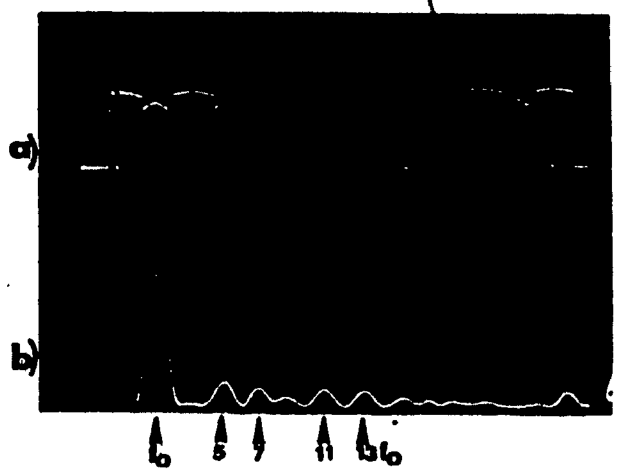

IMO Scheme #2 (Table 3.7)

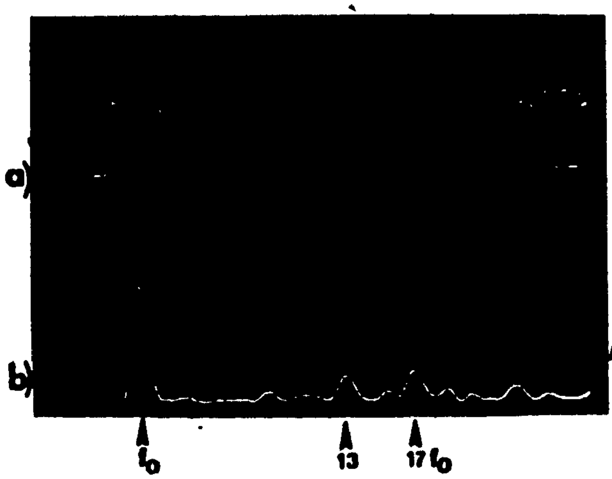

IMO Scheme #3 (Table 3.9)

Fig. 3.20: Simulated waveforms associated with different schemes of three to three phase DMO & IMO FCC at f_o = 75 Hz.

a) Output line voltage, V_{AB}.

b) Respective frequency spectrum.

3.8 Design Criteria

Some FCC design aspects regarding component ratings, control logic and component protection are discussed in this section.

3.8.1 Component Ratings

The component ratings presented here have been derived under steady state operating conditions. Although these are not the worst case ratings, they are nevertheless essential for the completion of the converter 'base' design. Once 'base' design values have been established, worst case values can be estimated from; specified overload conditions and the interaction between circuit stray inductances and circuit snubber components.

In determining the current ratings for each of the nine FCC switches, it is noted that the worst case condition interval is 120°. Conduction of more than 120° interval for any switch is equivalent to short circuiting the source, which is not desirable. Therefore, with inductive load;

- Peak switch current, $\hat{I}_s$ = Peak rated load line current, $\hat{I}_\ell$,
- RMS switch current, $I_R = \hat{I}_\ell/\sqrt{6}$
- Average switch current, $\bar{I}_{av} = \dfrac{2\hat{I}_\ell}{3\pi}$.

Finally, the 'base' peak switch blocking voltage V_{FB} is equal to the respective peak input line to line source voltage.

3.8.2 Control Logic

FCC have special logic control requirements because of the complexities of associated power circuits and power conversion requirements. The aspects include: the derivation of the appropriate switching functions, the processing of the gating signals from their respective functions, and finally the development of the circuitry required to implement the above mentioned functions and signal processing.

Deriving the gating/timing signals for DMO FCC is simpler than the IMO FCC signals. There are three input voltages and three components F_1, F_2, F_3 of converter transfer function. These two waveforms combine to produce the required gating signals. These can be explained by a block diagram shown in Fig. 3.21a. The derivation and implementation of this control signals and circuits are described in Appendix B.

The first step in organizing the IMO FCC control logic requirements (for the techniques illustrated in Figs. 3.12-3.19) is to observe that the respective output voltage waveform (i.e. Figs. 3.12e, 3.14e) are identical to the ones obtained with standard 3-ϕ PWM inverters. Therefore, the converter depicted in Fig. 3.1 can be viewed as a standard six-switch inverter (Fig. 3.22) supplied sequentially from input voltages V_{ab}, V_{ac}, V_{bc}, V_{ba}, V_{ca}, V_{cb}. This means that when, for example, input voltage V_{ab} is most positive the six-switch equivalent for the nine-switch converter is as shown in Fig. 3.22.

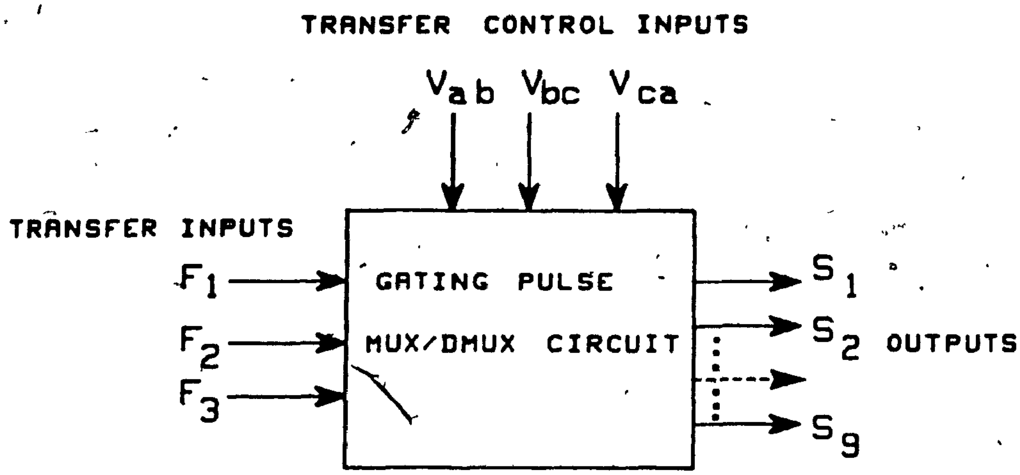

a) DMO cycloconverter.

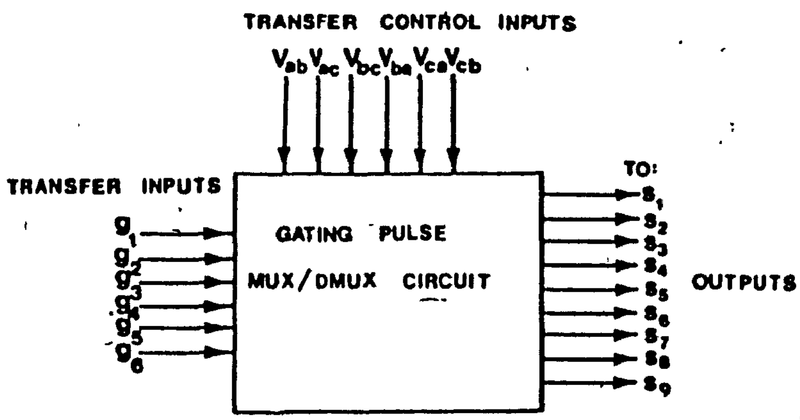

b) IMO cycloconverter.

Fig. 3.21: Block diagram representation of the process of deriving gating signals.

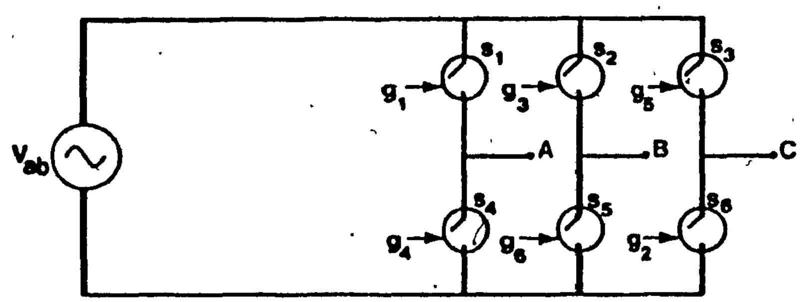

Fig. 3.22: Equivalent three-phase bridge inverter.

The exact correspondence between input voltages and groups of switches comprising the six-switch equivalent inverter, is shown in Table 3.14. This table also establishes the correspondence between the gating signals (g_1 - g_6) of the equivalent six-switch and the real nine-switch converter circuits as a function of the predominant (on of six) input voltage.

From these data and with reference to Figs. 3.1 and 3.22 the FCC control logic requirements are established as follows:

i) A PWM control technique that satisfies output voltage and input current requirements is first chosen. References [33], [37]-[39] comprise a good 'menu' to chose from.

ii) The gating signals g_1 to g_6 (Table 3.14) required to implement the aforementioned PWM technique on the equivalent six-switch inverter (Fig. 3.22) are next specified.

iii) A multiplexing/demultiplexing circuit (Fig. 3.21b) which assigns signals g_1 - g_6 to the nine IMO FCC switches (S_1-S_9) according to the Truth Table 3.14 is finally constructed by using standard logic blocks (Appendix B).

Table 3.14

	V_{ab}	V_{ac}	V_{bc}	V_{ba}	V_{ca}	V_{cb}
g_1	s_1	s_1	s_4	s_4	s_7	s_7
g_2	s_6	s_9	s_9	s_3	s_3	s_6
g_3	s_2	s_2	s_5	s_5	s_8	s_8
g_4	s_4	s_7	s_7	s_1	s_1	s_4
g_5	s_3	s_3	s_6	s_6	s_9	s_9
g_6	s_5	s_8	s_8	s_2	s_2	s_5

3.8.3 Component Protection

Providing effective switch protection in FCC circuits is a more difficult task than with most other converter circuits. The reason is that load current commutation in IMO FCC circuits must take place without the presence of free-wheeling doides. To illustrate this problem consider, for simplicity the chopper circuit shown in Fig. 3.23.

In this circuit it is assumed that switches SW_1 and SW_2 are of the (four quadrant) type shown in Fig. 3.1 and that the chopper is operating with continuous load current I_o. The obvious difficulty with this circuit is that the conduction intervals (and therefore gating signals) of SW_1 and SW_2 must be exactly complementary. Otherwise, if they overlap the two switches will be destroyed from the resulting short circuit across the dc source while if they do not overlap the two switches will again be destroyed from the release of the circuits inductive energy. Since a precisely complementary

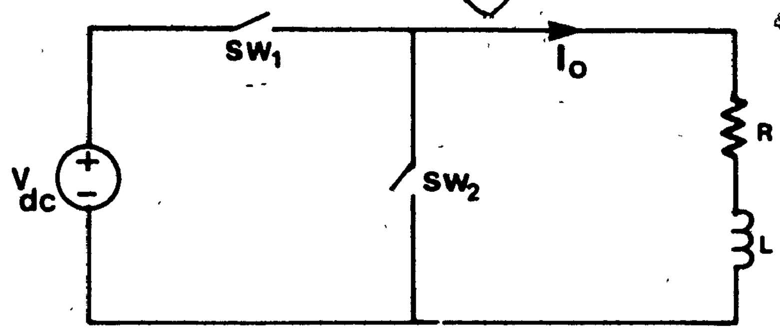

Fig. 3.23: A DC - to - DC converter circuit.

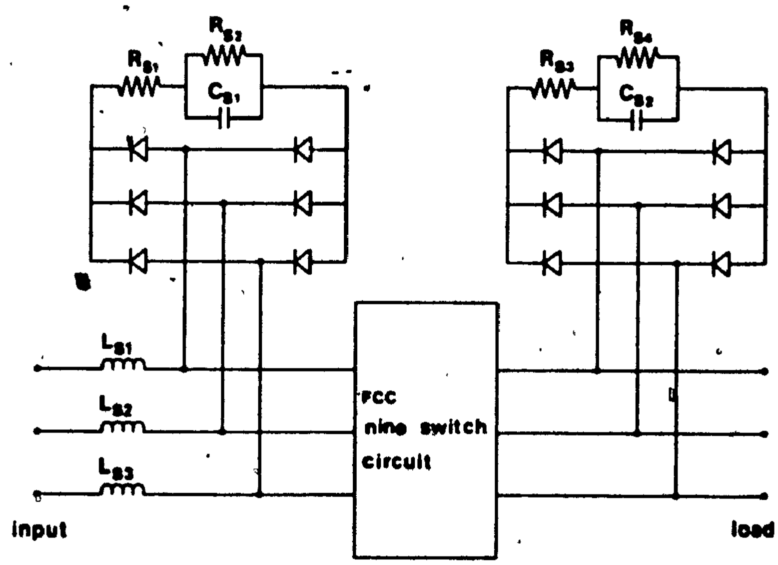

Fig. 3.24: The cycloconverter circuit showing protective elements.

switch performance cannot be guaranteed, special emphasis must be placed on the choice of proper snubber networks. An example of such a network is shown in Fig. 3.24. The function of each (network) component is as follows:

- Reactors L_{S1-2-3} facilitate current transition (i.e. commutation) from a turning off to a turning on switching device.
- Front-end snubber rectifier diverts input currents to storage element C_{S1} during converter normal or accidental switching transients.
- Load-end snubber rectifier diverts load currents to storage element C_{S2} during converter normal or accidental switching transients.
- Snubber capacitors C_{S1} and C_{S2} limit resulting over voltages during abovementioned transients.
- Resistors R_{S2} and R_{S4} act as energy 'bleeding' elements for C_{S1} and C_{S2}.
- Resistors R_{S1} and R_{S3} provide critical damping to the L-R-C path comprised by the snubber circuit components.

Finally, the design basis for this snubber circuit are provided in ref. [40].

3.9 Design Example and Experimental Results

In this section, some of the selected theoritical results obtained in sections 3.4 and 3.5 are verified experimentally on 3 phase 1KVA laboratory units with the following example;

- Rated KVA: 1 p.u. KVA/ph.
- Rated voltage: 1 p.u. V_{rms} (line to neutral)
- Input frequency: 60 Hz
- Output frequency: variable

Thus, from the above specifications, let

- 1 p.u. KVA/phase = 1000 VA
- 1 p.u. V_{rms}/phase = 115 V
- 1 p.u. rms current = $\frac{1000}{3 \cdot 115}$ = 2.9 A
- 1 p.u. impedance = $\frac{115}{2.9}$ = 40 ohm

Therefore, the base switch ratings are

- Peak switch current, $\hat{I}_s = \sqrt{2} \cdot 2.9 = 4.1$ A
- RMS switch current, $I_R = \frac{\hat{I}_\ell}{\sqrt{3}} = \frac{4.1}{\sqrt{3}} = 2.37$ A
- Average switch current, $\bar{I}_{av} = \frac{2\hat{I}_\ell}{3\pi} = 0.87$ A

Experimental results obtained with IMO cycloconverter constructed with the specific component values derived here are shown in Figs. 3.25 to 3.29. These experimental waveforms have been recorded by using DATA 6000 waveform analyser to display their respective frequency spectrum. Fig. 3.25 shows the output line voltage and output phase current for f_i= 60 Hz, f_o= 60 Hz for IMO scheme #1. Fig. 3.26 shows the output and input voltage and currents and their frequency spectra for the same scheme. Their frequency spectra is in close agreement with the spectra shown in Figs. 3.12f and a)

b)

a) Output line voltage, V_{AB}

b) Output phase current, I_A,

Fig. 3.25: Experimental input/output voltage/current waveforms obtained with three-phase to three-phase FCC for IMO Scheme #1.

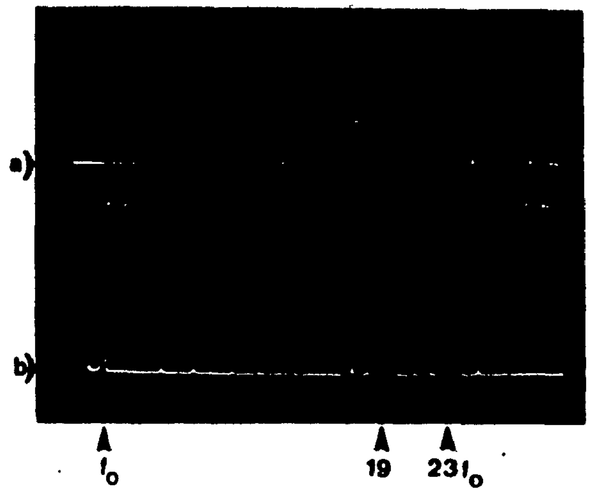

A. a) Output line voltage, V_{AB} (Fig. 3.12e).
b) Respective frequency spectrum (Fig. 3.12f).

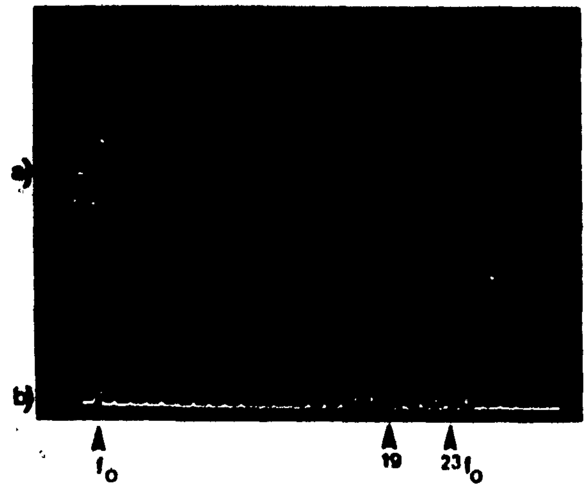

B. a) Output line current, I_A.
b) Respective frequency spectrum.

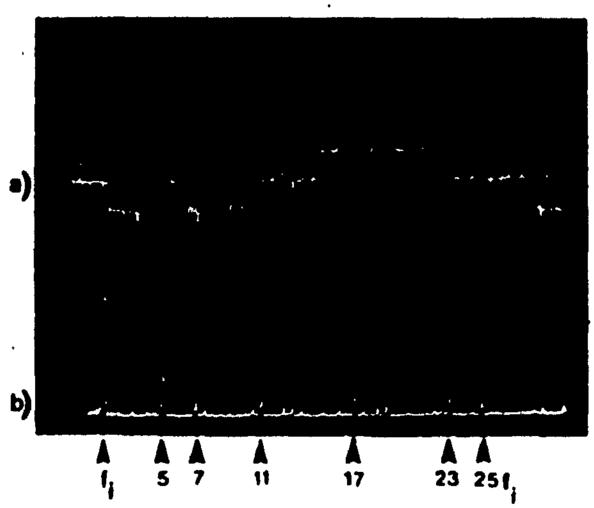

C. a) Input current, I_a (Fig. 3.13e).
b) Respective frequency spectrum (Fig. 3.13f).

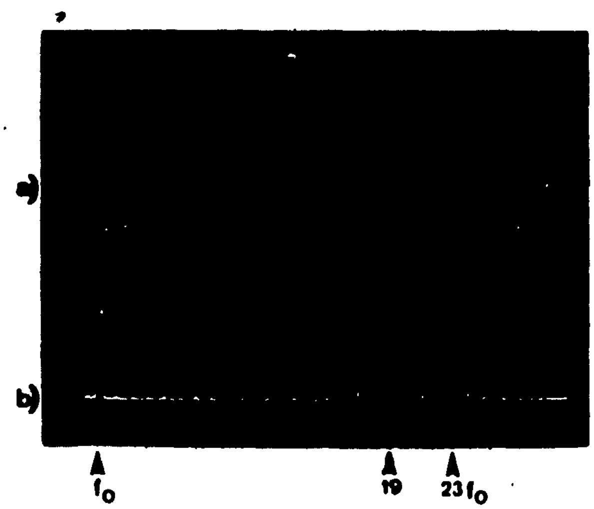

D. a) Output phase current, $I_{A'}$.
b) Respective frequency spectrum.

Fig. 3.26: Experimental input/output voltage/current waveforms obtained with three-phase to three-phase FCC for IMO Scheme #1, delta connected resistive load at M_f= 0.8, f_i= 60 Hz, and f_o=60 Hz.

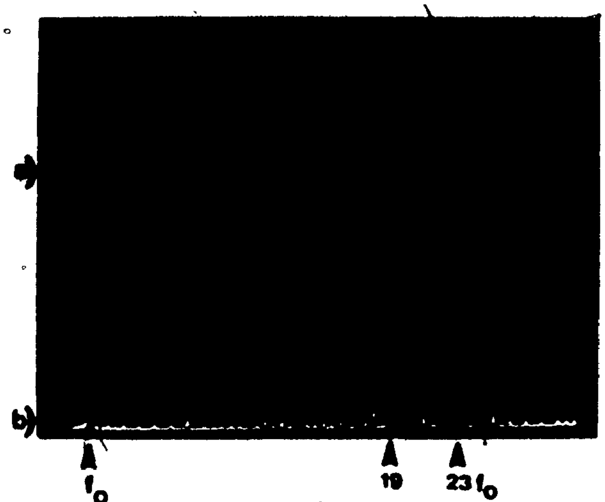

A. a) Output line voltage, V_{AB}.
b) Respective frequency spectrum.

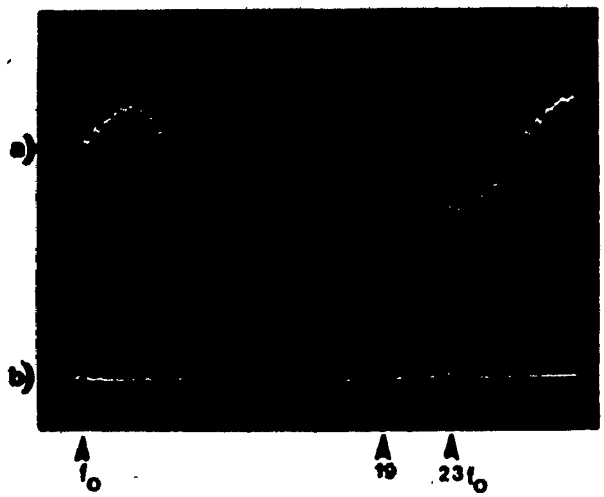

B. a) Output line current, I_A.
b) Respective frequency spectrum.

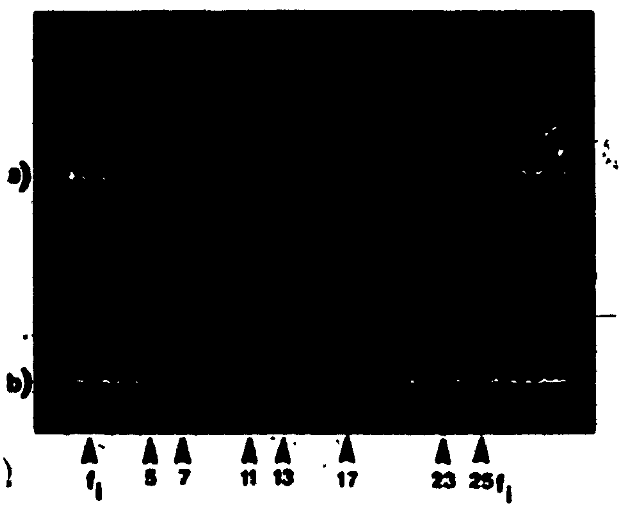

C. a) Input current, I_a.
b) Respective frequency spectrum.

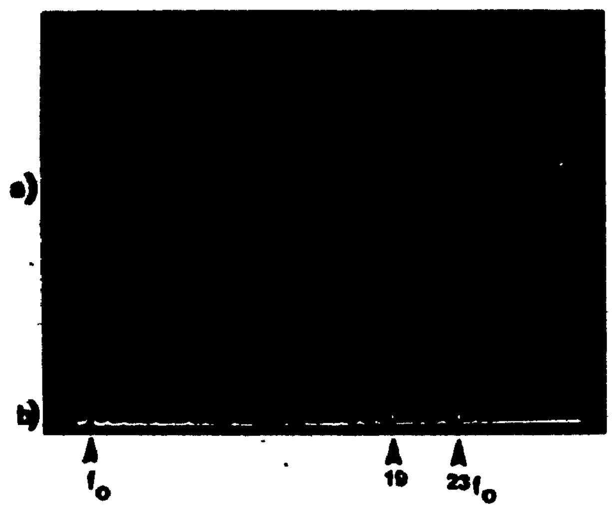

D. a) Output phase current, I_A'.
b) Respective frequency spectrum.

Fig. 3.27: Experimental input/output voltage/current waveforms for IMO Scheme #1 with delta connected R-L load (p.f. = 0.8), at M_f = 0.8, f_i = 60 Hz and f_o = 60 Hz.

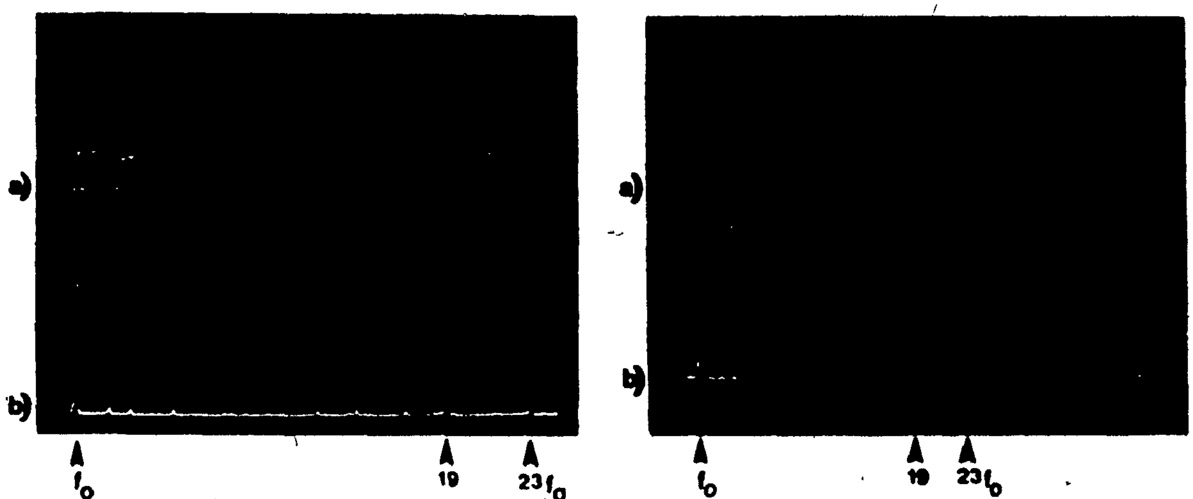

A. a) Output voltage, V_{AB} at 75 Hz.
b) Respective frequency spectrum.

B. a) Output voltage, V_{AB} at 90 Hz.
b) Respective frequency spectrum.

Fig. 3.28: Experimental output voltages for IMO Scheme #1 at different output frequency with M_f = 0.8 and delta connected resistive load.

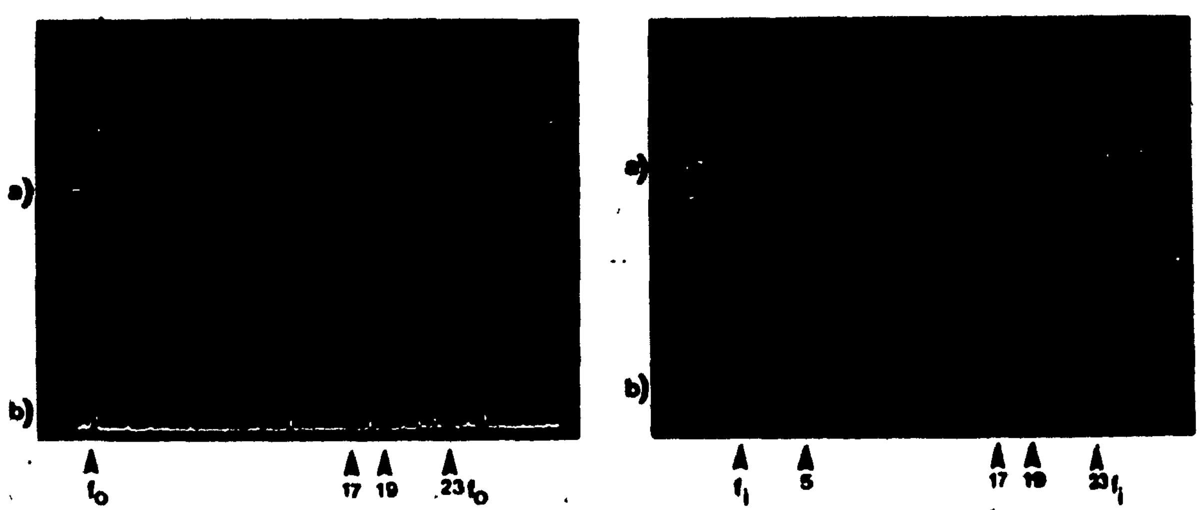

A. a) Output line voltage, V_{AB} (Fig. 3.16).
b) Respective frequency spectrum.

B. a) Input current, I_a (Fig. 3.17).
b) Respective frequency spectrum.

Fig. 3.29: Experimental input/output voltage/current waveforms for IMO scheme #3, delta connected resistive load at M_f = 0.8, f_i = 60 Hz, f_o = 60 Hz.

3.13f. Fig. 3.27 shows the same waveforms for a resistive-inductive load, i.e. p.f. 0.8. Output currents have become sinusoidal in this case. Figs. 3.28 A and B show output voltage waveforms at f_o = 75 Hz and 90 Hz respectively. IMO scheme #3 output voltage and input current waveforms are shown in Figs. 3.29 A and B. They agree with the predicted spectra of Figs. 3.16f and 3.17f. All these waveforms are unfiltered. Filtering will obviously improve the quality of waveforms.

3.10 Conclusions

A comprehensive analysis for several FCC schemes for three phase to three phase conversion has been presented in this chapter. Performance evaluation and related design data are provided for implementation of the structures. Detailed input current, output voltage harmonic analysis has shown that the proposed schemes yield effective suppression of low-order harmonics while they can offer up to 100 percent output-to-input voltage transfer ratio.

A method for generating the required converter gating signals and a snubber circuit for providing effective switch protection have also been discussed.

Simulated results are provided for comparison purpose. Finally, predicted FCC features such as input/output waveforms, associated harmonic spectra, and voltage transfer ratio have been verified experimentally on 1 KVA experimental breadboards.

CHAPTER 4

THREE PHASE TO SINGLE PHASE CYCLOCONVERTER

4.1 Introduction

There are many single phase applications, where variable frequency power is required. These types of loads could be normally supplied from a single-phase to single-phase cycloconverter. However, this can cause unbalance in three phase ac mains if a substantial amount of power is required. An alternative solution is to supply the variable frequency single phase load from a three-phase to single-phase cycloconverter, thereby distributing equal stresses on all three input phases.

The three phase to single phase cycloconverter could be of half-bridge or full bridge configuration depending on the output power requirement. The four switch configuration (half-bridge) requires less number of components and simpler control logic units than the six switch (full-bridge) configuration. However, full-bridge converter configuration is versatile and can deliver twice the amount of power than the half-bridge converter.

The object of this chapter is to select the most suitable scheme, the control logic circuit and subsequently analyse the various configurations to suit different types of load requirements.

Finally, experimental results from a prototype cycloconverter are compared and verified with the analytically predicted results.

4.2 Converter Configurations

This three phase to single phase FCC configuration is derived from the generalized circuit configuration, Fig. 2.1, Chapter 2 by setting number of input phases, N=3 and number of output phases, M=1. Six switch full-bridge converter configuration capable of frequency/voltage transformation from three phase ac source to single phase ac, is shown in Fig. 4.1. This converter consists of six bilateral switches. This arrangement is particularly suitable when a neutral connection is unavailable. A converter structure with identical performance features of Fig. 4.1 employing only four switches is shown in Fig. 4.2. This topology is particularly suitable when a neutral from the ac source is available. However, the input current spectrum of this configuration is not as good as with the full bridge converter. Also an extra switch, S_4 becomes necessary for output voltage control.

4.3 Direct Mode of Operation (DMO) FCC

DMO FCC as discussed earlier in subsection 2.2.1, Chapter 2 requires only one switching function. Uniform PWM switching function (Fig. 3.3, Chapter 3) can be applied for both of these configurations. No attempt has been made to implement Venturini's scheme as his proposed sinusoidal PWM (Fig. 3.4, Chapter 3) has the serious disadvantage of low voltage gain. The equations for output voltage and input current waveforms for three to single phase cycloconversion

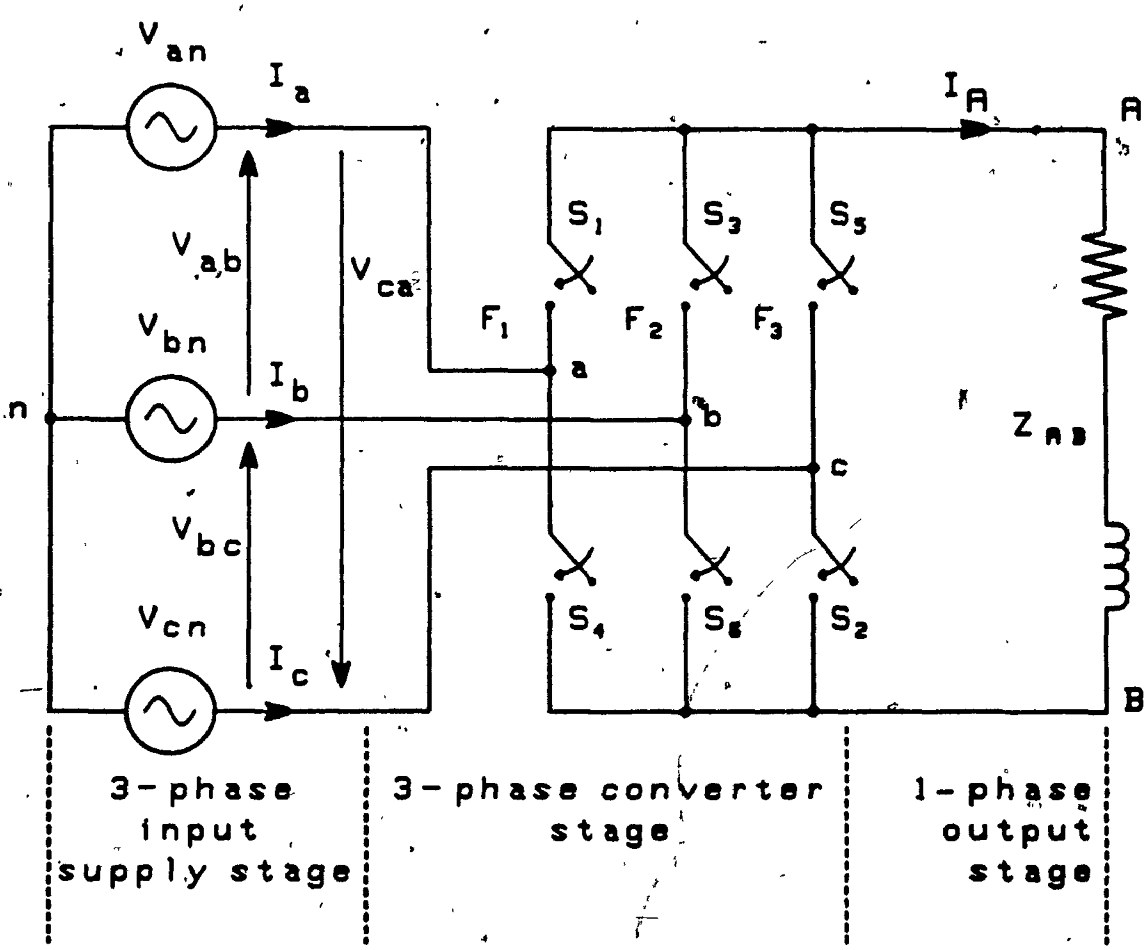

Fig. 4.1: Simplified circuit diagram of the proposed three-phase to single-phase FCC in full bridge configuration with no neutral available.

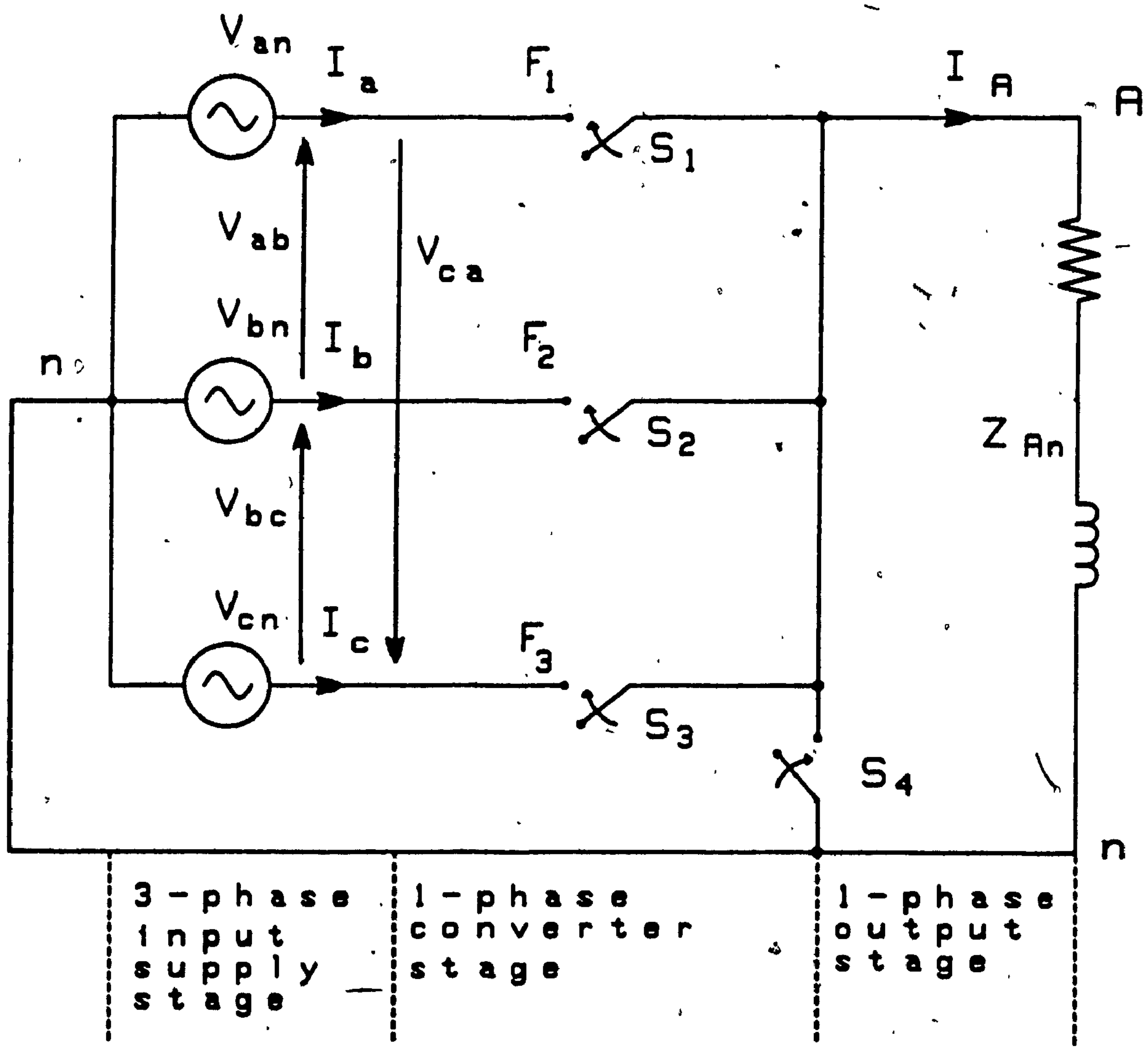

Fig. 4.2: Simplified circuit diagram of the proposed three-phase to single-phase FCC in half-bridge configuration with neutral available.

under DMO can be derived from the generalized equation ((2.1), Chapter 2) as follows,

$$V_{AN}=\frac{3A_1V_1}{2}\cos(\omega_o t)+\sum_{n=2,5,8}^{\infty}\frac{3A_nV_i}{2}\cos((n\omega_s+\omega_i)t)$$
$$+\sum_{n=4,7,10}^{\infty}\frac{3A_nV_i}{2}\cos((n\omega_s-\omega_i)t) \qquad (4.1)$$

and

$$I_a=\frac{A_1I_o}{2}\cos(\omega_i t)+\sum_{n=2,5,8}^{\infty}\frac{A_nI_o}{2}\cos((n\omega_s+\omega_o)t)$$
$$+\sum_{n=4,7,10}^{\infty}\frac{A_nI_o}{2}\cos((n\omega_s-\omega_o)t) \qquad (4.2)$$

Voltage control can be achieved by suitable modulation of the pulse widths. This principle has been discussed in sub-section 3.3.2 of Chapter 3.

4.3.1 Full Bridge Configuration Scheme #1

A simplified circuit diagram of the full bridge FCC, analysed in this subsection is shown in Fig. 4.1. Output voltage and input current waveforms are shown in Figs. 4.3 and 4.4. Corresponding frequency spectrum is tabulated in Tables 4.1 and 4.2. The voltage utilization as predicted in (2.17b), Chapter 2, is 96% of input phase voltage. However, the output voltage contains low order 8th and 10th harmonics of magnitude 0.19 and 0.14 respectively. Input current fundamental is 55% of output current. This is in a way

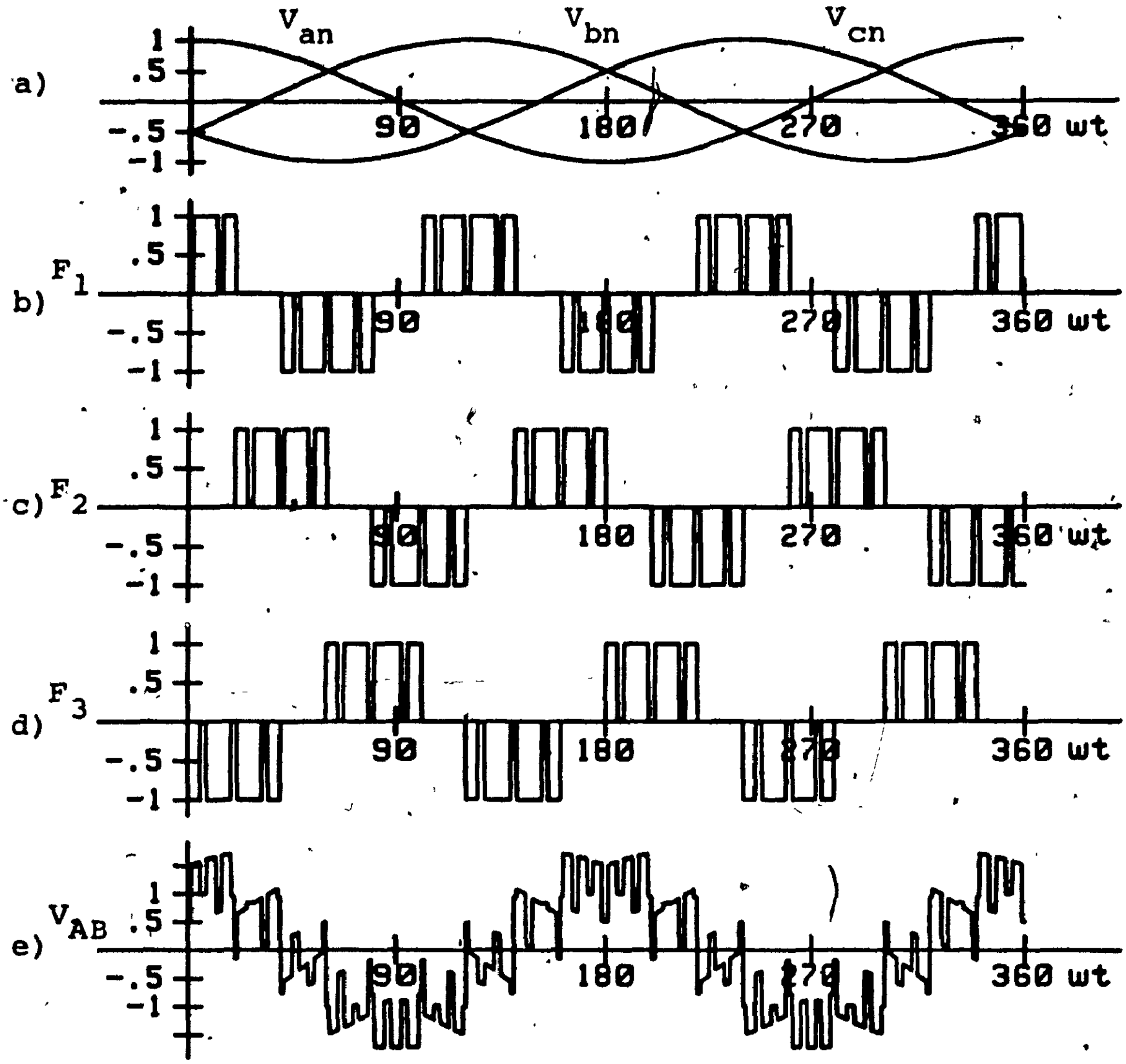

Fig. 4.3: Output voltage waveform obtained with three to single-phase full-bridge configuration DMO FCC scheme #1.
a) Three input phase voltages.
b) - d) F_1, F_2, F_3 switching function components.
e) Resulting output line voltage, V_{AB}.

TABLE 4.1

FREQUENCY SPECTRA OF WAVEFORMS ASSOCIATED WITH FCC OUTPUT VOLTAGE SHOWN IN FIG. 4.3

Harmonic coefficients of switching function (Fig. 4.3b)		Harmonic coefficients of resulting output phase voltage V_{AN}, (Fig. 4.3e) for $f_o = 120$ Hz $= 2 f_i$		
			Amplitude, V_{AN}	
Order (n)	Amplitude (A_n)	Order (kf_o)	(1) p.u.	(1) %
1	1.10	f_o	0.96	96
3	--	$8f_o$	0.19	19
5	0.22	$10f_o$	0.14	14
		$17f_o$	0.09	9
7	0.16			
		$19f_o$	0.07	7
9	--			
		$26f_o$	0.06	6
11	0.10			
		$35f_o$	0.04	4
13	0.09			
15	--			
17	0.07			
19	0.06			

(1) Input phase voltages have been taken as 1 p.u. volt and 100% volt.

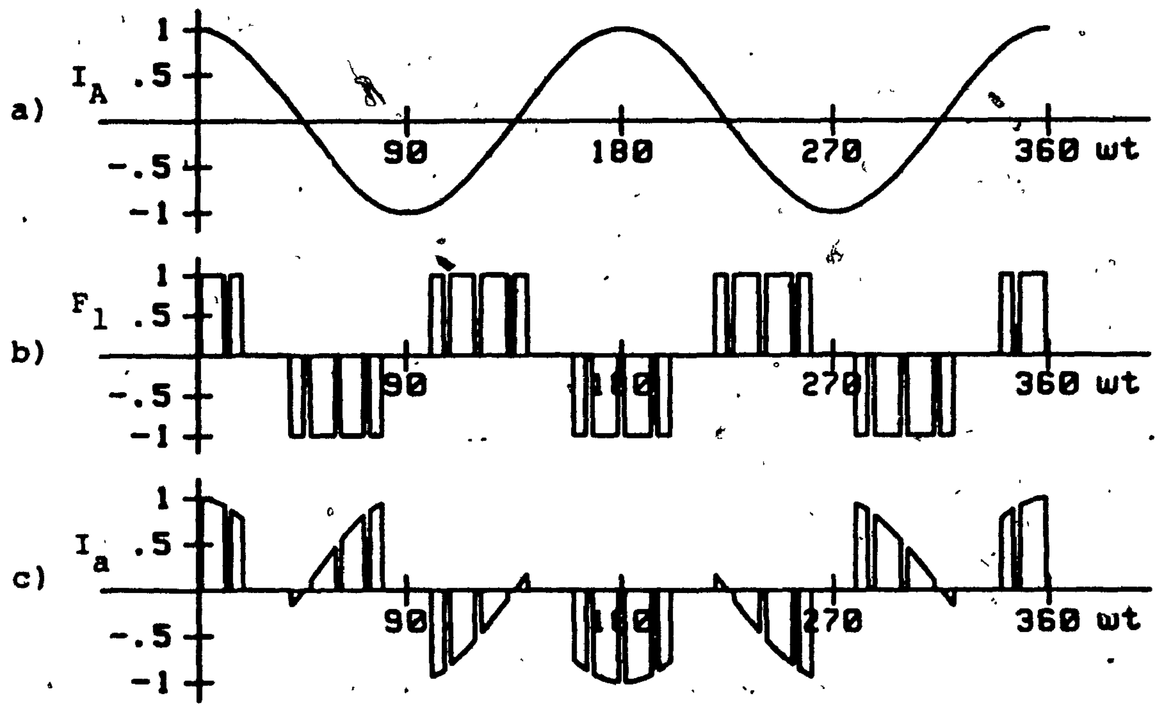

Fig. 4.4: Input current waveform obtained with three to single-phase full-bridge configuration DMO-FCC Scheme #1.

a) Output current, I_A.

b) F_1 switching function component.

c) Resulting input current, I_a.

TABLE 4.2					
FREQUENCY SPECTRA OF WAVEFORMS ASSOCIATED WITH FCC INPUT CURRENT SHOWN IN FIG. 4.4					
Harmonic coefficients of switching function (Fig. 4.4b)		Harmonic coefficients of resulting input phase current I_{an}, (Fig. 4.4c) for $f_o = 120$ Hz $= 2f_i$			
			Amplitude, I_{an}		
Order (n)	Amplitude (A_n)	Order (kf_i)	(1) p.u.	(1) %
1	1.10	f_i	0.55	55
3	--	$5f_i$	0.55	55
5	0.22	$13f_i$	0.11	11
7	0.16	$17f_i$	0.11	11
9	--	$19f_i$	0.08	8
11	0.10			
13	0.09			
15	--			
17	0.07			
19	0.06			

1) Output phase currents have been taken as 1 p.u. current and 100% current.

desirable as the capacity of the switching elements will be less than the rated output current. However, it contains 5th harmonics of the same amplitude (55%) as the fundamental.

4.3.2 Half Bridge Configuration Scheme #1

The circuit diagram of half-bridge FCC, analysed in this sub-section is shown in Fig. 4.2. Output voltage and input current waveforms and the respective frequency spectra are illustrated in Figs. 4.5 and 4.6 and tabulated in Tables 4.3 and 4.4. Amplitude of fundamental component of the output voltage is 83% (column 4, Table 4.3) of the input voltage. As expected it contains low order harmonics, but it is relatively free of sub-harmonic components. The low order harmonics are 3.5th, 5.5th and their amplitudes are 42% and 21% of input voltage respectively.

Amplitude of the fundamental component of input current is 28% of output current. It also contains 2nd, 4th and 5th harmonic component of amplitude 0.33, 0.14 and 0.28 respectively.

For half-bridge configuration IMO schemes are not generally feasible. Because the 3 switch configurations is insufficient to achieve the IMO principle.

4.4 Indirect Mode of Operation (IMO) FCC

Indirect mode of operation FCCs require two analytically independent stages of conversion. Therefore, different combination of rectifying and inverting switching functions are possible. The practical equations for output voltage and

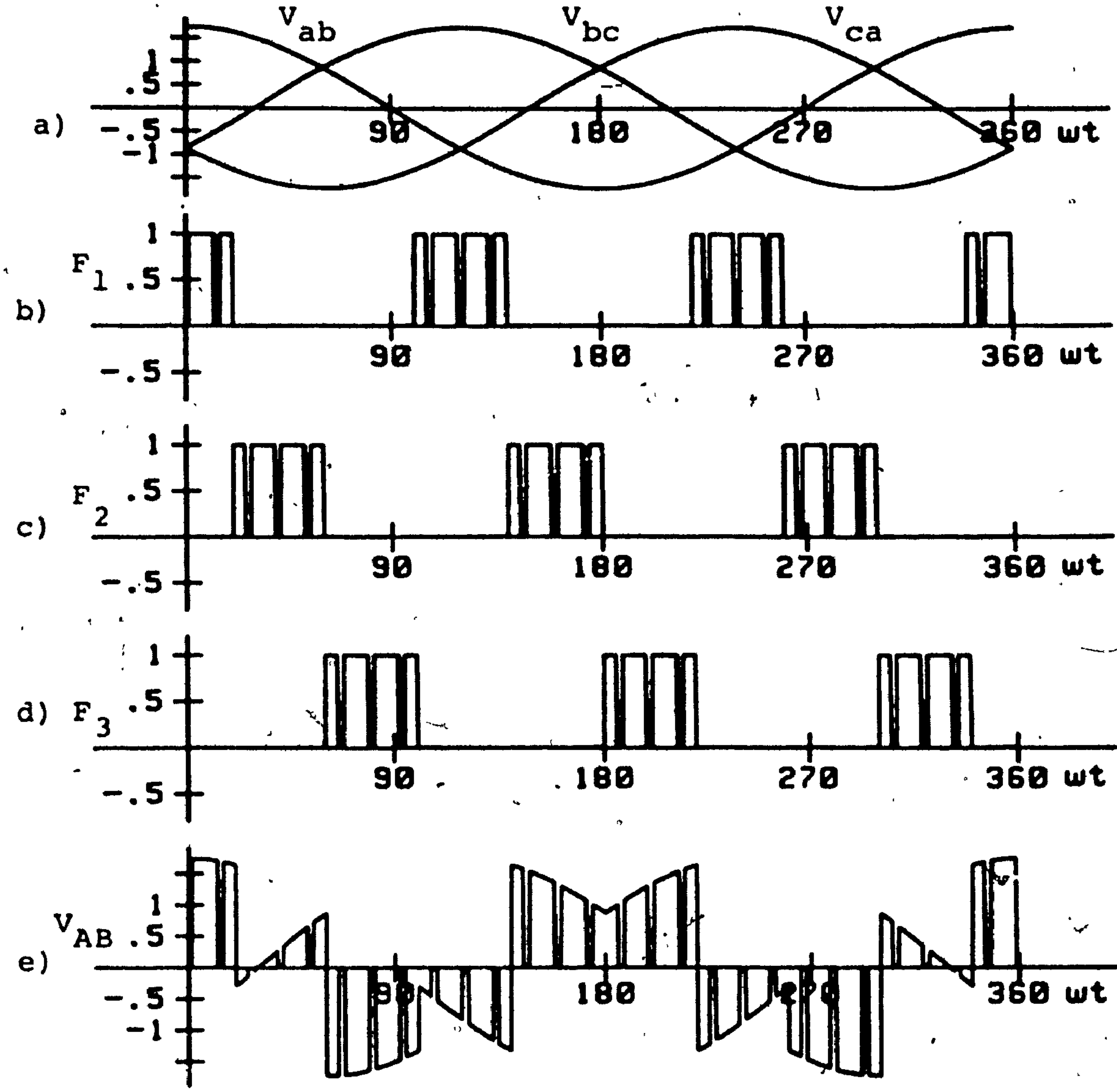

Fig. 4.5: Output voltage waveform obtained with three-phase to single-phase half-bridge configuration DMO FCC Scheme #1.

TABLE 4.3				
FREQUENCY SPECTRA OF WAVEFORMS ASSOCIATED WITH FCC OUTPUT VOLTAGE SHOWN IN FIG. 4.5				
Harmonic coefficients of switching function (Fig. 4.5b)		Harmonic coefficients of resulting output phase voltage V_{AN}, (Fig. 4.5e) for f_o = 120 Hz = 2 f_i		
			Amplitude, V_{AN}	
Order (n)	Amplitude (A_n)	Order (kf_o)	(1) p.u.	(1) %
dc	0.33			
1	0.55	f_o	0.83	83
2	0.28	$3.5f_o$	0.42	42
4	0.14	$5.5f_o$	0.21	21
5	0.11	$8.0f_o$	0.17	17
7	0.08	$10.0f_o$	0.12	12
8	0.07	$12.5f_o$	0.10	10
10	0.06	$14.5f_o$	0.08	8
16	0.04	$17.0f_o$	0.08	8
17	0.03	$19.0f_o$	0.06	6
19	0.03	$21.5f_o$	0.06	6

(1) Input phase voltages have been taken as 1 p.u. volt and 100% volt.

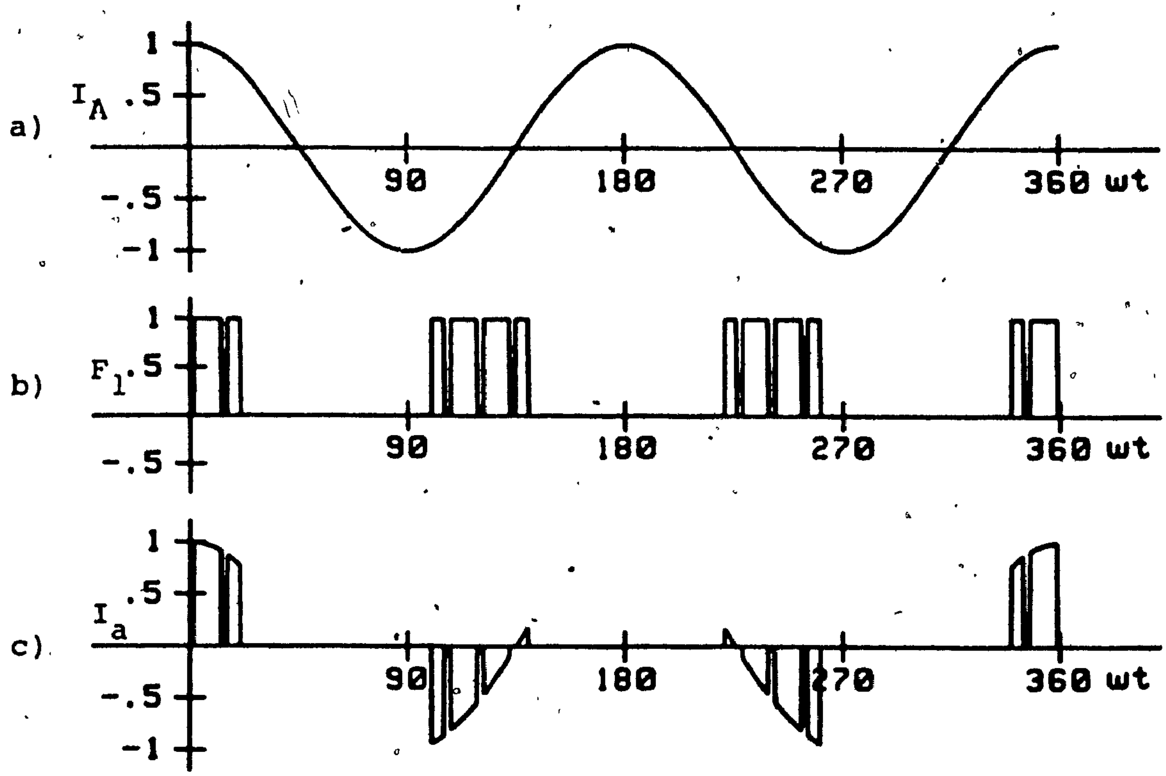

Fig. 4.6: Input current waveform obtained with three-phase to single-phase half-bridge configuration, DMO FCC Scheme #1.

TABLE 4.4

FREQUENCY SPECTRA OF WAVEFORMS ASSOCIATED WITH FCC INPUT CURRENT SHOWN IN FIG. 4.6

Harmonic coefficients of switching function (Fig. 4.6b)		Harmonic coefficients of resulting input phase current I_{an}, (Fig. 4.6c) for f_o = 120 Hz = $2f_i$		
		Amplitude, I_{an}		
Order (n)	Amplitude (A_n)	Order (kf_i)	(1) p.u.	(1) %
dc	0.33			
1	0.55	f_i	0.28	28
2	0.28	$2f_i$	0.33	33
4	0.14	$4f_i$	0.14	14
5	0.11	$5f_i$	0.28	28
7	0.08	$8f_i$	0.14	14
8	0.07	$10f_i$	0.07	7
10	0.06	$13f_i$	0.07	6
16	0.04	$14f_i$	0.07	7
17	0.03	$17f_i$	0.06	6
19	0.03	$19f_i$	0.04	4

1) Output phase currents have been taken as 1 p.u. current and 100% current.

input current for IMO FCC can be derived from the generalized equations as follows;

$$V_{AN}=\frac{3A_1B_1V_i}{2}\cos(\omega_o t)+\frac{3A_1V_i}{2}\sum_{k=3,5,7}^{\infty}B_k\cos(k\omega_o t)$$

$$+\frac{3V_i}{2}\sum_{k=1,3,5}^{\infty}\;\sum_{n=6,12,18}^{\infty}B_k(A_{n-1}+A_{n+1})\cos((k\omega_o\pm n\omega_i)t) \tag{4.3}$$

and

$$I_a=\frac{A_1B_1I_o}{2}\cos(\omega_i t)+\frac{B_1I_o}{2}\sum_{n=3,5,7}^{\infty}A_n\cos(n\omega_i t)$$

$$+\frac{I_o}{2}\sum_{n=1,3,5}^{\infty}\;\sum_{k=6,12,18}^{\infty}A_n(B_{k-1}+B_{k+1})\cos((n\omega_i\pm k\omega_o)t) \tag{4.4}$$

In this case the output voltage waveshape is similar to the three-phase FCC. Input current waveshape is different than the three-phase FCC input current as in this case only one current (single phase) is flowing in the load circuit rather than the three currents in three-phase case. All the waveforms have been computed at a output frequency of 120 Hz. The modulation schemes employed (for full-bridge FCC) in this case can be grouped as follows;

a) Rectifying function single pulse and inverting function MSPWM, Scheme #1.

b) Rectifying function MSPWM and inverting function single pulse, Scheme #2.

c) Rectifying and inverting functions are both MSPWM, Scheme #3.

d) Rectifying and inverting functions are both single pulse, Scheme #4.

4.4.1 IMO FCC Scheme #1

The rectifying function is single pulse and inverting function is MSPWM for this scheme. Resulting output voltage waveforms and corresponding spectrum are shown in Fig. 4.7 and Table 4.5. In this case the output frequency is 120Hz($=2f_i$). Consequently, the inverting switching frequency is also 120Hz, which is shown in Fig. 4.7d. Amplitude of the fundamental component of the resultant output voltage is 95% of input voltage. In this Scheme the low order harmonics are very insignificant. Dominant harmonics occur at $13f_o$ and its amplitude is 25% of input voltage. This dominant harmonic can be displaced further away from fundamental by simply increasing the number of pulses per cycle in the inverting switching function, i.e. increasing the switching frequency.

Input current waveform and its frequency spectrum are shown in Fig. 4.8 and Table 4.6. Amplitude of the fundamental component is 50% of the output current. But it also contains 3rd and 5th harmonics of considerable amplitudes. Their magnitudes are 31% and 17% respectively.

4.4.2 IMO FCC Scheme #2

In this scheme the rectifying SF and inverting SF are MSPWM and single pulse respectively. Duration of the single

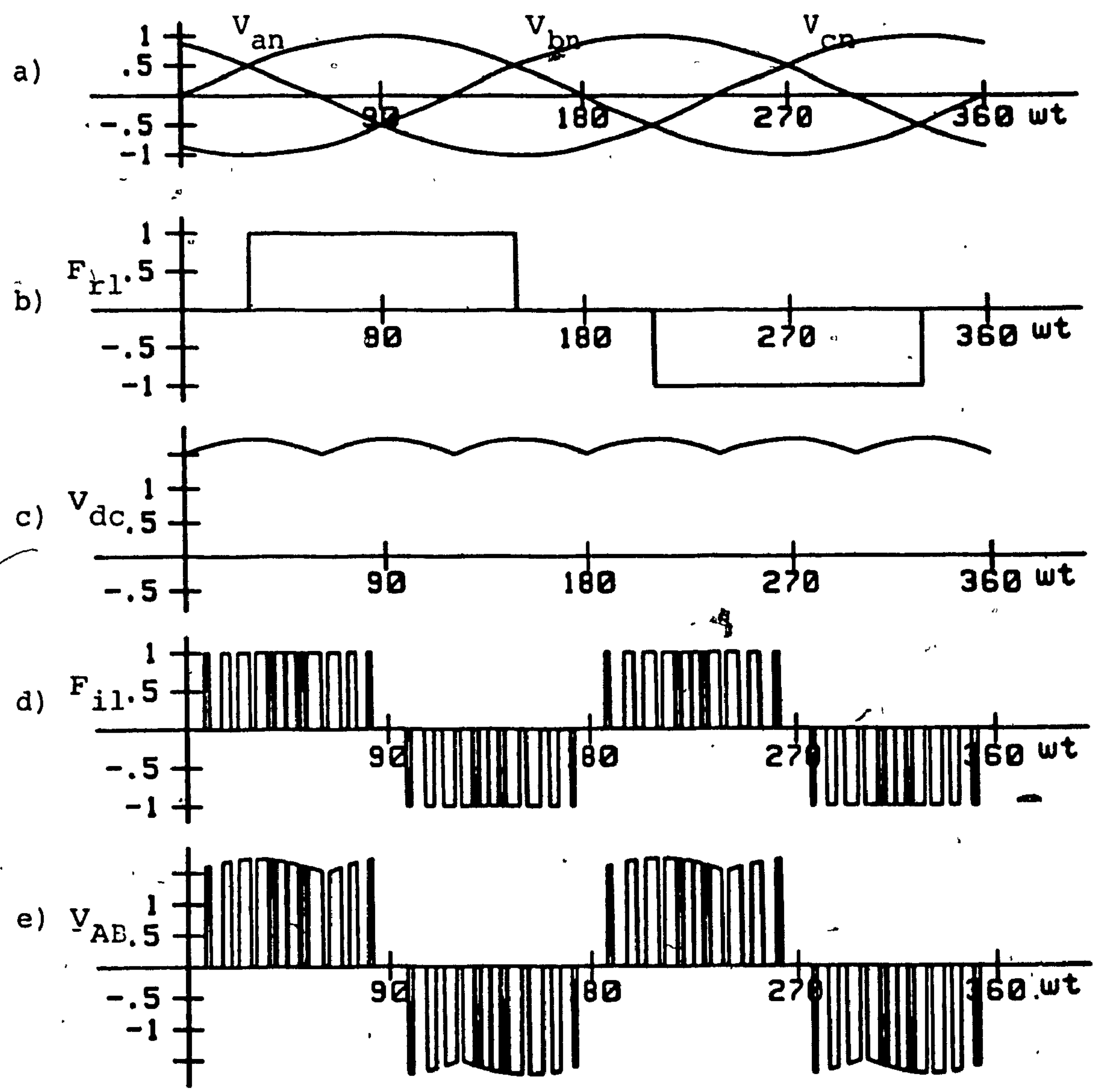

Fig. 4.7: Output voltage obtained with IMO Scheme #1.
a) Input phase voltages.
b) Fictitious rectifier SF (one of the three).
c) Fictitious rectifier voltage.
d) Fictitious inverter SF (one of the three).
e) Resulting output line voltage, V_{AB}.

TABLE 4.5						
FREQUENCY SPECTRA OF WAVEFORMS ASSOCIATED WITH FCC OUTPUT VOLTAGE SHOWN IN FIG. 4.7						
Harmonic coefficients of rectifier and inverter switching function (Fig. 4.7b and 4.7d)				Harmonic coefficients of resulting output phase voltage, V_{AN} (Fig. 4.7e) for $f_o = 120$ Hz $= 2f_i$		
Rectifier SF		Inverter SF		Amplitude, V_{AN}		
Order (n)	Amplitude (A_n)	Order (k)	Amplitude (B_k)	Order (kf_o)	(1) p.u.	(1) %
1	1.10	1	0.99	f_o	0.95	95
3	--	3	--	$2f_o$	0.03	3
5	0.22	5	--	$4f_o$	0.03	3
7	0.16	7	0.01	--	--	-
11	0.10	11	0.10	--	--	-
13	0.09	13	0.26	--	--	-
17	0.07	17	0.26	$11f_o$	0.10	10
19	0.06	19	0.10	$13f_o$	0.25	25
23	0.05			$17f_o$	0.25	25

(1) Input phase voltages have been taken as 1 p.u. volt and 100% volt.

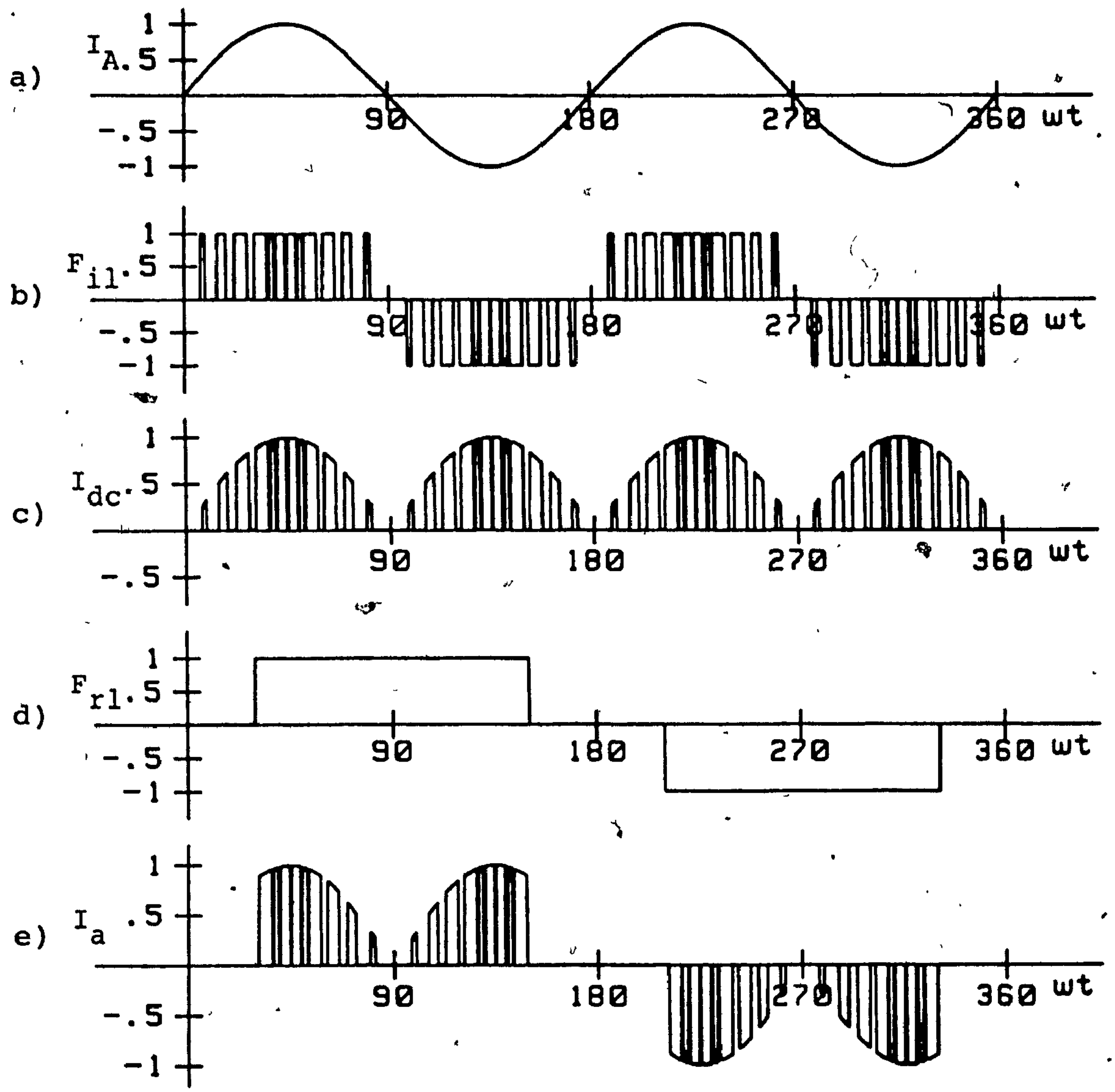

Fig. 4.8: Input current waveform obtained with IMO Scheme #1.

a) Output current , I_A.
b) Fictitious inverter switching function.
c) Fictitious rectifier current.
d) Fictitious rectifier SF.
e) Resulting input current, I_a.

TABLE 4.6

FREQUENCY SPECTRA OF WAVEFORMS ASSOCIATED WITH FCC INPUT CURRENT SHOWN IN FIG. 4.8

Harmonic coefficients of inverter and rectifier switching function (Fig. 4.8b and 4.8d)				Harmonic coefficients of resulting input phase current, I_{an}, (Fig. 4.8e) for f_o = 120 Hz = $2f_i$		
Inverter SF		Rectifier SF		Amplitude, I_{an}		
Order (k)	Amplitude (B_k)	Order (n)	Amplitude (A_n)	Order (kf_i)	(1) p.u.	(1) %
1	0.99	1	1.10	f_i	0.50	50
3	--	3	--	$3f_i$	0.31	31
5	--	5	0.22	$5f_i$	0.17	17
7	0.01	7	0.16	$7f_i$	0.05	5
11	0.10	11	0.10	$9f_i$	0.03	3
13	0.26	13	0.09	$11f_i$	0.01	1
15	--	15	--	$13f_i$	0.03	3
17	0.26	17	0.07	$17f_i$	0.01	1
19	0.10	19	0.06			

(1) Output phase currents have been taken as 1 p.u. current and 100% current.

pulse is 180^{o}, i.e. $\delta = 180^{o}$. This is possible ($\delta = 180^{o}$) as the required output is single phase. Output voltage waveform and its respective spectrum is shown in Fig. 4.9 and Table 4.7. Amplitude of output voltage fundamental is 110% i.e. greater than the input phase voltage. However, it contains low order harmonics and sub-harmonics. It also contains a dc component. However, its magnitude is insignificant (0.0096).

Input current waveform and its frequency spectra are shown in Fig. 4.10 and Table 4.8. Fundamental component is 64% of the output current and is free from sub-harmonic components. It contains low order harmonics of high amplitude. Third and fifth harmonics have the magnitude of 0.21 each.

4.4.3 <u>IMO FCC Scheme #3</u>

Rectifying and inverting SF employed in this scheme are both MSPWM. However, frequency control is achieved by varying the switching frequency of the inverting function. The frequency spectrum and output voltage waveshape are shown in Table 4.9 and Fig. 4.11. By the introduction of SPWM in the inverting function, the output voltage and the input current spectra have considerable improvement. Output voltage does not contain any subharmonics. However, voltage utilization is 86% of the input voltage which is less than IMO scheme #2. The frequency spectrum contains harmonics at $8f_o$, $11f_o$, $13f_o$, and their magnitudes are 7%, 14% and 16% of

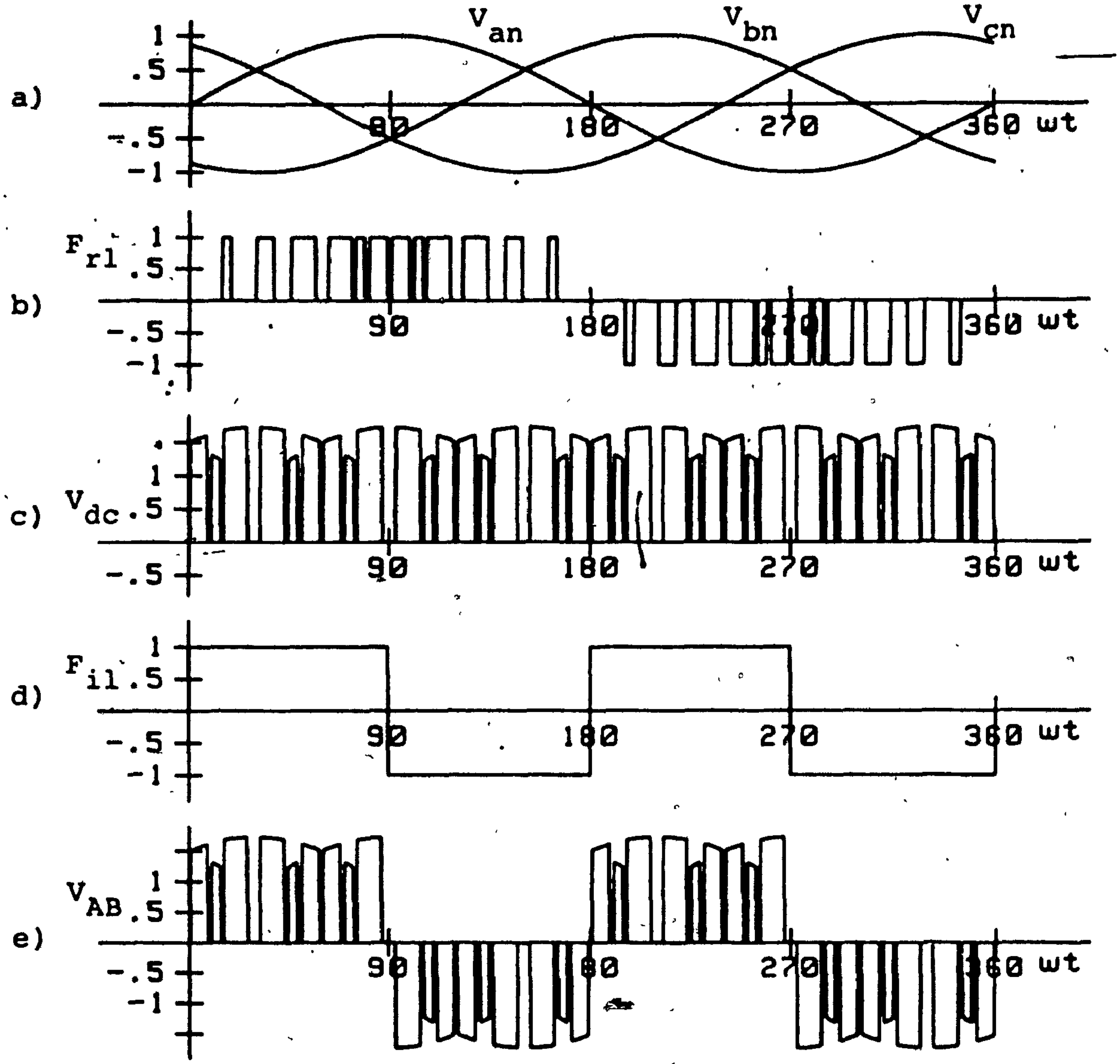

Fig. 4.9: Output voltage waveform obtained with IMO Scheme #2.

TABLE 4.7

FREQUENCY SPECTRA OF WAVEFORMS ASSOCIATED WITH FCC OUTPUT VOLTAGE SHOWN IN FIG. 4.9

Harmonic coefficients of rectifier and inverter switching function (Fig. 4.9b and 4.9d)				Harmonic coefficients of resulting output phase voltage, V_{AN} (Fig. 4.9e) for $f_o = 120$ Hz $= 2f_i$		
Rectifier SF		Inverter SF		Amplitude, V_{AN}		
Order (n)	Amplitude (A_n)	Order (k)	Amplitude (B_k)	Order (kf_o)	(1) p.u.	(1) %
				dc	0.0096	0.96
1	0.99	1	1.27	f_o	1.10	110
3	--	3	0.42	$2f_o$	0.02	2
				$3f_o$	0.37	37
5	--	5	0.26	$4f_o$	0.02	2
7	--	7	0.18	$5f_o$	0.22	22
				$6f_o$	0.03	3
9	--	9	0.14	$7f_o$	0.18	18
11	--	11	0.12	$8f_o$	0.08	8
				$9f_o$	0.15	15
13	--	13	0.10	$10f_o$	0.08	8
15	--	15	0.09	$11f_o$	0.18	18
17	0.11	17	0.08			
19	0.26	19	0.07			

(1) Input phase voltages have been taken as 1 p.u. volt and 100% volt.

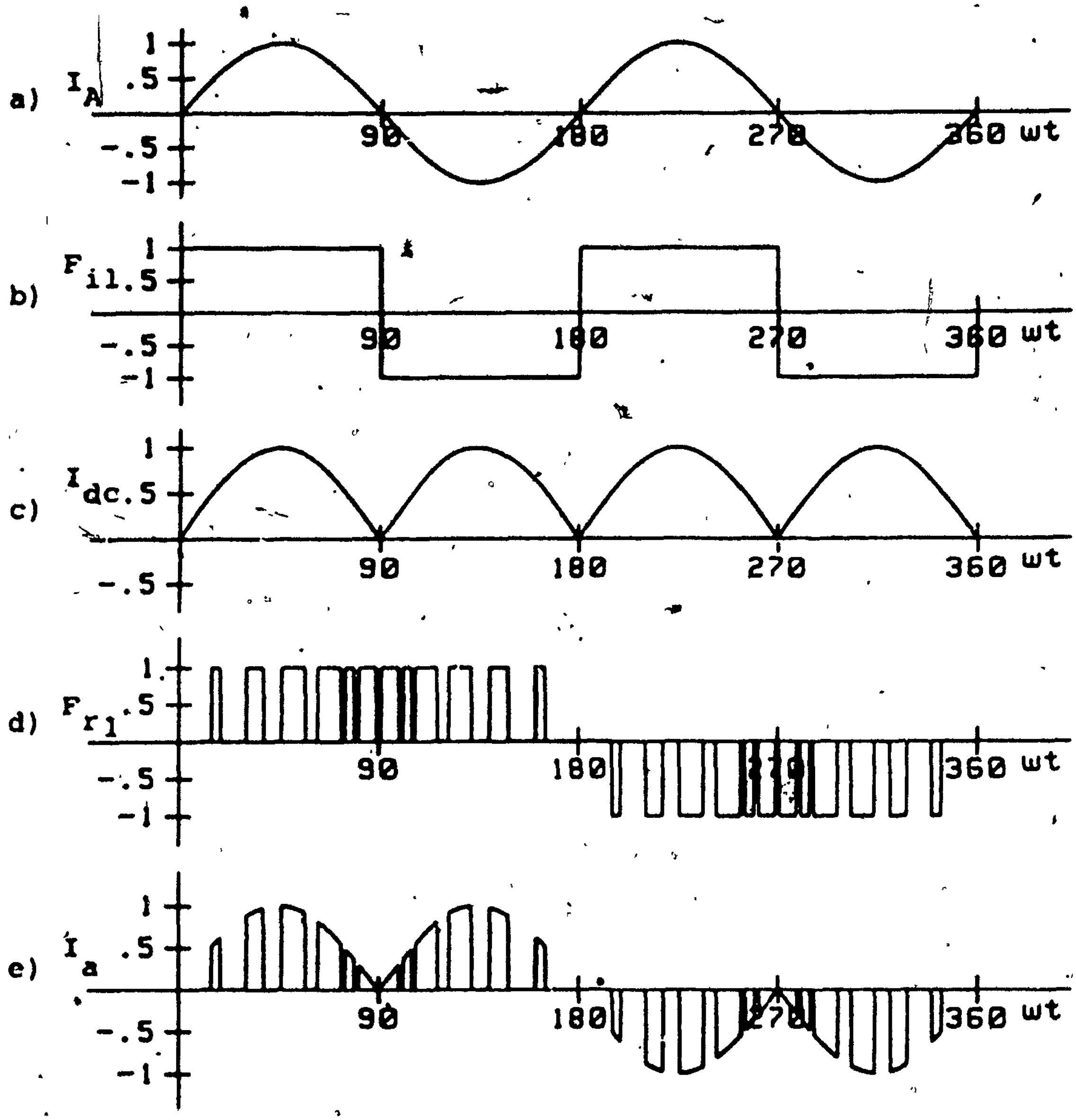

Fig. 4.10: Input current waveform obtained with IMO Scheme #2.

TABLE 4.8						
FREQUENCY SPECTRA OF WAVEFORMS ASSOCIATED WITH FCC INPUT CURRENT SHOWN IN FIG. 4.10						
Harmonic coefficients of inverter and rectifier switching function (Fig. 4.10b and 4.10d)				Harmonic coefficients of resulting input phase current, I_{an}, (Fig. 4.10e) for $f_o = 120$ Hz $= 2f_i$		
Inverter SF		Rectifier SF		Amplitude, I_{an}		
Order (k)	Amplitude (B_k)	Order (n)	Amplitude (A_n)	Order (kf_i)	(1) p.u.	(1) %
1	1.27	1	0.99	f_i	0.64	64
3	0.42	3	--	$3f_i$	0.21	21
5	0.26	5	--	$5f_i$	0.21	21
7	0.18	7	--	$7f_i$	0.04	4
9	0.14	11	--	$9f_i$	0.04	4
11	0.12	13	--	$13f_i$	0.01	1
13	0.10	15	--	$15f_i$	0.06	6
15	0.09	17	0.11	$17f_i$	0.09	9
17	0.08	19	0.26	$19f_i$	0.12	12

(1) Output phase currents have been taken as 1 p.u. current and 100% current.

input voltage respectively.

Input current waveform and its corresponding frequency spectrum is shown in Fig. 4.12 and Table 4.10 respectively. Fundamental component of the input current has an amplitude of 50% of the output current. It also contains 3rd and 5th harmonics of amplitude 25% of the output current.

4.4.4 IMO FCC Scheme #4

Applying single pulse modulation to both rectifying and inverting functions enhances the amplitude of fundamental component of output voltage to a maximum of 122% of input voltage (Fig. 4.13). However, it contains sub-harmonics. Moreover, it behaves as a six-pulse rectifier containing 5th and 7th harmonics of amplitude 24% and 18% respectively. It also contains a 3rd harmonic component of amplitude 41%.

As expected, input current (Fig. 4.14) frequency spectra contains 3rd and 5th harmonic components of amplitude 28% and 9% of the output current. Amplitude of the fundamental current is 0.65 of output current.

This scheme is particularly suitable when a boost in the output fundamental is the main design requirement rather than the converter overall performance.

4.5 Output Frequency Lower than Input Frequency Waveforms

All the output waveforms studied until now are at a higher frequency than the input frequency, i.e. $f_o > f_i$. However the proposed FCCs are capable of generating output

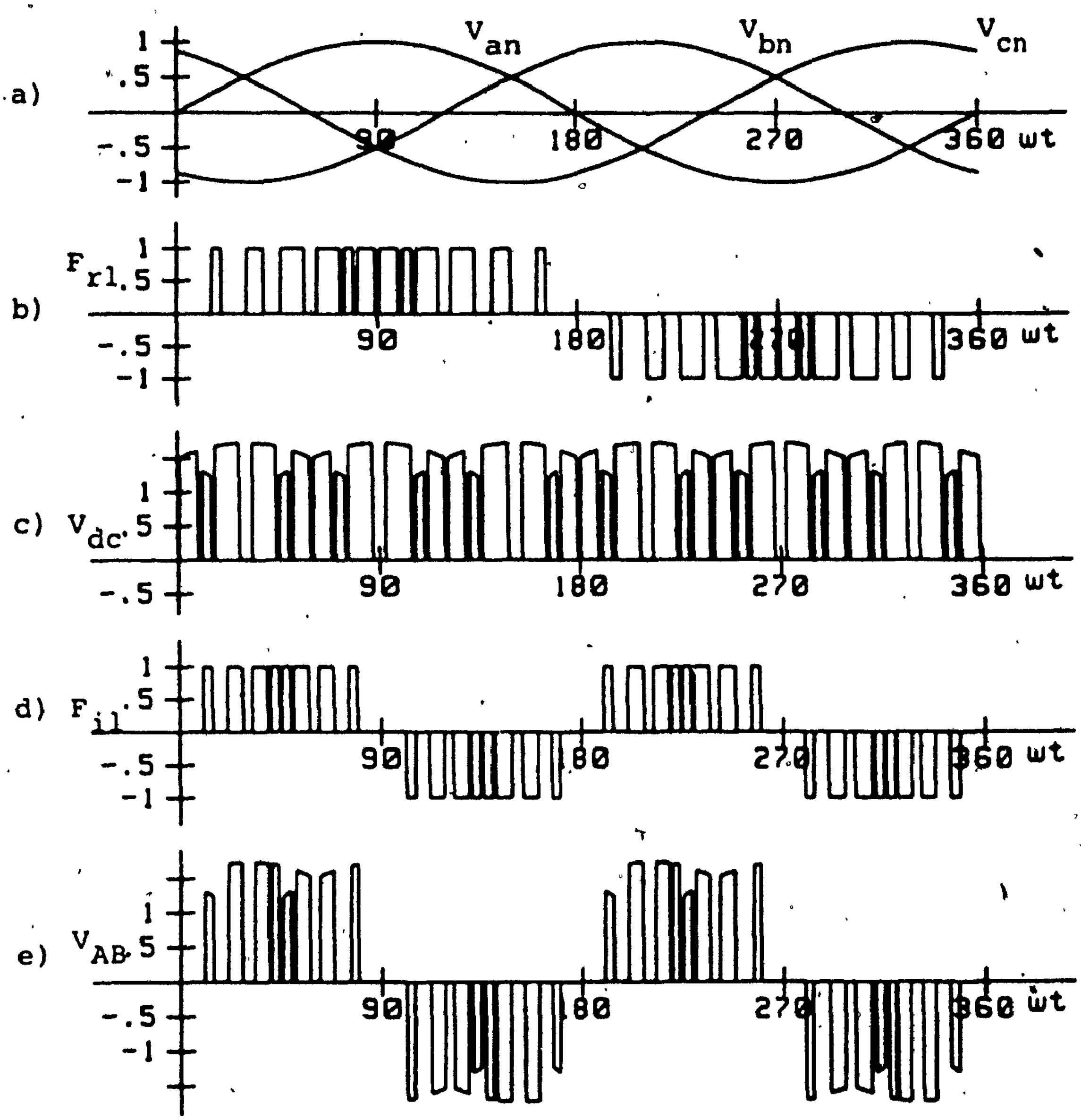

Fig. 4.11: Output voltage waveform obtained with IMO Scheme #3.

TABLE 4.9

FREQUENCY SPECTRA OF WAVEFORMS ASSOCIATED WITH FCC OUTPUT VOLTAGE SHOWN IN FIG. 4.11

Harmonic coefficients of rectifier and inverter switching function (Fig. 4.11b and 4.11d)				Harmonic coefficients of resulting output phase voltage, V_{AN} (Fig. 4.11e) for $f_o = 120$ Hz $= 2f_i$		
Rectifier SF		Inverter SF		Amplitude, V_{AN}		
Order (n)	Amplitude (A_n)	Order (k)	Amplitude (B_k)	Order (kf_o)	(1) p.u.	(1) %
1	0.99	1	0.99	f_o	0.86	86
3	--	3	--	$4f_o$	0.009	.9
5	--	5	--	$8f_o$	0.07	7
7	--	7	0.01	$11f_o$	0.14	14
9	--	9	--	$13f_o$	0.16	16
11	--	11	0.10	$17f_o$	0.22	22
13	--	13	0.26			
15	--	15	--			
17	0.11	17	0.26			
19	0.26	19	0.10			

(1) Input phase voltages have been taken as 1 p.u. volt and 100% volt.

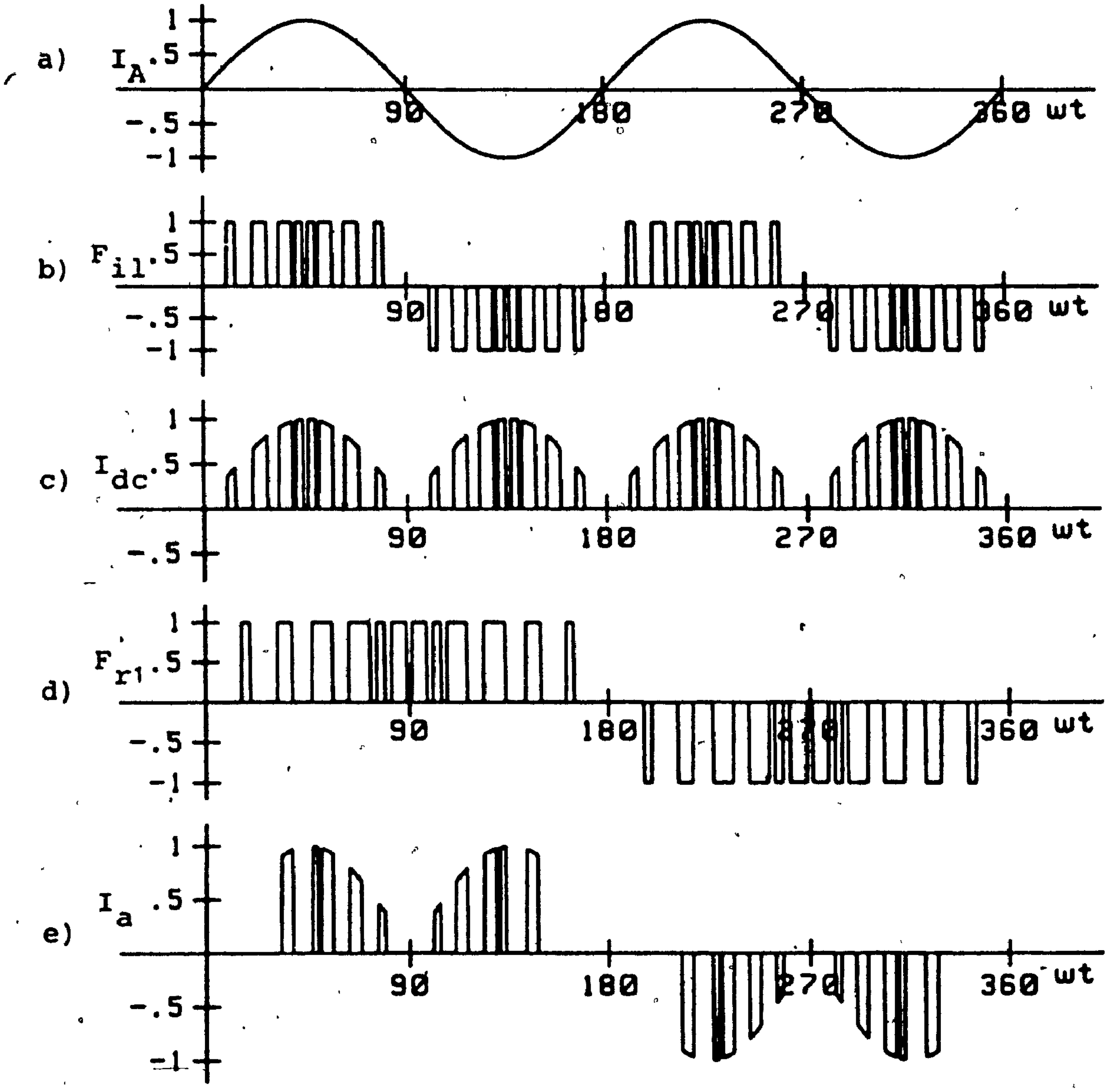

Fig. 4.12: Input current waveform obtained with IMO Scheme #3.

TABLE 4.10

FREQUENCY SPECTRA OF WAVEFORMS ASSOCIATED WITH FCC INPUT CURRENT SHOWN IN FIG. 4.12

Harmonic coefficients of inverter and rectifier switching function (Fig. 4.12b and 4.12d)				Harmonic coefficients of resulting input phase current, I_{an}, (Fig. 4.12e) for $f_o = 120$ Hz $= 2f_i$		
Inverter SF		Rectifier SF		Amplitude, I_{an}		
Order (k)	Amplitude (B_k)	Order (n)	Amplitude (A_n)	Order (kf_i)	(1) p.u.	(1) %
1	0.99	1	0.99	f_i	0.50	50
3	--	3	--	$3f_i$	0.25	25
5	--	5	--	$5f_i$	0.25	25
7	0.01	7	--	$7f_i$	0.04	4
11	0.10	11	--	$9f_i$	0.07	7
13	0.26	13	--	$11f_i$	0.06	6
15	--	15	--	$13f_i$	0.06	6
17	0.26	17	0.11	$15f_i$	0.02	2
19	0.10	19	0.26	$17f_i$	0.07	7

(1) Output phase currents have been taken as 1 p.u. current and 100% current.

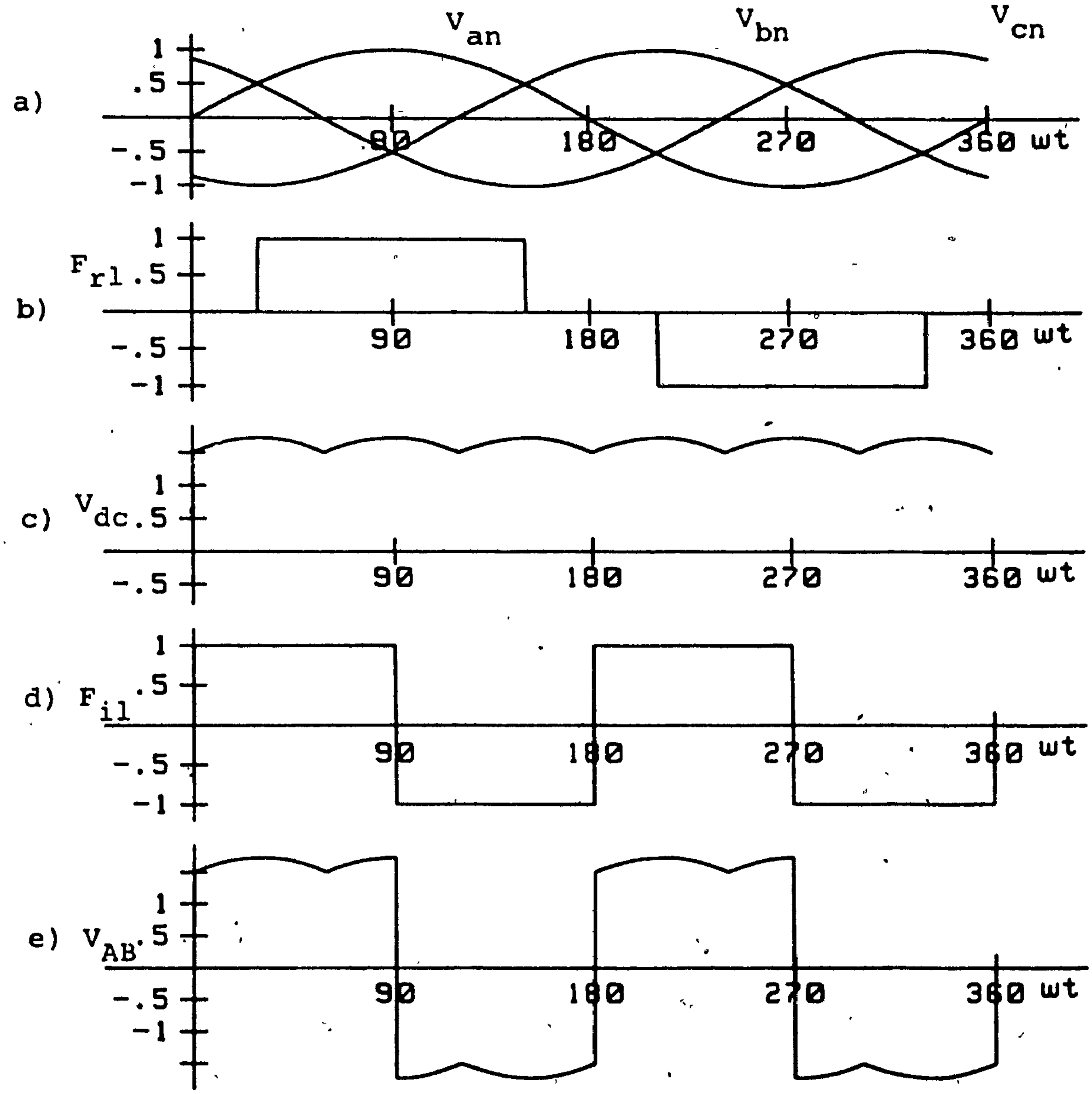

Fig. 4.13: Output voltage waveform obtained with IMO Scheme #4.

TABLE 4.11						
FREQUENCY SPECTRA OF WAVEFORMS ASSOCIATED WITH FCC OUTPUT VOLTAGE SHOWN IN FIG. 4.13						
Harmonic coefficients of rectifier and inverter switching function (Fig. 4.13b and 4.13d)				Harmonic coefficients of resulting output phase voltage, V_{AN} (Fig. 4.13e) for $f_o = 120$ Hz $= 2f_i$		
Rectifier SF		Inverter SF		Amplitude, V_{AN}		
Order (n)	Amplitude (A_n)	Order (k)	Amplitude (B_k)	Order (kf_o)	(1) p.u.	(1) %
				dc	0.011	1.1
1	1.10	1	1.27	f_o	1.22	122
				$2f_o$	0.04	4
3	--	3	0.42	$3f_o$	0.41	41
5	0.22	5	0.26	$4f_o$	0.04	4
				$5f_o$	0.24	24
7	0.16	7	0.18	$6f_o$	0.01	1
9	--	9	0.14	$7f_o$	0.18	18
11	0.1[illegible]	11	0.12	$9f_o$	0.14	14
13	0.09	13	0.10	$11f_o$	0.11	11
				$13f_o$	0.09	9
15	--	15	0.09	$15f_o$	0.08	8
				$17f_o$	0.07	7
17	0.07	17	0.08	$19f_o$	0.06	6
19	0.06	19	0.07			

(1) Input phase voltages have been taken as 1 p.u. volt and 100% volt.

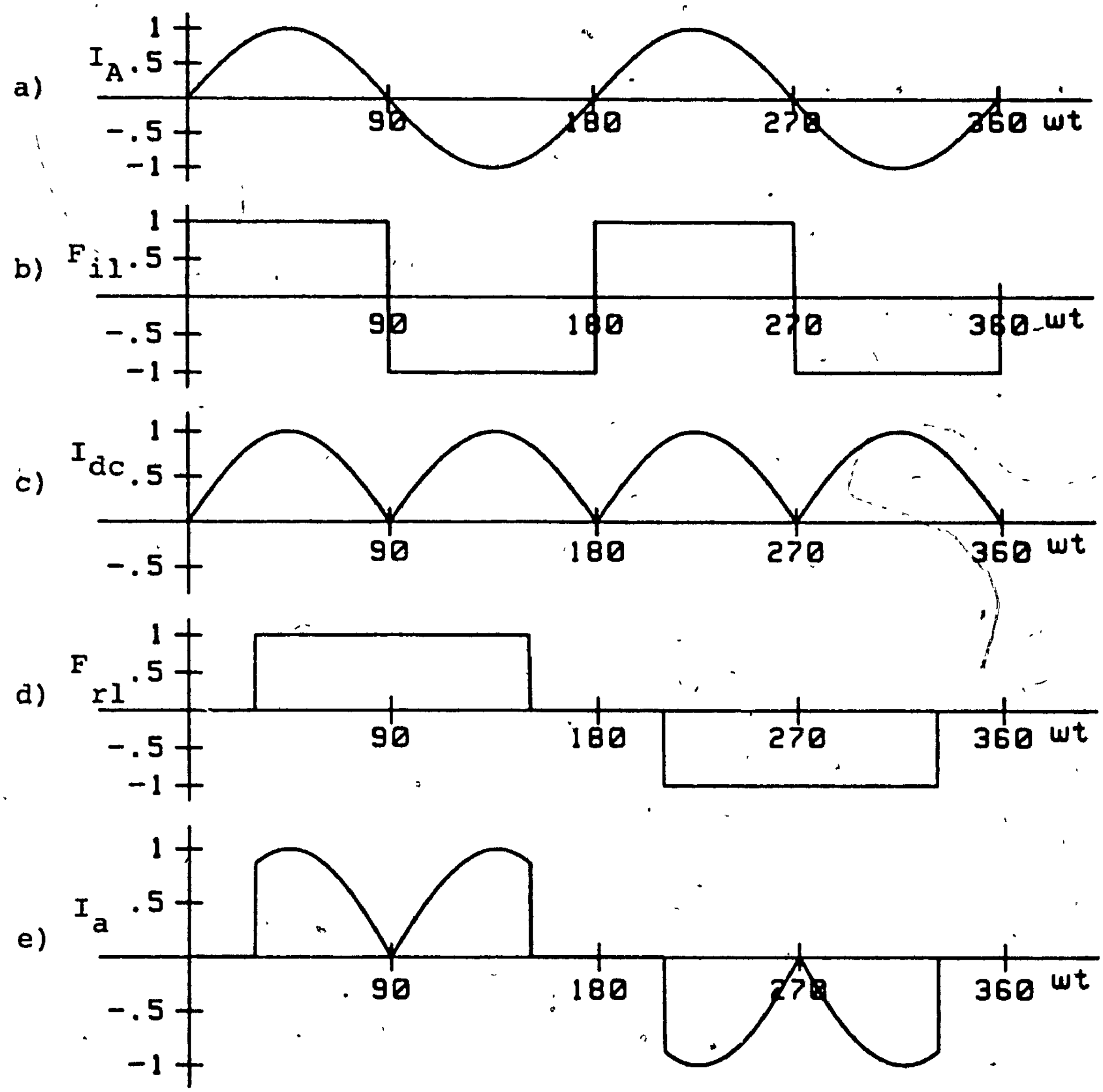

Fig. 4.14: Input current waveform obtained with IMO Scheme #4.

TABLE 4.12

FREQUENCY SPECTRA OF WAVEFORMS ASSOCIATED WITH FCC INPUT CURRENT SHOWN IN FIG. 4.14

Harmonic coefficients of inverter and rectifier switching function (Fig. 4.14b and 4.14d)				Harmonic coefficients of resulting input phase current, I_{an}, (Fig. 4.14e) for f_o= 120 Hz = $2f_i$		
Inverter SF		Rectifier SF		Amplitude, I_{an}		
Order (k)	Amplitude (B_k)	Order (n)	Amplitude (A_n)	Order (kf_i)	(1) p.u.	(1) %
1	1.27	1	1.10	f_i	0.65	65
3	0.42	3	--	$3f_i$	0.28	28
5	0.26	5	0.22	$5f_i$	0.09	9
7	0.18	7	0.16	$7f_i$	0.03	3
9	0.14	9	--	$9f_i$	0.08	8
11	0.12	11	0.10	$11f_i$	0.01	1
13	0.10	13	0.09	$13f_i$	0.07	7
15	0.09	15	--	$15f_i$	0.03	3
17	0.08	17	0.07	$17f_i$	0.04	4
19	0.07	19	0.06	$19f_i$	0.04	4

(1) Output phase currents have beent aken as 1 p.u. current and 100% current.

which is at lower frequency than the input source. To establish this capability, one of the schemes i.e. IMO Scheme #1 waveforms i.e. output voltage and input current are analytically drawn with their corresponding spectrum in Figs. 4.15 and 4.16 for a frequency of $f_i = 60$ Hz, $f_o = 30$ Hz. Output voltage and input current frequency specrtra are shown in Figs. 4.15f and 4.16f respectively.

4.6 Design Requirements

The design component values are the same as with the three-phase cycloconverter components i.e. the ratings of switches remain the same only fewer number of switches, six and four are employed in this case. The control logic requirement is also the same except for the fact that it becomes much more simpler than three phase case as the number of switches employed in this Scheme are less.

The control logic and its implementation requirements are discussed in Appendix B.

4.7 Experimental Results

To verify key predicted results in this chapter Scheme #1 for structure #1 (Fig. 4.1) hardware implementation is sought. A 1 KVA three-phase to single-phase cycloconverter working under DMO principle has been constructed and tested.

Fig. 4.17A shows the output voltage at a frequency of 120 Hz. The frequency spectrum agrees well with the analytically predicted results of Table 4.1. Fig. 4.17B shows the experimental input current and, its spectrum there

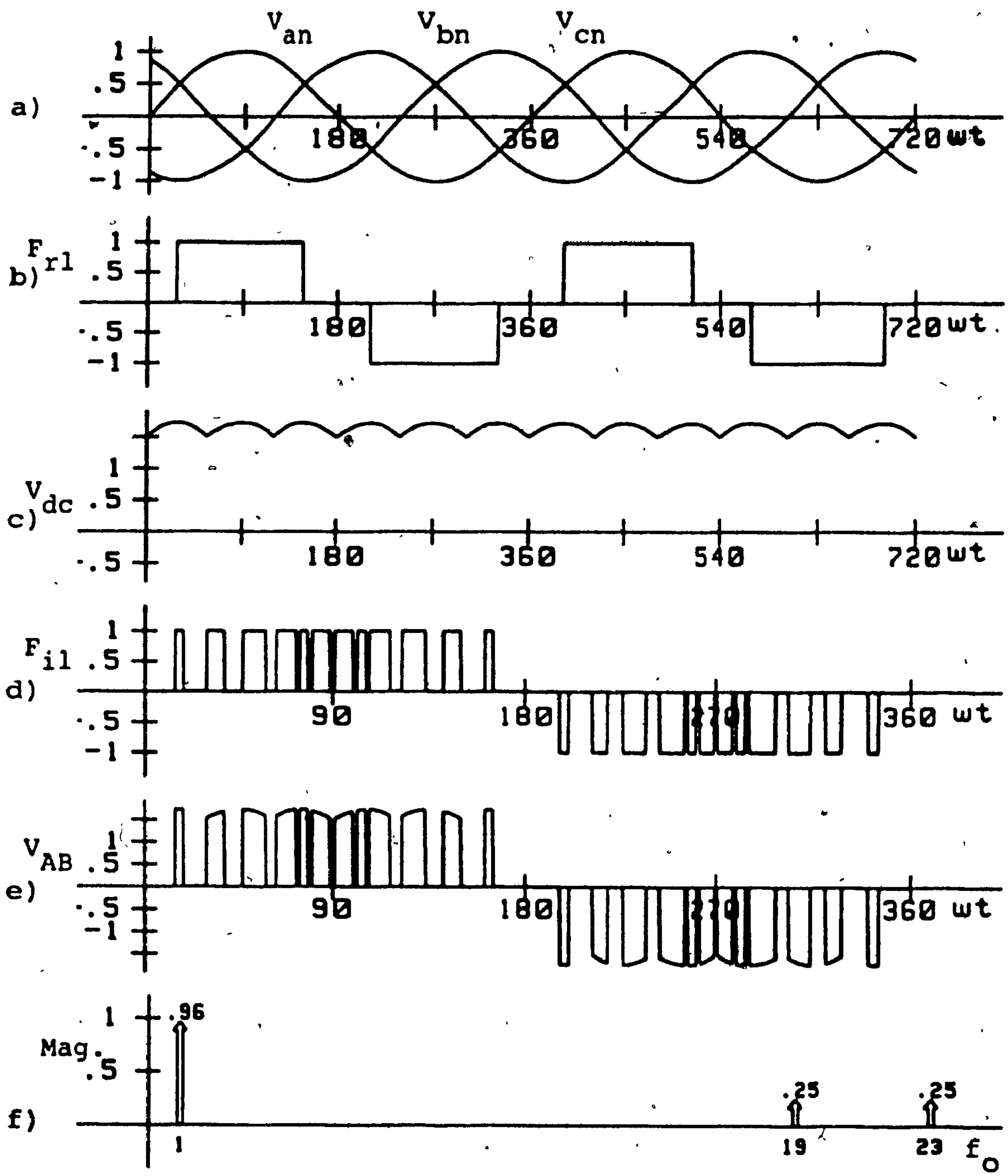

Fig. 4.15: Output voltage waveform obtained with three phase to single-phase full-bridge IMO FCC Scheme #1 at f_i= 60 Hz, f_o= 30 Hz. Respective frequency spectrum is shown in "f".

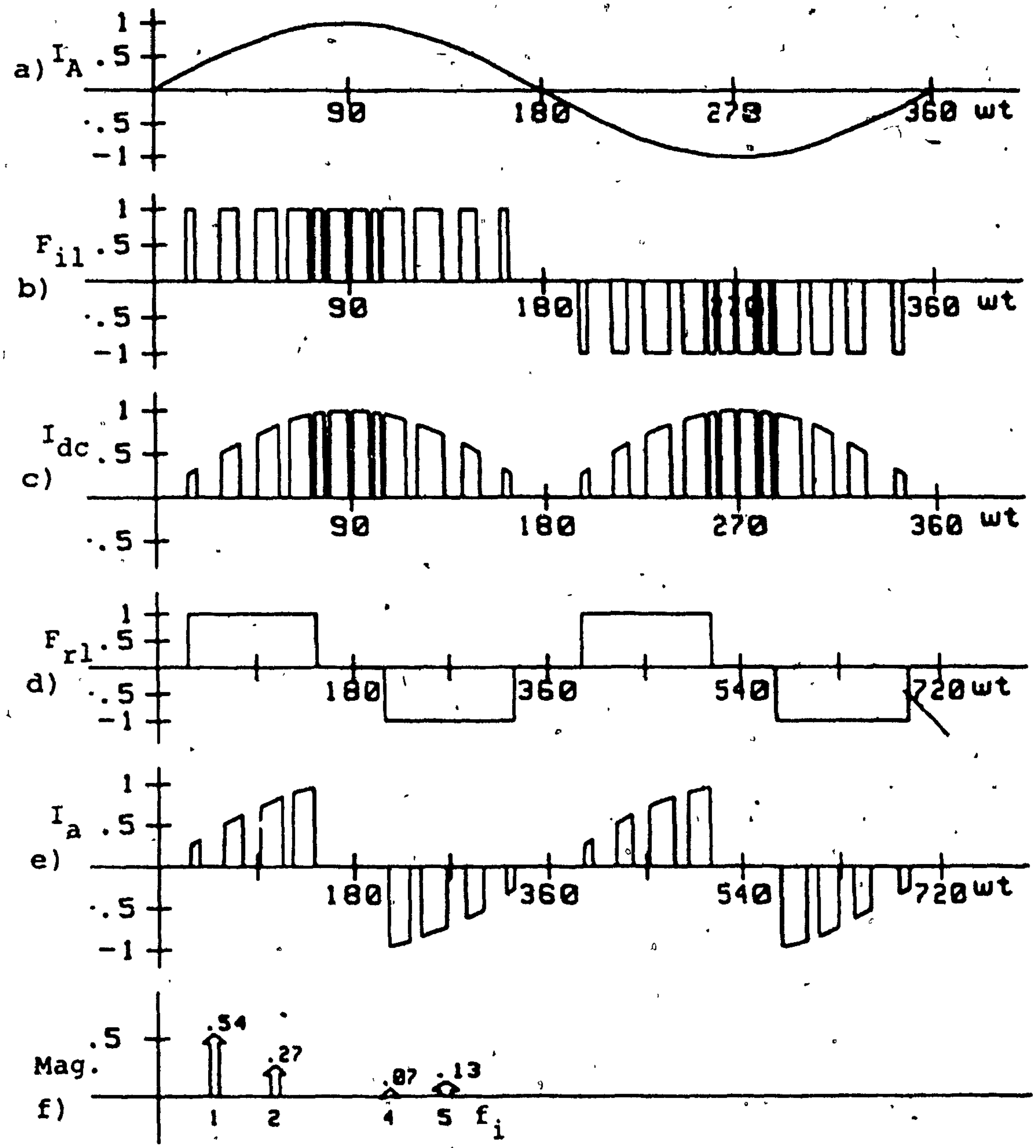

Fig. 4.16: Input current waveform obtained with three to single phase full-bridge IMO FCC Scheme #1 at f_i = 60 Hz, f_o = 30 Hz. Respective frequency spectrum is shown in "f".

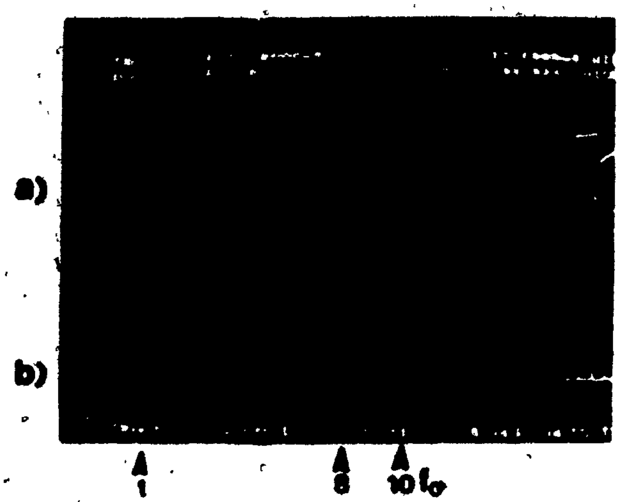

A. a) Output voltage, V_{AB} (Fig. 4.3).
b) Respective frequency spectrum.

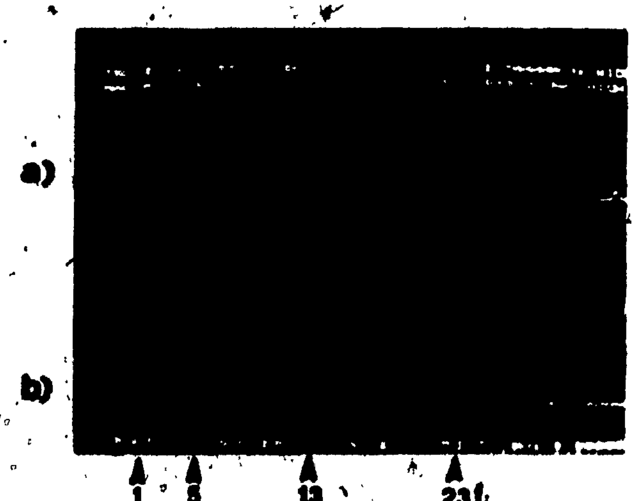

B. a) Input current, I_a (Fig. 4.4).
b) Respective frequency spectrum.

Fig. 4.17: Experimental input/output voltage/current waveforms obtained with full bridge three to single phase DMO FCC Scheme #1 at f_o = 120 Hz and M_f = 1 for resistive load.

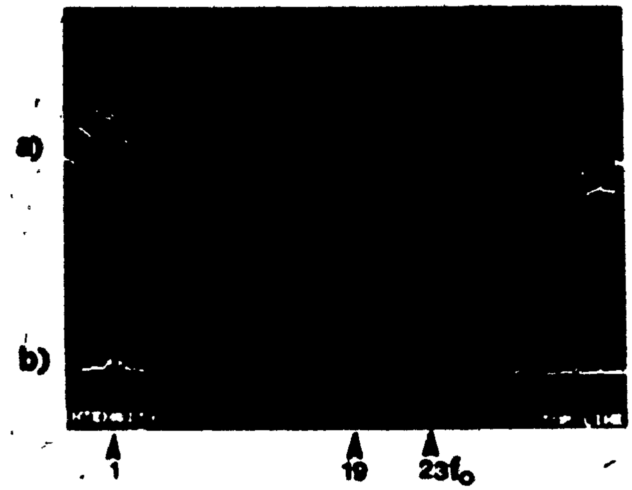

A. a) Output voltage, V_{AB}
b) Respective frequency spectrum

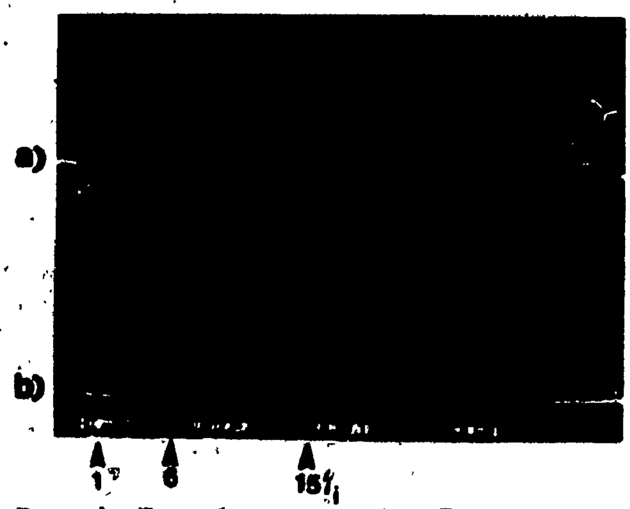

B. a) Input current, I_a.
b) Respective frequency spectrum.

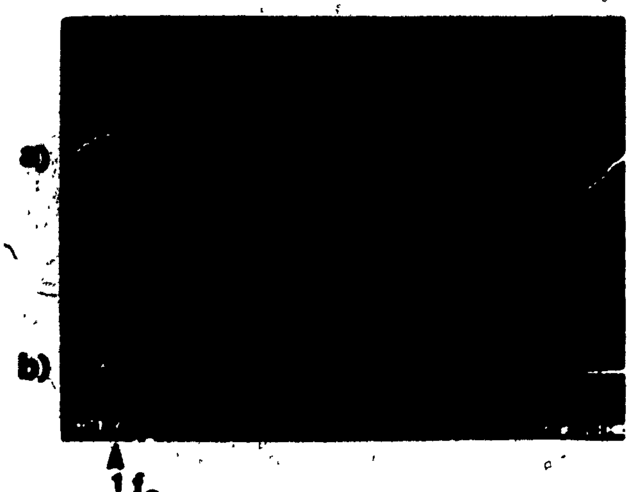

C. a) Output current, I_A.
b) Respective frequency spectrum.

Fig. 4.18: Experimental input/output voltage/current waveforms obtained with full bridge three to single phase DMO FCC Scheme #1 at f_o = 120 Hz and M_f = 1 for R-L load (p.f. = 0.8).

too have close agreement with analytically predicted results (Table 4.2).

Fig. 4.18 shows the same results for a load power factors of 0.8. Output current (Fig. 4.18C) in this case is sinusoidal. Output voltage (Fig. 4.18A) and input current (Fig. 4.18B) spectra have improved due to the filtering effect of the load.

4.8 Discussion and Conclusions

The several conversion schemes discussed in this chapter have improved voltage utilization, sinusoidal output voltage and input current. Most of the schemes described do not generate output or input sub-harmonics. Any suitable structure combined with specific scheme can suit various type of load requirements.

Finally, the feasibility of a proposed scheme has been tested and verified on a 1KVA laboratory prototype unit.

CHAPTER 5

SINGLE PHASE TO THREE PHASE CYCLOCONVERTER

5.1 Introduction

Use of balanced three phase ac mains allows for the most efficient and economical use of electrical power. This is mainly because three phase electrical equipment, such as 3-phase induction motors are significantly more efficient and economical than their single phase counterparts. In many instances, however, extension of 3-phase power lines to rural and light industrial areas is not economical. Consequently, these areas are supplied from single phase mains. A typical solution to this problem has been the use of single to three phase frequency changers, whose cost is often only a fraction of the cost of providing full 3-phase service. For this reason several phase conversion systems [41]-[42] have been developed and are in wide use today. These systems are either rotary or static. A brief description of how they function and of their limitations is as follows:

Fig. 5.1a shows a simplified circuit diagram of a rotary phase converter. It consists of rotary transformer and associated capacitors. The rotary transformer is actually a polyphase squirrel-cage induction motor without a shaft. At no load capacitors current, I_{cap}, flows into the rotary transformer, I_A''. At light load capacitors current, I_{cap} flows into the rotary, I_A'', and also to the load circuit, I_A. As the load current requirements increase, most of the capacitor current flows to the external load circuit.

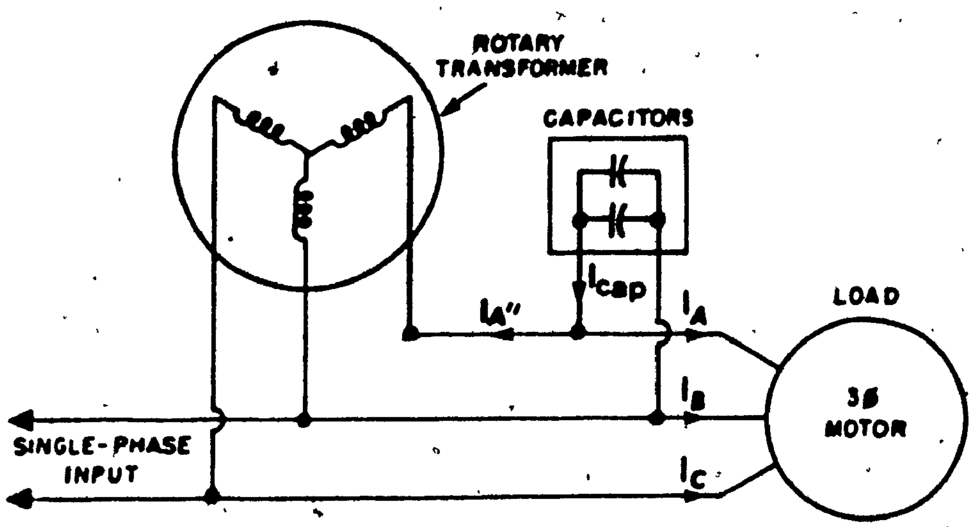

a) Rotary converter

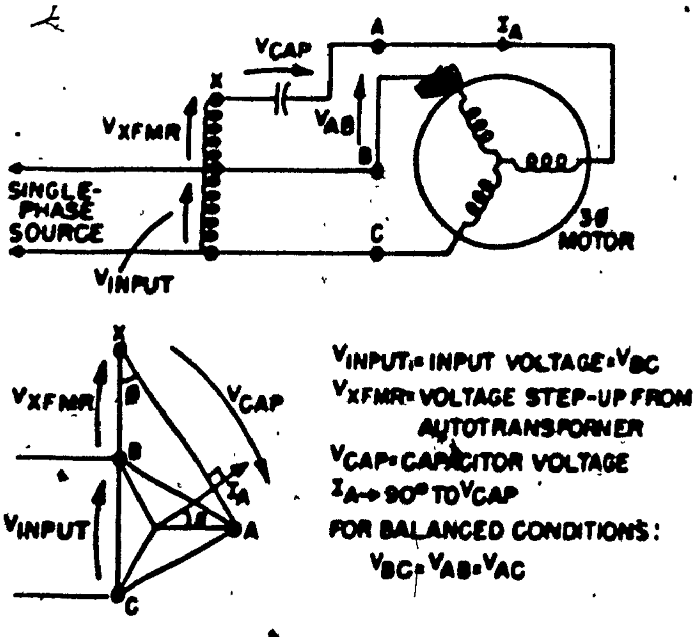

b) Static converter

Fig. 5.1: Simplified diagram of rotary and static phase converters.

The main advantage of rotary converter is; that the unit is cost effective and many motors can be operated under varying load conditions with the same rotary converter. However, the major disadvantage is the reduced lock rotor torque (sometimes 50% or less) which is a obvious problem with high starting torque loads. The no load losses are also high. The loss ratio, compared to static converter, could be as high as 10:1.

The static converter illustrated in Fig. 5.1b consists of an autotransformer and capacitors. Phase A current is generated by the capacitor. Balanced output supply can be achieved by the proper design of the autotransformer and by suitable choice of the capacitance values. This converter has the advantage of very low no-load losses and the ability to adjust or balance the load motor currents thereby improving the performance of the motor. The main problem of this converter is the supply of balanced current for all the three phases for different load conditions. Other limitations are; wide variation from the given load point should be avoided and breakdown torque is limited because of the reduced capacitor current (I_A) at overload [43].

It is reported [44] that static frequency converters capable of supplying balanced three phase voltage under varying load conditions are feasible. However, these converters [44] use conventional reactors and capacitors in conjunction with four thyristors.

The single to three phase frequency changer proposed (Fig. 5.2) in this chapter is also static but it employs semiconductor components for phase transformation. Additional passive components such as inductors and capacitors (for input/output filtering) may or may not be required according to customer specifications. Since it employs semiconductor switches, the proposed phase converter has the following merits.

i) It allows for full voltage control (zero to rated voltage) which in turn allows smooth starting of induction motors by employing constant Volt/Hz speed control.

ii) Resulting converter input current is sinusoidal.

The demerits are:

i) Output voltage of this phase converter contains third harmonic component of same amplitude as fundamental. However, this third harmonics can be filtered by employing a tuned line to line filter .

ii) Voltage utilization is low (55% of input voltage). This problem can however be solved by the use of a matching step-up transformer.

Finally, analytically predicted results are verified on an experimental 1 KVA prototype unit.

5.2 Fundamentals

The basic principle of operation for this single phase to three converter can be derived from the general equation

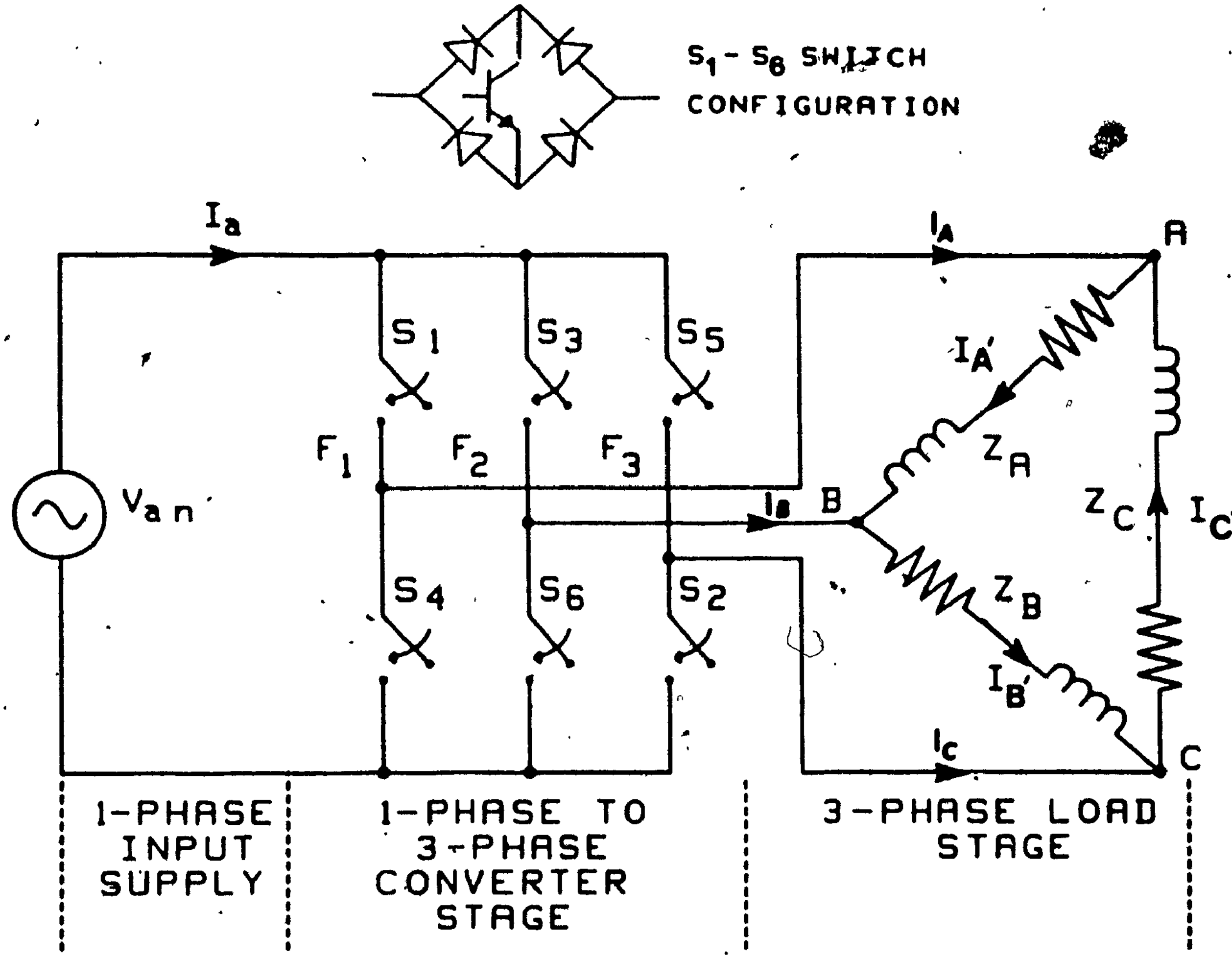

Fig. 5.2: Simplified circuit diagram of the proposed single to three phase converter.

(2.1) in Chapter 2, by setting the number of input phases, N=1 and number of output phase, M=3.

$$\begin{bmatrix} V_{AB} \\ V_{BC} \\ V_{CA} \end{bmatrix} = \frac{A_1 V_i}{2} \begin{bmatrix} \cos((\omega_s \pm \omega_i)t) \\ \cos((\omega_s \pm \omega_i)t - n240^o) \\ \cos((\omega_s \pm \omega_i)t - n120^o \end{bmatrix}$$

$$+ \sum_{n=2,3,4,\ldots}^{\infty} \frac{A_n V_i}{2} \begin{bmatrix} \cos((n\omega_s \pm \omega_i)t) \\ \cos((n\omega_s \pm \omega_i)t - n240^o) \\ \cos((n\omega_s \pm \omega_i)t - n120^o) \end{bmatrix} \qquad (5.1)$$

and respectively the input current equation is given by;

$$[I_a] = \frac{3A_1 I_o}{2} \cos(\omega_i t) + \sum_{n=2,5,8}^{\infty} \frac{3A_n I_o}{2} \cos((n\omega_s + \omega_o)t)$$

$$+ \sum_{n=4,7,10}^{\infty} \frac{3A_n I_o}{2} \cos((n\omega_s - \omega_o)t) \qquad (5.2)$$

Equation (5.1) and Tables 5.1-5.3 show that output voltages are balanced for all frequency ranges. It contains low order harmonics and their magnitudes are constant due to a fixed gating signal pattern. It should be noted here that the order of the harmonics vary according to the output frequency. However, this scheme is proposed here for fixed frequency application at 60 Hz ($f_i = f_o = 60$ Hz). The amplitude of the fundamental is given by $\frac{A_1 V_i}{2}$, (5.1). The input current spectrum is found to be very favourable and it does not inject any low order harmonics to input supply lines.

5.3 Physical Structure

A circuit configuration capable of transforming single phase input power to three phase output power is shown in Fig. 5.2. This structure consists of six bilateral switches as shown on top of the Fig. 5.2. Although this structure is suitable for variable frequency single to three phase conversion, only fixed frequency operation (at 60 Hz) is considered and analysed here. IMO condition is not applicable to this structure as imbalance occurs in the output voltages. Only DMO condition is applied to this structure.

5.4 Analysis of the Converter

The concept of FCC is used for the analysis of the converter and to explore the possibility of finding a quality single phase to three phase static phase converter. Since the intended use of the converter is for a fixed frequency operation, it is analysed at a output frequency which is same as the input frequency. Indirect mode of operation is discarded as imbalance occurs in output voltages (V_{AB1}= 0.95, V_{BC1}= 0.63).

Three DMO output voltage waveforms V_{AB}, V_{BC} and V_{CA} are plotted in Figs. 5.3, 5.4 and 5.5 respectively. Their spectra are shown in Tables 5.1, 5.2 and 5.3 respectively. Although the waveshape of V_{BC} is different from the waveshapes of the other two line voltages, their spectra are same. Fundamental component of output voltage is 55% of input voltage. This is in accordance to the predicted value in (5.1). The spectrum contains 3rd harmonic of the same amplitude as given by the second and third terms of (5.1). This 3rd harmonics (and higher harmonics) can however, be filtered by a 3rd harmonic trap (filter). The spectrum also contains harmonics of order 9, 11, 13 and 15 and of magnitude 11, 11, 8 and 8 percent respectively of the fundamental.

Respective input current waveform and its corresponding spectrum are shown in Fig. 5.6 and Table 5.4. Input current can be filtered for harmonic by suitable means to obtain a near sinusoidal waveshape. The harmonic content of the input current is as follows, 11th, 13th harmonics of magnitude 19 and 14 percent. Amplitude of the fundamental component is 96% of the output current.

5.5 Design Criteria

This converter requires only 6 gating signals for the 6 bilateral switches. The switches are composed of 4 diodes and a gate turn-off device, i.e. transistor. In near future these bilateral switches will be available (in sufficient power) in modular integrated forms. In designing the digital control (firing) circuit, the following need to be considered:

i) Deriving the 6 gating signals.

ii) Applying the 6 gating signals.

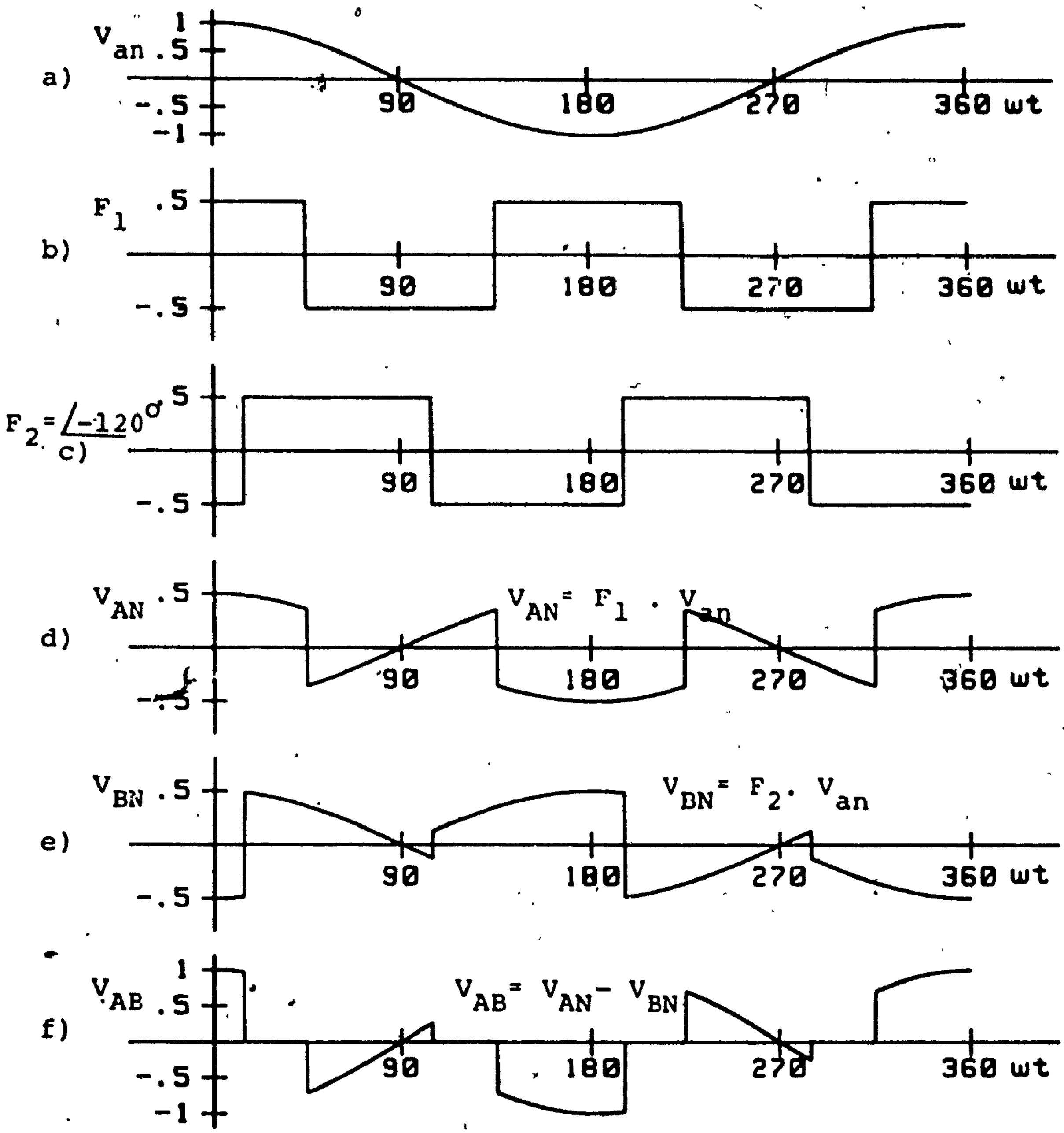

Fig. 5.3: Output voltage, V_{AB} waveform obtained with single to three phase converter.

TABLE 5.1

FREQUENCY SPECTRA OF WAVEFORMS ASSOCIATED WITH FCC OUTPUT VOLTAGE SHOWN IN FIG. 5.3

Harmonic coefficients of switching function (Fig. 5.3b)		Harmonic coefficients of resulting output line voltage V_{AB}, (Fig. 5.3) for $f_o = 60$ Hz $= f_i$		
		Amplitude, V_{AB}		
Order (n)	Amplitude (A_n)	Order (kf_o)	(1) p.u.	(1) %
1	1.27	f_o	0.55	55
3	0.42	$3f_o$	0.55	55
5	0.26	$9f_o$	0.11	11
7	0.18	$11f_o$	0.11	11
9	0.14	$13f_o$	0.08	8
11	0.12	$15f_o$	0.08	8
13	0.10			
15	0.09			
17	0.08			
19	0.07			

(1) Input phase voltages have been taken as 1 p.u. volt and 100% volt.

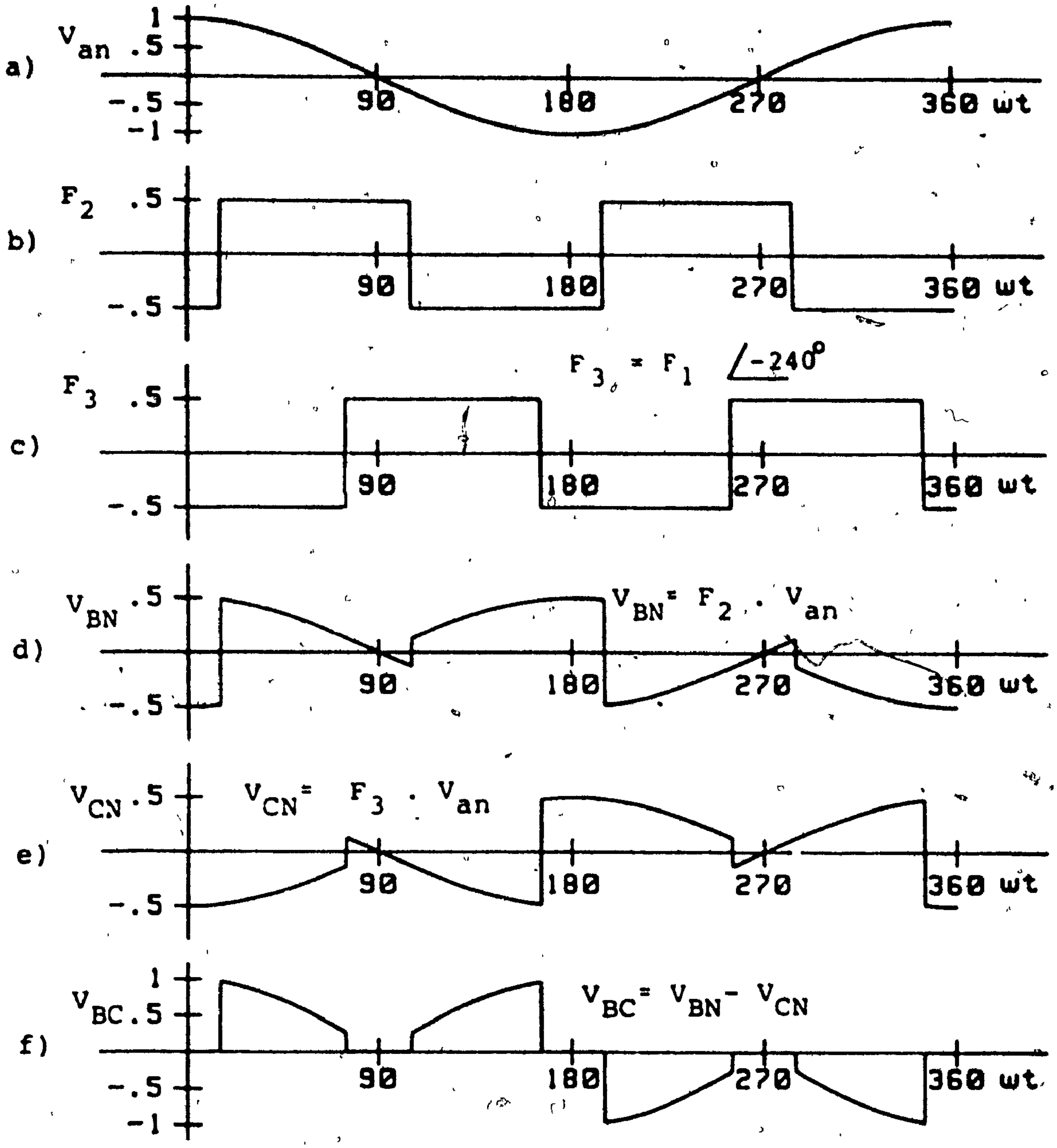

Fig. 5. 4: Output voltage, V_{BC} waveform obtained with single to three phase converter.

TABLE 5.2

FREQUENCY SPECTRA OF WAVEFORMS ASSOCIATED WITH FCC OUTPUT VOLTAGE SHOWN IN FIG. 5.4

Harmonic coefficients of switching function (Fig. 5.4b)		Harmonic coefficients of resulting output line voltage V_{BC}, (Fig. 5.4f) for $f_o = 60$ Hz $= f_i$		
		Amplitude, V_{BC}		
Order (n)	Amplitude (A_n)	Order (kf_o)	(1) p.u.	(1) %
		f_o	0.55	55
1	1.27			
3	0.42	$3f_o$	0.55	55
5	0.26			
7	0.18	$9f_o$	0.11	11
9	0.14	$11f_o$	0.11	11
11	0.12			
13	0.10	$13f_o$	0.08	8
15	0.09			
17	0.08	$15f_o$	0.08	8
19	0.07			

(1) Input phase voltages have been taken as 1 p.u. volt and 100% volt.

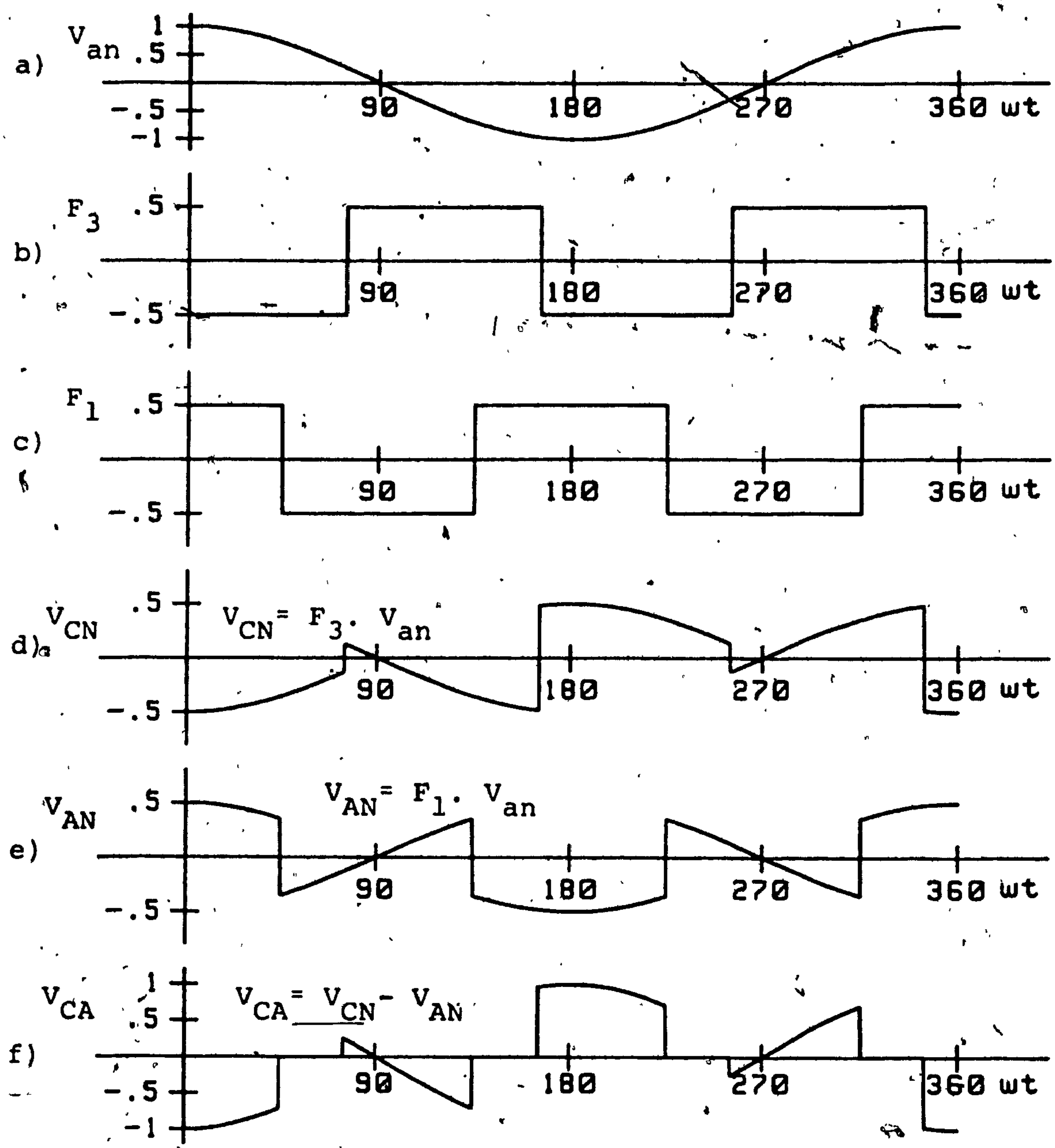

Fig. 5.5: Output voltage, V_{CA} waveform obtained with single to three phase converter.

TABLE 5.3

FREQUENCY SPECTRA OF WAVEFORMS ASSOCIATED WITH FCC OUTPUT VOLTAGE SHOWN IN FIG. 5.5

Harmonic coefficients of switching function (Fig. 5.5b)		Harmonic coefficients of resulting output line voltage V_{CA}, (Fig. 5.5f) for f_o= 60 Hz = f_i		
		Amplitude, V_{CA}		
Order (n)	Amplitude (A_n)	Order (kf_o)	(1) p.u.	(1) %
1	1.27	f_o	0.55	55
3	0.42	$3f_o$	0.55	55
5	0.26			
7	0.18	$9f_o$	0.11	11
9	0.14			
11	0.12	$11f_o$	0.11	11
13	0.10			
15	0.09	$13f_o$	0.08	8
17	0.08	$15f_o$	0.08	8
19	0.07			

(1) Input phase voltages have been taken as 1 p.u. volt and 100% volt.

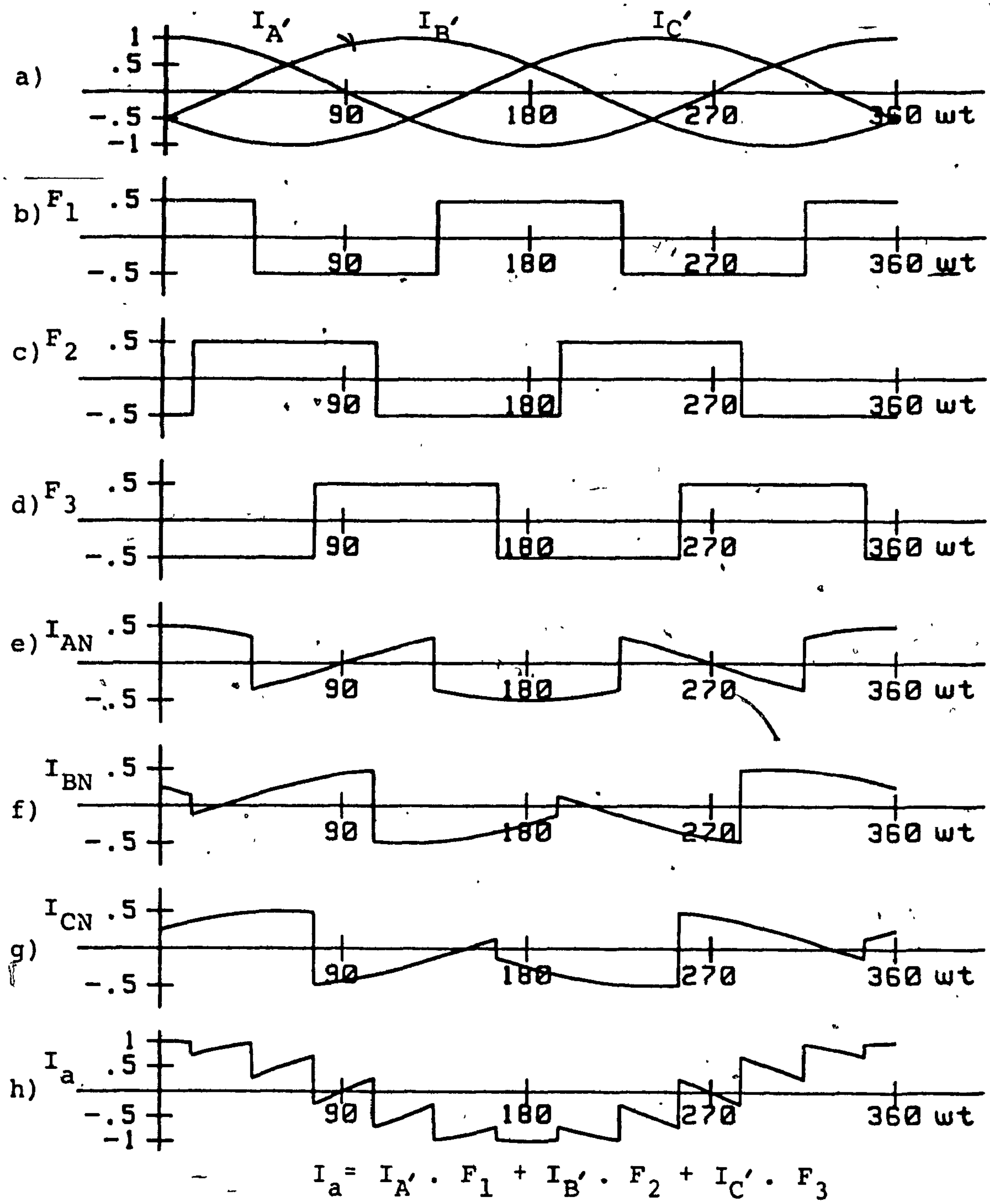

Fig. 5.6: Input current, I_a waveform obtained with single to three phase converter.

TABLE 5.4

FREQUENCY SPECTRA OF WAVEFORMS ASSOCIATED WITH FCC INPUT CURRENT SHOWN IN FIG. 5.6

Harmonic coefficients of switching function (Fig. 5.6b)		Harmonic coefficients of resulting input phase current I_{an}, (Fig. 5.6h) for f_o = 60 Hz = f_i		
			Amplitude, I_{an}	
Order (n)	Amplitude (A_n)	Order (kf_i)	(1) p.u.	(1) %
1	1.27	f_i	0.96	96
3	0.42			
5	0.26	$11f_i$	0.19	19
7	0.18			
9	0.14	$13f_i$	0.14	14
11	0.12			
13	0.10	$23f_i$	0.09	9
15	0.09			
17	0.08			
19	0.07			

1) Output phase currents have been taken as 1 p.u. current and 100% current.

The 6 gating signals are shown in Fig. 5.7a, which are pulses of 180^{o} duration. The voltage control can be achieved by introducing notches in the middle of the pulses as shown in Fig. 5.7b, or by reducing the pulse duration. These six gating signals are applied directly to the gates of the six switches.

5.6 Experimental Results

The experimental results obtained with this phase converter for various load conditions are shown in Figs. 5.8 to 5.10. Fig. 5.8A shows the output line voltage, input current, output line current and output phase currents for a resistive load. Output line voltages V_{AB}, B_{BC} and V_{CA} and their respective spectra are shown in Fig. 5.8B, C and D. The experimental voltage and current waveshapes and their corresponding spectra have close agreement with the analytically predicted results in Tables 5.1, 5.2 and 5.3. Thus, it is shown that they produce balanced output voltages. Input current and its spectrum is shown in Fig. 5.9A which agrees with the predicted spectrum shown in Table 5.4. Output phase and line currents and their spectra are shown in Fig. 5.9B and C respectively.

The same output voltage and current for delta connected R-L load of 0.8 power factor is shown in Fig. 5.10. They also agree with expected waveshape of voltages and currents.

a)

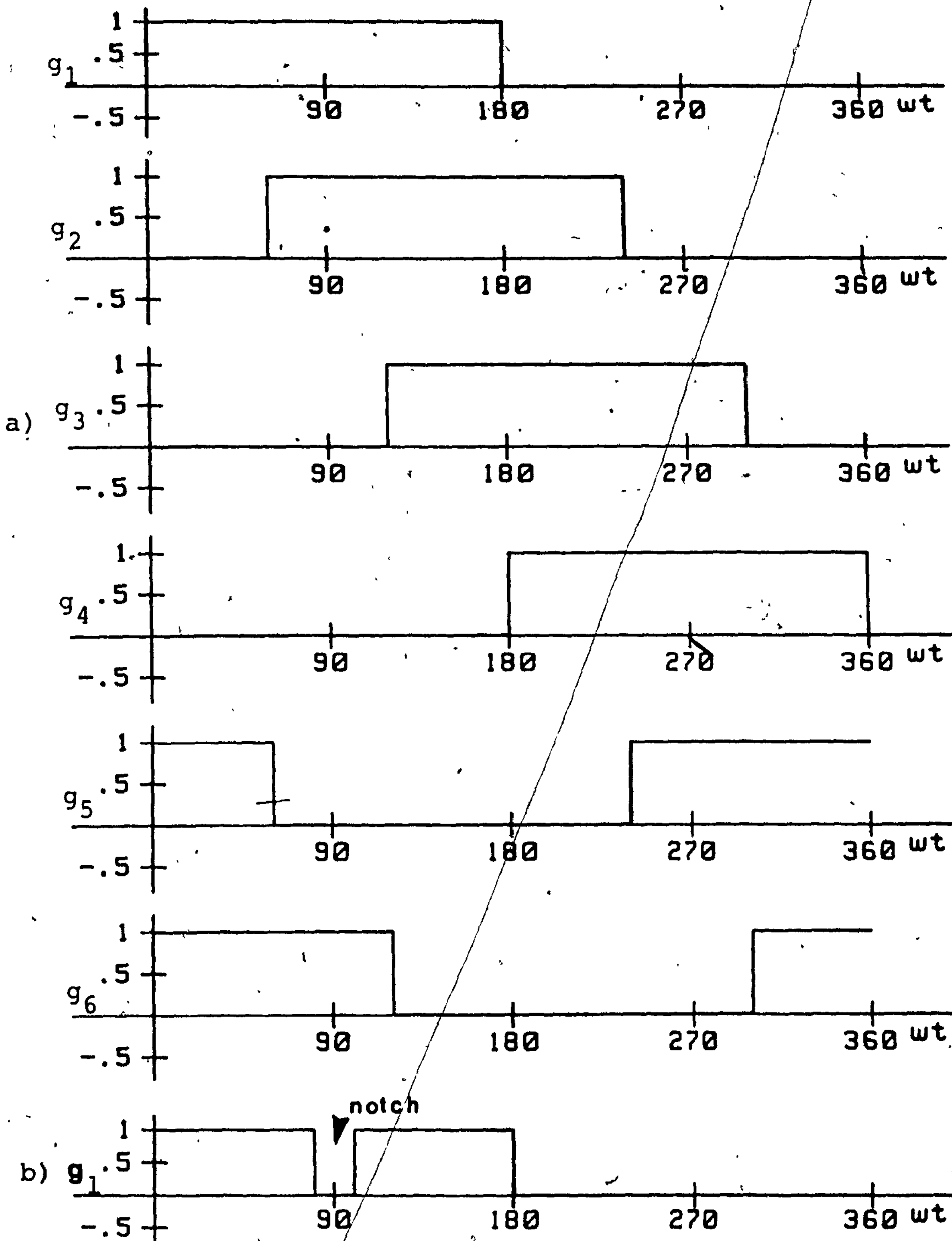

Fig. 5.7: Gating signals of the single to three phase converter.
a) g_1-g_6 gating signals.
b) Output voltage control by introducing notch.

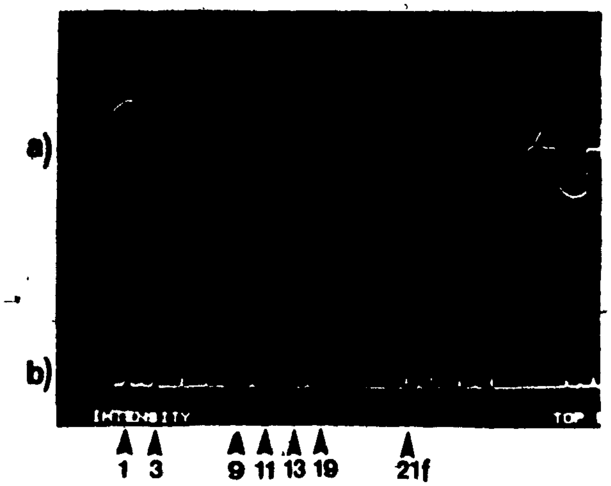

A. a) Output line voltage, V_{AB}.
b) Input current, I_a.
c) Output line current, I_A.
d) Output phase current, I_A' .

B. a) Output line voltage, V_{AB}.
b) Respective frequency spectrum.

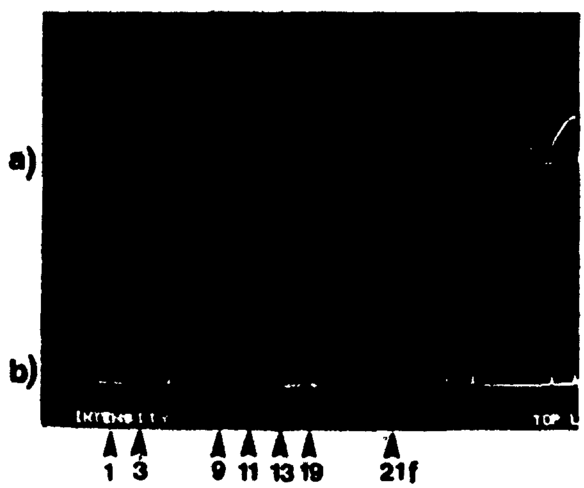

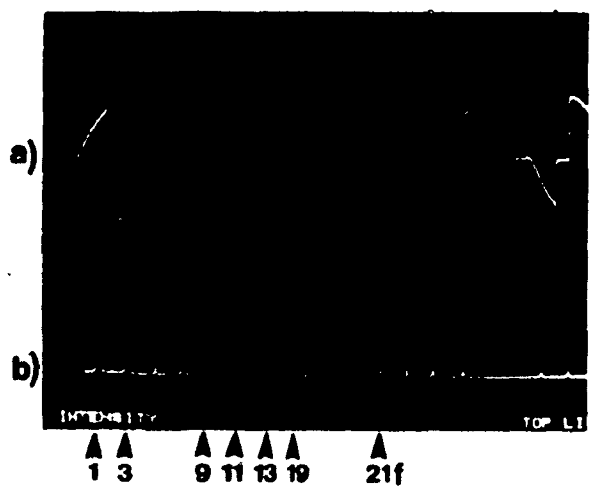

C. a) Output line voltage, V_{BC}.
b) Respective frequency spectrum.

D. a) Output line voltage, V_{CA}.
b) Respective frequency spectrum.

Fig. 5.8: Experimental input/output voltage/current waveforms obtained with the proposed single to three phase converter for delta connected resistive load.

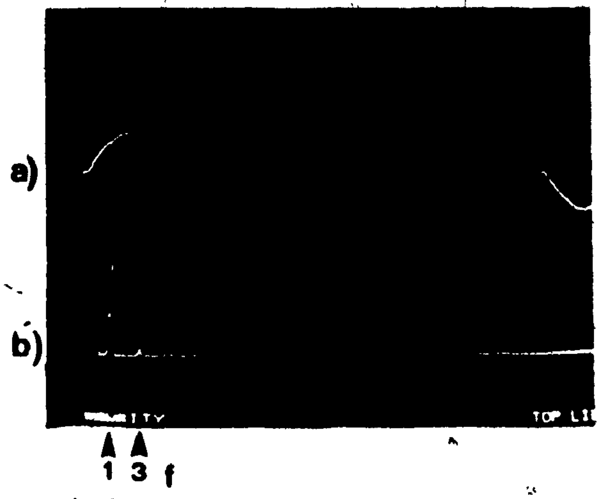

A. a) Input current, I_a.

b) Respective frequency spectrum.

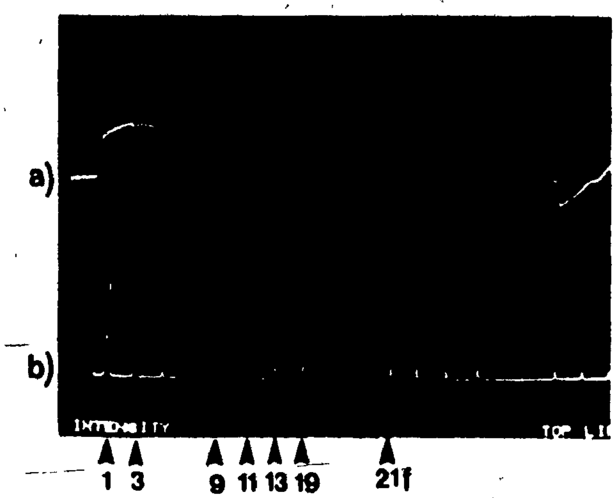

B. a) Output phase current, I_A'.

b) Respective frequency spectrum.

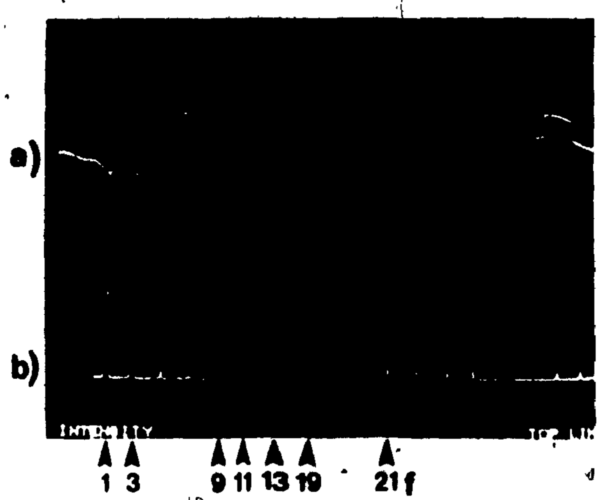

C. a) Output line current, I_A.

b) Respective frequency spectrum.

Fig. 5.9: Experimental input/output current waveforms obtained with the proposed single to three phase converter for delta connected resistive load.

A. a) Output line voltage, V_{AB}.
b) Input current, I_a.
c) Output line current, I_A.
d) Output phase current, I_A'.

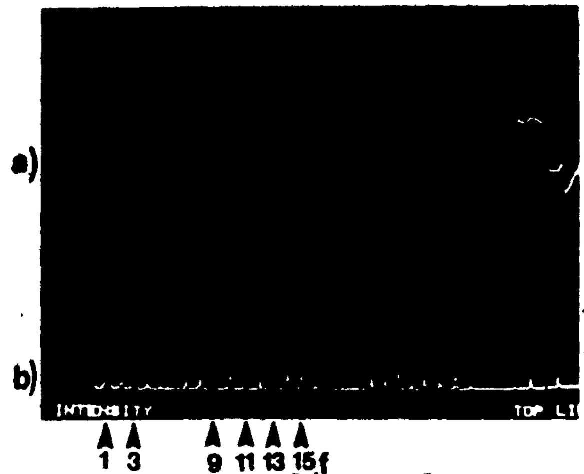

B. a) Output line voltage, V_{AB}.
b) Respective frequency spectrum.

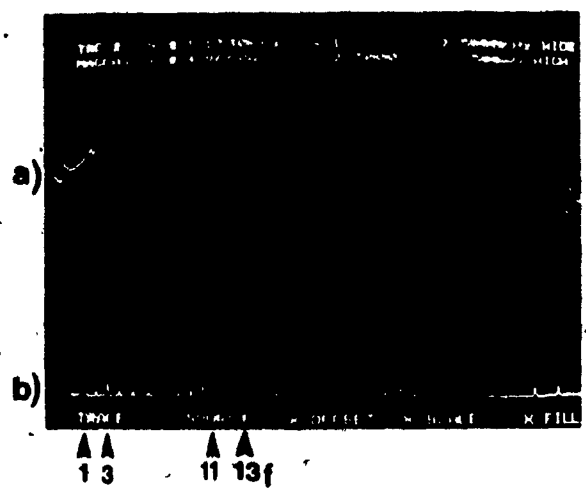

C. a) Input current, I_a.
b) Respective frequency spectrum.

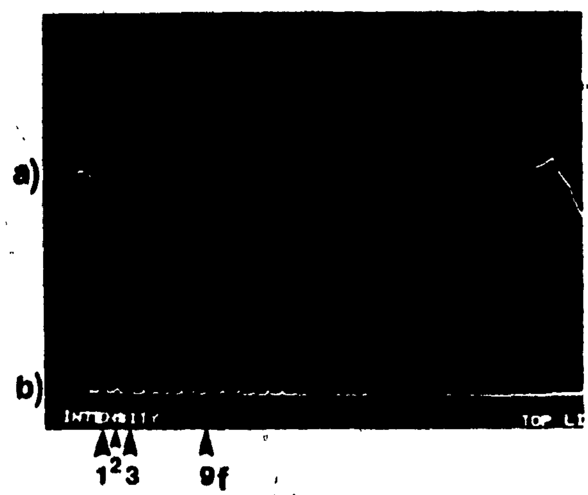

D. a) Output line current, I_A.
b) Respective frequency spectrum.

Fig. 5.10: Experimental input/output voltage/current waveforms obtained with the proposed single to three phase converter for delta connected R-L load (p.f. = 0.8).

5.7 Discussion and Conclusions

This chapter provides a comprehensive analysis of a phase converter structure capable of providing three phase power from existing single phase ac mains employing the principle of cycloconversion. The proposed converter provides balanced three phase output power. However, output voltages contain low order harmonics which can be easily filtered. The simple control logic circuit and standard six-switch configuration of the proposed scheme makes it attractive economically as well as practically.

Experimental results proves the validity of analytically predicted results of this new phase converter structure.

CHAPTER 6

CYCLOCONVERTERS FOR HIGH FREQUENCY LINK APPLICATIONS

6.1 Introduction

The possible applications of Forced Commutated Cycloconverters for low to medium frequency conversion have already been described in the previous chapters. This chapter investigates the use of FCCs for high frequency applications and in particular in the role of high frequency links (HFLs). Such links are widely used as intermediate stage circuits to provide simultaneous power conditioning and ohmic isolation of input and output stages.

High frequency links have shown a number of significant advantages in the area of static power conversion and conditioning. These advantages include; reduction in the size of magnetics, elimination of dc link components, capability for independant control of real and reactive power components, bilateral control of power flow, precise output voltage and input current waveshaping, [45]-[47], etc. Because of these advantages high frequency links are now employed in applications which require light-weight ac/dc and ac/ac power supplies. Some of the applications include; switch-mode rectifiers, battery chargers, and high frequency power distribution buses which are employed in 60 Hz and 400 Hz UPS. Moreover, HFLs have been recently proposed for linking asynchronously independent [48] utility lines and for linking utilities with industrial users.

So far most of the technical literature in this area focuses on thyristor based technology mainly because of the large power ratings envisaged and the established superior performance of thyristors in high power applications. Recent developments in the power semiconductor have shown that for low to medium power levels the bipolar power transistor is by far the most economical choice in many applications. In the present day power transistor with superior switching speeds are available in integrated-insulated packages which allow the implementation of novel circuit topologies that require only small size reactive components thus contributing to the overall reduction in converter size and weight. Several such HFL topologies are discussed and thoroughly analyzed in this chapter. Although some of these topologies are previously known [49]-[50], they have been treated here for the first time as a family of circuits with common functional characteristics. In particular three HFL circuit configurations (Figs. 6.1, 6.7 and 6.12) and two mode of operation (Figs. 6.2, 6.5) are discussed in this chapter. Each of these circuits is compatible with one of the following source phase to load phase configurations;

i) Three phase source to three phase load with no neutral available (Fig. 6.1).

ii) Three phase source to single phase load with no neutral available (Fig. 6.7).

iii) Three phase source to single phase load with neutral available (Fig. 6.12).

The two modes of operation i.e. the direct and indirect mode of operation (DMO and IMO) have already been described in Chapter 2. For each case the best combination of circuit topology and mode of operation has been sought for optimum system performance. For each of the aforementioned combinations this chapter presents;

i) A detailed functional description for the resulting HFL power conversion system.

ii) Respective input current and output voltage waveforms (Figs. 6.2, 6.3, etc.).

iii) Detailed harmonic analysis of the above with emphasis on respective voltage gain characteristics. (Tables 6.1-6.10).

Finally some predicted results are experimentally verified (Figs. 6.15 and 6.16) on 1 KVA laboratory prototype units.

6.2 Practical FCC Circuits for HFL Applications

The generalized N-input M-output voltage/frequency/phase static transformer (or FCC) topology shown in Fig. 2.1, Chapter 2 can be readily used to realize practical HFL-FCC circuits once the number of input/output phases (N,M) have been specified. Some of the examples treated in this chapter are shown in Fig. 6.2.

6.2.1 Three Phase to Three Phase HFL-FCC Circuit

Fig. 6.1 shows the simplified HFL-FCC circuit topology that results from the generalized case described in (Fig. 2.1, Chapter 2), by setting the number of input and output phases equal to three (i.e. N=M=3). This HFL topology is useful in cases where a fixed frequency, fixed voltage three phase ac power supply is used as a common source for several loads with different variable frequency (e.g. from dc to 400 Hz) variable voltage supply requirements (these loads are assumed to include their respective frequency step down converters). Other applications include; static VAR compensators and/or dedicated three phase high frequency loads.

Output voltage and input current equations are same as described in (3.7), (3.8); (3.14) and (3.15) in Chapter 3 for DMO and IMO respectively. One efficient scheme each for DMO and IMO are considered and analysed here.

6.2.1.1 DMO HFL-FCC Characteristics

The waveforms of the elements $f_{1,1}$, $f_{1,2}$ and $f_{1,3}$ of the converter "switching matrix" $[F_d(\omega_s t)]$ are shown in Fig. 6.2.b, c, d. The respective spectrum of these waveforms is shown in column 2 of Table 6.1. The main advantage with this type of switching waveforms is that they yield maximum possible output to input voltage gain (i.e. ≈0.827) for the DMO. However, the principle disadvantage is that they generate output voltage waveforms (Fig. 6.2.e) with low order harmonics of significant amplitude. This is shown in

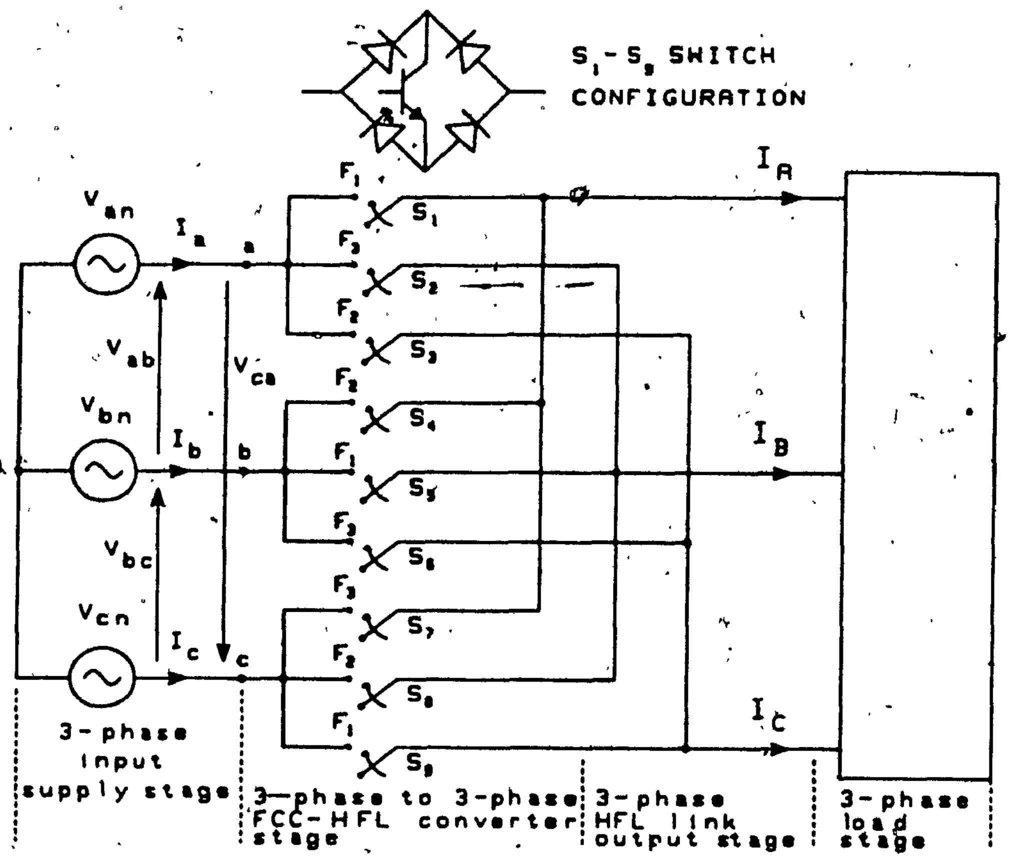

Fig. 6.1: Simplified circuit diagram of the proposed three-phase to three-phase FCC-HFL topology.

columns 3, 4 and 5 of Table 6.1. These three columns also illustrate the amplitudes of all other significant components of the generated FCC-HFL output voltage (line to line) waveforms. Respective DMO output/input currents and switching matrix waveforms are shown in Fig. 6.3. Table 6.2 provides the amplitudes of all significant components of the input current ~~waveforms~~ shown in Fig. 6.3. It is worth noting that the resulting input current does not contain any low order harmonics provided that $f_o \gg f_i$.

Output voltage control can be achieved by introducing notches at the centre of the pulses as shown in Fig. 6.4.

6.2.1.2 IMO HFL-FCC Characteristics

IMO is a two step process. In this method, input voltage is, first rectified into dc voltage, and then it is inverted to obtain the desired frequency at the output. Output frequency is varied by varying the inverter frequency. MSPWM switching function consists of a number of pulses and as such, some of the pulses may be lost at that high frequency due to finite switching time of the inverter switches. Therefore, inverter switching function cannot be PWM SF. Therefore, only one scheme where rectifier function in MSPWM and inverter function is single pulse is considered for analysis.

Respective output voltage and input current results are presented here for the indirect mode of operation (IMO). In particular, Fig. 6.5 shows the waveform of the $f_{1,1}$ element

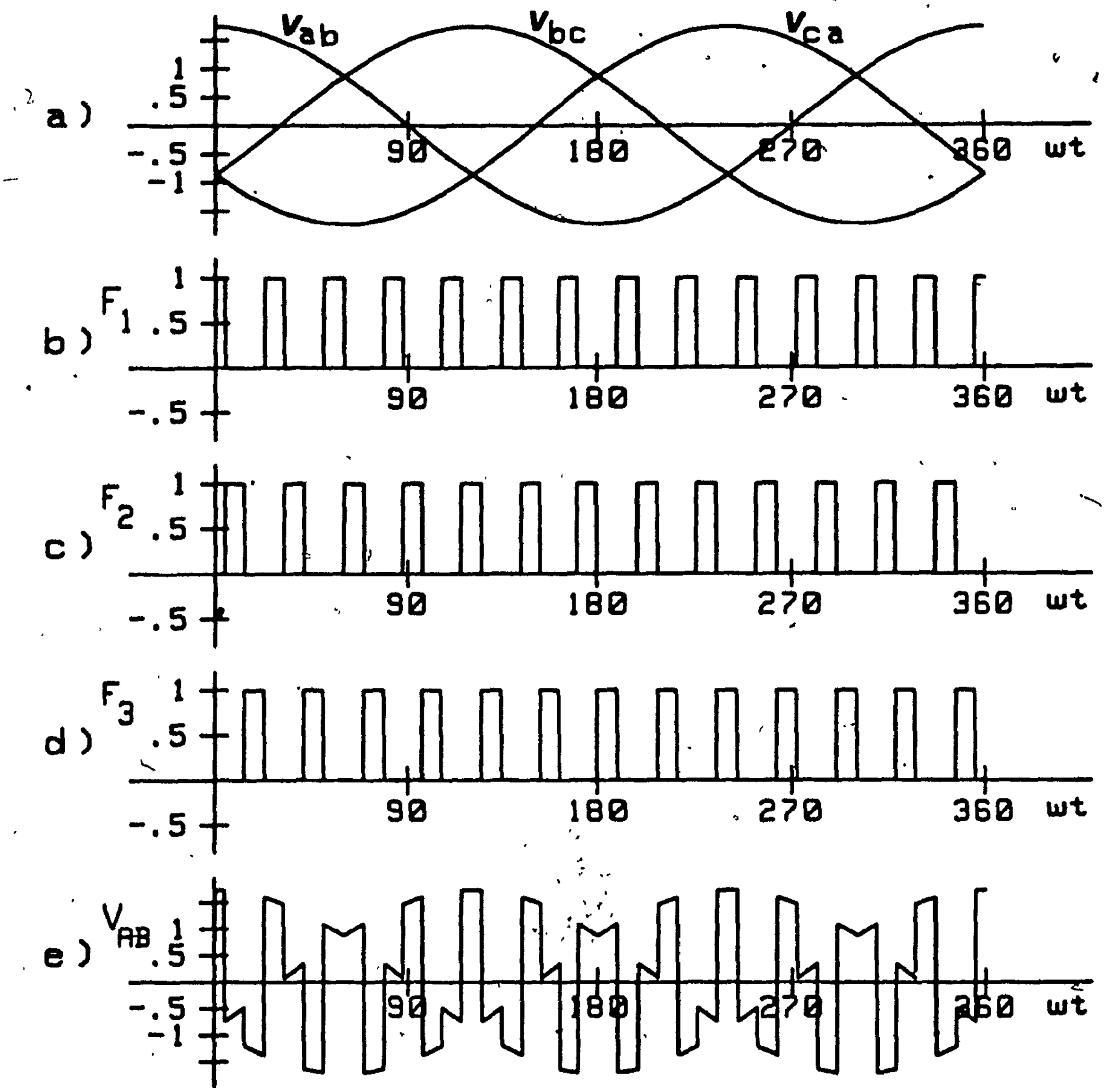

Fig. 6.2: High frequency output voltage waveform obtained with three-phase to three-phase DMO FCC-HFL topology.
a) Three input line voltages.
b) - d) F_1, F_2, F_3 switching function components.
c) Resulting output line voltage, V_{AB}.

TABLE 6.1

FREQUENCY SPECTRA OF WAVEFORMS ASSOCIATED WITH FCC HIGH FREQUENCY OUTPUT VOLTAGE SHOWN IN FIG. 6.2

Harmonic coefficients of switching function (Fig. 6.2b)		Harmonic coefficients of resulting output line voltage V_{AB}, (Fig. 6.2e) for f_o= 720 Hz = $12f_i$		
			Amplitude, V_{AB}	
Order (n)	Amplitude (A_n)	Order (kf_o)	(1) p.u.	(1) %
dc	0.33			
1	0.55	f_o	0.83	83
2	0.28	$2f_o+3f_i=2.25f_o$	0.42	42
4	0.14	$4f_o+3f_i=4.25f_o$	0.21	21
5	0.11	$5.5f_o$	0.17	17
7	0.08	$7.5f_o$	0.12	12
8	0.07	$8.75f_o$	0.10	10
10	0.06	$10.75f_o$	0.08	8
16	0.04	$12f_o$	0.08	8
17	0.03	$14f_o$	0.06	6
19	0.03	$18.5f_o$	0.05	5

(1) Input line voltages have been taken as 1 p.u. volt and 100% volt.

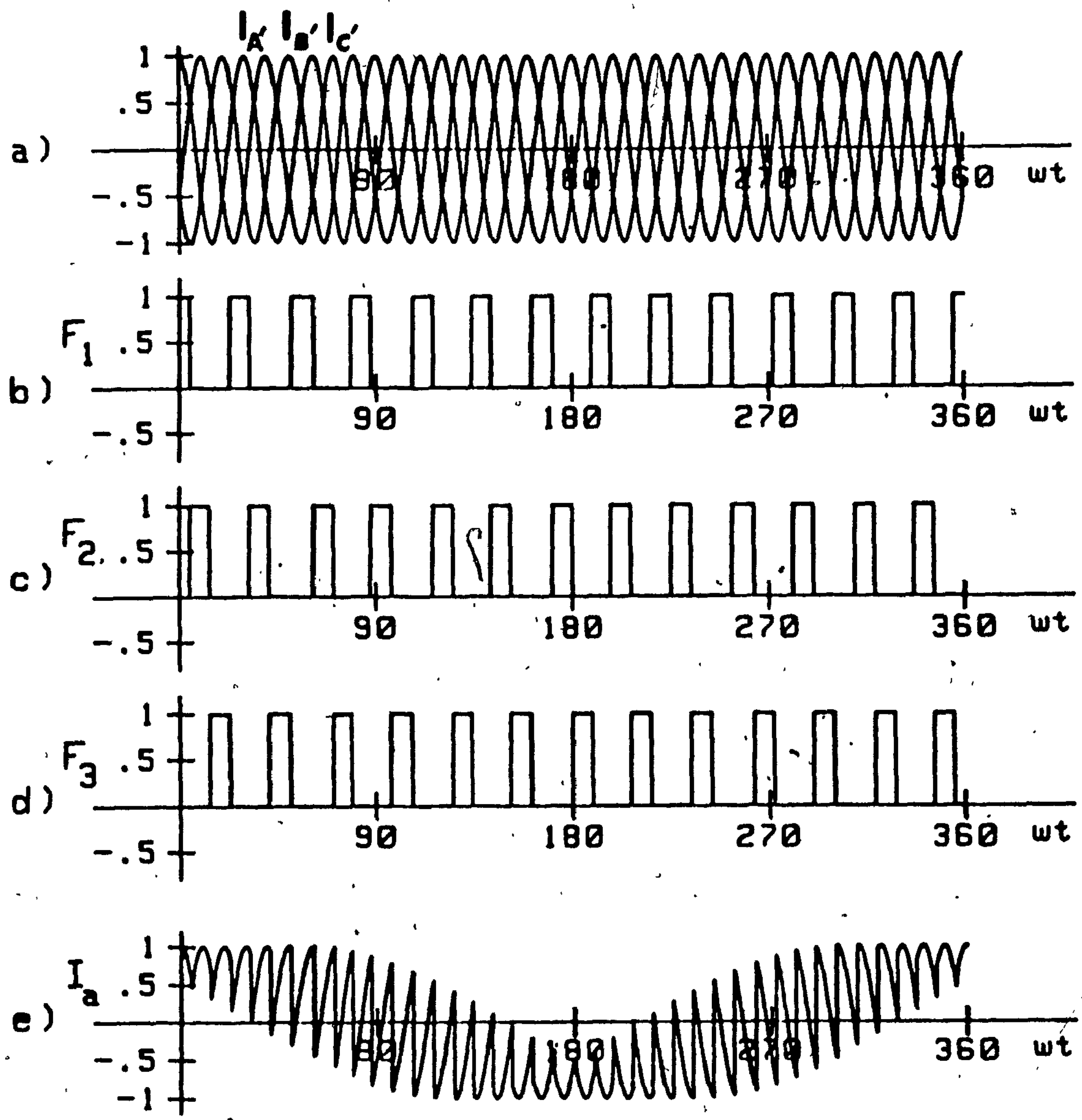

Fig. 6.3: Input current waveform obtained with three-phase to three-phase DMO FCC-HFL topology.
a) Three output phase currents.
b) - d) F_1, F_2, F_3 switching function components.
c) Resulting input current, I_a.

TABLE 6.2

FREQUENCY SPECTRA OF WAVEFORMS ASSOCIATED WITH FCC INPUT CURRENT SHOWN IN FIG. 6.3

Harmonic coefficients of switching function (Fig. 6.3b)		Harmonic coefficients of resulting input phase current I_{an}, (Fig. 6.3e) for f_o = 720 Hz = $12f_i$		
			Amplitude, I_{an}	
Order (n)	Amplitude (A_n)	Order (kf_i)	(1) p.u.	(1) %
dc	0.33			
1	0.55	f_i	0.83	83
2	0.28	$2f_i+3f_o=38f_i$	0.42	42
4	0.14	$4f_i+3f_o=40f_i$	0.21	21
5	0.11	$77f_i$	0.17	17
7	0.08	$79f_i$	0.12	12
8	0.07			
10	0.06			
16	0.04			
17	0.03			
18	0.03			

1) Output phase current has been taken as 1 p.u. current and 100% current.

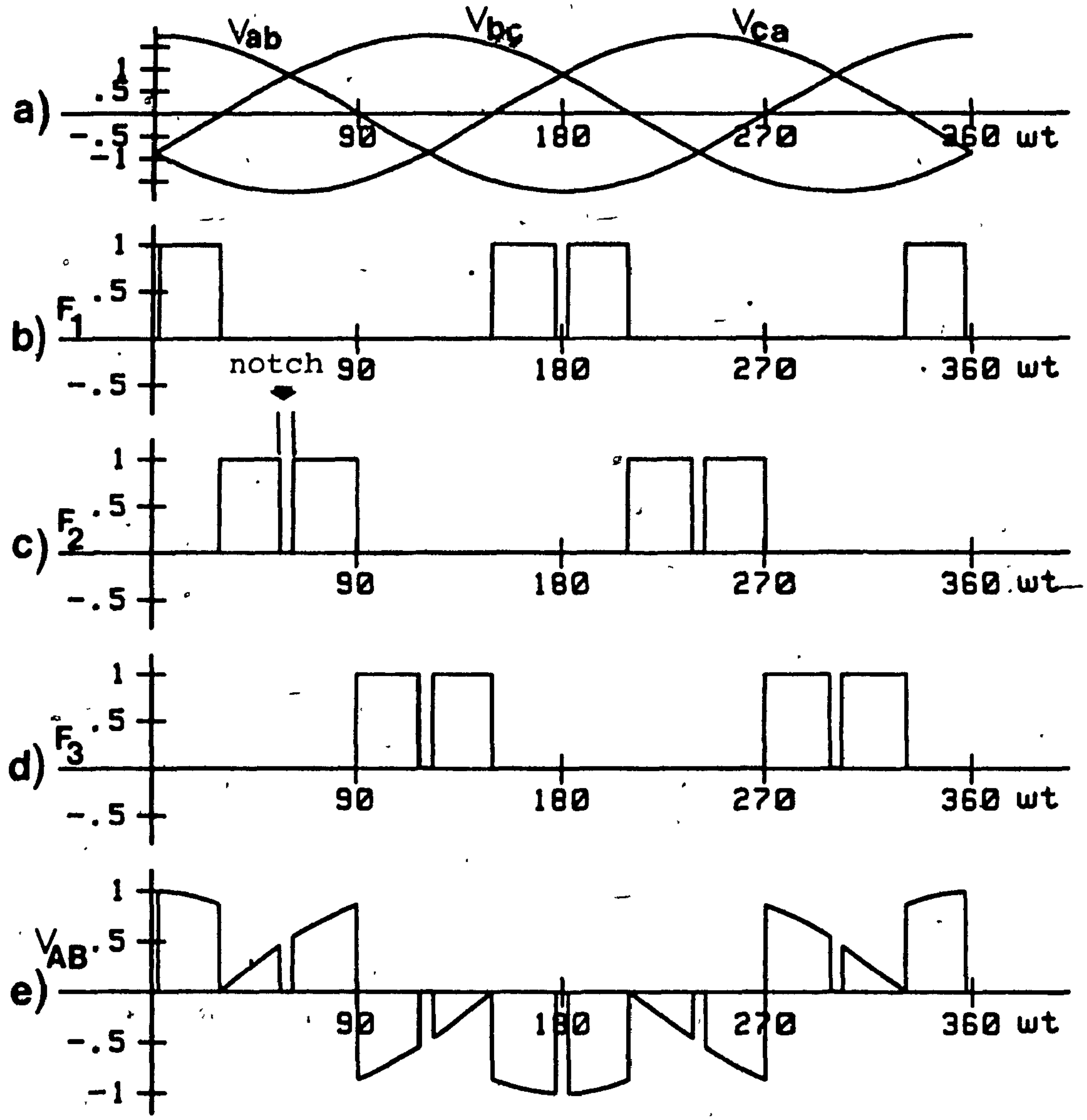

Fig. 6.4: Output voltage control for DMO_FCC-HFL topology by introducing notches.

of the fictitious rectifier switching matrix $[F_r(\omega_i t)]$ while Fig. 6.5d shows corresponding waveform for the fictitious inverter switching matrix $[F_i(\omega_o t)]$. Also the waveform of one of the resulting HFL line to line output voltages V_{AB} is shown in Fig. 6.5e. Similar waveforms regarding HFL input current are shown in Fig. 6.6.

Complementary information for the abovementioned voltage/current/'switching matrix' waveforms is given in Tables 6.3 and 6.4. It can be seen from column 6 of Table 6.3 that the IMO mixed modulation scheme provides a good voltage gain (i.e. 0.96). Moreover, as shown in Table 6.4 column 5 the respective HFL input currents are free of low order harmonic components.

6.2.2 Three Phase to Single Phase HFL-FCC Circuits

Three phase to single phase conversion can be achieved by two structure, i.e. full-bridge (6 switch) or half-bridge (4 switch). Input and output current and voltage equations shown in (4.1), (4.2) and (4.3), (4.4) in Chapter 4 are equally valid for high output frequency. These two structures are analysed below.

6.2.2.1 Full-bridge Configuration

Fig. 6.7 shows a simplified FCC-HFL circuit topology that results from the generalized cycloconverter structure (shown in Fig. 2.1, Chapter 2) by setting the number of input phases N=3 and the number of output phases M=1. This HFL

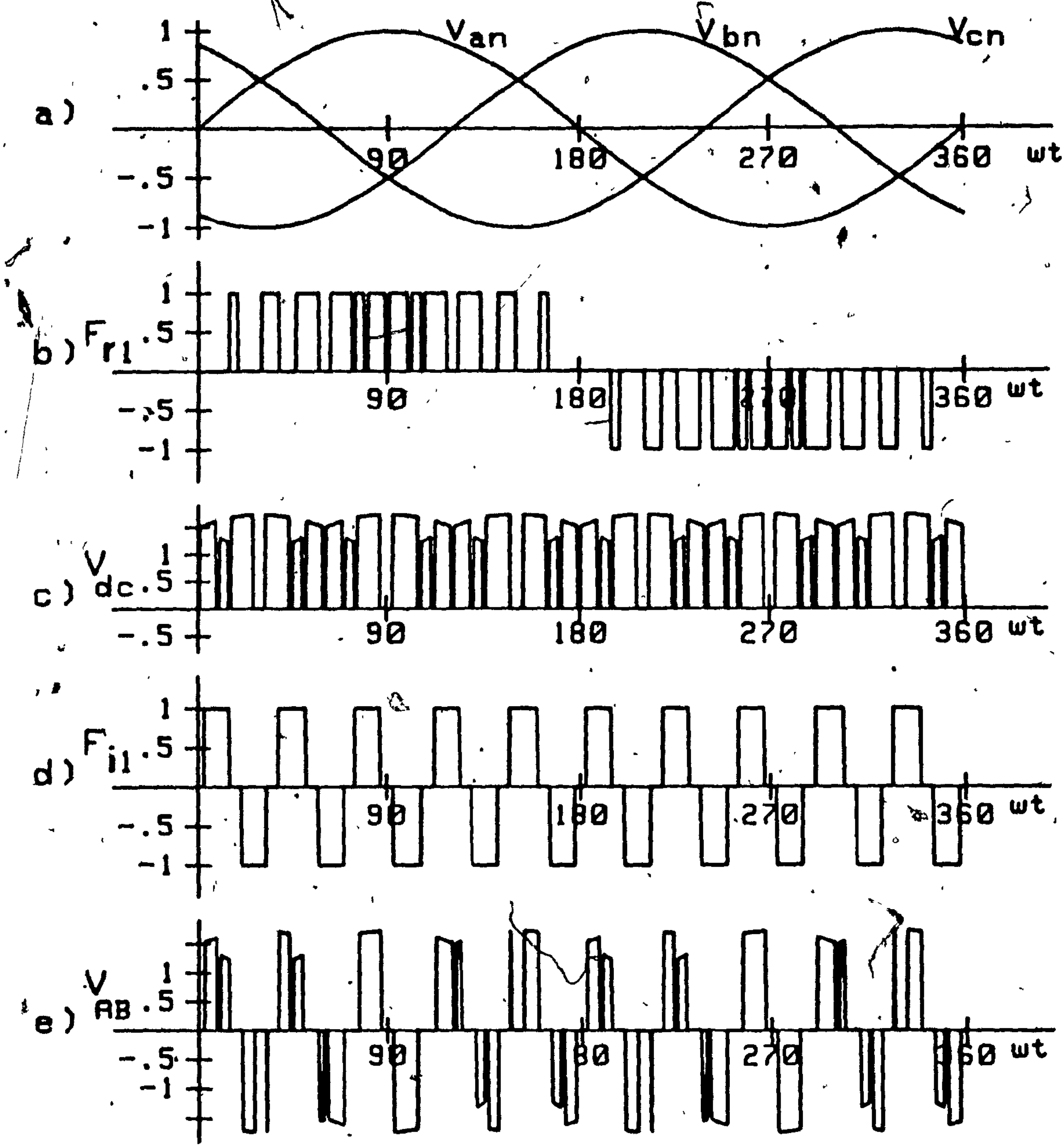

Fig. 6.5: High frequency output voltage waveform obtained with three to three phase IMO FCC-HFL topology. a) Three input phase voltages. b) Fictitious rectifier SF. c) Fictitious rectifier voltage. d) Fictitious inverter SF. e) Resulting output line voltage, V_{AB}.

TABLE 6.3

FREQUENCY SPECTRA OF WAVEFORMS ASSOCIATED WITH HIGH FREQUENCY FCC OUTPUT VOLTAGE SHOWN IN FIG. 6.5

Harmonic coefficients of rectifier and inverter switching function (Fig. 6.5b and 6.5d)				Harmonic coefficients of resulting output phase voltage, V_{AN} (Fig. 6.5e) for $f_o = 720$ Hz $= 12f_i$		
Rectifier SF		Inverter SF		Amplitude, V_{AN}		
Order (n)	Amplitude (A_n)	Order (k)	Amplitude (B_k)	Order (kf_o)	(1) p.u.	(1) %
				dc	0.00329	0.329
				$0.5f_o$	0.01	1
1	0.99	1	1.10	f_o	0.96	96
				$1.5f_o$	0.075	7.5
3	--	3	--	$2f_o$	0.055	5.5
				$2.5f_o$	0.013	1.3
5	--	5	0.22	$3.5f_o$	0.075	7.5
				$4f_o$	0.109	10.9
7	--	7	0.16	$4.5f_o$	0.067	6.7
				$5f_o$	0.224	22.4
9	--	9	--	$5.5f_o$	0.017	1.7
				$6f_o$	0.042	4.2
11	--	11	0.10	$6.5f_o$	0.076	7.6
				$7f_o$	0.082	8.2
13	--	13	0.09	$8f_o$	0.009	0.9
				$8.5f_o$	0.018	1.8
15	--	15	--	$9f_o$	0.022	2.2
				$9.5f_o$	0.009	0.9
17	0.11	17	0.07	$10f_o$	0.008	0.8
19	0.26	19	0.06			

(1) Input phase voltages have been taken as 1 p.u. volt.

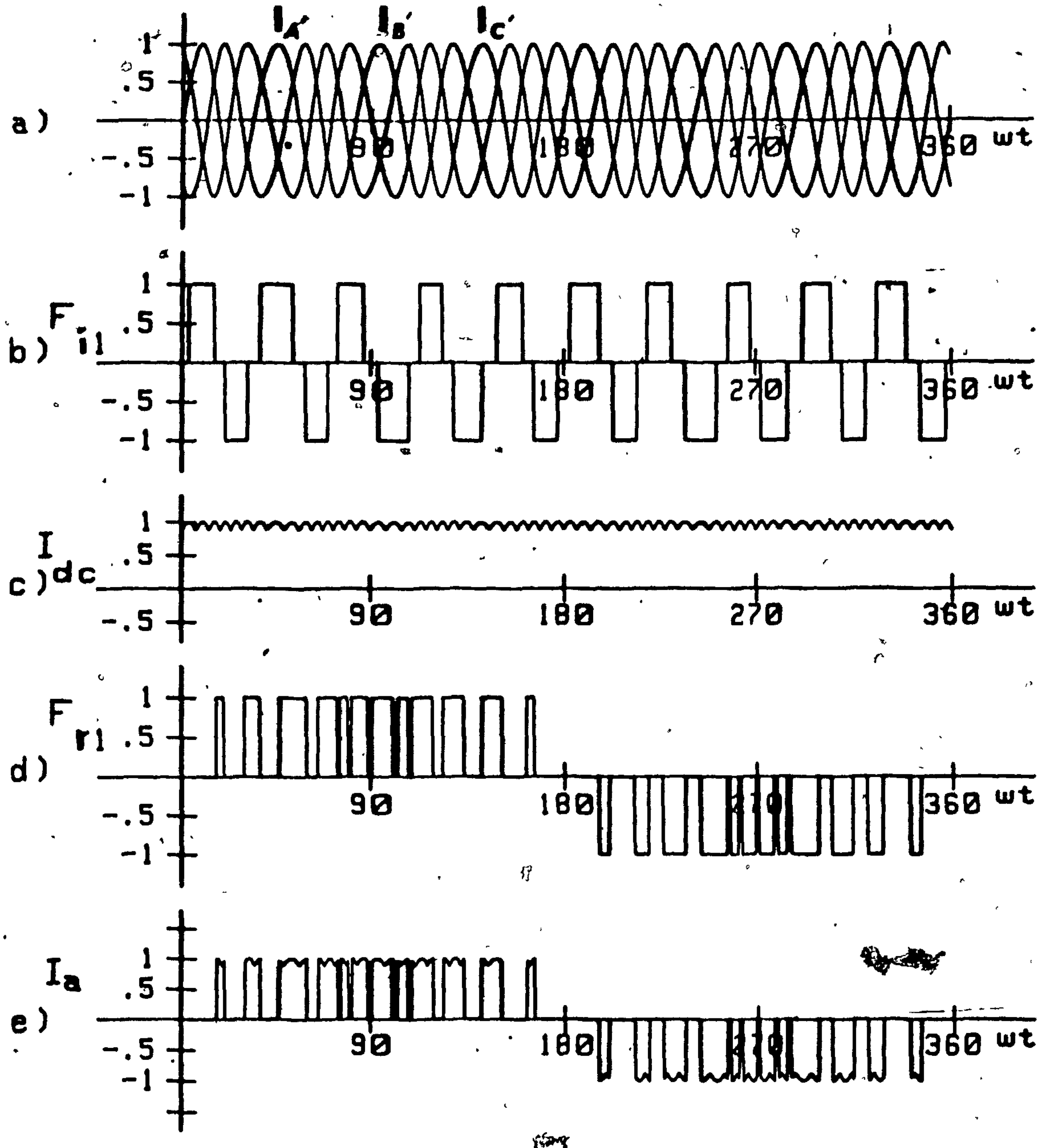

Fig. 6.6: Input current waveform obtained with three to three phase IMO FCC-HFL topology.

TABLE 6.4						
FREQUENCY SPECTRA OF WAVEFORMS ASSOCIATED WITH FCC INPUT CURRENT SHOWN IN FIG. 6.6						
Harmonic coefficients of inverter and rectifier switching function (Fig. 6.6b and 6.6d)				Harmonic coefficients of resulting input phase current, I_{an}, (Fig. 6.6e) for f_o = 720 Hz = $12f_i$		
Inverter SF		Rectifier SF		Amplitude, I_{an}		
Order (k)	Amplitude (B_k)	Order (n)	Amplitude (A_n)	Order (kf_i)	(1) p.u.	(1) %
1	1.10	1	0.99	f_i	0.954	95.4
3	--	3	--	$25f_i$	0.006	0.6
5	0.22	5	--	$29f_i$	0.109	10.9
7	0.16	7	--	$31f_i$	0.245	24.5
9	--	9	--	$35f_i$	0.246	24.6
11	0.10	11	--			
13	0.09	13	--			
15	--	15	--			
17	0.07	17	0.11			
19	0.06	19	0.26			

(1) Output phase currents have been taken as 1 p.u. current and 100% current.

topology is particularly suitable for ac/dc power conversion process (such as switch-mode rectifiers) that incorporates stages of high frequency ohmic isolation [47]. They can also be employed for any of the applications considered in sub-section 6.2.1.

Moreover, the HFL circuit topology can function equally well either with DMO or IMO. Again, the waveforms of the elements $f_{1,1}$, $f_{1,2}$ and $f_{1,3}$ of the converter DMO 'switching matrix' $[F_d(\omega_s t)]$ are shown in Fig. 6.8b, c and d. Fig. 6.8e shows the waveform of the resulting HFL output line to line voltage V_{AB}. Respective HFL input current waveforms are shown in Fig. 6.9. Complementary information regarding the harmonic composition of the abovementioned waveforms is tabulated in Tables 6.5 and 6.6. In particular column 5 of Table 6.5 shows that the maximum amplitude of the fundamental component of V_{AB} is approximately 96% of the respective amplitudes of the input line voltage and also that V_{AB} contains significant low order harmonics. However as expected, no subharmonic components are present in the V_{AB} spectrum. Similarily column 3 of Table 6.6 shows that the resulting three HFL input currents, although discontinuous, do not contain any low order harmonics. These features allow effective filtering of unwanted current harmonics employing smaller size input filter components.

Output voltage and input current waveforms and their associated frequency spectra for IMO are shown in Figs. 6.10, 6.11 and Tables 6.7 and 6.8 respectively. This mode of

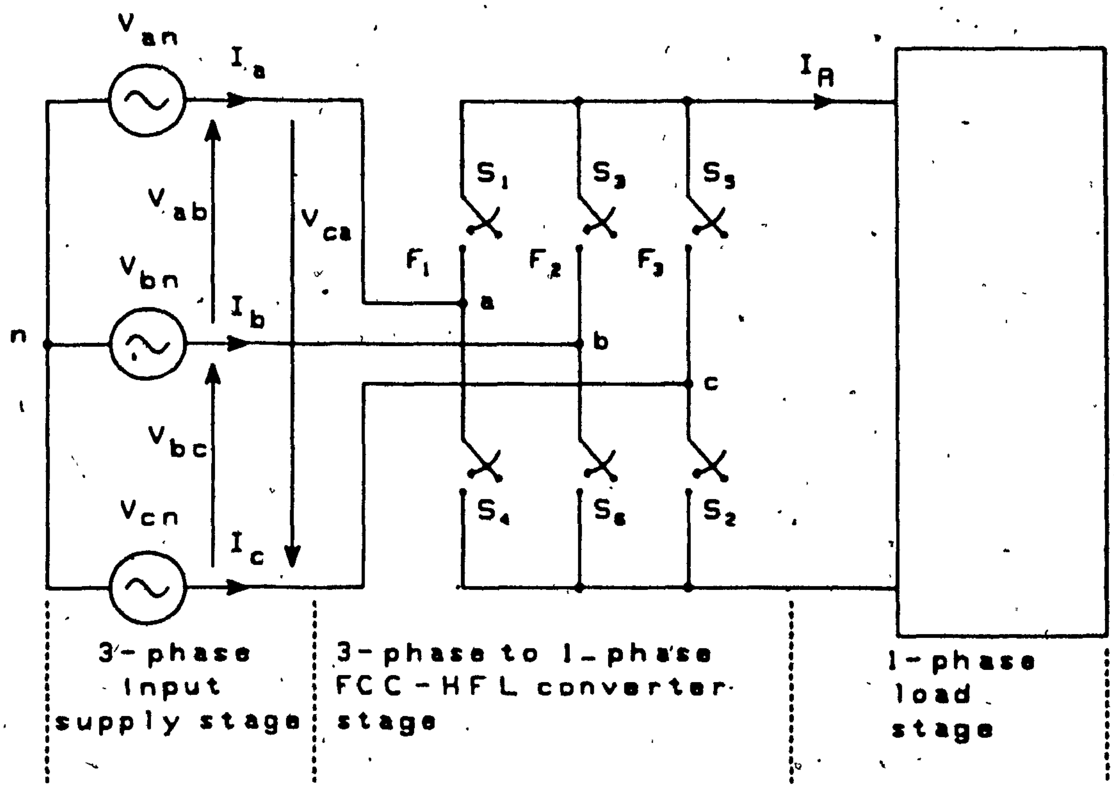

Fig. 6.7: Simplified circuit diagram of the proposed three-phase to single-phase FCC-HFL topology with no neutral available.

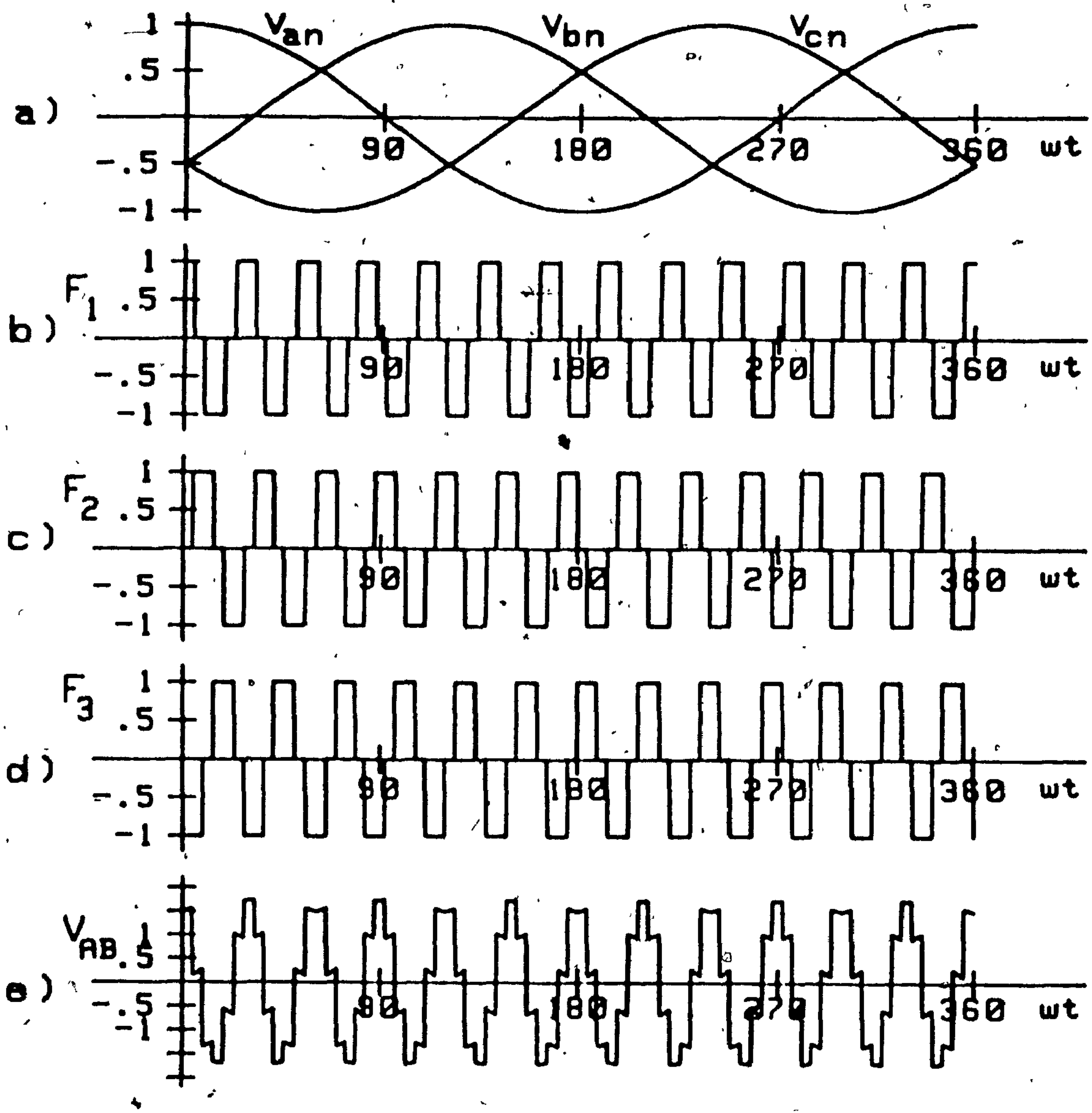

Fig. 6.8: High frequency output voltage waveform obtained with three-phase to single-phase (full-bridge) DMO FCC-HFL topology.

TABLE 6.5

FREQUENCY SPECTRA OF WAVEFORMS ASSOCIATED WITH FCC HIGH FREQUENCY OUTPUT VOLTAGE SHOWN IN FIG. 6.8

Harmonic coefficients of switching function (Fig. 6.8b)		Harmonic coefficients of resulting output phase voltage V_{AN}, (Fig. 6.8e) for $f_o = 720$ Hz $= 12f_i$		
		Amplitude, V_{AN}		
Order (n)	Amplitude (A_n)	Order (kf_o)	(1) p.u.	(1) %
1	1.10	f_o	0.96	96
3	--	$5.5f_o$	0.19	19
5	0.22	$7.5f_o$	0.14	14
		$12f_o$	0.09	9
7	0.16			
		$14f_o$	0.07	7
9	--			
		$18.5f_o$	0.06	6
11	0.10			
		$25f_o$	0.04	4
13	0.09			
15	--			
17	0.07			
19	0.06			

(1) Input phase voltages have been taken as 1 p.u. volt and 100% volt.

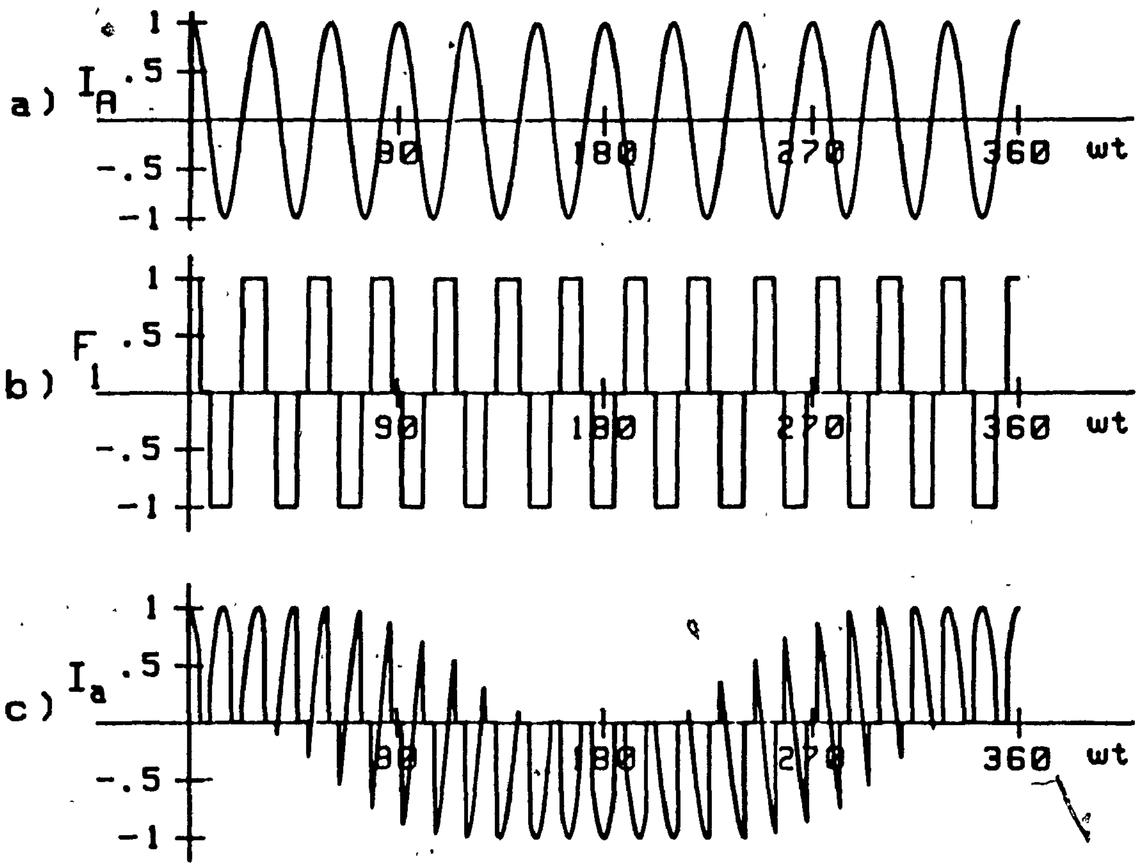

Fig. 6.9: Input current waveform obtained with three to single-phase (full bridge) DMO FCC-HFL topology.

TABLE 6.6

FREQUENCY SPECTRA OF WAVEFORMS ASSOCIATED WITH FCC INPUT CURRENT SHOWN IN FIG. 6.9

Harmonic coefficients of switching function (Fig. 6.9b)		Harmonic coefficients of resulting input phase current I_{an}, (Fig. 6.9c) for $f_o = 720$ Hz $= 12f_i$		
Order	Amplitude	Amplitude, I_{an}		
(n)	(A_n)	Order (kf_i)	(1) p.u.	(1) %
1	1.10	f_i	0.55	55
3	--	$25f_i$	0.55	55
5	0.22	$53f_i$	0.11	11
7	0.16	$77f_i$	0.11	11
9	--	$79f_i$	0.08	8
11	0.10			
13	0.09			
15	--			
17	0.07			
19	0.06			

1) Output phase currents have been taken as 1 p.u. current and 100% current

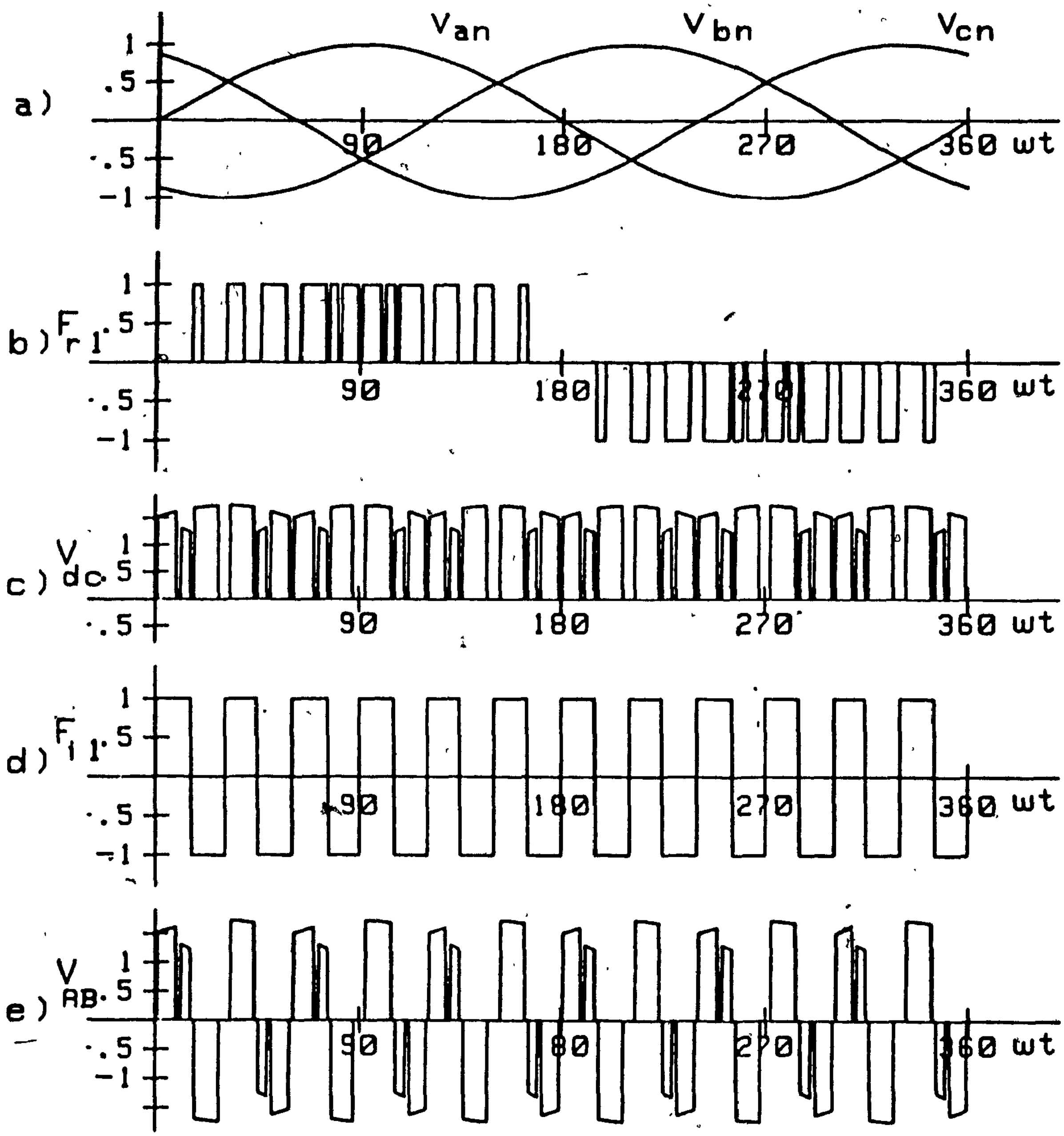

Fig. 6.10: High frequency output voltage waveform obtained with three-phase to single-phase (full bridge) IMO FCC-HFL topology.

TABLE 6.7

FREQUENCY SPECTRA OF WAVEFORMS ASSOCIATED WITH FCC OUTPUT VOLTAGE SHOWN IN FIG. 6.10

Harmonic coefficients of rectifier and inverter switching function (Fig. 6.10b and 6.10d)				Harmonic coefficients of resulting output phase voltage, V_{AN} (Fig. 6.10e) for f_o= 720 Hz = $12f_i$		
Rectifier SF		Inverter SF		Amplitude, V_{AN}		
Order (n)	Amplitude (A_n)	Order (k)	Amplitude (B_k)	Order (kf_o)	(1) p.u.	(1) %
				dc	0.00134	0.13
				$0.5f_o$	0.0738	7.38
1	0.99	1	1.27	f_o	1.05	105.0
				$1.5f_o$	0.012	1.2
3	--	3	0.42	$2f_o$	0.045	4.5
				$2.5f_o$	0.139	13.9
5	--	5	0.26	$3f_o$	0.5	50.0
				$3.5f_o$	0.049	4.9
7	--	7	0.18	$4f_o$	0.064	6.4
				$4.5f_o$	0.062	6.2
9	--	9	0.14	$5f_o$	0.171	17.1
				$5.5f_o$	0.059	5.9
11	--	11	0.12	$6f_o$	0.028	2.8
				$6.5f_o$	0.065	6.5
13	--	13	0.10	$7f_o$	0.251	25.1
				$7.5f_o$	0.017	1.7
15	--	15	0.09	$8f_o$	0.008	0.8
17	0.11	17	0.08			
19	0.26	19	0.07			
23	0.26	23	0.06			

(1) Input phase voltages have been taken as 1 p.u. volt and 100% volt.

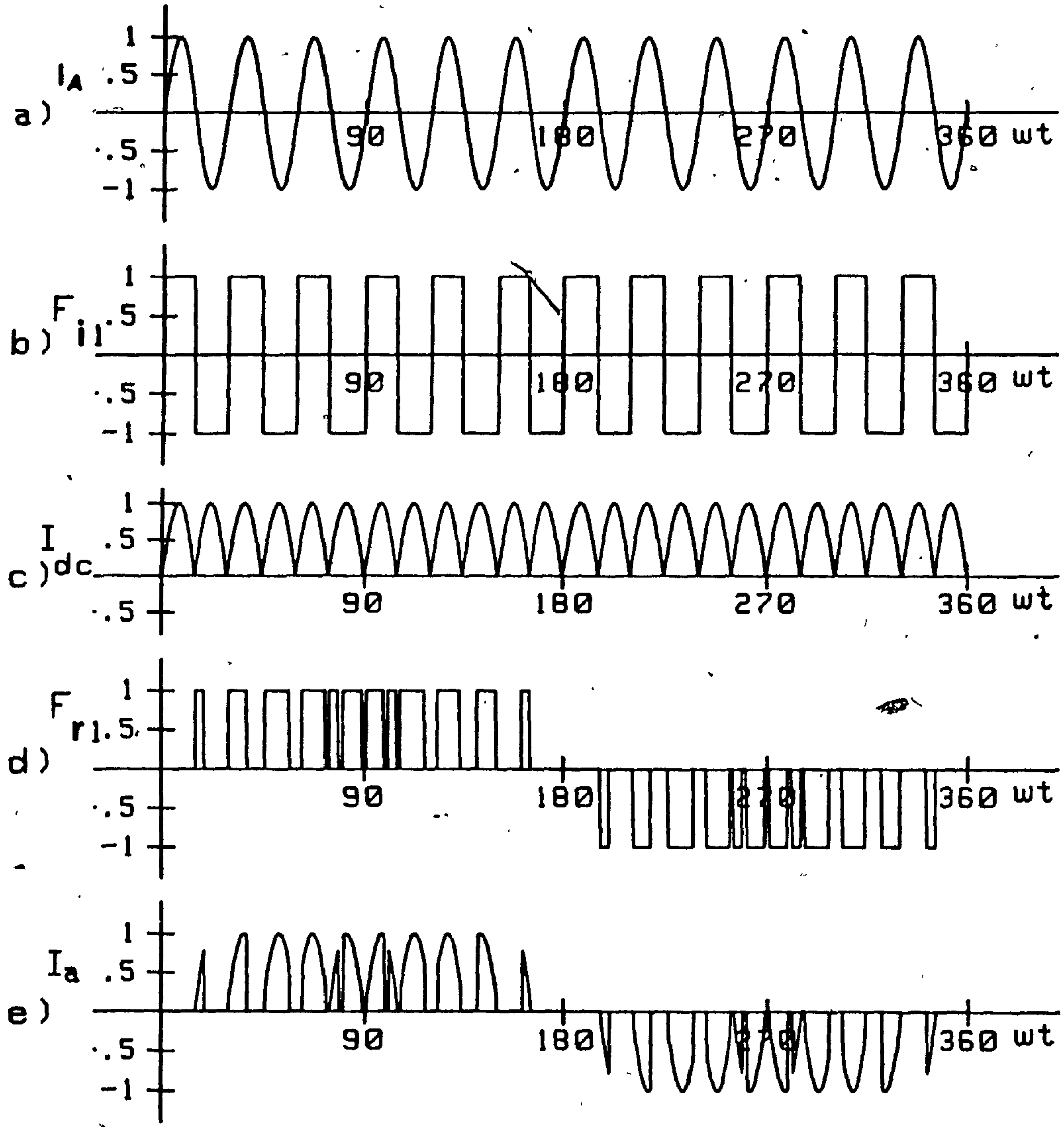

Fig. 6.11: Input current waveform obtained with three-phase to single-phase (full bridge) IMO FCC-HFL topology.

TABLE 6.8

FREQUENCY SPECTRA OF WAVEFORMS ASSOCIATED WITH FCC INPUT CURRENT SHOWN IN FIG. 6.11

Harmonic coefficients of inverter and rectifier switching function (Fig. 6.11b and 6.11d)				Harmonic coefficients of resulting input phase current, I_{an}, (Fig. 6.11e) for f_o= 720 Hz = $12f_i$		
Inverter SF		Rectifier SF		Amplitude, I_{an}		
Order (k)	Amplitude (B_k)	Order (n)	Amplitude (A_n)	Order (kf_i)	(1) p.u.	(1) %
1	1.27	1	0.99	f_i	0.609	60.9
3	0.42	3	--	$5f_i$	0.055	5.5
5	0.26	5	--	$7f_i$	0.276	27.6
7	0.18	7	--	$11f_i$	0.016	2.6
9	0.14	9	--	$13f_i$	0.032	3.2
11	0.12	11	--	$17f_i$	0.059	5.9
13	0.10	13	--	$19f_i$	0.177	17.7
15	0.09	15	--			
17	0.08	17	0.11			
19	0.07	19	0.26			

(1) Output phase currents have been taken as 1 p.u. current and 100% current.

operation results in high gain i.e. 105% at the output but contains subharmonics and low order harmonic components. Input current spectrum is fairly good.

6.2.2.2 Half-bridge Configuration

Fig. 6.12 shows a three-phase to single-phase FCC-HFL circuit topology that results from the one shown in Fig. 6.7 by removing the three top or bottom switches [49]. The fourth switch S_4 has been introduced to allow for output voltage control. This topology is particularly useful when the neutral terminal of the ac source is available.

The converter DMO switching matrix $[F_d(\omega_s t)]$, elements are shown in Fig. 6.13b, c and d. Resulting HFL output voltage, is illustrated in Fig. 6.13e. The spectrum of the output voltage is tabulated in Table 6.9. Column 4 (Table 6.9) shows that the maximum amplitude of the fundamental component of output voltage is approximately 83%, of the respective amplitude of the input voltage. As expected it contains low order harmonics. However, it is free from sub-harmonic components. Input current waveform, I_a is shown in Fig. 6.14. Respective spectra for input currents are shown in Table 6.10. Column 3 shows that it do not contain any low order harmonics, although HFL input ac currents are discontinuous.

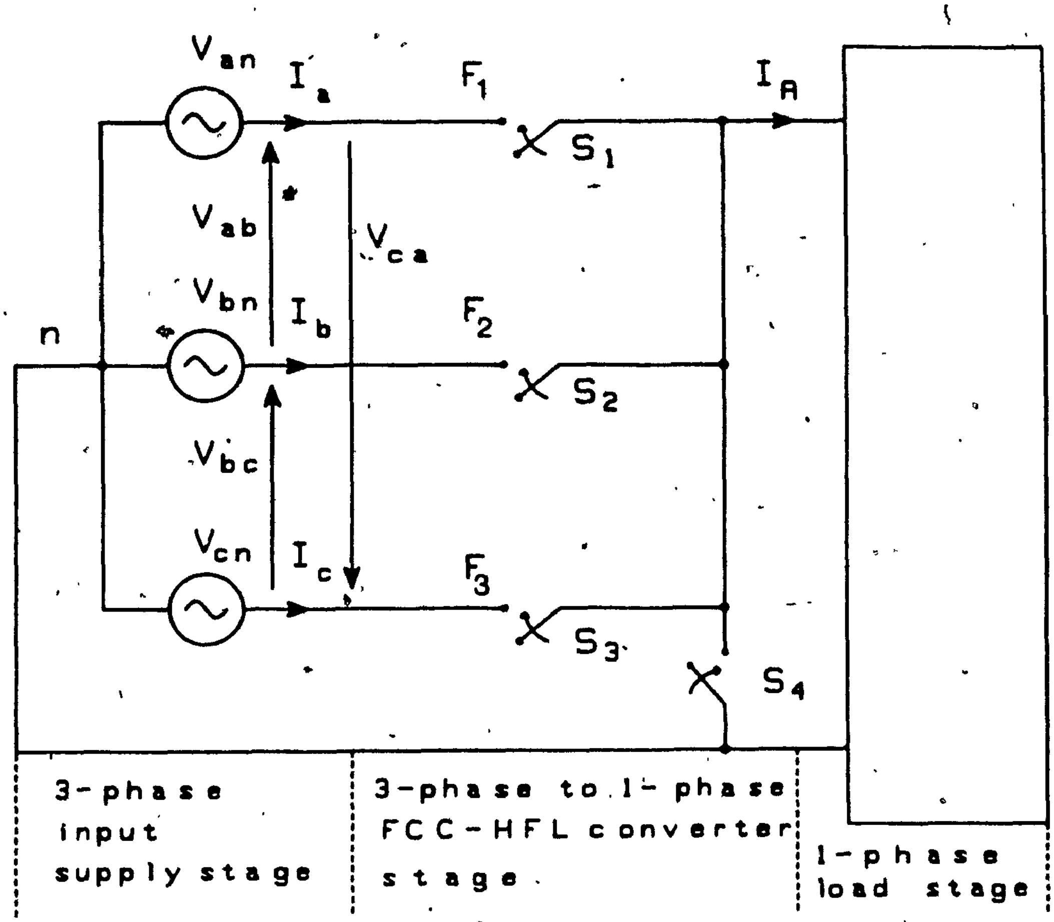

Fig. 6.12: Simplified circuit diagram of the three-phase to single-phase FCC-HFL topology with neutral connection available.

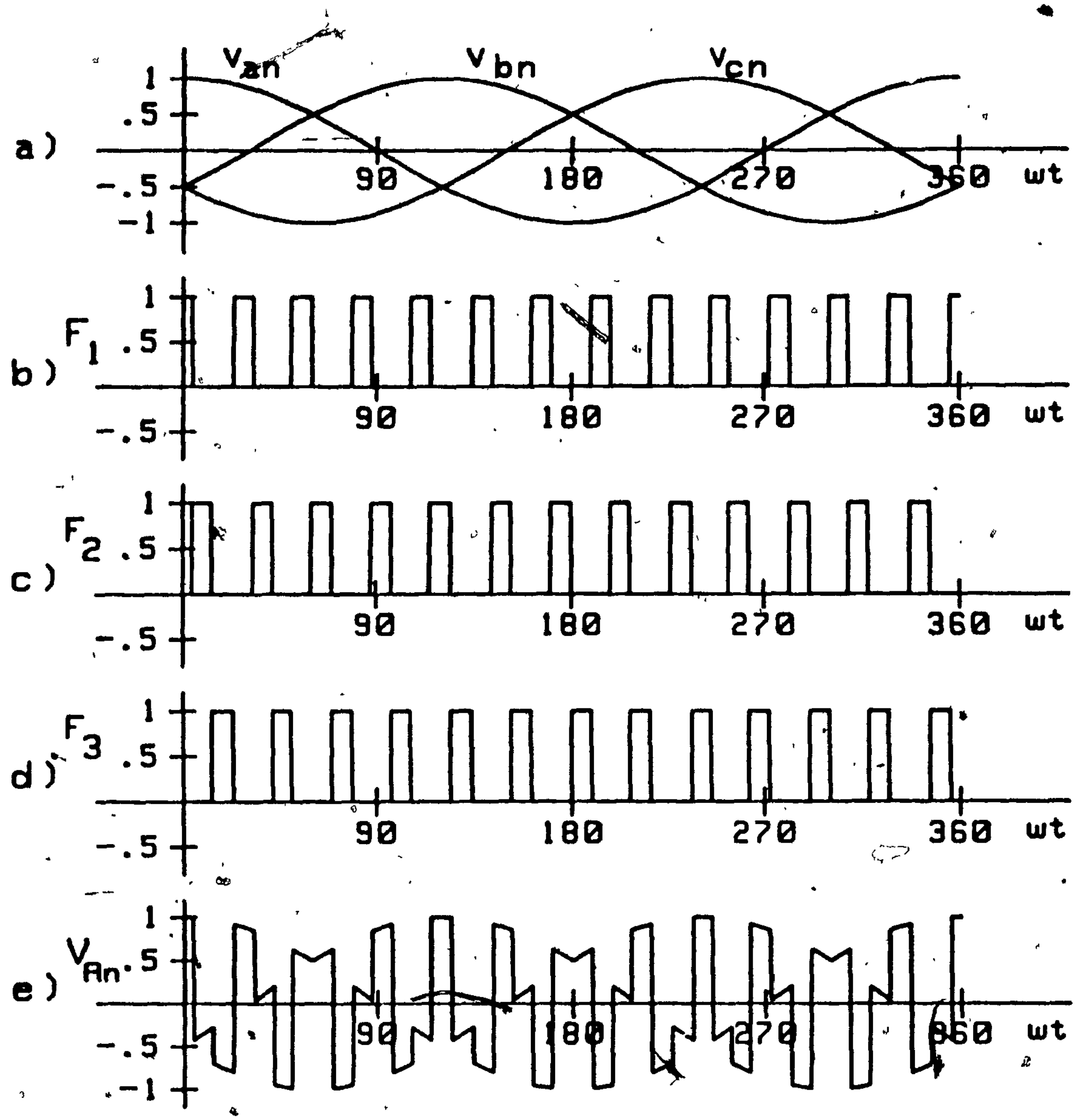

Fig. 6.13: High frequency output voltage waveform obtained with three-phase to single-phase (half bridge) DMO FCC-HFL topology.

TABLE 6.9

FREQUENCY SPECTRA OF WAVEFORMS ASSOCIATED WITH FCC HIGH FREQUENCY OUTPUT VOLTAGE SHOWN IN FIG. 6.13

Harmonic coefficients of switching function (Fig. 6.13b)		Harmonic coefficients of resulting output phase voltage V_{AN}, (Fig. 6.13e) for $f_o = 720$ Hz $= 12f_i$		
			Amplitude, V_{AN}	
Order (n)	Amplitude (A_n)	Order (kf_o)	(1) p.u.	(1) %
dc	0.33			
1	0.55	f_o	0.83	83
2	0.28	$2.25f_o$	0.42	42
4	0.14	$4.25f_o$	0.21	21
5	0.11	$5.5f_o$	0.17	17
7	0.08	$7.5f_o$	0.12	12
8	0.07	$8.75f_o$	0.10	10
10	0.06	$10.75f_o$	0.08	8
16	0.04	$12f_o$	0.08	8
17	0.03	$14f_o$	0.06	6
19	0.03	$18.5f_o$	0.05	5

(1) Input phase voltages have been taken as 1 p.u. volt and 100% volt.

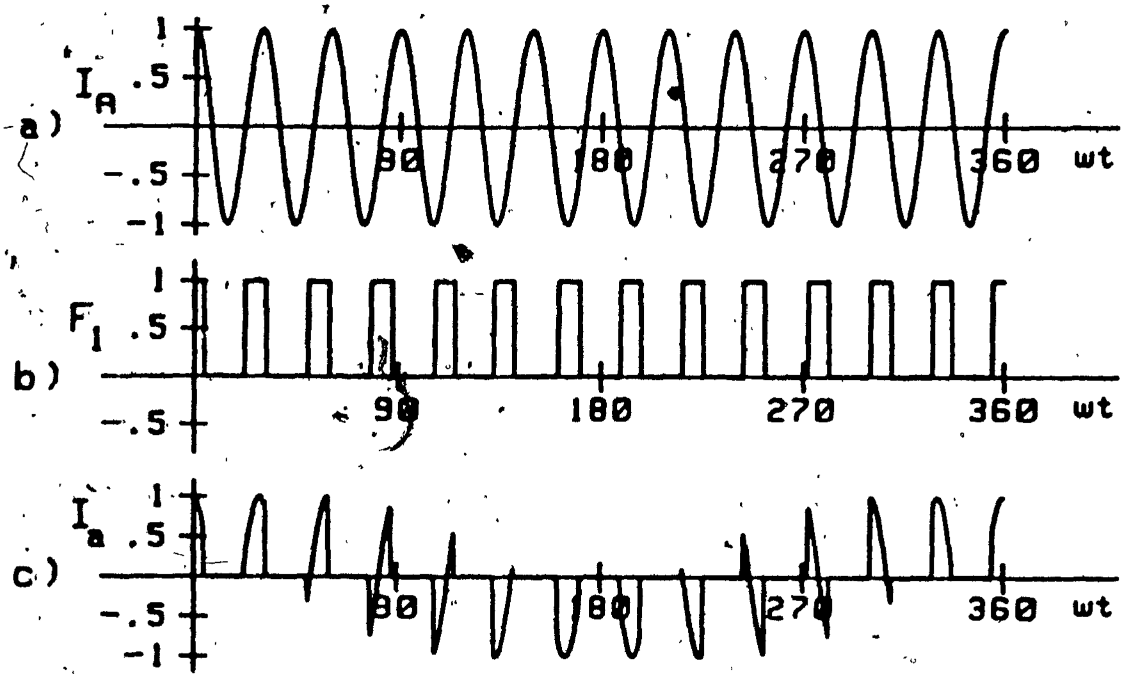

Fig. 6.14: Input current waveform obtained with three-phase to single-phase (half-bridge) DMO FCC-HFL topology.

TABLE 6.10				
FREQUENCY SPECTRA OF WAVEFORMS ASSOCIATED WITH FCC INPUT CURRENT SHOWN IN FIG. 6.14				
Harmonic coefficients of switching function (Fig. 6.14b)		Harmonic coefficients of resulting input phase current I_{an}, (Fig. 6.14c) for f_o = 720 Hz = $12f_i$		
			Amplitude, I_{an}	
Order (n)	Amplitude (A_n)	Order (kf_i)	(1) p.u.	(1) %
dc	0.33			
1	0.55	f_i	0.28	28
2	0.28	$12f_i$	0.33	33
4	0.14	$14f_i$	0.14	14
5	0.11	$25f_i$	0.28	28
7	0.08	$38f_i$	0.14	14
8	0.07	$40f_i$	0.07	7
10	0.06	$53f_i$	0.07	6
16	0.04	$64f_i$	0.07	7
17	0.03			
19	0.03			

1) Output phase currents have been taken as 1 p.u. current and 100% current

6.3 Experimental Results

To demonstrate the feasibility of the proposed FCC-HFL topologies and their associated switching control schemes two 1 KVA experimental prototypes were implemented for the topologies shown in Figs. 6.1 and 6.7. Key experimental results obtained with these prototypes are shown in Figs. 6.15 and 6.16. In particular Fig. 6.15 shows the output line voltage V_{AB} (Fig. 6.5) and the input line current, I_a (Fig. 6.6) for the case of three phase to three phase IMO FCC-HFL topology (Fig. 6.1). Also Fig. 6.16 shows the output line voltage, V_{AB} (Fig. 6.8) and the input line current, I_a (Fig. 6.9) for three-phase to single-phase DMO FCC-HFL topology (Fig. 6.7). Their spectra agree with respective simulated results (Tables 6.5 and 6.6).

6.4 Conclusions

Several FCC-HFL topologies and two modes of operation have been presented and evaluated in this chapter. It has been shown theoretically and experimentally that FCC's can be successfully employed in various HFL applications and in particular for cases where bilateral power flow and compact packaging are required. Also it has been demonstrated that through the use of appropriate mode and switching function FCC-HFL circuits can be made to yield output voltage and input current waveforms with low harmonic content and insignificant amplitude derating.

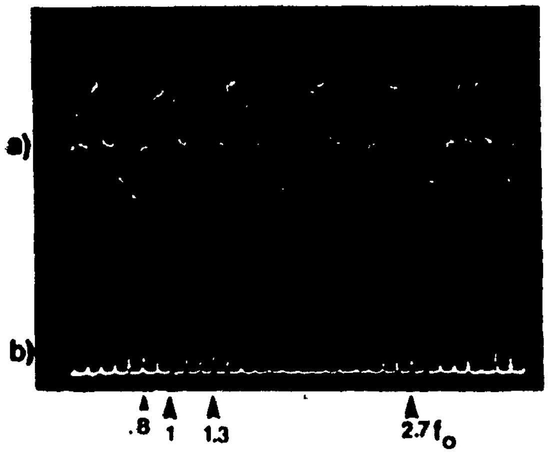

A. a) Output line voltage, V_{AB} (Fig. 6.5e).
b) Respective frequency spectrum.

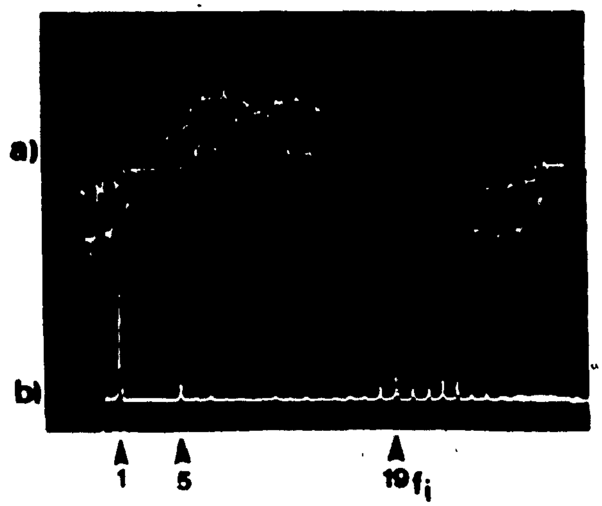

B. a) Input current, I_a (Fig. 6.6e).
b) Respective frequency spectrum.

Fig. 6.15: Experimental input/output voltage/current waveforms obtained with three to three-phase FCC-HFL (Fig. 6.1) IMO topology at f_o = 600 Hz, f_i = 60 Hz for resistive load.

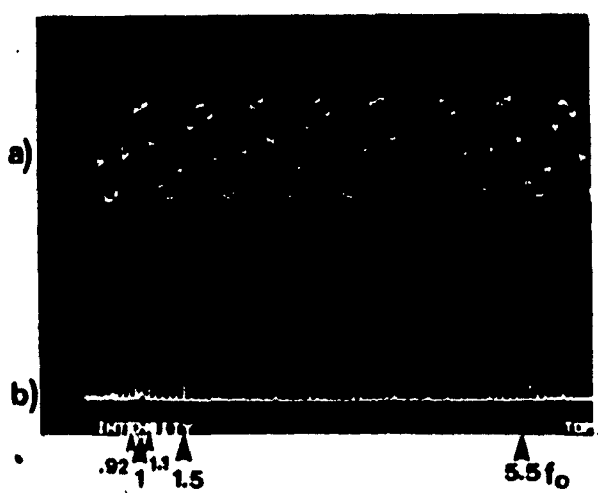

A. a) Output line voltage, V_{AB} (Fig. 6.8e).
b) Respective frequency spectrum.

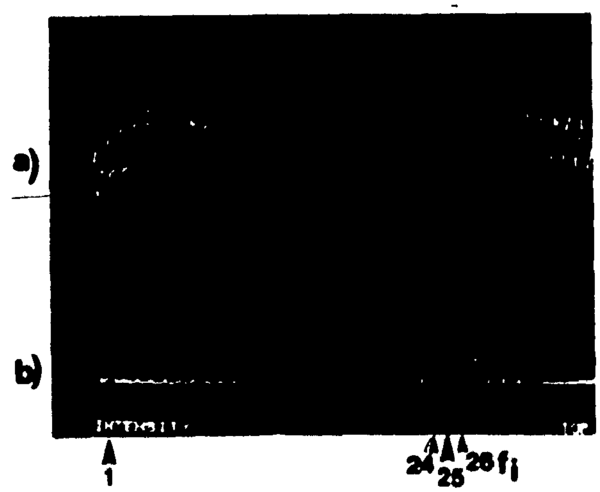

B. a) Input current, I_a (Fig. 6.9c).
b) Respective frequency spectrum.

Fig. 6.16: Experimental input/output voltage/current waveforms obtained with full-bridge three to single-phase FCC-HFL (Fig. 6.7) DMO topology at f_o = 720 Hz, f_i = 60 Hz for resistive load.

Moreover, the generalized synthesis approach regarding circuit topologies presented in Chapter 2, can be used to obtain suitable topologies for any combination of HFL input to output number of phases.

Finally key predicted results have been verified experimentally on laboratory prototype units.

CHAPTER 7

SUMMARY, CONCLUSIONS AND RECOMMENDATIONS

7.1 Summary and Conclusions

Some Forced Commutated Cycloconverter (FCC) structures to suit different types of loads have been investigated in this thesis. Depending on a particular load characteristics and specifications, various FCC topologies and combinations of switching functions have been studied. A generalized matrix model of FCC has been developed, which has been later used to analyse different types of FCCs. Cycloconverter control strategies employing direct and indirect modes of operation (DMO and IMO) have been identified. Respective FCC analyses have shown that IMO offers the best combination of voltage gain and low harmonic distortion. However, it requires a considerable more complex conceptual and hardware realization.

In particular the contributions of this thesis by chapter are as follows:

In Chapter 2 it has been shown that complex FCC structures could be analytically and physically represented by a generalized matrix model. This model has been used to investigate different FCC structures operating under DMO and IMO.

In Chapter 3 three-phase to three-phase FCCs under DMO and IMO conditions have been investigated. Some advanced PWM techniques, which have yielded minimum possible harmonic distortion of the input/output waveforms along with maximum possible voltage utilization have been proposed and employed. It has been shown that IMO voltage gain could be increased up to 0.95 of input voltage without any significant harmonics. This is a significant improvement since existing control strategies yield only 0.5 (output to input) voltage transfer ratio. For FCC under DMO condition the voltage gain has been shown to be only 0.83%. However, DMO control logic is significantly simpler. Also an evaluation of all the proposed FCC structures and control schemes has been provided which facilitates the selection of best scheme for specific load characteristics and requirements.

Three phase to single phase FCCs have been investigated in Chapter 4. It has been shown that these new FCC structures have better performance in terms of voltage utilization, harmonic content and subharmonics than any other known structures. Experimental results have been employed to confirm these conclusions.

Next, the search for an efficient single to three phase FCC has led to a novel converter structure whose principles of operation are described in Chapter 5. This new FCC structure is recommended for fixed frequency single phase to three-phase power conversion applications in rural areas. It has been shown that this new phase converter is simple, light weight, economical, efficient and uses no bulky reactive components. The validity of these conclusions has again been verified experimentally.

Finally, the proposed three-phase to three and single-phase FCCs have been further investigated in Chapter 6 for potential use in high frequency link (HFL) applications. It has been shown theoretically and experimentally that the proposed FCCs can be successfully employed in various HFL applications and in particular for cases where bilateral power flow and compact light weight packaging are required.

In summary all FCC structures proposed and treated in this thesis exhibit significantly improved performance than respective known FCC structures. They are light weight and compact as no bulky reactive components are necessary. Moreover, some key theoreticaly results have been verified experimentally in order to prove their validity.

7.2 Suggestions for Future Work

Most of the analysis and design of static FCC topologies discussed in this thesis have been performed under steady state operating condition. Further investigation is therefore required in the areas of transient performance and stability of the FCCs. Some input/output filters are necessary for the subject FCCs, but no filter design has been provided in this thesis. Further study is required to design these input/output filter components to suit particular customer specifications. A reduction in complexity and size of FCC control logic circuitry can be investigated by employing VLSI techniques. Converter protection for the proposed FCC structures can be further investigated.

REFERENCES

[1] L. Gyugyi and B.P. Pelly, Static Power Frequency Changes: Theory, Performance and Application, Wiley-Interscience, New York, 1976.

[2] V.R. Stefanovic, "Present trends in variable speed ac drives", Conference Record, IPEC-Tokyo, 1983, pp. 438-449.

[3] B.K. Bose, Power Electronics and AC Drives, Prentice-Hall, New Jersey, 1986.

[4] K.M. Chirgwin, L.J. Stratton and J.R. Toth, "Precise frequency power generation from an unregulated shaft", AIEE Trans. Appl. and Ind., Vol. 79, No. 52, Pt. II, Jan. 1961, pp. 442-451.

[5] R. Chauprade and A. Abbondanti, "Variable speed drives: modern concepts and approaches", Conference Record, IEEE-ISPCC, 1982, pp. 20-37.

[6] R.A. Pearman, Power Electronics Solid State Motor Control, Reston Publishing Company, Inc., Virginia, 1980.

[7] T.A. Kneschke, "Static frequency converter for SEPTA's Wayne junction traction substation", IEEE Trans. Ind. Appl., Vol. IA-21, No. 2, March/April 1985, pp. 295-300.

[8] T.A. Lipo and P.C. Krause, "Analysis and simplified representation of a rectifier-inverter induction motor drive", IEEE Trans. Power Appar. & Sys., Vol. PAS-88, No. 5, May 1969, pp. 588-596.

[9] P.D. Ziogas, Y.G. Kang and V.R. Stefanovic, "Rectifier inverter frequency changers with suppressed dc link components", Conference Record, IEEE-IAS, 1985, pp. 1180-1189.

[10] F.E. Gentry, F.W. Gutzwiller, N. Holonyak, Jr. and E.E. Von Zastrow, Semiconductor Controlled Rectifiers, Principles and Applications of p-n-p-n Devices, Prentice-Hall, N.J., 1964.

[11] S.B. Dewan and A. Straughen, Power Semiconductor Circuits, John Wiley & Sons, New York, 1975.

[12] P.D. Ziogas, Y.G. Kang and V.R. Stefanovic, "Optimum System design of a three-phase PWM rectifier-inverter type frequency changer", Conference Record, IEEE-IAS, 1984, pp. 908-919.

[13] B.R. Pelly, "Power Semiconduction devices - a status review", Conference Record, IEEE-ISPCC, 1982, pp. 1-19.

[14] F. Wesselak, "Thyristor convertors with natural commutation", Siemens Review, No. 12, pp. 405-410, December, 1965.

[15] W. Faust, "Static frequency changers for 16 2/3-cycle railway network", The Brown Boveri Review, pp. 519-525, Aug./Sept. 1964.

[16] D.G. Fink and H.W. Beaty, Standard Handbook for Electrical Engineers, McGraw-Hill Book Company, 1978.

[17] B.R. Pelly, Thyriston Phase-controlled Converters and Cycloconverters, Wiley-Interscience, 1971.

[18] P.D. Ziogas, S.I. Khan and M.H. Rashid, "Some improved forced commutated cycloconverter structures", IEEE Trans. Ind. Appl., Vol. IA-21, No. 5, pp. 1242-1253, Sept./Oct. 1985.

[19] P.D. Ziogas, S.I. Khan and M.H. Rashid, "Analysis and design of forced commutated cycloconverter structures with improved transfer characteristics", IEEE Trans. Ind. Electronics, Vol. IE-33, No. 3, pp. 271-280, Aug. 1986.

[20] L.A. Hazeltine, "An improved method of and apparatus for converting electric power", British Patent No. 218.675, Jan. 4, 1926.

[21] M. Schenkel, "Eine unmittelbare asynchrone umrichtung fur niederfrequente bahnneutze", Electr. Bahnen, 8, pp. 69-73, 1932.

[22] J. Von Issendorff, "Der gesteuerte umrichter", Wiss. Veroff. Siemens, 14, pp. 1-31, 1935.

[23] C. Ehrensperger, "Static converter with current and voltage smoothers for flexibly coupling a three-phase 50 cycle network with a single-phase 16 2/3-cycle network", Brown Bovery Rev., Vol. 21, No. 6, pp. 96-112, 1934.

[24] H. Rissik, Mercury Arc Current Convertors, Sir Issac Pitman & Sons, 1935.

[25] H. Rissik, The Fundamental Theory of Arc Convertors, Chapman & Hall, 1939.

[26] A.R. Daniels and D.T. Slattery, "New power convertor technique employing power transistors", Proc. IEE, Vol. 125, No. 2, pp. 146-150, Feb. 1978.

[27] A.R. Daniels and D.T. Slattery, "Application of power transistors to polyphase regenerative power convertors", Proc. IEE, Vol. 125, No. 7, July 1978.

[28] J. Rodriguez, "A new control technique for ac-ac converters", Third IFAC Symposium, Lausanne, Switzerland, 1983, pp. 203-208.

[29] M. Venturini, "A new sine wave in, sine wave out conversion technique eliminates reactive elements", in Proc. Powercon 7, 1980, E3-1-E3-15.

[30] K.J. Maytum and D. Colman, "The implementation and future potential of the Venturini converter", Proc. of the Conference on Drives/Motors/Controls, Harogate, England, October, 1983.

[31] S.I. Khan, P.D. Ziogas and M.H. Rashid, "Forced commutated cycloconverters for high frequency link applications", in Conf. Rec., IEEE-IAS, 1986, pp. 476-487.

[32] P. Wood, Switching Power Converters, Van Nostrand Reinhold Company, New York, 1981.

[33] H.S. Patel and R.G. Hoft, "Generalized techniques of harmonic elimination and voltage control in thyristor inverters: Part I, harmonic elimination", IEEE Trans. Ind. Appl., Vol. IA-9, pp. 310-317, May-June 1973.

[34] H.S. Patel and R.G. Hoft, "Generalized techniques of harmonics elimination and voltage control in thyristor

inverters: Part II, voltage control techniques", IEEE Trans. Ind. Appl., Vol. IA-10, pp. 666-673, July-Aug. 1974.

[35] M. Boost and ~~N.~~ Marinos, "Rectifier optimization", Dept. Elect. Eng., Concordia University, Montreal Canada, Tech. Rep., Dec. 1982.

[36] B.D. Bedford and R.G. Hoft, Principles of Inverter Circuits, John Wiley & Sons, New York, 1964.

[37] T. Ohnishi and H. Okitsu, "A novel PWM technique for three phase inverter/converter", Conference Record, IPEC-Tokyo, 1983, pp. 384-395.

[38] A. Schonung and H. Stemmber, "Static frequency changers with subharmonics control in conjunction with reversible variable speed ac drives", Brown-Boveri Review, pp. 555-557, Aug./Sept. 1964.

[39] R. Bonert and Ru-Song Wu, "Improved three phase pulse width modulator for overmodulation", Conference Record, IEEE-IAS, 1984, pp. 784-786.

[40] J.B. Rice, "Design of snubber circuits for thyristor converters", Power Semiconductor Applications, Vol. I, pp. 21-24, IEEE Press, 1972, edited by J.D. Harden, Jr. and F.B. Golden.

[41] Claude M. Hertz, "Current techniques in phase conversion systems", Conference Paper No. 78A3, IEEE Rural Electric Power Conference, Minneapolis, Minn., May 1-2, 1978, pp. 35-49.

[42] T.C. Jongsma, "The application of phase converters", Electrical/Electronic Showcase '79, Winnipeg, Manitoba, May 2, 1979.

[43] R.L. Chhabra, L.H. Soderholm, and L.F. Charity, "Voltage effects on phase converter operated three-phase motors", Trans. of the ASAE, 1973, pp. 500-503.

[44] S.B. Dewan and M. Showleh, "Steady-state analysis of static single-phase to three-phase converters", Conference Record, IEEE-IAS, 1981, pp. 910-916.

[45] L. Gyugyi and F. Cibulka, "The high-frequency base converter - a new approach to static high-power converter", IEEE Trans. Ind. Appl., Vol. IA-15, No. 4, pp. 420-429, July/August, 1979.

[46] P.M. Espelage and B.K. Bose, "High-Frequency link power conversion", IEEE Trans. In. Appl., Vol. IA-13, No. 5, pp. 387-394, Sept./Oct., 1977.

[47] S. Manias and P.D. Ziogas, "A novel sinewave in AC to DC converter with high-frequency transformer isolation", IEEE Trans. Ind. Electronics, Vol. IE-32, No. 4, pp. 430-438, November, 1985.

[48] T. Fukao and M. Matsui, "Basic characteristics of cycloconverter for linking commercial and high frequency distribution lines", Conference Record, IEEE-IAS-1985, pp. 975-983.

[49] V.C. Jones and B.K. Bose, "A frequency step-up cycloconverter using power transition in inverse-series

mode", Int. J. Electronics, Vol. 41, No. 6, pp. 573-587, 1976.

[50] X. Ma, "High-performance PWM frequency changers", IEEE Trans. Ind. Appl, Vol. IA-22, No. 2, pp. 267-280, March/April 1986.

[51] Shahidul I. Khan, M.H. Rashid and P.D. Ziogas, "Design aspects of logic control circuits for direct frequency changers", in Conf. Rec., IEEE-IECON, 1985, pp. 277-284.

APPENDICES

APPENDIX A

HARMONIC ANALYSIS OF [3 X 3] DMO CYCLOCONVERTER

The practical equation for DMO cycloconverter is given by;

$$V_o(L\omega_o t) = [V_i(\omega_i t)][S_{dh}(\omega_s t)]$$

$$= V_i[\cos(\omega_i t) \quad \cos(\omega_i t - 120^o) \quad \cos(\omega_i t - 240^o)] \cdot \begin{bmatrix} A_\ell \cos(\ell\omega_s t) \\ A_\ell \cos(\ell\omega_s t - \ell 120^o) \\ A_\ell \cos(\ell\omega_s t - \ell 240^o) \end{bmatrix}$$

$$= \tfrac{1}{2} V_i A_\ell [\cos(\ell\omega_s + \omega_i)t + \cos((\ell\omega_s + \omega_i)t - (\ell + 1)\ 120^o)$$

$$+ \cos((\ell\omega_s + \omega_i)t - (\ell + 1)\ 240^o)]$$

$$+ \tfrac{1}{2} V_i A_\ell [\cos(\ell\omega_s - \omega_i)t + \cos((\ell\omega_s - \omega_i)t - (\ell - 1)\ 120^o)$$

$$+ \cos((\ell\omega_s - \omega_i)t - (\ell - 1)\ 240^o)]$$

$$= \frac{3}{2} V_i A_\ell \cos[(\ell\omega_s \pm \omega_i)t]$$

$$= \frac{3}{2} A_\ell V_i \cos[(\ell\omega_o + (\ell \pm 1)\omega_i)t], \quad \text{for } \ell = n = (3I \mp 1),$$

$$I = 1,2,3,\ldots \text{ integer}$$

$$= 0 \qquad \text{for } \ell \neq (3I \mp 1)$$

APPENDIX B

DESIGN OF CONTROL LOGIC CIRCUIT

Designing a proper control circuit for a cycloconverter is very important. Direct and indirect cycloconversion modes have different logic circuit configurations and requirements. A general Boolean expression for a three phase to three phase cycloconverter operating under IMO (section a) and DMO (section b) principle is first developed, which is then reduced for three phase to single phase operation.

a. IMO Control Logic Circuit

Selection of the specific cycloconverter switch control strategy is based on several considerations [51] which include:

(i) Overall converter voltage gain

(ii) Converter switching frequency

(iii) Quality of generated output voltages/input currents.

A strategy for 9 switch configuration that provides good voltage gain and yields good quality output voltages at moderate switching frequencies is illustrated in Figs. B1 and B2. Specifically, Fig. B1 shows the switch timing diagram for the fictitious rectification stage while Fig. B2.c shows the respective diagram for the fictitious inversion stage. Furthermore, Fig. B2.a illustrates the PWM (MSPWM) technique employed to improve the quality of the cycloconverter output voltage while Fig. B2.b shows one of three resulting output line to line voltages. The remaining step in conceptualizing

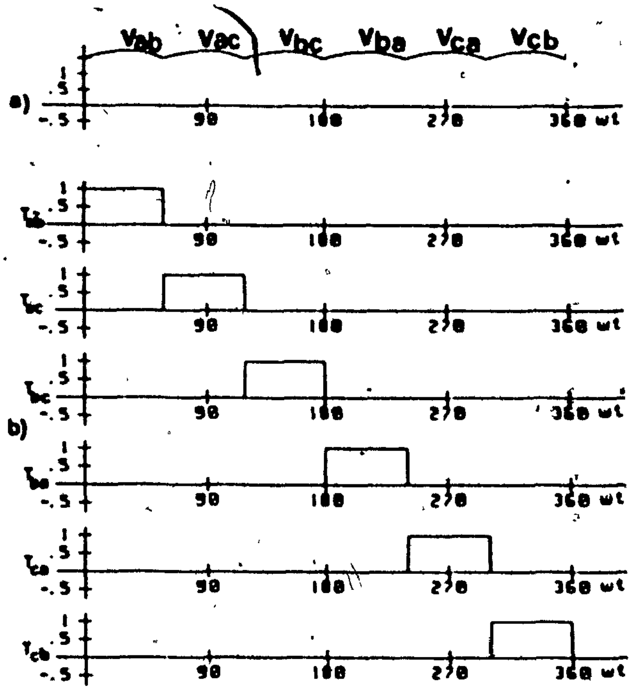

Fig. B1: Timing diagram for rectification stage.
a) The fictitious rectifier output voltage.
b) Six rectifier timing signals.

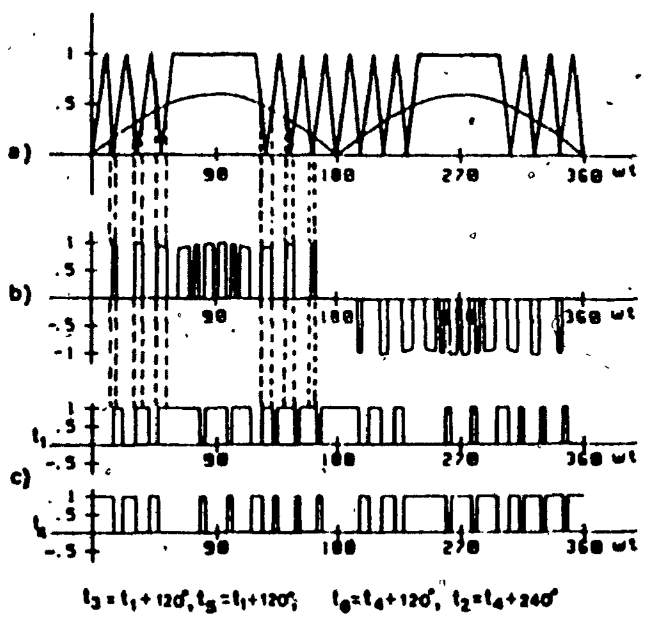

Fig. B2: Timing diagram for inversion stage.
a) Reference sine and triangular wave.
b) Output voltage.
c) Two complementary inverter timing signals.

the cycloconverter switch control strategy involves the derivation of the nine switch (S_1 to S_9) gating signals (g_1 to g_9) from the switch timing diagrams shown in Figs. B1 and B2. This is accomplished by considering that the converter simultaneously performs the 'rectification' and 'inversion' functions by activating the appropriate subset among the set of nine cycloconverter switches. The resulting 'truth-table' is presented in Table B1.

Table B1

	V_{ab}	V_{ac}	V_{bc}	V_{ba}	V_{ca}	V_{cb}
g_1	S_1	S_1	S_4	S_4	S_7	S_7
g_2	S_6	S_9	S_9	S_3	S_3	S_6
g_3	S_2	S_2	S_5	S_5	S_8	S_8
g_4	S_4	S_7	S_7	S_1	S_1	S_4
g_5	S_3	S_3	S_6	S_6	S_9	S_9
g_6	S_5	S_8	S_8	S_2	S_2	S_5

Hardware Implementation

A block diagram representation of the hardware required for the all digital implementation of the subject cycloconverter PWM control strategy is shown in Figs. B3 and B4. The associated logic components have been for convenience, divided into two sections each of which performs a distinct control logic task, as follows:

<u>'Rectifier' logic section</u>: The block diagram for this section is shown in Fig. B3. This logic section performs the task of producing the six 'rectifier' timing signals shown in Fig. B1.b. Consequently, it is comprised of the following main components:

i) A delta-wye step-down transformer is used for input line voltage sensing. The output of this transformer provides the six zero cross points for the three input line voltages. It is also used to sense a number of input line faults, such as: input over/under voltage, improper phase rotation, etc. The zero-cross sensing is implemented by employing six properly biased voltage comparators.

ii) A digital delay circuit comprised of monostables is used to produce the rectifier timing signals (Fig. B1.b), which is then fed to the combinational circuit to produce the desired gating signals, g_1 to g_9.

<u>'Inverter' logic section</u>: The block diagram for this section is shown in Fig. B4. The sine reference waveform, Fig. B2.a is stored in an EPROM and the respective triangular waveform is obtained from suitable (cascaded) UP-DOWN counters. The points of intersection between the two waveforms are determined through the use of digital comparators (also cascaded for greater accuracy).

Finally, both the 'rectifier' and 'inverter' timing signals are combined together to produce the required gating

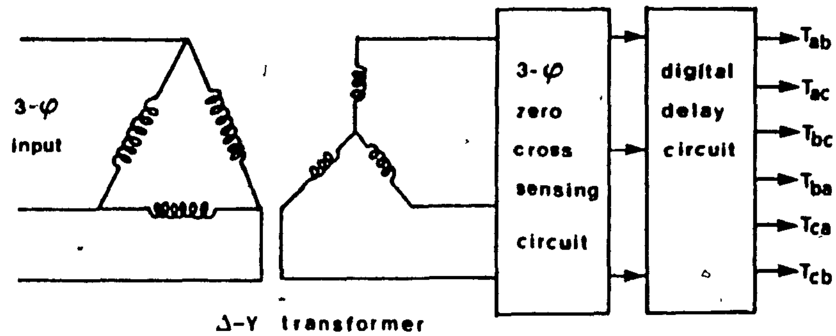

Fig. B3: Rectifier logic block diagram.

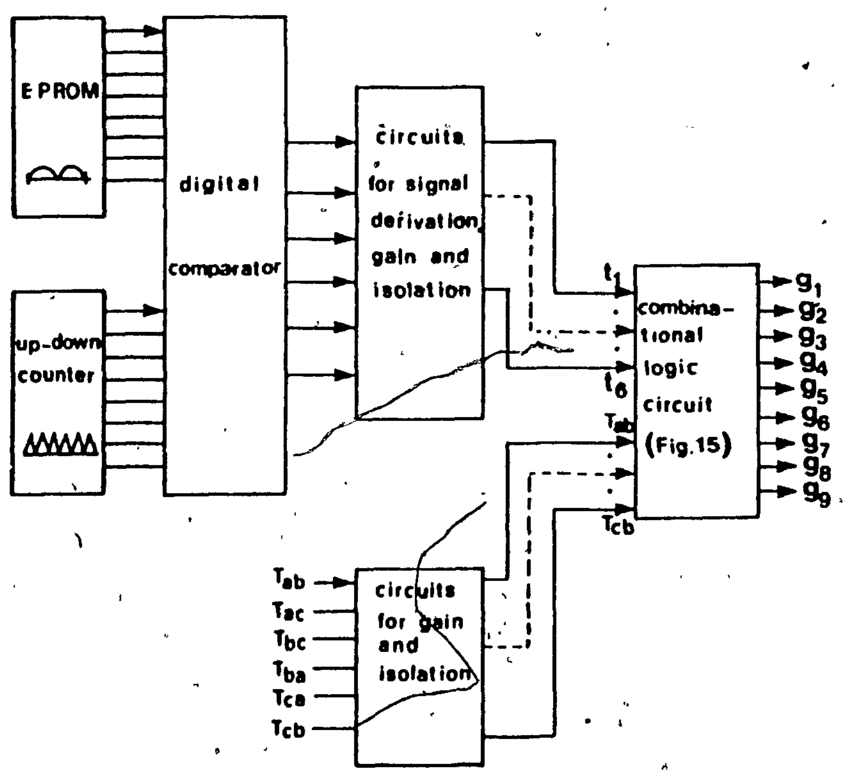

Fig. B4: Inverter logic and gating signal block diagram.

signals (g_1 to g_9) according to the Truth Table B1 by suitable digital components.

The Boolean equations for the gating signals can be written (from Table B1) as follows:

$$g_1 = (T_{ab} + T_{ac}) \cdot t_1 + (T_{ba} + T_{ca}) \cdot t_4$$
$$g_2 = (T_{ab} + T_{ac}) \cdot t_2 + (T_{ba} + T_{ca}) \cdot t_5$$
$$g_3 = (T_{ab} + T_{ac}) \cdot t_3 + (T_{ba} + T_{ca}) \cdot t_6$$
$$g_4 = (T_{cb} + T_{ab}) \cdot t_4 + (T_{bc} + T_{ba}) \cdot t_1$$
$$g_5 = (T_{cb} + T_{ab}) \cdot t_5 + (T_{bc} + T_{ba}) \cdot t_2$$
$$g_6 = (T_{cb} + T_{ab}) \cdot t_6 + (T_{bc} + T_{ba}) \cdot t_3$$
$$g_7 = (T_{cb} + T_{ca}) \cdot t_1 + (T_{ac} + T_{bc}) \cdot t_4$$
$$g_8 = (T_{cb} + T_{ca}) \cdot t_2 + (T_{ac} + T_{bc}) \cdot t_5$$
$$g_9 = (T_{cb} + T_{ca}) \cdot t_3 + (T_{ac} + T_{bc}) \cdot t_6$$

The combinational circuit required to implement these expressions is shown in Fig. B5.

For a three-phase to single-phase cycloconverter operating under IMO principle, only six switches are required. Therefore only gating signals g_1 to g_6 need to be generated in this case.

b. DMO Control Strategy Logic Circuit

Cycloconverters operating under DMO principle is simpler than IMO principle as DMO is a single step process. Referring to Fig. B6 the Boolean expressions for 9 switch configuration (three-phase to three-phase cycloconverter) can be written as follows;

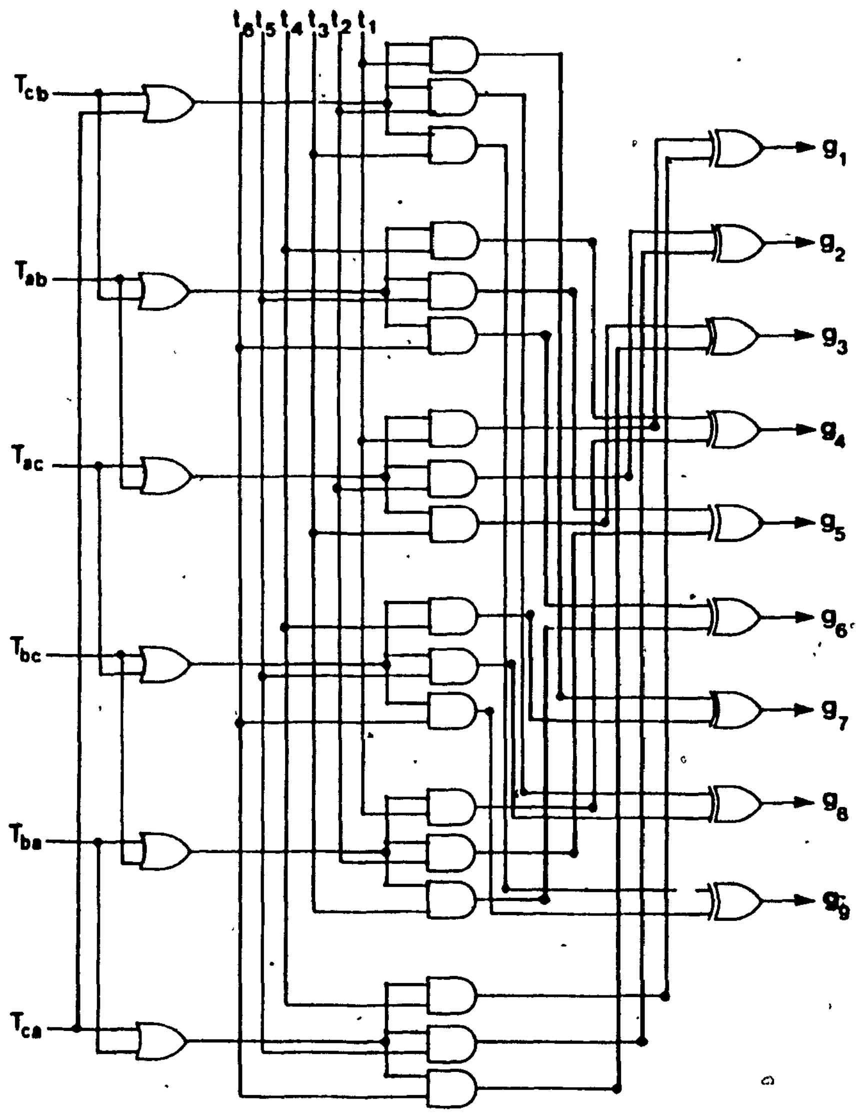

Fig. B5: The logic circuit for producing the final gating signals g_1-g_9.

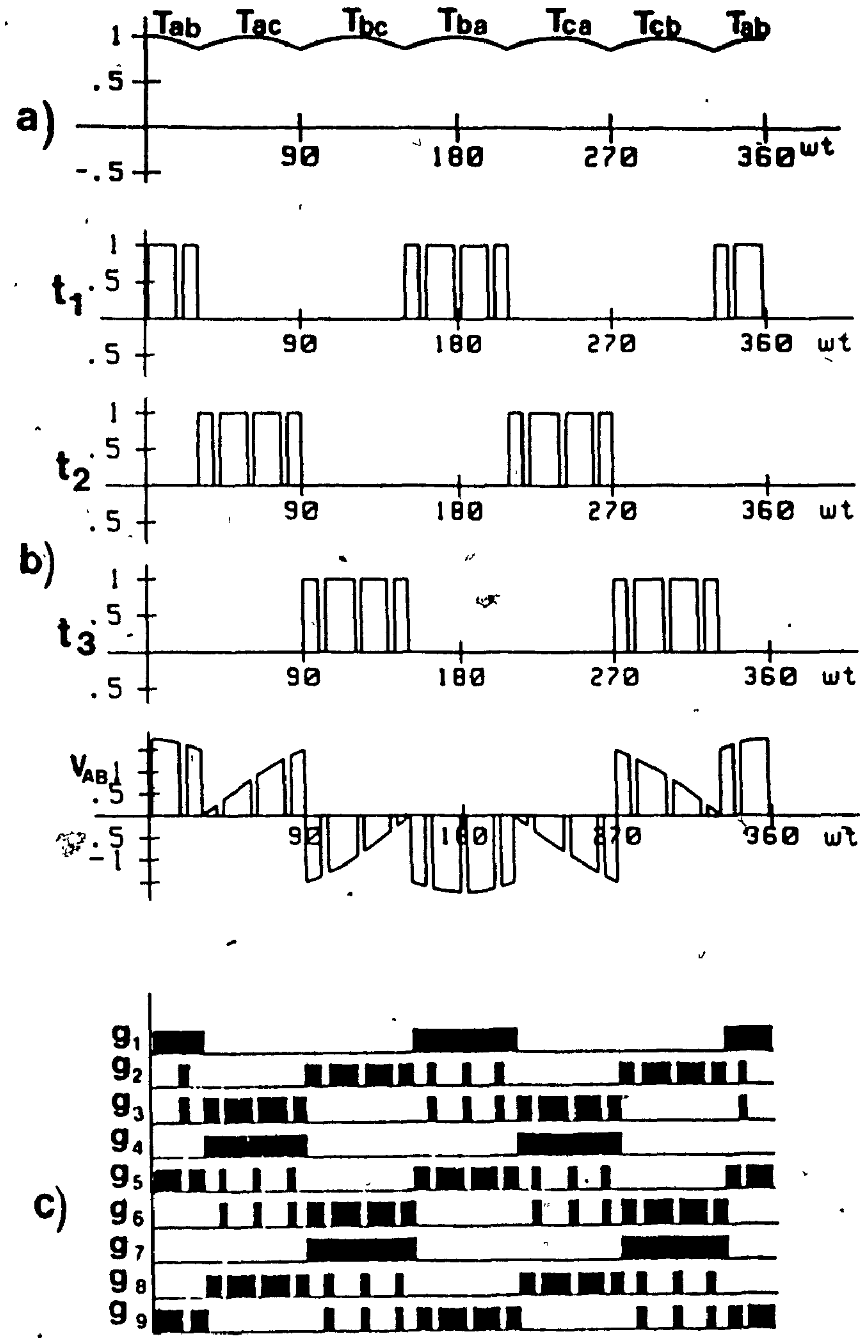

Fig. B6: Timing diagram for DMO cycloconversion.

$$g_1 = (T_{ab} + T_{ba}) \cdot t_1 + (T_{ab} + T_{ba}) \cdot \bar{t}_1$$
$$g_2 = (T_{bc} + T_{cb}) \cdot t_3 + (T_{ab} + T_{ba}) \cdot \bar{t}_1$$
$$g_3 = (T_{ac} + T_{ca}) \cdot t_2 + (T_{ab} + T_{ba}) \cdot \bar{t}_1$$
$$g_4 = (T_{ac} + T_{ca}) \cdot t_2 + (T_{ac} + T_{ca}) \cdot \bar{t}_2$$
$$g_5 = (T_{ab} + T_{ba}) \cdot t_1 + (T_{ac} + T_{ca}) \cdot \bar{t}_2$$
$$g_6 = (T_{bc} + T_{cb}) \cdot t_3 + (T_{ac} + T_{ca}) \cdot \bar{t}_2$$
$$g_7 = (T_{bc} + T_{cb}) \cdot t_3 + (T_{bc} + T_{cb}) \cdot \bar{t}_3$$
$$g_8 = (T_{ac} + T_{ca}) \cdot t_2 + (T_{bc} + T_{cb}) \cdot \bar{t}_3$$
$$g_9 = (T_{ab} + T_{ba}) \cdot t_1 + (T_{bc} + T_{cb}) \cdot \bar{t}_3$$

The hardware implementation is similar to IMO implementation. The only difference is in the logic block configuration, which is described by the above equations.

For three phase to single phase cycloconverter only 6 gating signals will be required.

APPENDIX C

COMPUTER PROGRAM FOR IMO FCC SIMULATION

```
10    !THIS PROGRAM SIMULATES IMO FCC (THREE TO THREE OR SINGLE PHASE) SHOWN
        IN FIG.4.7 ON HEWLETT PACKARD MINI-COMPUTERS USING BASIC LANGUAGE
20    DIM Ta(9),Tb(4),Tc(4),Fa(1440),Fb(2000),Fc(2400),Xdc(1440),Xa(1440)
30    DIM Tai(200),Fd(1440)
40    Wo=60.   ! OUTPUT FREQUENCY
50    CALL Rectfn(Ta(*),Fa(*),Fb(*),Fc(*))
70    CALL Rectout(Fa(*),Fb(*),Fc(*),Xdc(*))
80    CALL Hirosi(3,.8,Kp,Tai(*))
90    CALL Invout(Wo,Kp,Tai(*),Fd(*),Xdc(*),Xa(*))
100   CALL Sines(Ta(*))
110   CALL Mplot(20,34,1.2,-1.2,Fa(*))
120   CALL Mplot(36,50,1.9,-.8,Xdc(*))
130   CALL Mplot(52,66,1.2,-1.2,Fd(*))
140   CALL Mplot(68,86,1.9,-1.9,Xa(*))
150   END
160   SUB Rectfn(Ta(*),Fa(*),Fb(*),Fc(*))
170    !THIS SUBROUTINE CALCULATES RECTIFIER S.F.(SINGLE PULSE MODULATION)
180     Ta(1)=30.
190     Ta(2)=Ta(1)+120.
200     Ta(3)=210.
210     Ta(4)=Ta(3)+120.
220     Ij=4
230     FOR I=1 TO 4
240       Tb(I)=Ta(I)+120.
250       Tc(I)=Ta(I)+240.
260       PRINT I;Ta(I),Tb(I);Tc(I)
270     NEXT I
280    !CALCULATION OF SWITCHING FUNCTION:RESOLUTION IS .25 DEG.
290     Jj=1
300     FOR J=1 TO Ij STEP 2
310       FOR I=Jj TO 1440
320         Xf=.25*I
330         IF Xf>Ta(J) THEN
340           Fa(I)=1
350         ELSE
360           Fa(I)=0
370         END IF
380         IF Xf>Ta(J+1) THEN GOTO R1
390       NEXT I
400 R1: !   NEXT Angle
410       Jj=I
420     NEXT J
```

```
430    FOR I=721 TO 1440
440      Fa(I)=-Fa(I)
450    NEXT I
460    FOR I=1 TO 1440
470      Ib=120*4
480      Fb(I+Ib)=Fa(I)
490      Ic=240*4
500      Fc(I+Ic)=Fa(I)
510    NEXT I
520    FOR I=1441 TO 1920
530      Fb(I-1440)=Fb(I)
540    NEXT I
550    FOR I=1441 TO 2400
560      Fc(I-1440)=Fc(I)
570    NEXT I
580   SUBEND
590   SUB Rectout(Fa(*),Fb(*),Fc(*),Xdc(*))
600   !THIS SUBROUTINE CALCULATES FICTITIOUS RECTIFIER OUTPUT VOLTAGE
610     DIM Y(120)
620     DEG
630     FOR I=1 TO 1440
640       Ya=.25*I
650       Xa=Fa(I)*SIN(Ya)
660       Yb=Ya-120
670       Xb=Fb(I)*SIN(Yb)
680       Yc=Ya-240
690       Xc=Fc(I)*SIN(Yc)
700       Xdc(I)=(Xa+Xb+Xc)
710            PRINT I;Xdc(I)
720       IF Xdc(I)>SQR(3) THEN Xdc(I)=Xdc(I-1)     !  A CHECK
730     NEXT I
740       !GOTO R5 ! ONLY USED WHEN 30 DEG SHIFT IS NOT DESIRED
750       !THIS PORTION IS TO SHIFT RECT. OUTPUT BY 30 DEG
760     FOR I=1 TO 120
770       Y(I)=Xdc(I)
780     NEXT I
790     FOR I=121 TO 1440
800       Xdc(I-120)=Xdc(I)
810     NEXT I
820     FOR I=1321 TO 1440
830       Xdc(I)=Y(I-1320)
840     NEXT I
850 R5: !
860   SUBEND
870   SUB Hirosi(L,Sm,Kp,Tai(*))
880    !THIS SUBROUTINE CALCULATES INVERTER S.F.(MSPWM)
890     DIM S(20),C(20),Y(90),X(90),T(90)
900     Tol=.0001
910     Kp=2*L+1
920     Kp1=Kp-1
930     FOR I=1 TO Kp1
940       S(I)=((-1)^I)*(3*Kp/PI)
950     NEXT I
```

```
960      FOR I=1 TO Kpl STEP 2
970        C(I)=I+1
980      NEXT I
990      FOR I=2 TO Kpl STEP 2
1000       C(I)=-I
1010     NEXT I
1020    ! CALCULATION OF INTERCEPT OF TRIANGLE & SINE WAVE
1030     Y(1)=Sm
1040     X(1)=PI/2.
1050     FOR J=1 TO Kpl
1060       FOR I=1 TO 50
1070         K=I+1
1080         X(K)=(Y(I)-C(J))/S(J)
1090         Y(K)=Sm*SIN(X(K))
1100         Xx=ABS(X(K)-X(K-1))
1110         IF Xx<Tol THEN GOTO H1
1120       NEXT I
1130 H1:   T(J)=X(I)
1140     NEXT J
1150     FOR Kc=1 TO Kpl
1160       Kc1=Kp-Kc
1170       Kc2=Kpl+Kc
1180       Kc3=2*Kpl+Kc
1190       Kc4=3*Kpl+Kc
1200       T(Kc2)=2*PI/3-T(Kc1)
1210       T(Kc3)=PI/3+T(Kc)
1220       T(Kc4)=PI-T(Kc1)
1230     NEXT Kc
1240     Kp5=4*Kpl-1
1250     FOR J=1 TO Kp5
1260       M=4*Kpl-J
1270       FOR I=1 TO M
1280         IF T(J)>T(J+I) THEN
1290           GOTO H2
1300         ELSE
1310           GOTO H3
1320         END IF
1330 H2:     Aux=T(J)
1340         T(J)=T(J+I)
1350         T(J+I)=Aux
1360 H3:   NEXT I
1370     NEXT J
1380     Kp4=4*Kpl
1390     FOR I=1 TO Kp4
1400       Tai(I)=T(I)*180./PI
1410       PRINT I,Tai(I)
1420     NEXT I
1430   SUBEND
1440   SUB Invout(Wo,Kp,Tai(*),Fd(*),Xdc(*),Xa(*))
1450    !THIS SUBROUTINE CALCULATES INVERTER OUTPUT VOLTAGE AT fo(=Wo)
1460     Wil=60.
1470     Wsl=Wo
```

```
1480    Perd=Wil/Wsl
1490    Period=360.*Perd
1500    Kp4=4*(Kp-1)
1510    Kpr=Kp4+1
1520    Kpt=2*Kp4
1530    Ij=Kpt
1540    FOR I=Kpr TO Kpt
1550      J=I-Kp4
1560      Tai(I)=Tai(J)+180.
1570    NEXT I
1580    FOR I=1 TO Ij
1590      Tai(I)=Tai(I)*Perd
1600      PRINT I;Tai(I)
1610    NEXT I
1620    FOR I=1 TO 10
1630      Dreqd=Period*I
1640      IF Dreqd 360.>THEN GOTO I1
1650    NEXT I
1660 I1:Iprod=I
1670    FOR I=1 TO Iprod
1680      FOR J=1 TO Ij
1690        Jp=Ij*I+J
1700        Tai(Jp)=Tai(J)+Period*I
1710      NEXT J
1720    NEXT I
1730    Nang=Jp
1740    PRINT Perd,Period,Iprod,Nang
1750    Jj=1
1760    FOR J=1 TO Nang STEP 2
1770      IF Tai(J)>360. THEN GOTO I2
1780      FOR K=Jj TO 1440
1790        Xi=.25*K
1800        IF Xi>Tai(J) THEN
1810          Fd(K)=1
1820        ELSE
1830          Fd(K)=0
1840        END IF
1850        IF Xi>Tai(J+1) THEN GOTO I3
1860      NEXT K
1870 I3:  Jj=K
1880    NEXT J
1890 I2:Iend=Iprod*2-1
1900    FOR I=1 TO Iend
1910      Inum=4*180*Perd*I
1920      FOR J=Inum TO 1440
1930        Fd(J)=-Fd(J)
1940      NEXT J
1950    NEXT I
1960    FOR I=1 TO 1440
1970      Xa(I)=Fd(I)*Xdc(I)
1980          PRINT I;Xa(I)
1990    NEXT I
2000 SUBEND
```

```
2010 SUB Sines(Ta(*))
2020  !THIS SUBROUTINE PLOTS THE INPUT VOLTAGES
2030   GINIT
2040   GRAPHICS ON
2050     !PLOTTER IS 705,"HPGL"   TO GET A HARD COPY
2060     !OUTPUT 705;"VS 4"  IT SLOWS DOWN THE SPEED OF PLOTTER
2070   DEG
2080   LDIR 90
2090   CSIZE 2.6
2100   VIEWPORT 5,16,20,96
2110   WINDOW 1.2,-1.2,-40,402
2120   AXES .5,90
2130   LORG 6!LABEL Y AXIS
2140   FOR I=90 TO 360 STEP 90
2150     MOVE -.1,I
2160     LABEL I
2170     IF I=360 THEN
2180       MOVE -.02,390
2190       CSIZE 2.9
2200       LABEL "wt"
2210     END IF
2220   NEXT I
2230   CSIZE 2.6
2240   LORG 8 ! LABELLING X AXIS
2250   FOR I=-1.0 TO 1.0 STEP .5
2260     IF I=0 THEN 2290
2270     MOVE I,-.4
2280     LABEL I
2290   NEXT I
2300   FOR H=0 TO 2
2310     MOVE 0,0
2320     FOR X=0 TO 360
2330       IF H=0 THEN DRAW SIN(X),X
2340       IF H=1 THEN DRAW SIN(X-120),X
2350       IF H=2 THEN DRAW SIN(X-240),X
2360     NEXT X
2370   NEXT H
2380 SUBEND
2390 SUB Mplot(Vlft,Vrt,Wlft,Wrt,Plotp(*))
2400  !THIS SUBROUTINE CALCULATES DIFFERENT S.F./OUTPUT VOLTAGE WAVEFORMS
2410   DEG
2420   LDIR 90
2430   CSIZE 2.6
2440   VIEWPORT Vlft,Vrt,20,96
2450   WINDOW Wlft,Wrt,-40,402
2460   AXES .5,90
2470   LORG 6  ! LABELIING Y AXIS
2480   FOR I=90 TO 360 STEP 90
2490     MOVE -.15,I
2500     LABEL I
2510     IF I=360 THEN
2520       CSIZE 2.9
```

```
2530        MOVE -.02,390
2540        LABEL "wt"
2550      END IF
2560    NEXT I
2570    CSIZE 2.6
2580    LORG 8  ! LABELLING X AXIS
2590    FOR I=-1.0 TO 1.0 STEP .5
2600      IF I=0 THEN M1
2610      MOVE I,-.4
2620      LABEL I
2630 M1:NEXT I
2640    MOVE 0,0
2650    FOR X=1 TO 1440
2660      DRAW Plotp(X),X/4
2670    NEXT X
2680  SUBEND
```